



The University of
Nottingham

University of Nottingham

Polymer Composites Group

Division of Materials, Mechanics and Structures

Faculty of Engineering

Characterisation of Tack for Automated Tape Laying

January 2011

By

Richard James Crossley
MEng. (Hons.)

GEORGE GREEN LIBRARY OF
SCIENCE AND ENGINEERING

Thesis submitted to the University of Nottingham for the degree of Doctor of Philosophy

Abstract

Automated Tape Laying (ATL) trials using low cost wind energy suitable material and mould tools have been conducted. New materials proved problematic during ATL lay-up and observations of the ATL process show that the prepreg tack and stiffness properties significantly affect lay-up performance. Prepreg tack has not been widely researched within the composites industry due to the absence of a standardised method for characterisation. A new tack and stiffness test has therefore been developed which is representative of the ATL process. The new test was used to investigate the response to process and material variables. Two failure modes were observed and compared to those found in Pressure Sensitive Adhesives (PSA). Failure modes are associated with the viscoelastic stiffness of the resin. High stiffness appears to result in interfacial failure turning to cohesive failure when stiffness is reduced. A peak in tack is observed to correspond with the transition in failure mode leading to the conclusion that prepreg tack is the result of a chain system rather than a single property. The chain system consists of an interface and bulk components each having individual time and physical variable dependant properties.

Tack and stiffness is shown to conform to the Williams-Landel-Ferry (WLF) time-temperature superposition principle for both cohesive and interfacial failure modes. Cohesive viscoelastic and surface energy interface failure mechanisms may be theoretically linked via the Lennard-Jones energy well with molecular jumps triggered by thermal vibrations. This analogy allows both failure phenomenon to simultaneously follow the time temperature superposition principle and is typically demonstrated in LJ dynamic mechanical modelling. The theoretical analogy is used in the explanation of experimental results where tack is essentially thought of as a low energy non-covalent molecular bond or reaction.

The experimental technique developed here could allow for the standardisation of tack and stiffness specification for manufacturers. The application of results to ATL production is explored and demonstrated using ATL equipment. The results show that optimum lay-up conditions may be explored offline using the new tack and stiffness test. Results also show promising signs that the WLF relationship could be exploited to greatly increase lay-up speed and consistency, increasing the attractiveness of the process to wind turbine blade manufacturers. A theoretical results curve is also presented which may allow manufacturers to determine the effect of changes in surface conditions and resin properties on tack.

Acknowledgements

The author would like to thank his academic supervisors Dr Peter Schubel and Professor Nick Warrior for their advice and support during this work and Dr Davide De Focatiis for his guidance and interest.

I would also like to thank all the partners of the Affordable Innovative Rapid Production of Wind Energy Rotor-blades (AIRPOWER) project under which this work was carried out. The AIRPOWER project was co-funded by the Technology Strategy Board's Collaborative Research and Development program, following open competition.

The Technology Strategy Board is an executive body established by the Government to drive innovation. It promotes and invests in research, development and the exploitation of science, technology and new ideas for the benefit of business. Increasing sustainable economic growth in the UK and improving quality of life. For more information visit www.innovateuk.org

I would also like to thank my partner Ruth Elmer for all her support and encouragement.

Nomenclature

Abbreviations

AFP	<i>Automated Fibre Placement</i>
AIRPOWER	<i>Affordable Innovative Rapid Production of Offshore Wind Energy Rotor-blades</i>
APL	<i>Automated Ply Lamination</i>
ATL	<i>Automated Tape Laying</i>
ATW	<i>Automated Tape Winding</i>
BEM	<i>Blade Element Momentum theory</i>
BIAX	<i>Bi-axial</i>
BPA	<i>Bisphenol-A</i>
CFW	<i>Continuous Filament Winding</i>
CSM	<i>Chopped Strand Mat</i>
CTL	<i>Contour Tape Laying</i>
DC	<i>Dahlquist's Criterion</i>
DSC	<i>Differential scanning calorimetry</i>
FAW	<i>Fibre Areal weight</i>
FW	<i>Filament Winding</i>
GFRP	<i>Glass Fibre Reinforced Plastic</i>
GPC	<i>Gel Permeation Chromatography</i>
HLU	<i>Hand Lay-Up</i>
LJ	<i>Lennard-Jones two parameter molecular adhesion model</i>
OCA	<i>Occupational Contact Allergy</i>
PSA	<i>Pressure Sensitive Adhesives</i>
PU	<i>Polyurethane</i>
PVC	<i>Poly Vinyl Chloride</i>
RH	<i>Relative Humidity</i>
RIFT	<i>Resin Infusion under Flexible Tooling</i>
SAOS	<i>Small Amplitude Oscillatory Shear rheometry</i>
THF	<i>Tetrahydrofuran</i>
TRIAx	<i>Tri-axial</i>
TSB	<i>Technology Strategy Board</i>
TTS	<i>Time Temperature Superposition</i>
UD	<i>Unidirectional</i>
UV	<i>Ultra Violet</i>
VART	<i>Vacuum Assisted Resin Transfusion</i>
VF	<i>Volume Fraction</i>
VI	<i>Vacuum infusion</i>
VOC	<i>Volatile Organic Compound</i>
WBL	<i>Weak Boundary Layer</i>
WE	<i>Wind Energy</i>
WLF	<i>Williams-Landel-Ferry time temperature superposition equation</i>

Symbols

A	Area	[m ²]
a _t	Time shift factor (WLF)	
b	Tape width	[mm]
C ₁	WLF constant	
C ₂	WLF constant	
E	Young's Modulus	[GPa]
E _a	activation energy	[kJ/mol]
F _p	Average peel force	[N]
F	Force	[N]
G	Work of adhesion	[J/m ²]
G'	Shear storage modulus	[Pa]
G''	Shear loss modulus	[Pa]
h	Layer thickness	[mm]
M _n	Number average molecular weight	[g/mol]
M _w	Weight average molecular weight	[g/mol]
P	pressure	[MPa]
P	peel Resistance	[N/mm]
P	Polydispersity	
R	Universal gas constant	[J/mol K]
R _a	Surface roughness average	[μm]
RH	Relative humidity	[%]
S	Shear stress	[N/m ²]
T	Temperature	[°C]
T ₀	Reference temperature	[°C]
T _g	Glass transition temperature	[°C]
V	Separation velocity	[mm/min]
W _{adh}	Work of adhesion	[J/m ²]
Z	Extension	[mm]
ε	Strain	
η	Viscosity	[MPas]
ρ	Density	[kg/m ³]
σ	Standard deviation	
σ	Tensile strength	[MPa]
ω	Frequency	[Rad/s]
$\dot{\gamma}$	Strain rate	[s ⁻¹]
δ	Phase angle	[°]

Contents

Abstract	2
Acknowledgements	3
Nomenclature.....	4
1 Introduction	9
1.1 Turbine blade demand.....	9
1.2 Turbine blade design	11
1.2.1 <i>Size</i>	<i>11</i>
1.2.2 <i>Geometry</i>	<i>12</i>
1.2.3 <i>Materials.....</i>	<i>13</i>
1.3 Existing production methods	20
1.4 Automated forming processes	25
1.5 Aims and objectives.....	30
1.6 Theme of this work.....	31
2 Literature review	32
2.1 Prepreg materials.....	32
2.1.1 <i>Production</i>	<i>32</i>
2.1.2 <i>Specification and supply</i>	<i>33</i>
2.1.3 <i>Resin chemistry and cure.....</i>	<i>36</i>
2.2 Automated tape laying	37
2.3 Prepreg flexural rigidity	40
2.4 Prepreg tack.....	41
2.4.1 <i>Definition.....</i>	<i>41</i>
2.4.2 <i>Commercial characterisation</i>	<i>42</i>
2.4.3 <i>Experimental characterisation.....</i>	<i>43</i>
2.5 Pressure sensitive adhesives.....	44
2.5.1 <i>Probe testing.....</i>	<i>44</i>
2.5.2 <i>Peel testing.....</i>	<i>53</i>
2.5.3 <i>Shear testing.....</i>	<i>63</i>
2.6 Rheology	63
2.7 Adhesives theory	69
2.8 Polymer melts	71
2.8.1 <i>Basic molecular principles</i>	<i>71</i>
2.8.2 <i>Molecular description.....</i>	<i>73</i>
2.8.3 <i>Melt behaviour.....</i>	<i>74</i>
2.8.4 <i>Diffusion</i>	<i>76</i>
2.8.5 <i>Time-temperature dependant behaviour</i>	<i>76</i>
2.8.6 <i>Mathematical models.....</i>	<i>78</i>
2.8.7 <i>Molecular adhesion.....</i>	<i>78</i>
2.8.8 <i>Dynamic molecular modelling</i>	<i>80</i>
2.8.9 <i>Molecular characterisation.....</i>	<i>81</i>
3 Experimental methodology	83
3.1 General approach	83
3.2 ATL feasibility study	84
3.2.1 <i>Materials.....</i>	<i>85</i>
3.2.2 <i>Equipment</i>	<i>85</i>
3.3 Tack and stiffness test.....	88
3.3.1 <i>Operation</i>	<i>88</i>
3.3.2 <i>Equipment</i>	<i>89</i>

3.3.3	<i>Specimens</i>	91
3.3.4	<i>Accuracy</i>	91
3.3.5	<i>Analysis</i>	93
3.3.6	<i>Repeatability study</i>	95
3.3.7	<i>Controlling uncertainty</i>	96
3.4	Commercial prepreg tack characterisation	99
3.5	Effect of variables on tack and stiffness	101
3.5.1	<i>Tack and stiffness tests</i>	101
3.5.2	<i>Control of variables</i>	103
3.6	Rheology	106
3.7	Time temperature superposition investigation	107
3.8	ATL applicability study	109
4	Results and observations	112
4.1	ATL feasibility trials	112
4.2	Commercial prepreg characterisation	117
4.2.1	<i>Roll position effects</i>	117
4.2.2	<i>Face position effects</i>	118
4.2.3	<i>Overall characterisation</i>	118
4.3	Effect of tack variables	120
4.3.1	<i>Temperature</i>	120
4.3.2	<i>Feed rate</i>	123
4.3.3	<i>Surface roughness</i>	124
4.3.4	<i>Release agents</i>	127
4.3.5	<i>Compaction force</i>	128
4.3.6	<i>Surface material</i>	130
4.3.7	<i>Contact temperature</i>	132
4.3.8	<i>Resin type</i>	133
4.3.9	<i>Fibre areal weight</i>	134
4.3.10	<i>Fibre type</i>	134
4.3.11	<i>Resin content</i>	136
4.3.12	<i>Fibre architecture</i>	137
4.3.13	<i>Stiffness summary</i>	139
4.3.14	<i>Tack summary</i>	140
4.4	Rheology	142
4.5	Time temperature superposition	143
4.5.1	<i>Gel permeation chromatography</i>	143
4.5.2	<i>Differential scanning calorimetry</i>	145
4.5.3	<i>Rheology</i>	145
4.5.4	<i>Peel testing</i>	148
4.6	ATL applicability study	154
4.6.1	<i>Prepreg tack in commercial conditions</i>	154
4.6.2	<i>ATL trials</i>	157
5	Discussion	159
5.1	Tack and stiffness methodology	159
5.2	Effect of variables on tack and stiffness	161
5.2.1	<i>Temperature</i>	161
5.2.2	<i>Feed rate</i>	162
5.2.3	<i>Surface roughness</i>	163
5.2.4	<i>Release agent</i>	163
5.2.5	<i>Compaction force</i>	164
5.2.6	<i>Surface type</i>	165
5.2.7	<i>Resin type</i>	165
5.2.8	<i>Contact temperature</i>	166
5.2.9	<i>FAW</i>	166
5.2.10	<i>Fibre type</i>	167

5.2.11	Resin content	169
5.2.12	Fibre architecture.....	170
5.3	Time temperature superposition investigation	171
5.3.1	DSC	171
5.3.2	GPC	171
5.3.3	Rheology	171
5.3.4	Tack and stiffness results.....	172
5.4	Results Summary.....	173
5.4.1	Stiffness	173
5.4.2	Tack.....	173
5.4.3	Molecular theory	178
5.5	Commercial prepreg	182
5.6	ATL feasibility and application	183
5.6.1	Performance observations.....	183
5.6.2	Applicability results	184
5.6.3	Tape performance.....	186
6	Conclusions	189
6.1	Tack and stiffness.....	189
6.1.1	Method and observations	189
6.1.2	Variable effects.....	190
6.1.3	Time temperature superposition	192
6.1.4	Molecular theory	192
6.2	Prepreg characterisation	193
6.3	ATL development.....	194
6.3.1	Feasibility	194
6.3.2	Application.....	195
6.4	Major conclusions.....	196
7	Recommendations and future work	199
7.1	Tack and stiffness.....	199
7.2	Prepreg.....	200
7.3	ATL	200
	Appendix	202
	A. Publications arising from this thesis	202
	B. Calibration of rolling friction and backing film	203
	C. Analysis of single level results.....	204
	D. Analysis of temperature sweep results.....	205
	E. Statistical confidence.....	206
	References	208

1 Introduction

The increasing demand for wind turbines has led to a shortage in turbine blade supply (Chapter 1.1). Current turbine blade production involves a significant amount of manual glass fibre placement leading to long production times, high labour costs and poor part consistency (Chapter 1.3). Manufacturers are now seeking to improve production by utilising automated production methods. However, for reasons of design and efficiency suitable automated processes are limited to those capable of producing large blade components (>60m long) with unidirectional fibres running along the length (Chapter 1.2). Automated Tape Lay-up (ATL), traditionally utilised for aerospace applications, is believed to be the most appropriate candidate for development.

1.1 Turbine blade demand

The release of CO₂ gasses into the atmosphere when burning fossil fuels is now recognised as a major contributor towards global warming [1]. The United Nations have agreed through the Kyoto protocol to reduce emissions in the developed world with a cost penalty for every tonne of CO₂ produced exceeding agreed limits [2]. The tax penalty for CO₂ emissions coupled with increasing cost of oil and gas, as finite resources become depleted, have allowed emission free renewable energy resources to increase in affordability. Therefore, wind power has become increasingly popular as a zero emissions means of generating electricity. Wind power has proven to be cost effective and reliable in comparison to other renewable energy sources. For the year 2008, 36% (8,484 MW) of the European Union's (EU) newly installed capacity was wind energy, making it the fastest growing electricity source [3]. Wind power has seen an exponential growth in demand for installed capacity which is set to continue with annual growth of 17%, hampered marginally by the financial crisis in 2009 (Fig 1-1).

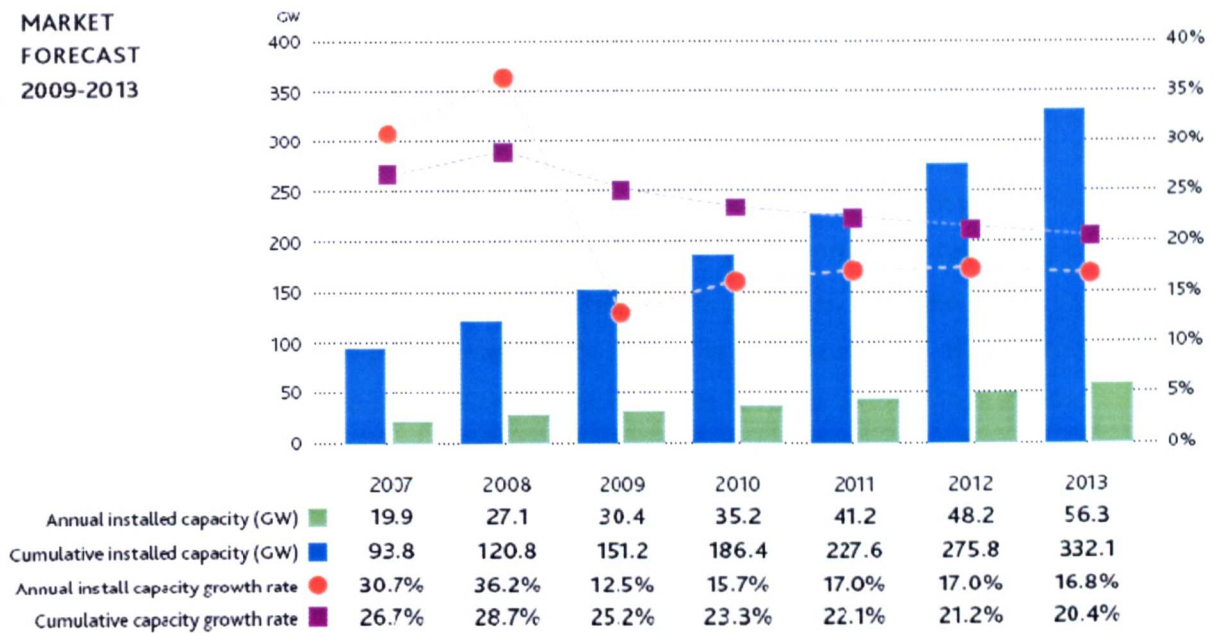
**MARKET
FORECAST
2009-2013**


Fig 1-1 GWEC world market forecast for installed wind power capacity [4]

Blades account for approximately 13% of the total cost of the turbine [5]. Blade manufacturing is now one of the largest single applications of engineered composites in the world. In 2007 more than 200,000 metric tonnes of finished blade structures were completed, consisting of [6]:-

- Glass fibre – 100,240 tonnes
- Carbon fibre – 2,090 tonnes
- Thermoset resin (primarily epoxy and vinyl ester) – 82,550 tonnes
- Core (balsa and foam) – 8,160 tonnes
- Metal (finishing and bolts) – 6,800 tonnes

With these values expected to rise, production increases are required to meet demand. The stagnation in the growth of large turbine installations (>2 MW) during 2007 was said to be the result of component shortages, particularly blades [7]. This overwhelming demand has caused manufacturers to seek automated methods to improve production efficiency and satisfy demand [8].

1.2 Turbine blade design

1.2.1 Size

The kinetic energy or power contained in moving air is a function of velocity and swept area [9]. An increase in turbine diameter results in a squared increase in power output. This relationship allows a greater power yield per installation cost, reducing the overall cost per kW. This saving drives manufacturers to produce turbines with increasingly large rotor diameters. Reducing the blade mass is necessary to allow production of larger turbines. Simple scaling laws suggest that the turbine blade mass should increase at a cubed rate proportionally with rotor diameter [10]. However, a 2.65 exponential mass increase has been observed in practice [9, 11]. This favourable deviation is attributed to improvements in blade materials, mostly the strength to weight ratio of composites [11]. Technological advances in materials have allowed the wind energy market to capitalise on larger turbines with a significant increase in large (>2MW) turbine installations accounting for more than half of all installed capacity across Europe in 2006 [7].

The continued trend of increasing turbine diameter installations appears to have reached a plateau at 126m diameter with 62m long blades in 2004 (Fig 1-2). The plateau is generally attributed to the increasing design, production, transport and installation costs. However, increasing financial support from government organisations may allow larger blades to be developed in future. One such development is the Clipper Wind 'Britannia project', a 10MW turbine expected to have 72m blades [12].



Fig 1-2 The largest wind turbine diameters from 1980 to 2008 [7]

1.2.2 Geometry

High rotor aerodynamic efficiency is desirable and is typically maximised within the limits of affordable production. It is widely accepted that not all of the winds kinetic energy may be utilised and that wind turbine efficiency cannot exceed 59.3%, commonly referred to as the Betz limit [10, 13]. This concept along with tip losses and rotational losses is embodied in the Blade Element Momentum (BEM) method, which is used to define the optimum blade geometry for aerodynamic performance [14]. The BEM method is also used to define the aerodynamic loads. The blade may then be modelled as a simple encastré beam [9]. The main aerodynamic load causes the blade to deflect towards the tower in the 'flatwise' direction. The increasing bending moment towards the root indicates that structural requirements also determine blade shape, with increasing influence towards the hub. Areas approaching the hub require thicker aerofoils to increase structural efficiency [15]. Other operational loads tend to be proportional to blade mass under gravitational, centrifugal and inertial forces [16].

An efficient rotor blade defined by BEM will typically consist of a complex shape with several aerofoil profiles blended at an angle of twist terminating at a circular flange (Fig 1-3) [10, 17]. To reduce mould complexity and manufacturing costs several deviations from the ideal shape are likely, including:-

- Reducing the angle of twist
- Linearization of the change in chord length

Such simplifications are detrimental to rotor efficiency [18] and are unlikely to be tolerated by manufacturers without significant justification. The introduction of new moulding techniques and materials has allowed production of increasingly complex blade shapes. However, production economics and practicalities are likely to dictate final geometry. Turbine suppliers are now capable of the cost effective production of blades with optimisation features such as; an angle of twist up to 16° , variable chord length up to 4.2m and multiple aerofoil geometries, with quoted efficiencies of up to 51% for a 90m rotor [19].

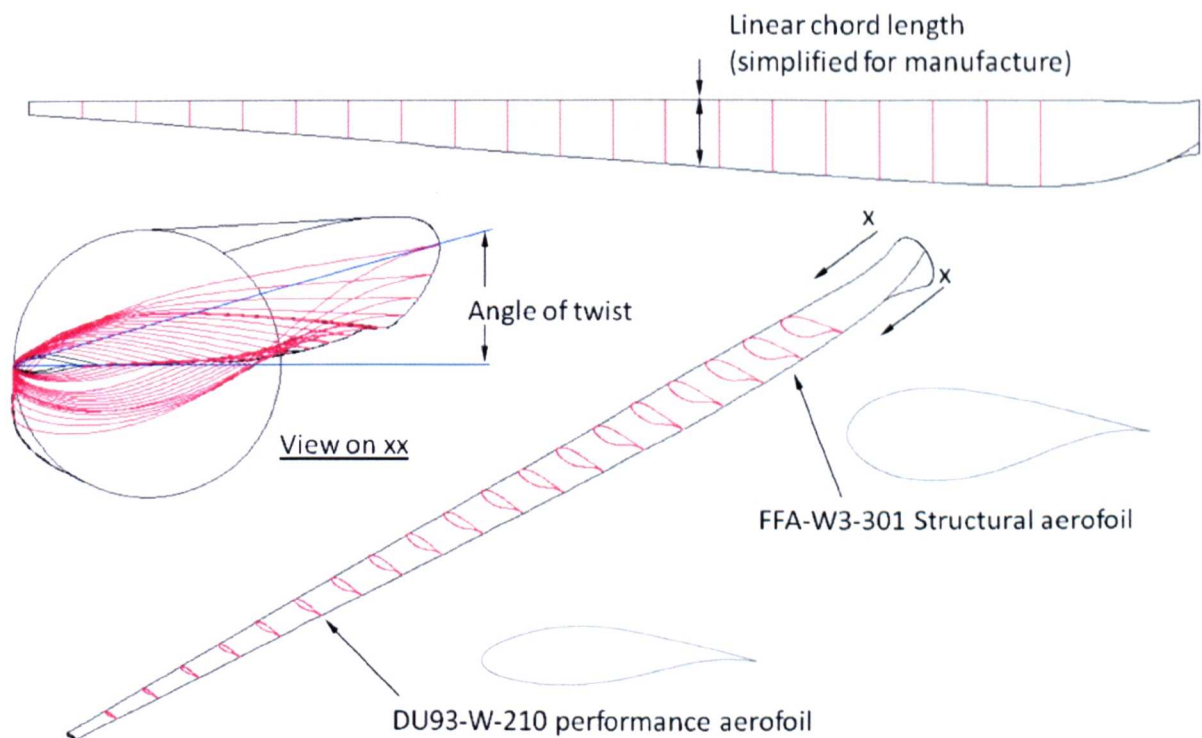


Fig 1-3 A typical modern commercial blade with multiple aerofoil profiles, angle of twist and linear chord length increase

1.2.3 Materials

Composite materials allow the necessary complex aerofoil blade shapes to be formed and are used by all wind turbine market leaders. They also offer superior structural capabilities and resistance to corrosion. They are generally formed into a laminate which consists of layers of fibres encased in a polymer resin matrix. Two laminates may be separated by a foam core to form a sandwich panel which increases flexural rigidity with minimal weight increase. An almost endless combination of sandwich configurations, matrix, fibres and foam core components are utilised, tailored to suit the application and load case. The typical component and laminate configuration for wind turbine blades is reviewed here in order to assess the ability of automation methods to handle such materials.

Resin Matrix

Thermoset resins are the only resin type currently utilised by mainstream turbine manufacturers. Thermoset resins can be formed easily and then cured at elevated temperature, solidifying in the required shape by an irreversible chemical reaction. These isotropic materials allow load transfer between the reinforcement fibres, other duties include [20]:-

- Protecting notch sensitive fibres from abrasion

- Protecting fibres from moisture, oxidation and chemicals
- Providing shear, transverse tensile and compression properties
- Governing the thermo-mechanical performance

Epoxy and polyester resin systems are favoured by rotor blade manufacturers for their widespread existing working knowledge, availability, performance and ease of production. They are general purpose resins with inapplicable alternatives selected for their fire and chemical resistance. Polyester resins offer versatility, good physical and mechanical properties, are readily available and cost effective [20]. Polyester resins were once the most popular resin type for rotor blade manufacture. However, their use has declined in all but one leading supplier of rotor blades, generally due to the increase in performance demands and the reduction in cost of superior epoxy resins. Additionally, polyester resins are incompatible with desirable higher modulus carbon fibres with mainstream surface treatments. A major contribution to the decline in polyester use can be attributed to health and safety risks [21]. Epoxy resins now dominate consumption, superior in most respects to polyester resins, which are generally preferred simply on the grounds of cost [22]. They are typically tougher than polyesters, shrink less and have good resistance to heat distortion. The ability of epoxy resins to be partially cured so that prepregs can be supplied offers increased flexibility in manufacturing. A direct comparison of properties (Table 1-1) highlights the advantages of epoxy.

Table 1-1 A comparison of the two resins most commonly used in wind turbine blades

Criteria	Epoxy	Polyester
Estimated use in turbine rotors	70%	30%
Availability and expertise	Excellent	Excellent
Health and safety issues	occupational contact allergy (OCA) dermatitis[23] (minor)	Regulated volatile organic compound emissions[21] (major cost implications)
Common forming processes	Prepreg lay-up vacuum infusion	Wet lay-up vacuum infusion
Common curing processes	Elevated temperature under Vacuum	Ambient or elevated temperature with or without vacuum
Non - compatible fibres	Some CSM binding agents	Mainstream carbon
Shrinkage on cure	3-4% [24, 25]	4-8% [22]
Density (ρ)[22]	1.1-1.4 Mg/m ³	1.2-1.5 Mg/m ³
Young's modulus (e)[22]	3-6 GPa	2-4.5 GPa
Tensile strength (σ)[22]	0.035-0.1 GPa	0.004-0.09 GPa
Failure strain (ϵ)[22]	1-6%	2%

Fibres

Fibres carry the majority of the structural load. Consequently, the essential property of a fibre is defined as the elastic modulus. It must be significantly stiffer than the matrix, which allows it to carry and transfer the load applied to the composite [20]. Since the fibre is the main load bearing component it must also have sufficient strength to avoid failure. Glass fibres are the most popular fibre reinforcement utilised by all of the leading rotor blade producers [26]. There are several types of glass fibres available each with a unique chemical composition and favourable properties. Although E-glass was originally designated by its excellent electrical insulation properties it also offers relatively high mechanical strength, durability at low cost with good availability and working knowledge [27]. Therefore, E-glass dominates consumption in both the rotor blade and general composite market. S-glass is designated for its increased strength and is likely to be limited to local reinforcement of highly stressed areas due to higher cost. S-glass is mostly used by manufacturers using polyester resins since those using epoxy are likely to prefer superior carbon fibres which are not compatible with polyester resins [28]. Carbon fibres are the predominant reinforcement material used to achieve high stiffness and strength. These fibres offer superior mechanical and fatigue properties in comparison to glass fibre [20]. At present, due to increased cost, carbon fibres are restricted in use to local reinforcement of highly stressed areas. However, recent large blade designs with complete carbon slender spars have been produced [28]. Therefore, the focus of wind energy carbon fibre has been on moderate to low stiffness and high failure strain properties, which better conform to the glass fibre properties of which they are to be integrated [11]. An extensive range of commercially available fibre types exist. For comparison, more general published data is also available (Table 1-2) [20].

Table 1-2 A comparison of typical fibre reinforcements used in turbine blades [20]

<i>Fibre</i>	<i>E Glass Std. grade</i>	<i>S2 - Glass High strength</i>	<i>T300 Carbon Low grade</i>	<i>T1000G Carbon High grade</i>
Density [Kg/m ³]	2570	2470	1760	1800
Modulus [GPa]	72.5	88	230	294
UT Strength [MPa]	3331	4600	3530	6370
UT Strain [%]	2.5	3	1.5	2.2

Fibre volume fraction and orientation

Fibre volume fraction and orientation also affects the overall strength and stiffness of the finished laminate [22, 29]. It is desirable to achieve a high fibre volume fraction to maintain the overall high strength provided by the fibres. The volume fraction that may

be achieved is typically dependent on the fibres and forming process [30]. Recently implemented vacuum infusion processes offer superior VF of 50-60% when compared to 40% achievable by hand lay-up. Mechanical performance is also effected by processing defects such as voids, resin rich or dry fibre areas [31]. The highest fibre volume fraction and laminate mechanical performance is typically achieved using continuous unidirectional fibres. Short fibre composites generally have reduced performance due to reduced volume fraction and alignment [22]. The prediction of composite strength in transverse and shear loading is also possible [22]. These predictions and experimental results indicate that composite materials are considerably stronger in the fibre direction. Fibre architecture is therefore chosen carefully to suit loading conditions with a range of commercially available formats:-

- *Unidirectional (UD)*, Continuous fibres lie in a single direction held in position by a minimal amount of cross stitching or a binding agent. Ideally suited for polar axial loading conditions the finished composite is highly anisotropic. This fibre orientation is utilised in the spar cap region of the rotor blade well suited to the intensive loads which run along the blade length.
- *Bidirectional (Biax)*, Continuous fibres are situated normal to each other achieved by either a woven fabric or by layering unidirectional fabrics. Bidirectional fabrics are used in two dimensional and shear loading conditions to avoid transverse loading of the fibres. They may be utilised in shear webs and within laminates of other blade components. Biax and UD fibres may also be combined to produce a tri-axial (triax) fabric with improved strength in the UD fibre direction.
- *Random*, Fibres are randomly orientated and can be either continuous or chopped, known as chopped strand mat (CSM). This type of fibre alignment typically results in inferior mechanical properties. Randomly orientated fibres have the advantage of being in plane isotropic facilitating simpler stress predictions with lower material costs. They may be utilised in non-structural areas.

Manufacturers typically use a range of fibre orientations in a lay-up sequence to give the required mechanical performance at specific areas of the blade (Fig 1-4).

Sandwich core

Core materials are used by all wind turbine manufacturers typically within trailing edge panels and shear webs to prevent buckling. Core sandwich constructions produce a stiff, light economic structure [20]. Using a low density core material increases flexural rigidity with no significant weight penalty. The core supports lateral loads experienced by the laminate component through shear, therefore the relevant properties are shear

strength and modulus [27]. The sandwich concept relies on the laminates being kept at constant thickness under loading, a small degree of compression of the core material causes a significant decrease in flexural rigidity [27]. Traditional methods for calculating the flexural rigidity of sandwich beams and shear stress of their core material are well defined [20]. Four types of core materials exist; honeycomb, corrugated, foam and balsa. Corrugated and honeycomb cores are not typically used in turbine blades due to their high cost and incompatibility with vacuum resin infusion methods. Mostly foam or cellular plastic cores are utilised. Any polymer, thermoset and thermoplastic alike can be expanded in several different manners. The density ranges available signify that a nearly limitless scope of properties are achievable to suit any application [27]. Two common foam materials used in the manufacture of blades are Poly Vinyl Chloride (PVC) foam and Polyurethane (PU) foam [16]. PVC is usually favoured due to its superior mechanical properties and temperature tolerance. Both balsa and foam may be used depending on the material cost and availability. Foam is usually favoured as it is in line with expertise and supply chain. Similarly, manufacturers utilising wood hybrids are likely to prefer balsa.

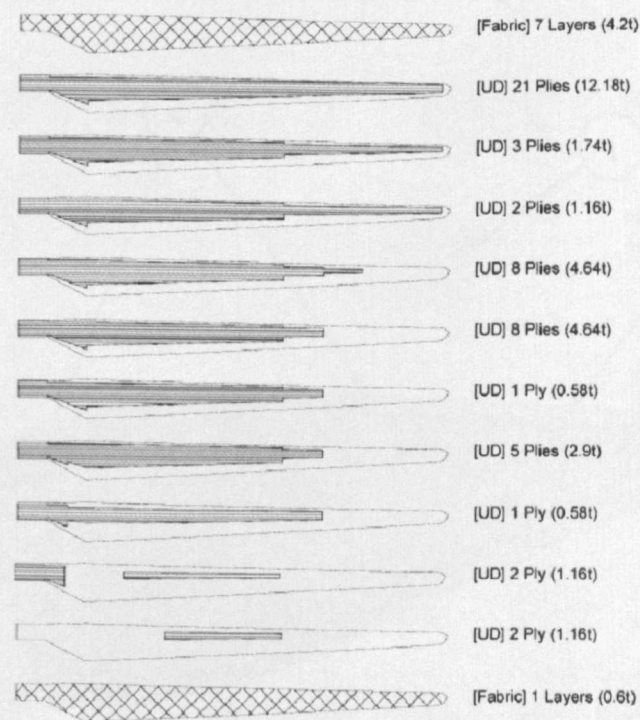


Fig 1-4 Typical fibre lay-up sequence for a 23m blade [17]

Components

To maintain aerodynamic shape and withstand the required loads, a typical blade design will have several distinguishable areas within an assembly which have significant differences in material usage (Fig 1-5):-

1. *Outer coating*, an aerodynamically significant smooth surface resistant to soiling, environmental weathering and UV corrosion. Typically a gel coat.
2. *Sandwich shell*, responsible for maintaining the blade's aerodynamic shape, resistant to panel buckling, lightning and bird strike. Typically, thin (>3mm) multi-axial E-glass fibre laminates with a lightweight foam or balsa core.
3. *Laminate spar caps*, structural components carrying high flapwise bending moments caused by aerodynamic loading. Typically a thick (>20mm) E glass continuous unidirectional fibre in the laminate which may incorporate high S glass or carbon fibres. It is critical that the fibres are laid along the blade length.
4. *Shear webs*, structural components to carry shear forces developed from flapwise bending moments and gravitational loading. Typically, thick (>10mm) multi-axial E glass fibre laminates with a lightweight core.

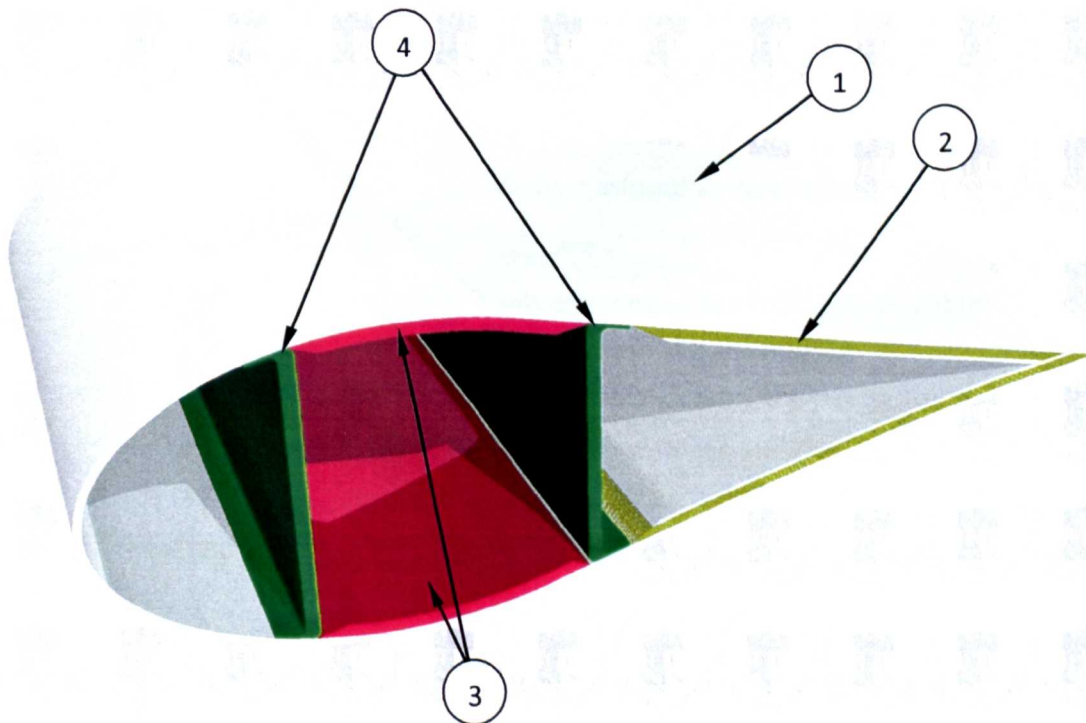


Fig 1-5 Typical components of a wind turbine blade cross section determined by composite material usage

Assembly

The type of process chosen for component construction generally dictates blade assembly. Two major design variations have emerged. A blade manufacturer who utilises filament winding (FW) will typically separate the main structural loading component to produce a central closed box section which is better suited to this method (Fig 1-6). The central box section may be integrated with foam cores and unidirectional material in the shear web and spar cap regions. Manufacturers who utilise vacuum infusion (VI) will typically integrate the spar cap material into the blade shell with separate shear web components. Production of a central box spar may also be carried out by VI.

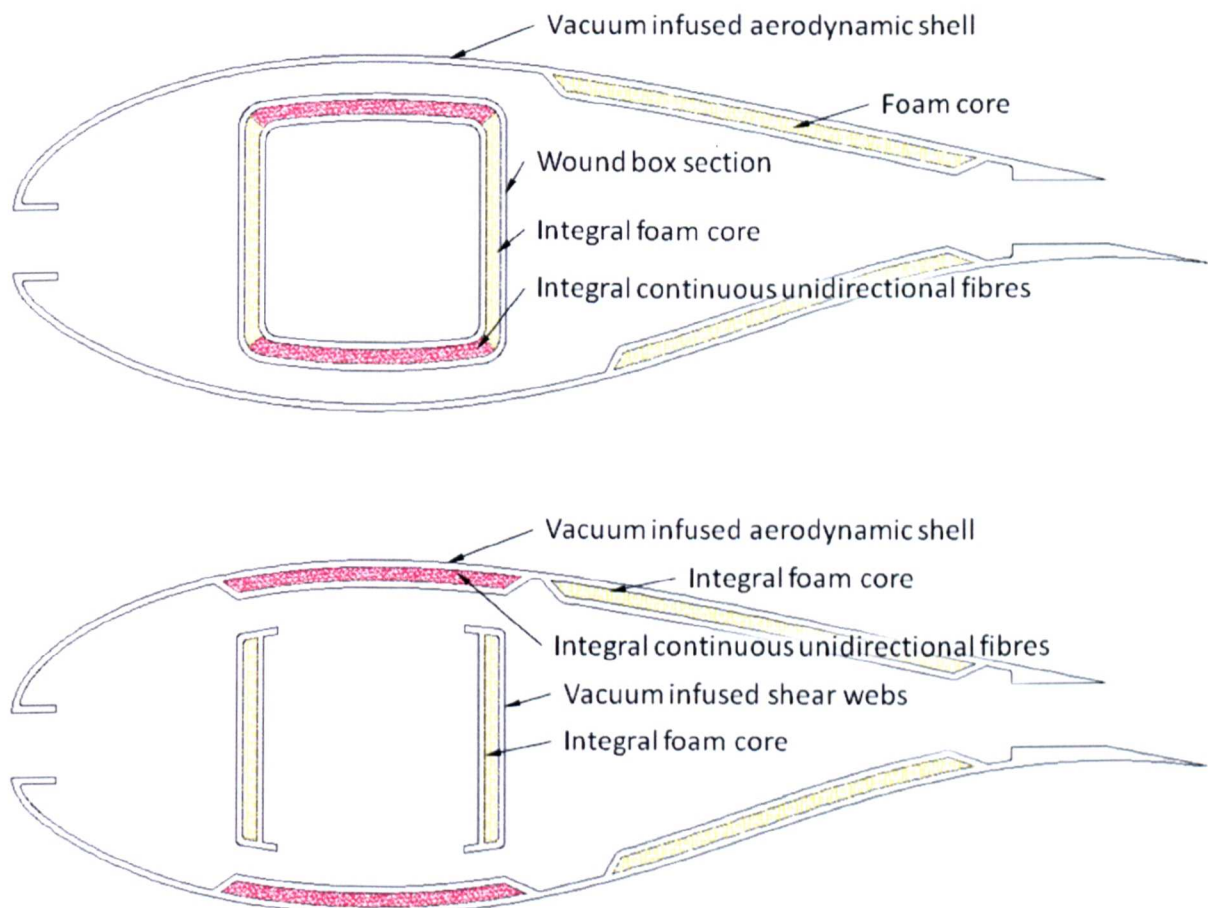


Fig 1-6 Two typical blade designs incorporating either a box section produced by FW (top) or shear webs (bottom) typically produced by VI

1.3 Existing production methods

Prepreg and vacuum Infusion (VI) have mostly replaced wet lay-up as the mainstream manufacturing process for rotor blade production. These methods are flexible but rely on the manual positioning of materials. Filament winding is the most successful historical attempt at automation. However, difficulties in forming the trailing edge prevented large scale production of the full blade component. Despite this drawback, many blades with filament wound structural box section spars have been produced. Therefore, fibre winding is included within existing production methods.

Wet lay-up

Until recently wet lay-up techniques, used traditionally in the boat building industry [11], were favoured for turbine blade production. Wet lay-up production suffers from poor repeatability, high labour content and health issues. This process has now been replaced by vacuum resin infusion or prepreg methods in all of the top ten suppliers. Low volume production may still continue in smaller companies or to cover excess production. Wet lay-up is the simplest method used for forming composite materials. The fibres are laid out over a mould and wetted out with a premixed resin by hand using a brush or roller. This method demands longer curing times as the resin needs to remain viscous throughout the lengthy rolling process. The quality and strength of the laminate relies heavily on the skill of the workforce. It has no guaranteed repeatability and produces relatively low fibre volume fractions [32]. A typical cycle time for using wet lay-up techniques on a 40m blade is 2 days [33] with increased scrap and re-work due to human error. The wet lay-up process results in parts with inconsistent fibre orientations with strands separating from the fibre preform mat due to excess handling. The process also results in an uneven surface on the inner skin resulting in poor bonding of the blade shells in final assembly [32].

Significant health and safety risks are associated with polyester wet lay-up techniques. Harmful Volatile Organic Compounds (VOCs), primarily styrene, are released during the curing process [21]. New and increasingly tightening legislation exists limiting the styrene content in air. The clean air requirement for workshops has offset the cost of investing in improved forming methods against the cost of newly required ventilation equipment [32]. Despite its drawbacks the process remains attractive for its simplicity and low cost (Table 1-3).

Table 1-3 A summary of the wet lay-up forming process

Advantages		Disadvantages	
		Poor repeatability	
Low investment cost		Labour intensive	
Simple to learn		Quality is worker skill dependant	
Wide choice of materials and resins	Costly ventilation equipment required to meet health and safety legislation	Low fibre volume fractions (30 – 40%)	
		Long cure times (48hr cycle time)	
		Uneven bonding surface	

Vacuum infusion

Vacuum infusion moulding has recently increased in popularity in turbine blade production due to desires to improve working conditions, increase structural integrity and repeatability. A number of acronyms, patented technologies and processes have evolved relating to differences in the technical approach to resin infusion. Vacuum assisted resin transfer moulding (VARTM) has been used to describe the infusion process without reference to tooling. Resin infusion under flexible tooling (RIFT) is used to define a resin infusion process which involves a flexible surface such as a bagging film [34]. All such processes may be referred to as vacuum infusion (VI). VI turbine production involves arranging the dry fibres in a female mould tool (Fig 1-7) which may include channels or porous layers to facilitate resin flow. The mould tool and dry fibres are then covered with a sealed bag. The air between the bag and mould tool is removed creating a vacuum which draws the resin into the mould (Fig 1-8). The resultant component will have a single quality surface matching the mould tool and an inner surface suitable for bonding internal structural components.



Fig 1-7 Hand lay-up of dry fibres in a turbine blade mould [LM Glassfibre]

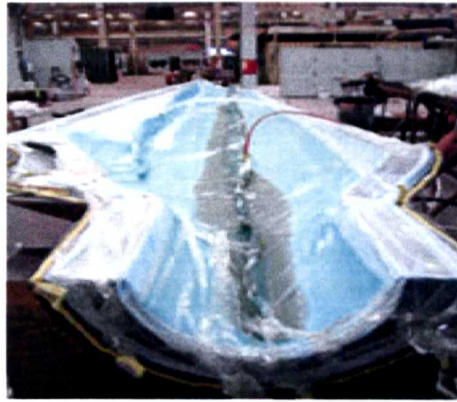


Fig 1-8 Resin impregnation during VI of a turbine blade shell [Tygavac]

Individual processes are distinguished by the methods used to ensure resin flows evenly to all areas without voids. The dominant impregnation mechanism is through thickness flow, thus the flow path through the relatively low permeability reinforcement is very short, and a high vacuum is relied upon to ensure that voids are reduced [30]. As the resin no longer needs to remain fluid throughout the lay-up process faster curing times can be achieved. Therefore, an overall cycle time of 24 hours is obtainable for a 40m blade [33]. The VI process has a reasonable level of flexibility with a novel approach being adopted by one manufacturer using a closed mould bladder process (Fig 1-9).

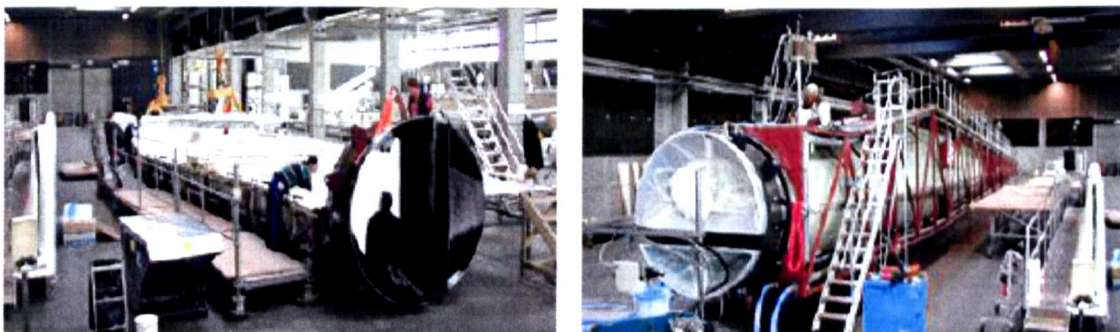


Fig 1-9 Hand lay-up of the laminate material in the open mould which is then closed ready for inflation of the bladder type vacuum bag [Siemens Wind]

In comparison to wet lay-up, VI processing has improved; cycle times, repeatability, working conditions, volume fractions and component quality. However, several difficulties remain (Table 1-4). In particular ensuring all fibres are fully wet-out by the resin [11]. Other negative attributes such as a high labour content and component inconsistencies result from the hand assembly of dry fibres which can also move during resin infusion.

Table 1-4 Characteristics of the Vacuum resin infusion process [34]

Advantages	Disadvantages
Compatible with epoxy and polyester resin systems.	Complex process with additional skills required compared to HLU.
Compatible with most conventional fabric reinforcements.	Sensitive to leaks.
Lower cost materials compared to prepreg.	Low viscosity requirements of resin may compromise mechanical and thermal properties.
Fewer health and safety issues.	Uneven flow may result in dry fabric areas and expensive scrap parts.
Relatively low tooling costs.	Poor repeatability due to hand positioning of fabrics which may move during resin flow.
Faster cure and cycle times (24hr).	High labour content.
Superior repeatability to hand lay-up (HLU).	
Superior achievable volume fraction to HLU.	
Microstructure is more uniform with reduced void content compared to HLU.	

The prepreg process

Prepreg hand lamination involves cutting plies into the required shape, removing the backing paper and placing them into a mould. Pressure is manually applied to ensure the ply conforms to the mould surface. Tack levels are formulated such that the material will remain in place throughout the lamination process but can be repositioned if necessary.

Prepreg is typically manufactured by laying fibres and resin between sheets of silicone paper or plastic film. The layers are then pressed or rolled, to ensure consolidation and wetting of the fibres, then partially cured to produce a flexible pre-impregnated aggregate [22]. The additional processing leads to an increased cost. Nevertheless, prepreg is still favoured for guaranteed resin matrix fibre compatibility, optimum volume fractions, reduced variability, ease of handling and improved placement accuracy [35]. Prepreg use is generally associated with high performance applications in the aerospace industry, which require high pressure and temperature cure in an autoclave [22]. An autoclave suitably sized for wind turbine rotor blades would incur excessive costs. Therefore, prepreps used by wind turbine manufacturers are cured under vacuum in a similar arrangement to vacuum resin infusion without gross resin flow. The prepreg material is laid up by hand, held in place due to its tacky consistency. Curing takes place at 80-120°C under vacuum. Limited harmful emissions are associated with prepreg, health concerns over occupational contact allergy dermatitis can be easily overcome [23].

Prepreg materials effectively begin to cure slowly at room temperature, limiting the shelf life. Therefore, freezer storage is required at additional cost. Prepreg material use

is somewhat restricted in blade production due to the associated additional costs (Table 1-5). However, prepreg offers the advantage of good fibre alignment during processing resulting in parts with lower fibre flaws and excellent predicted properties [32]. Again, this process suffers from a high labour content and inconsistencies associated with hand placement of fabrics.

Table 1-5 A summary of the prepreg forming process [11, 35]

Advantages	Disadvantages
Consistency in resin quality and material properties.	Increased materials cost compared to VI and hand lay-up.
Improved repeatability.	
Optimum fibre volume fractions.	May require freezer storage at increased cost.
Easier to cut and place accurately.	Hand assembly leading to high labour content and repeatability issues.
Minimal health and safety issues.	

Traditional filament winding

Filament Winding (FW) is primarily used in the fabrication of vessels and tubes. In this process the continuous strands of fibre are submerged in a resin bath and then spun around a cylindrical driven mandrel of the required shape [32]. FW use in the wind turbine industry is restricted to the production of a spar box section due to its inability to form the sharp trailing edges of aerofoils (Fig 1-10). FW box sections lack structural efficiency due to the inability to place longitudinal fibres [32]. This deficiency was overcome initially by simply increasing thicknesses consequently leading to excessive blade mass and material costs which become increasingly detrimental as blade length increases. Fully mechanised 38m rotor blade production was conducted using filament winding techniques in the 1980's. These glass polyester blades were said to be some of the heaviest ever produced [9]. This excessive mass together with the cost of materials and machinery lead to its withdrawal from use.

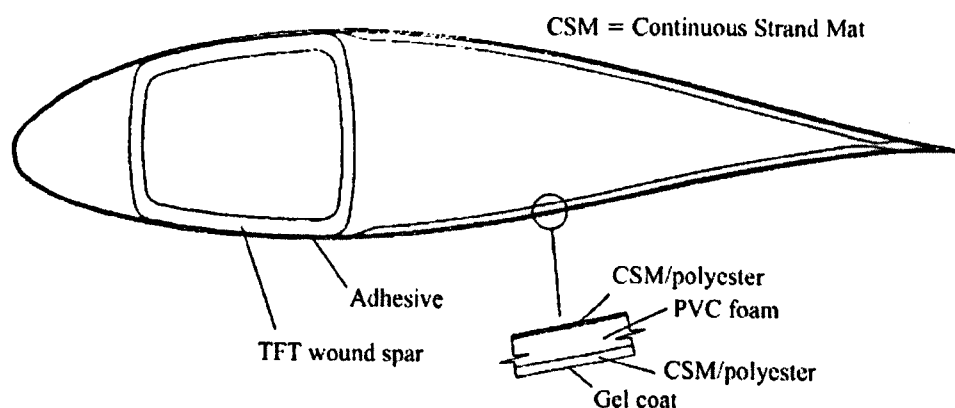


Fig 1-10 A typical blade with a filament wound box section spar [16]

1.4 Automated forming processes

With hand lay-up, considerable time is spent in the manual positioning of plies and accuracy is subject to the laminator's skill. Therefore, the process is labour intensive, lacks consistency and would benefit considerably from automation [36] (Table 1-6). Automated ply lamination (APL) seeks to resolve these issues by automated cutting, picking and placement of complete plies. Considerable technical difficulty is attributed to the prepreg tack level which must be low to allow backing paper removal but remain high enough to hold the lay-up together [37]. In general slow and complex development of automated lay-up has been attributed to the tacky and flexible nature of prepreg [36]. The APL method is unsuitable for the large curved surfaces of wind turbine blades and still requires significant manual intervention. Continuous lamination processes involve feeding prepreg from a roll and cutting and placing prepreg whilst traversing the mould surface in a layer by layer process. These processes are suitable, since the laminating head is able to follow the contours of the mould surface and remove backing paper in-situ. A suitable automated process would ideally meet the following criteria (Chapter 1.2):-

- Capable of producing components above 42m in length
- Capable of complex curved and twisted geometry
- Ability to lay unidirectional fibres along the length
- Capable of incorporating foam cores
- Ability to lay multiple fibre types in multiple directions
- Capable of achieving a high fibre volume fraction

A number of automated methods which have potential to produce turbine blade components are outlined (Table 1-7).

Table 1-6 The advantages of automation in turbine blade production

Advantage	Facilitator
<i>Reduced lay-up times</i>	Increased deposition rates through mechanisation allowing 24hr production
<i>Increased fibre volume fractions</i>	Improved alignment, compaction pressures
<i>Reduced labour content and cost</i>	Using a single machine operator
<i>Improved component repeatability</i>	Increased accuracy of material placement
<i>Reduced scrap rates</i>	Elimination of human error
<i>Reduced cycle times</i>	Integrated tool paths in design analysis
	Future possibility of in-situ curing

Table 1-7 Automated methods with potential for turbine blade production

Method	Typical product	Typical size (S,M,L)	Geometric flexibility
Automated Tape Laying (ATL)	Aerospace structural components	ALL	Curved surfaces / hollow sections
Automated Fibre Placement (AFP)		S,M	Smooth hollow sections only
Automated tape or tow winding	Pressure vessel	ALL	Smooth hollow sections only
Filament winding		ALL	Smooth hollow sections only

Automated Tape Laying (ATL)

The ATL process is used for the production of high performance parts in the aerospace industry [27]. The process involves robotic placement of relatively narrow (150-300mm [38]) strips of prepreg. Typically, the prepreg is heated and its backing tape is removed, it is then positioned and cut accordingly. These operations occur continuously within a material delivery head. The delivery head is robotically manoeuvred along an overhead gantry with multiple axis of travel (Fig 1-11). The working envelope is relatively large (20x4x3m [38]) and can be extended in the X axis to accommodate longer components such as turbine blades. The option of multiple heads working on a single gantry is also available. The material head will perform multiple passes in alternating directions to build up laminate layers of the required thickness and direction.

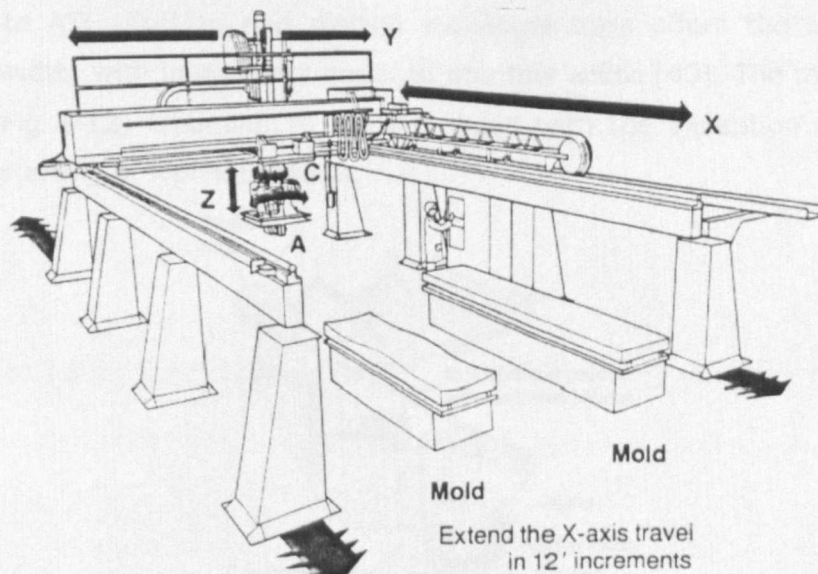


Fig 1-11 A typical ATL gantry system and working envelope [38]

The typical ATL configuration is most suitable for producing flat or gently curved surfaces and has been utilised by the aerospace industry to produce wing skin sections [27]. Sections of 9m length, 2m width and up to 22mm thickness have been produced

by Airbus [38]. Typical deposition rates are relatively high for aerospace production, between 16-26 kg/hour [38, 39]. ATL has the ability to form the gently curved profile of the blade and deposit unidirectional fibres along the blade length with increased accuracy. However, modifications would be required to increase deposition rates and reduce raw material costs in order to ensure success in turbine blade production. A comparison is made between the current ATL process and the hand VI methods for blade production (Table 1-8).

Table 1-8 ATL in comparison to VI hand lay-up methods

Advantages	Disadvantages
Reduced labour content.	High initial investment costs.
Improved repeatability.	Increased material costs.
Improved accuracy of fibre placement.	Additional programming costs.
Reduced scrap rate.	Low relative deposition rates in comparison to VI hand lay-up.
High fibre volume fractions.	

Automated Fibre Placement (AFP)

AFP involves the robotic placement of individual fibre tows in a similar machine configuration to ATL. Cutting and placing individual tows offers the advantage of a variable tape width, with increments equal to one tow width [40]. The material delivery head layout (Fig 1-12) is similar to the ATL head with the exception of independent cutting and restarting of individual tows.

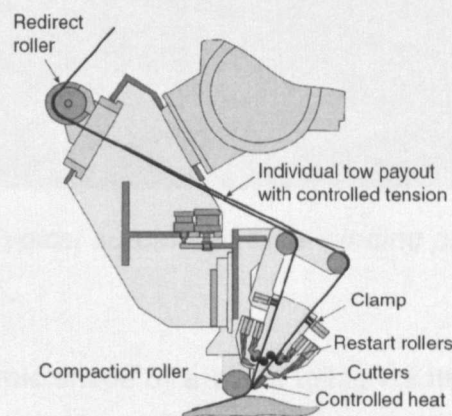


Fig 1-12 Typical AFP material delivery head configuration [40]

The robotic configuration is generally similar to ATL and can be tailored to suit manufacturer's requirements. Therefore, AFP has similar characteristics to ATL (Table 1-8) with additional flexibility in the ability to vary lay-up width which comes with

increased cost. The additional flexibility of AFP allows the production of more complex parts with increased machine and programming complexity which results in a reduced deposition rate for larger components.

Automated tape winding (ATW)

ATW is essentially ATL with a mandrel mould configuration and is often not distinguished as a separate process. ATW allows lay-up over a numerically controlled rotating mandrel to form closed hollow sections (Fig 1-13). Prepreg tape is laid using a material delivery head similar to that of ATL with the exception that material may be mounted away from the head accommodating larger rolls. The rotating mandrel allows continuous lay-up with fewer cuts resulting in improved deposition rates. Once the mandrel has been layered sufficiently thick, it is then cured in a secondary autoclave or vac bag process. The ATW process exhibits similar characteristics to ATL configured to produce tubular parts rather than flat panels. However, the ATW process performs faster deposition rates than ATL due to the reduced number of cutting operations with the exception of longitudinal directions. For longitudinal fibre direction cutting is still required resulting in deposition rates similar to that of ATL. Therefore, ATW offers no advantage over ATL for producing open curved surfaces or closed sections with a significant amount of longitudinal fibre placement, as found in blade components.



Fig 1-13 Typical automated tape winding process [41]

Modern filament winding

Production of the aerodynamic shape of a blade using traditional filament winding (FW) was eventually considered inefficient and problematic (Chapter 1.3). However, FW remains suitable for the production of a box section structural spar provided fibres can now be laid in an almost longitudinal direction. Recent advances have been made using the FW process which increase its potential [42]:-

- Increased precision resin baths for improved 'wet out' of fibres.

- A pin ring system to improve low winding angles (near longitudinal fibre directions).
- Online monitoring of fibre resin volume fractions.

Recent innovations allow the continuous filament winding (CFW) of thermoplastic glass reinforced tubing with a higher allowable strain, impact resistance and improved robustness [42]. Innovations have also allowed the inclusion of optical fibres for data transmission, strain and damage monitoring. CFW equipment (Fig 1-14) is readily available for the production of up to 4m diameter tube. The CFW process utilises a thermoset matrix with UV cure, reporting production rates of up to 50 meters per hour [43, 44]. Despite these recent advances in FW the problem of longitudinal fibre placement and inability to form sharp edges continues to limit this method to closed hollow gently rounded structures under radial and hoop stress loads.



Fig 1-14 Modern fibre winding equipment capable of producing 48m/hr of $\text{\O}600\text{mm}$ GFRP tube

Summary

Winding processes appear limited to the production of closed hollow sections. Development of winding processes for blade production should only be pursued if the manufacturer is content to be constrained to a structural box section spar design. Additionally, successful rapid production of the spar component requires an equally rapid method of shell production to be developed. AFP is considered a flexible process capable of producing all WTRB components. The process is very similar to ATL with the ability to lay individual tows resulting in a material delivery head with extra flexibility. However, such flexibility incurs additional cost and reduced deposition rates.

ATL is considered to have the most potential in satisfying the demands of automated turbine production; an existing technology with known material attributes offering the

flexibility to produce all blade components. ATL has proven capability in producing similar geometry aerospace components. However, the typical wind turbine component size and material thickness has yet to be achieved. Increased deposition rates and a reduction in material costs are required for the successful implementation of ATL in turbine blade production. Successful development has predicted cost savings of 8% per annum [45] in addition to; reduced labour content, improved repeatability, improved accuracy of fibre placement, reduced scrap rate and higher fibre volume fraction in laminates.

1.5 Aims and objectives

The primary aim of this project was to develop ATL for wind turbine blade production, requiring:-

- *A reduction in material cost*, switching from high cost toughened aerospace resins with carbon fibres to low cost simple epoxy BPA resins with E-glass fibres.
- *Wind turbine compatible materials*, Using low exotherm resins to allow the curing of thick laminates.
- *An increase in deposition rates*, Facilitated by increasing the FAW thickness of prepregs.
- *A reduction in tooling cost*, To produce low cost fibreglass tooling using typical wind turbine industry methods suitable for ATL.

Aims and objectives evolved with the project in reaction to problems which occurred in satisfying the primary aim. During the trials of these new materials tack and stiffness properties of the ATL prepreg were found to significantly affect lay-up performance. However, a reliable method of quantifying tack limited the understanding of the process and the ability to develop new materials. Therefore, a number of secondary aims emerged:-

- Develop a new method to quantify prepreg tack and stiffness
- Characterise existing prepreg
- Study the effects of variables

Throughout the experimental study results were occasionally confusing and contradictory to current composites industrial experience. However, greater understanding of tack was found within the Pressure Sensitive Adhesives (PSA) field where results were often related to polymer melt behaviour and rheology. These additional aims were then set to establish the applicability of PSA and polymer melt theories to prepreg tack and stiffness:-

- Relate results to PSA research
- Relate results to resin rheology
- Establish the applicability of the time-temperature-superposition principle
- Relate results to molecular theory

1.6 Theme of this work

The work presented here has formed part of a TSB funded research project entitled AIRPOWER. Several publications have resulted from this thesis (Appendix A). The project was concerned with the development of rapid automated techniques for the production of large scale off shore turbine blades with the integration of optical fibre sensors. The aim of this thesis was the development of ATL for wind turbine blade production. New low cost low exotherm ATL materials were developed but proved problematic in production and feasibility trials (Chapter 4.1). A review of the ATL process indicated that the success and performance of ATL is particularly sensitive to the tack and stiffness properties of prepreg materials (Chapter 5.6). However, the lack of a reliable method for quantifying tack limits the understanding of the process and ability to develop new materials. Therefore, a new test was developed which quantifies tack and stiffness during a simulated ATL application process (Chapter 3.3). The new tack and stiffness test was then used to investigate the effect of process and material variables (Chapter 3.5).

Greater understanding and explanation could be found in the comparison of results to those found in Pressure Sensitive Adhesives (PSA) research where results are related to polymer melt theory and rheology. The time temperature superposition principle, found applicable to PSAs, was also discovered to be applicable to the tack and stiffness of prepreps (Chapter 4.5). The theoretical implications of this relationship and rationalisation of results are then discussed (Chapter 5.4.3). Tack and stiffness results were then related to material tack performance during ATL lay-up in experimental trials. The application of the new characterisation method and newly discovered time temperature relationship for prepreg specification and ATL performance are discussed (Chapter 5). Major conclusions are then drawn on all aspects of this work suggesting standardisation of prepreg tack characterisation and significant improvements to automated prepreg processing may now be possible (Chapter 6 & 7).

2 Literature review

Review of literature and commercial experience regarding prepreg and the ATL process indicates that tack to the mould surface is considered to be a major component of successful lay-up. The ATL feasibility study confirms that both tack and stiffness of the prepreg play a vital role. Tack is also considered of equal importance in AFP and to a lesser extent in prepreg hand lay-up and fibre winding processes. Therefore, existing commercial and scientific background literature is reviewed for both prepreg tack and stiffness. The results and methods applied in the study of prepreg tack appear to have stemmed from the study of pressure sensitive adhesives (PSA) where tack has been studied more intensely. In the study of PSAs tack has been related to the rheological and molecular properties of the resin. An important relationship between the effects of time and temperature on PSA tack has been observed during cohesive failure which allows tack to be rationalised based on molecular theory. A background to molecular theory is required to discuss results from tack testing which are difficult to explain on the macro scale.

2.1 Prepreg materials

An overview of prepreg component materials and production processes utilising prepreg are available in the introduction (Chapter 1.2.3 and 1.3). The details of prepreg resin, impregnation methods and specification are discussed here.

2.1.1 Production

Prepreg is produced by impregnating reinforcement fibres with resin to form a pre-impregnated, hence 'prepreg', fabric which can be cut and positioned easily. Four types of prepreg production methods are typically utilised [46]; solution dip, solution spray, direct hot melt coat and film calendaring. Filming processes are said to be faster and cheaper, with solution methods utilised only when certain resin formulations prevent filming [46]. In each of the methods the resin is partially reacted, termed beta or b-stage, to give the correct degree of tack [46]. The hot melt film impregnation method was utilised for the production of prepregs used in this study. Hot melt film transfer prepegging consists of four basic operations [47]:-

1. A resin film of uniform thickness is produced on backing paper. Precise control of film thickness is essential to control final prepreg resin content.
2. The resin matrix impregnates the fibres in the impregnation zone (Fig 2-1). Pressure, temperature and line speed must be controlled to maintain the desired resin distribution.

3. The prepreg temperature is quickly reduced using a chill plate. Resin viscosity is reduced preserving fibre positions and resin distribution.
4. The prepreg may be slit to the required roll width and collected onto a take up reel and placed in cold storage.

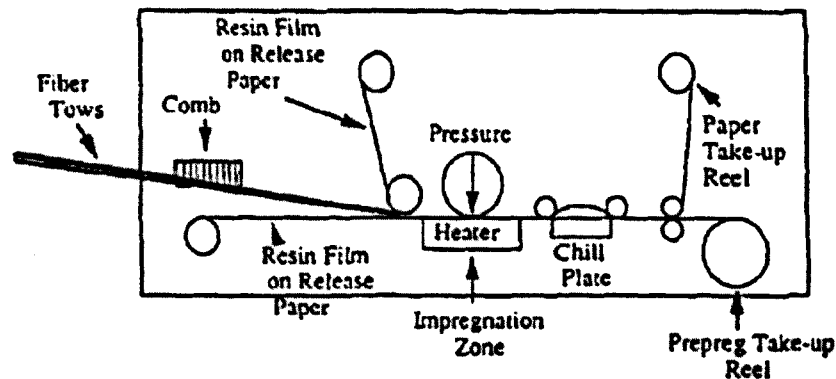


Fig 2-1 The hot melt film transfer prepregging process [47]

Stage two is considered the most important for maintaining impregnation quality [47]. Due to the nature thin films and fibre porosity impregnation may be subject to capillary and surface tension effects. Pressure is said to provide the driving force, temperature controls the resin viscosity and line speed controls the impregnation time where the temperature-pressure-velocity superposition principle between dimensionless variables is considered valid [47].

Resin content

High fibre content is beneficial in obtaining the highest mechanical properties. However, the resin matrix is required to transfer load between fibres. Therefore, when fibre loadings exceed 70% (by volume) a reduction in mechanical properties is generally observed, attributed to fibre to fibre contact [46]. A standard loading of 60-65% is said to attain the best compromise. It has been standard practice to produce prepreps with 50:50 ratio and induce a 10% bleed out during the vacuum bagging process, also beneficial in handling properties and washing out trapped air. However, this practice has been criticised for excessive waste in resin and ancillary bleed soak materials [46].

2.1.2 Specification and supply

Manufacturers tend to specify prepreg materials using a series of designations corresponding to material components, fibre areal weight (FAW) and architecture (Fig 2-2). Hand lay-up materials are typically supplied in rolls of one to 1.6m in width covered on both sides with embossed polythene film. ATL materials are generally supplied in rolls of 75, 150, 300 mm width, dependant on machine requirements, with a

wax coated release paper on the reverse (Fig 2-3). Tack values are specified as high, medium or low on datasheets relating to the tack level of the infused resin. Tack levels are measured by a combination of probe and subjective methods. Uncured prepreg stiffness is not specified.

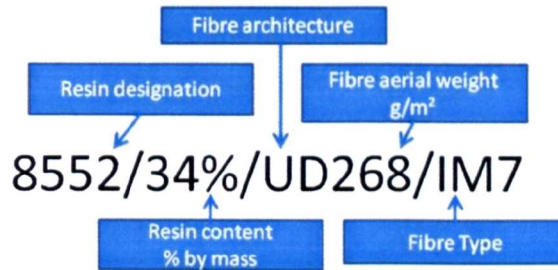


Fig 2-2 Typical manufacturer's prepreg designation and specification

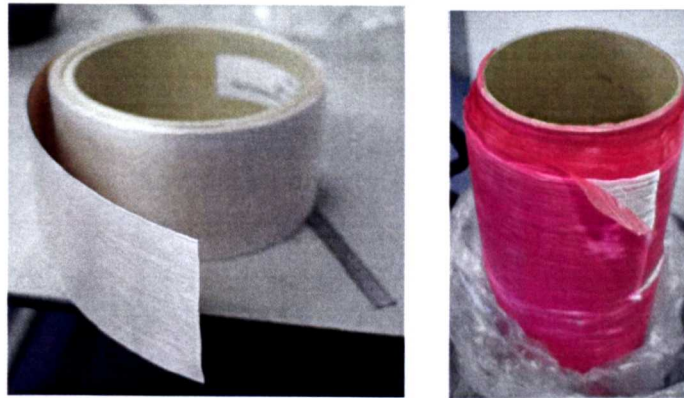


Fig 2-3 ATL prepreg tape roll (left) in comparison to hand lay-up prepreg

ATL aerospace prepreg

Existing aerospace ATL materials typically utilise a high cost high performance thermoset resin system (Table 2-1). A typical aerospace resin is described by manufacturers as amine cured, toughened epoxy recommended for structural applications requiring high strength, stiffness and damage tolerance. Resin content is kept low (typically 32% by wt., 40% by vol.) to ensure the overall mechanical performance is maintained.

High cost high strength carbon fibres (e.g. IM7/AS4) are typically utilised to give the highest strength to weight ratio. FAW rarely exceeds 200 g/m² resulting in a ply thickness of less than 0.2mm, suitable for the thin laminates required in aerospace panels. Only unidirectional (UD) fibres are utilised since the ATL is capable of placing fibre angles accurately to recreate multidirectional fabrics.

Table 2-1 A comparison of aerospace 8552 and wind energy prepreg resin

Designation	Description	Tensile properties	
		Strength	Modulus
8552	High performance amine cured toughened epoxy resin system	120 MPa	4.67 GPa
M19.1/M9.1F (High tack) M19.6/M9.6F (Medium tack) M19.6LT/M9.6FLT (Low tack)	Low exotherm, versatile cure temperatures (80-160°C) and pressures (0.5-5 Bar) suitable for vacuum bagging of thick components.	85 MPa	3.2 GPa

Hand lay-up wind energy prepreg

Existing wind energy prepregs typically consist of cost effective general epoxy resins suitable for a low pressure moulding process. In comparison to aerospace resin systems they are inferior in strength and modulus (Table 2-1). However, they are low cost and have a low exotherm ideally suited to the production of thick laminates using vacuum bag techniques. A range of low cost fibres and architectures are available to suit the various wind turbine components (Table 2-2). The inferior performance of wind energy grade prepregs (Table 2-3) is tolerated in return for significantly lower material cost, high deposition rates, low exotherm and the suitability for low pressure forming techniques.

Table 2-2 Wind energy prepreg fibre architecture and usage

Designation	Description	Component Usage
BB600/G	600 g/m ² Biaxial E glass (300 g/m ² at + and -45°)	Aerodynamic Shells, Shear webs
LBB1200/G	1200 g/m ² Triax E glass (566 g/m ² at 0°, 297 g/m ² at + and -45°)	All
UD1600/G	Unidirectional E glass 1600 g/m ² at 0°	Spar caps
UD600/CHS	Unidirectional high strength carbon fibre 600 g/m ² at 0°	High performance spar caps

Table 2-3 ATL aerospace and wind energy prepreg mechanical properties

Industry & process	Material	Tensile properties (Roll angle)	
		Strength (MPa)(°)	Modulus (GPa)(°)
Aerospace, ATL and autoclave	8552/34%/UD268/IM7	2570	160
	8552/34%/UD194/AS4	1900	135
Wind, Hand lay-up and vacuum bag	M9.6/45%/BB600/G	112(0), 514(45)	11(0), 21(45)
	M9.6/38%/LBB1200/G	512(0), 276(45)	23(0), 13(45)
	M9.1F/32%/UD1600/G	1312	51
	M9.6FLT/32%/UD600/CHS	1600	130

2.1.3 Resin chemistry and cure

Epoxy resins are polymers consisting of Bisphenol A (BPA) which takes its name from its constituents of two moles of phenol and a single mole of acetone [48]. BPA resin is produced by dehydrohalogenation reactions of Bisphenol A and chlorohydrins [49]. BPA-epichlorhydrin resins cannot be cross-linked by heat alone, even heating at 200°C has little effect. In order to convert the resins into cross-linked structures it is necessary to add a curing agent. For prepregs the curing agent is added at the time of prepregging. The curing reaction is then ongoing at the time of manufacture. The reaction tends to obey the kinetic rate equation [50] and therefore the reaction may be slowed by reducing temperature. A prepreg will then have its storage life specified as typically one month at ambient (23°C) and one year at freezer (-18°C) temperatures. The prepreg storage life is mostly limited by the loss of tack with age which may prevent hand lamination [51]. Therefore, shelf life is often referred to as tack life by manufacturers [52]. Although the handling properties may be reduced due to loss of tack, the finished laminate mechanical performance does not necessarily suffer until long after the tack life has expired [53].

Epoxy prepreg resin has a viscosity which allows forming at room temperature. Once positioned into the desired mould shape the prepreg is subjected to elevated temperatures, known as a cure cycle, where it solidifies or cures to form the required structure. Curing is the result of cross-linking which is the covalent bonding between polymer molecules. This curing process is irreversible and therefore the resin is known as a thermoset. The reaction results in a transition from a melt to a glass state where the process is exothermic [49]. Therefore, differential scanning calorimetry (DSC), which measures the heat flow of a sample, can be used to study cure kinetics and measure cure enthalpy [50]. An increase in cure enthalpy is associated with an increased reaction and therefore degree of cure [54].

2.2 Automated tape laying

The following section gives an in depth review of automated tape laying (ATL) and similar automated lamination methods, a general overview of the automation and the ATL process can be found in the introduction (Chapter 1.4). The ATL machine consists of a Gantry and tape dispensing head (Fig 2-4), where the gantry is responsible for the positioning of the tape head. The tape head is responsible for cutting and placement of the prepreg (Fig 2-5).

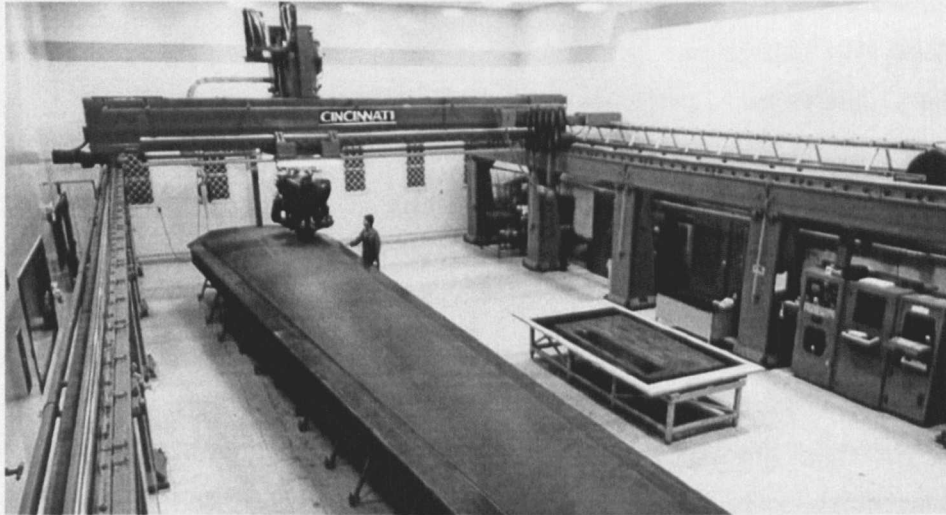


Fig 2-4 Typical gantry mounted ATL equipment [55].

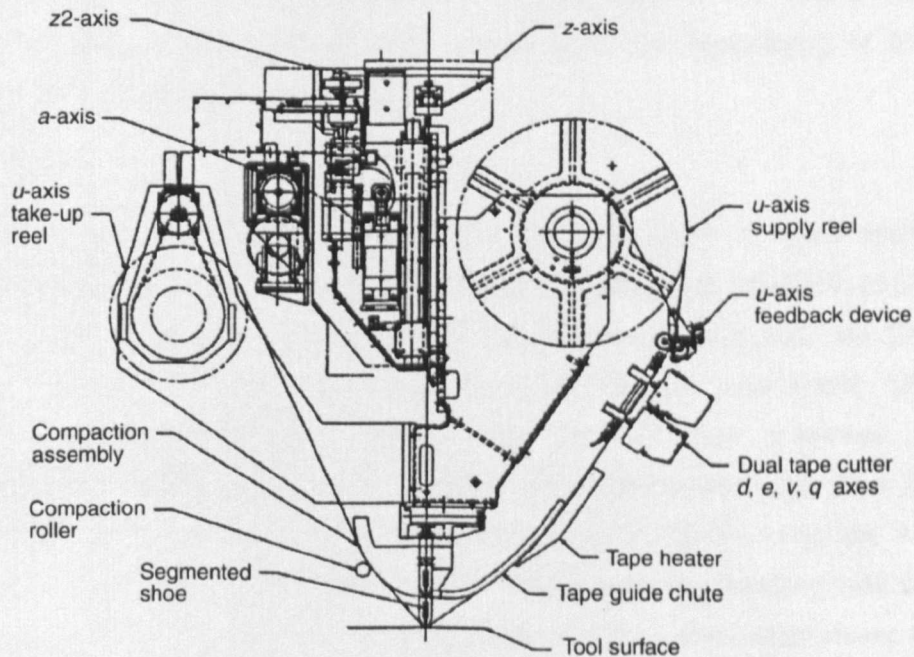


Fig 2-5 Typical ATL material dispensing head [56].

Cutting

Older machines such as the one used in this study utilise pneumatically operated fixed blades. Prepreg is held against a wear resistant plate by tape tension and cut from the prepreg side. The blades require accurate depth settings such that the prepreg is cut but the backing paper remains intact. Newer machines utilise ultrasonic cutting knives for improved performance [36, 57].

Lamination

In the lay-up process prepreg tape is guided off the spool and under a compaction tool head with the uncovered surface facing the mould. The compaction tool then holds the tape against the mould surface under a compaction force. The release paper is then removed onto a take up spool in a continuous process. Sufficient tack to the mould surface and subsequent plies is considered essential for successful lay-up [55, 58, 59]. It is also suggested that 'the tack levels should remain constant through the thickness of the ATL tape to ensure splitting does not occur' [55]. However, it is more sensible to define tape splitting as a result of poor impregnation leading to dry fibre bulk failure rather than 'internal tack failure'. Trapped air during lay-up is considered detrimental, related to increase void content within the finished laminate resulting in reduced mechanical strength [60]. Temperature, feed rate and compaction pressure are controlled throughout the process and are thought to influence the tack level and lamination quality. The ATL lamination process may be likened to other continuous placement methods like AFP, with subtle differences, such as the lack of backing paper [59] (Chapter 1.4). Similarities are also drawn with the laminating of thermoplastic tapes which occur at higher temperatures.

Temperature

Lay-up temperature may be increased locally at the point of tape application. For thermoset aerospace prepreg a typical fixed temperature of 26-43°C [55] is used to improve tack [61, 62]. It is recommended that temperature is reduced (low tack) for cutting operations and increased (high tack) for lay-up operations [58]. Special temperature considerations have been made for low tack prepregs where tape temperature was slightly increased (37-43°C) proportionately with feed rate. Lay-up temperatures on such occasions were found by experimentation using the ATL machine. Excessively low temperatures resulted in lack of tack and overheating was said to result in tape splitting [63]. The tack of AFP fibre tows are also controlled using temperature where tow guide chutes are chilled to prevent tack but heated using a gas torch at the point of lamination [59]. Again, there are no guidelines for appropriate temperature settings.

Feed rate and performance

Increased feed rate is generally desirable as it is directly proportional to deposition rate, where deposition rate may be used as an indicator of performance. Typical lay-up rates are between 16-26 kg/hour [39, 55]. However, there is said to be a critical minimum contact time which places a practical upper bound limit on the lay-up speed, greatly limiting the cost effectiveness of automated machines [64]. However, the author does not identify any changes in the critical contact time which may occur with changes in material temperature. Feed rate is adjusted throughout lay-up (Typical range 1-47,900 mm/min) to suit the difficulty of the particular operation and is usually reduced during cutting and at the start of lay-up. Dwelling or reducing feed rate over the ends or start of tape is recommended for improved tack performance [64].

Compaction force

A significant compaction force is applied using a roller or segmented shoe normal to the mould surface which is believed to increase tack and remove trapped air [61]. The compaction force is typically fixed throughout lay-up but may change between machines. A compaction force of 265-1300N is typical for a 150mm wide segmented shoe or roller [55]. Two lay-up behaviours have been identified as pressure and surface tension driven, where conformed or tacked area is dependent on either the applied contact pressure or the surface tension of the resin or rigid surface. In pressure driven lay-up a force velocity superposition principle is established, however, in the surface tension driven behaviour the applied force is considered unimportant [64]. In AFP the compaction roller is said to perform the function of bonding, tacking and de-bulking which prevents residual stresses, voids and warping by squeezing out trapped air pockets and increasing contact area [59].

Mould tooling

High cost, high tolerance ($\pm 0.035\text{mm}$ [65]), stiff alloy tooling is typically utilised which can withstand the compaction pressure of the ATL head. Mould contour angles may be limited to 15° from the horizontal which could easily be improved by demand since it is a mechanical configuration constraint imposed by the rotation limits of the delivery head. Surface energy of the mould is also considered applicable, since surface tension driven lay-up behaviour has been identified where it is suggested that lay-up on a low energy surface could be problematic [64]. The thermal properties of the tool material should also be considered if increased temperature lay-up is required. It is recommended that materials which act as a heat sink are best avoided. Such mould materials are blamed for rapid cooling of the relatively thin matrix preventing good

lamination. An epoxy mould tool was considered acceptable but a steel tool required thermal insulation using Mylar sheet [63].

Humidity & prepreg age

Humidity changes unintentionally based on local and seasonal climate conditions and has been found to effect tack and therefore lay-up performance in some cases [66]. The age of prepreg is also known to effect tack, where tack level appears to be the principal property determining the shelf life of prepreg [53]. Therefore, humidity and prepreg age appear to be two uncontrolled variables which are present in the ATL process and, along with prepreg batch variations, are occasionally thought responsible for failed or inconsistent lay-up.

2.3 Prepreg flexural rigidity

It has become necessary to quantify uncured prepreg stiffness to assist with the development of ATL for wind turbine blade production. Uncured flexural rigidity is most applicable as it reflects the bending of ATL tape as it is fed around the compaction shoe and forced to conform to the mould surface. A standard ASTM D1388 test (Fig 2-6) has been utilised previously in research [51]. No load is required since the uncured prepreg deforms significantly under its own weight. However, this does not allow a constant load comparison of materials with differing FAWs. The stiffness in bending or forming complex shapes may be affected by fibre weave and direction resulting in wrinkling [67]. Wrinkling is considered detrimental to mechanical performance and is not accepted by manufacturers using ATL, therefore it should be avoided and considered as a material failure if found during testing.

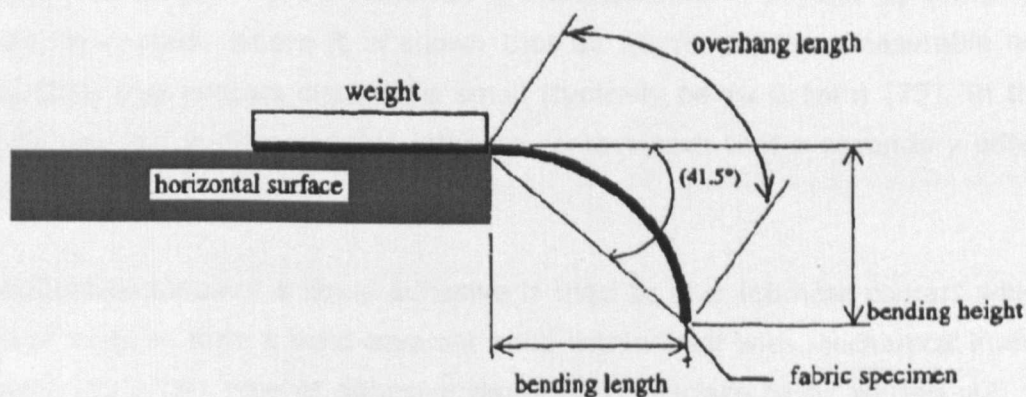


Fig 2-6 The ASTM D1388 uncured prepreg flexural rigidity test [51].

2.4 Prepreg tack

It has become necessary to quantify prepreg tack to assist with the development of ATL materials for wind turbine blade production. A complete review of existing resin, prepreg, and adhesive characterisation methods is undertaken in order to find a suitable method to quantify prepreg tack and stiffness which will allow a comparison of prepreg materials.

2.4.1 Definition

The term tack is used in the composites industry to describe instantaneous adhesion before the resin has set or cured with the study of tack said to be one of the open problems in adhesion science [68]. The definition of adhesion tends to be dependent on the discipline and scale of study. Adhesion may occur in all materials in any phase. However, only certain adhesive forces are relevant on the scale under investigation. On an atomic scale the smallest known particles of matter are believed to be held together by four forces, or fields, of nature. They are known as strong, weak, electromagnetic, and gravitational [69]. Fully understanding these fundamental forces is one of the greatest modern scientific challenges [70]. It is generally understood that the effects of the weak and strong forces are confined to the nucleus of the atom. Only the effects of gravity and electromagnetism are thought to extend into the realms of adhesion [71]. Since gravity is considered weak on a molecular scale it may be ignored. The electromagnetic forces, carried by the electron, are manifested in covalent bonds, coulomb force, ionic bonds and Van der Waals forces [71]. Covalent bonding is responsible for the chemical bonds which join elements to create molecules and polymers [72] studied intensively in the field of chemistry rather than adhesion. Therefore, the remaining lower energy non-covalent bonds are generally thought responsible for adhesion [71]. Adhesion is often studied in physics by bringing solids into intimate contact, where it is shown that all atoms display measurable adhesion provided their true contact distance is small (typically below 0.1nm) [73]. In this case extremely polished surfaces enable intimate contact such that a secondary adhesive is not required.

In the adhesives industry a liquid adhesive is used to give intimate contact which then hardens or cures to form a solid covalent bond within itself with mechanical interlocking at surfaces [73]. This type of adhesive requires the surface to be wetted out. Surface wetting is also a type of adhesion experienced by liquids. However, in this case the cohesive adhesion of like molecules and adhesive forces are comparable allowing the observation of the surface tension phenomenon.

The greatest appreciation of tack comes from the pressure sensitive adhesives (PSA) industry, where multiple definitions of tack are offered, generally defined as the resistance of an adhesive film to detachment of a substrate [74]. This resistance includes the effects of cohesive separation of the adhesive itself and adhesive separation of the resin and the substrate surface. PSA tack is regarded to be instantaneous adhesion occurring with short application times that generally result in adhesive rather than cohesive failure. For this reason tack is more likely to be associated with the probe test because of short application times [75]. Names such as quick stick, wet tack, finger tack, thumb tack, quick grab, quick adhesion and wettability have also been used in an attempt to better define tack as an instantaneous attractive force obtainable under light pressure application conditions [74].

The definition of prepreg tack originates from its handling characteristics, which are the prepregs ability to adhere to the mould and itself. However, tack should not be so overwhelming that a misplaced ply cannot be relocated easily [76]. Perceived tack may also be related to the ability of the prepreg to deform to the mould shape due to the presence of the fibres [77]. Historically, tack has been defined from a human perspective to describe adhesion which occurs quickly at room temperature, without special surface preparation, under finger application pressure. The term tack is now extended to include instantaneous adhesion which occurs within the ATL production environment.

2.4.2 Commercial characterisation

A search of international standards reveals the absence of a standardised method for determining prepreg tack [51]. However, several simple British standard methods exist relating to PSAs (Fig 2-7), with mechanised commercial versions also available at increased cost. These existing standardised methods bear little resemblance to the ATL process with the exception of the floating roller method. However, this method requires a separate application stage. The separate application stage signifies that only long contact times can be investigated, unreflective of the ATL process. A commercial prepreg tack testing machine is available from Accutac Inc. USA, which claims to be the industry standard for aeronautics utilised by Boeing [78]. However, there is an absence of published material detailing the operational method and supporting such claims. The excessive cost (>\$100k) of this machine also excludes it from use due to budget constraints.

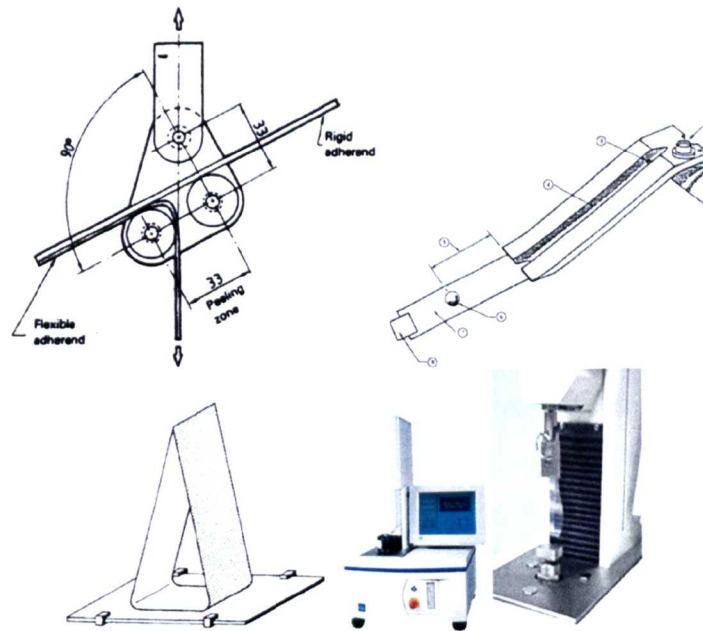


Fig 2-7 BS EN 1464:1994 Floating roller method for determining peel resistance (top left), BS EN 1721:1999 rolling ball tack (top right), the BS EN 1719:1999 Determination of loop tack (bottom left) and mechanised (bottom right) [79]

2.4.3 Experimental characterisation

Experimental prepreg tack research is conducted mostly to assist with prepreg development. Studies tend to use modified versions of British standard methods or established techniques from the PSA industry. The floating roller peel method (Fig 2-7) has had minimal use due to the lack of a defined application process. This method has been utilised to develop prepregs and demonstrate the effect of level of cure on tack [51].

The probe method taken from PSA testing has been favoured by most prepreg tack studies for its ability to achieve a controlled short application time and pressure. Such tests have concluded that the viscoelastic properties of the material are key to understanding tack along with the effects of the voids created by fibre surface patterns [80]. Tack has been modelled as a bulk viscoelastic property of the prepreg, with predictions of experimental results [77]. The effects of prepreg aging have been investigated using this method, showing the apparent decrease in energy of separation with increased age [54]. Prepreg tack has been found to be dominated by surface effects at low temperatures and viscoelastic mechanical properties at higher temperatures [81]. The effects of prepreg production variables such as impregnation temperature, pressure and line speed have been shown to affect resin content and uniformity of impregnation with a subsequent effect on prepreg tack [82]. The results

then allow prepreg manufacturers to adjust tack accordingly in a controllable scientific and experimentally verifiable manner correlated by selecting probe test settings verified by the study of human tack perception [76, 82]. Recent studies distinguish the effects of fibres on prepreg tack in comparison to resin films such as surface roughness caused by fibre patterns, irregular resin layer thickness and lack of cavitation [83].

2.5 Pressure sensitive adhesives

The Pressure Sensitive Adhesives (PSA) Industry is thought to be worth \$26 billion [84]; major competitors such as BASF and 3M offer products with a range of applications from packaging to surgical tapes [85]. Generally, a greater depth of research is carried out, since the product performance is dictated by tack properties. PSA tack is studied using adhesive resin films and flexible backing substrates. PSA probe, peel and shear tests are the most commonly used experimental methods for tack testing. Each method is used to determine a particular property relating to the function of the product. PSA tack is considered to be the ability to stick to a surface with light applied pressure and contact times, therefore, the probe test is favoured [75] (Chapter 2.5.1). Peel tests are used to quantify the ability of a tape to be peeled easily and cleanly or retained depending on the intended application [74, 75] (Chapter 2.5.2). Shear resistance is considered a purely cohesive property and is used to determine holding power under constant force, considered a creep property of the bulk resin [74] (Chapter 0).

2.5.1 Probe testing

The probe test has emerged as a popular analytical tool to evaluate the adhesive properties of PSAs. A thin resin layer is placed between two typically flat cylindrical parallel surfaces under quantified pressure and deflection (Fig 2-8). The tack and extension is then recorded during the separation of the two surfaces under a constant rate. Early versions of the test suffered from surface misalignment resulting in poor reproducibility. Alignment problems were improved in the mid 1980's. The ability to visualize the probe surface using a transparent contact and 45° mirror gave greater insight in the late 1990's.

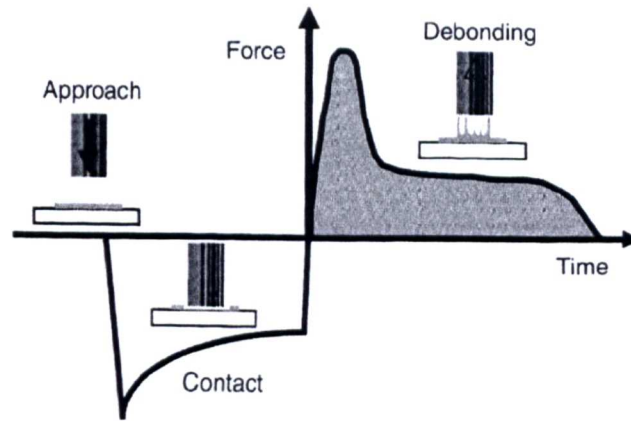


Fig 2-8 Probe test showing contact and debonding forces [75].

Three mechanisms of failure have been observed under tensile loading. When the interface between the resin and the surface is sufficiently weak, failure may occur by crack propagation from the edge. Failure may also occur by initiation and propagation of an internal crack. Cavitation and fibrillation of the resin is also considered a separate failure mode [86] (Fig 2-9). Results are presented as a stress strain curve. Stress is typically calculated using the probe surface area. The actual contact area of the resin is difficult to define using traditional methods. Complex optical methods have been used to measure the initial adhesive contact area [87]. As cavitation and fibrillation progresses the actual cross sectional area of the resin under strain remains unknown.

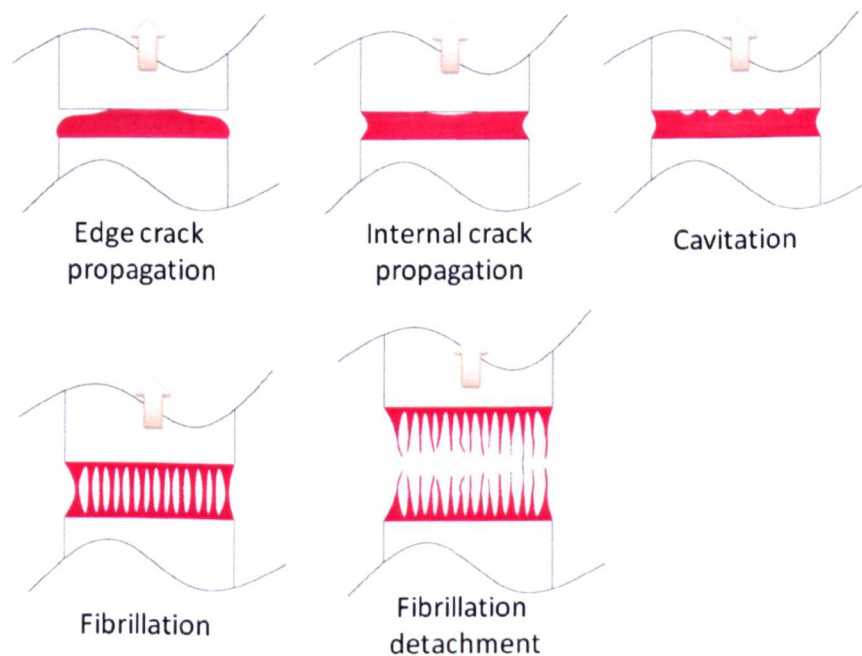


Fig 2-9 Adhesive failure modes observed in a flat probe tack test

The deformation of an adhesive layer under tensile stress has been divided into four main stages; homogeneous deformation, cavitation at the interface between the probe and adhesive, lateral expansion of the cavities and finally growth of a fibrillar structure [75]. An initial peak stress (σ_{\max}) has been observed at the onset of crack propagation or cavitation. In the case of cavitation a reasonable stress may be maintained throughout cavity growth and fibrillation until detachment of the fibrils occurs. The work of adhesion (W_{adh}) is expressed as the integral of tensile stress to failure (Fig 2-10). The shape of the curve also gives additional information regarding the type of failure. A single peak followed by a sharp drop in force after the peak indicates weak adhesion and interfacial crack propagation. As the level of adhesion increases the stress decrease after the peak is less pronounced and forms a distinct shoulder, which then reaches a plateau. This plateau in stress has been observed to form a second peak at higher elongation immediately preceding fibril detachment [75].

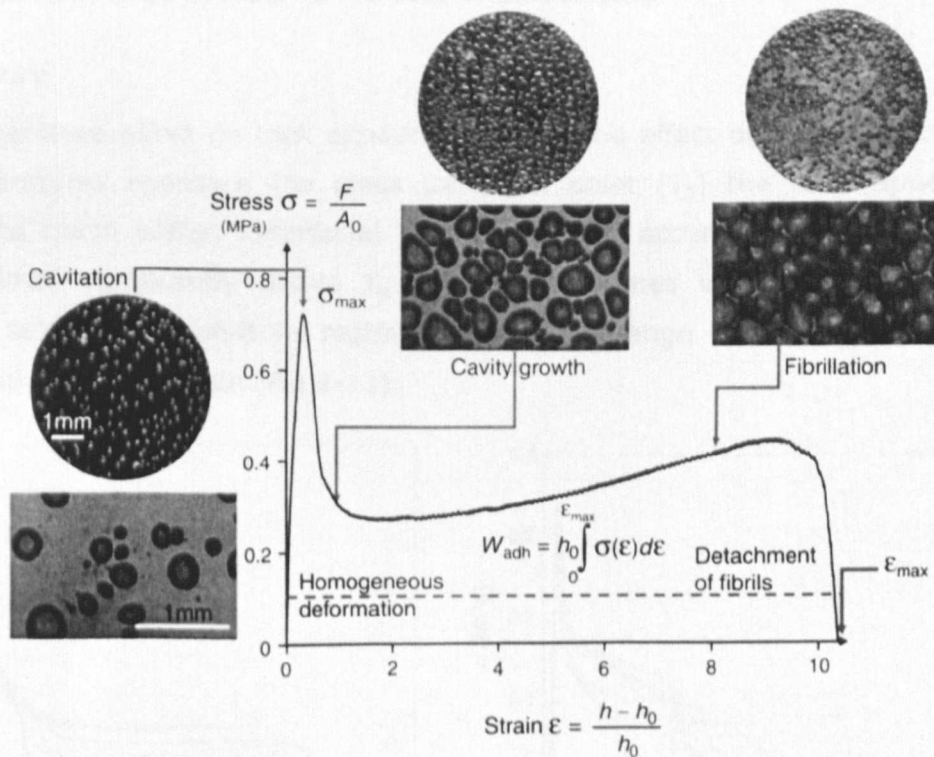


Fig 2-10 A typical probe test result for a sample exhibiting fibrillation [75]

A sharp peak appears to accompany failure at the surface and is therefore referred to as interfacial failure. Stress maintained at high extensions, sometimes resulting in a second peak, typically accompanies failure within the bulk of the resin, termed cohesive failure. Interfacial failure has been described as elastic due to the material behaviour during the test. Typically interfacial failure occurs fast with no residual resin remaining on the test surface. In contrast, cohesive failure occurs slowly with the formation of resin columns and fibrils. This failure mode is described as viscous, again due to the

material behaviour. Cohesive failure results in the deposition of resin on both test surfaces [68, 88]. The energy of adhesion has been found to be dependent on mode of failure, with significant adhesion energy only obtainable when bulk cavitation occurs. Adhesive energy of cohesive failure is dependent on the volume and deformation of the resin. Interfacial failure is limited to the total energy required for crack propagation [89].

Variable effects

The parameters of the probe test are usually specified to suit the product. Typical application pressure, contact time, feed rate and temperature reflect conditions of quick application under light pressure with moderate removal speeds at room temperature. Therefore, the majority of studies focus on changing resin properties and characterising performance under these conditions. However, a limited number of studies go on to adjust these variables in order to increase understanding.

Temperature

The temperature effect on tack appears linked to the effect on viscoelastic properties. As temperatures approach the glass transition point (T_g) the resin appears mostly elastic and much stiffer. Interfacial failure tends to occur at shorter extensions. At temperatures significantly above T_g the resin becomes viscous and shifts towards cohesive failure. This shift in regimes causes a change in results where stress is maintained at higher strain (Fig 2-11).

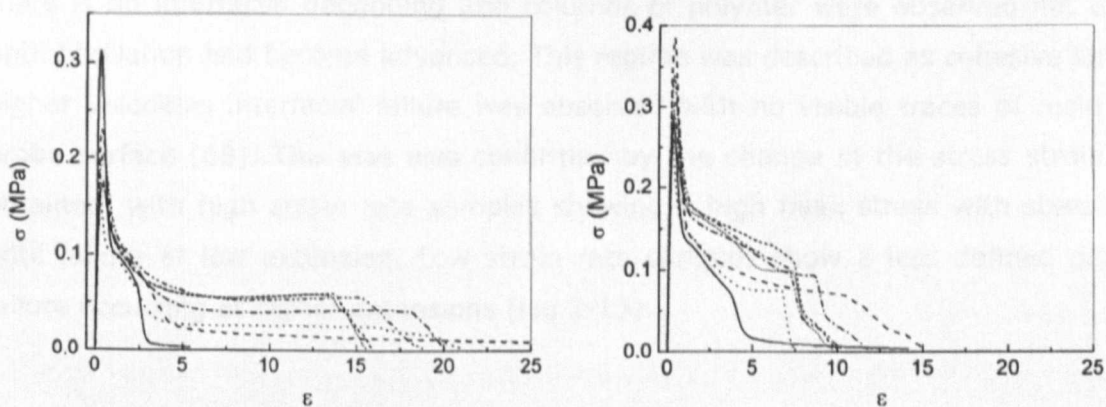


Fig 2-11 Probe stress (σ) strain (ϵ) curves for a number of polymer blends at 25°C (left) and -10°C (right) where $T_g \approx -50^\circ\text{C}$ [90]

The work of adhesion (W) has also been recorded over a temperature range for a number of polymer resins. In this case a peak was found to occur at roughly 40-60°C above T_g , for samples with a wide range of T_g (Fig 2-12). The rising tack was attributed to the increasing ability to deform and flow. A strong relationship was also observed

between W and creep compliance [91]. Temperatures approaching the T_g appear to show an interfacial brittle failure attributed to lack of adhesion and apparent incomplete contact. At temperatures higher than T_g the viscous behaviour of the resin allows good flow and complete contact. However, the resin itself now appears to fail in a cohesive flow process resulting in fibrillation.

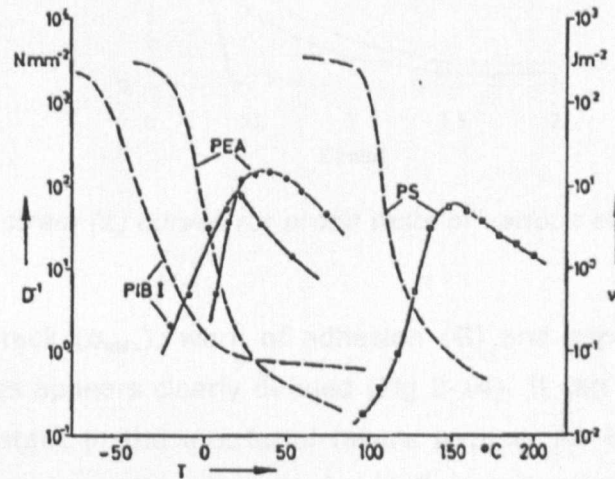


Fig 2-12 Work of adhesion (W) and reciprocal compliance (D^{-1})(dashed) for three polymers over a temperature (T) range [91]

Separation Rate

Under constant thickness, load and contact time, the strain rate at which the tensile part of the probe test is conducted has also been found to affect tack. At low rates, there is no interfacial debonding and columns of polymer were observed not to break until fibrillation had become advanced. This regime was described as cohesive failure. At higher velocities interfacial failure was observed with no visible traces of resin on the probe surface [68]. This was also confirmed by the change in the stress strain curves obtained, with high strain rate samples showing a high peak stress with steep decline until failure at low extension. Low strain rate samples show a less defined peak with failure occurring at higher extensions (Fig 2-13).

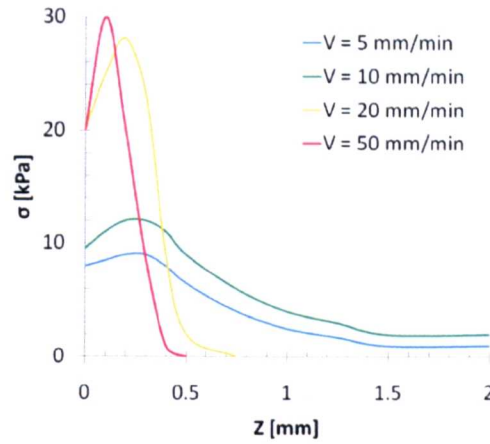


Fig 2-13 Stress (σ) strain (z) curves for probe tests of various extension rates (V)[68]

When plotting peak tack (σ_{\max}), work of adhesion (G) and separation rate transition between failure modes appears clearly defined (Fig 2-14). It can also be seen that σ_{\max} remains roughly constant in the interfacial failure regime. An intermediate regime is also observed near the transition, described as adhesion energy enhanced by viscous losses in the bulk. This third failure regime is only observable when considering work of adhesion (G) (Fig 2-15). Therefore, the peak stress gives a simple criterion to determine the failure type. However, it is said that the value of adhesion energy is more sensitive to the fracture mechanism and gives a better characterisation of the process of tack [68].

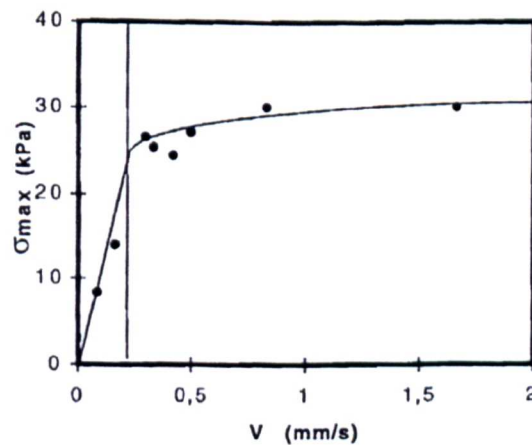


Fig 2-14 Maximum tack stress (σ_{\max}) as a function of separation rate (V) [68]

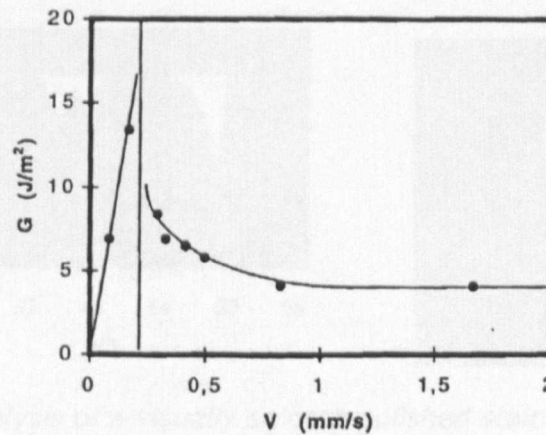


Fig 2-15 Work of adhesion (G) as a function of separation rate (V) [68]

Resin properties

Resin viscoelastic properties have been found to dictate the ability to deform and flow. A strong link between work of adhesion (W) and the glass transition temperatures T_g has been found with polymer resins of almost equal molecular weights [91] (Fig 2-12). The effect of molecular weight has also been found to significantly affect tack characteristics. The mode of failure has been seen to shift from cohesive failure to interfacial failure with increasing molecular weight, consistent with an increase in stiffness. The increase in stiffness is attributed to a higher molecular weight where stiffness may be reduced by the addition of a suitable low molecular weight component referred to as a tackifier [90].

Contact conditions

Contact time, rate, pressure and surface finish are all considered together as their effect appears linked to actual contact area. Poor adhesion at short contact times and light pressure are observed, believed to occur through a decrease in actual contact area. Other explanations include; lack of viscous flow, incomplete wetting and too high elastic modulus [92]. Probe surfaces without special preparation typically have a microscopic surface roughness resembling that of a hilly landscape [93] (Fig 2-16). Under constant application conditions a smoother surface has been found to increase peak tack (Fig 2-17). However, the increase is not simply explained as an increase in actual contact area but as a complex interaction between the probes surface and the nucleation of cavities [94]. The volume of air pockets trapped during the application stage and a change in stress distribution near the surface have also been considered to have an effect [95].

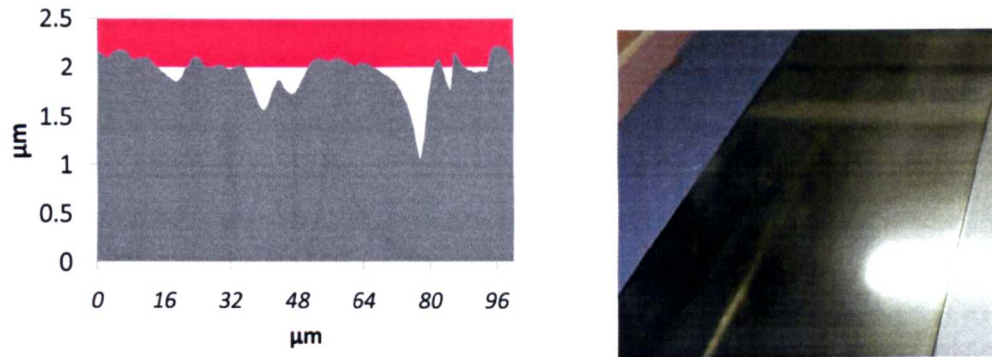


Fig 2-16 Surface analysis of a visually smooth polished stainless plate ($R_a=0.12\mu\text{m}$)

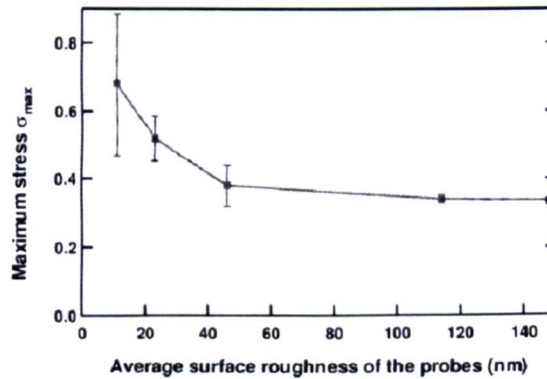


Fig 2-17 Experimental tack peak stress as a function of surface roughness [95]

Tack energy has been shown to increase as a function of contact time and contact pressure (Fig 2-18). Increased contact time may increase actual contact area through creep relaxation. In a similar way, increased pressure may result in increased actual area of contact through increased deformation of the resin. These results suggest that tack force or energy is directly proportional to true area of contact provided that; adhesion is contact limited, temperature and debonding rate are kept constant, and the variation in contact area does not affect the debonding mechanism [92].

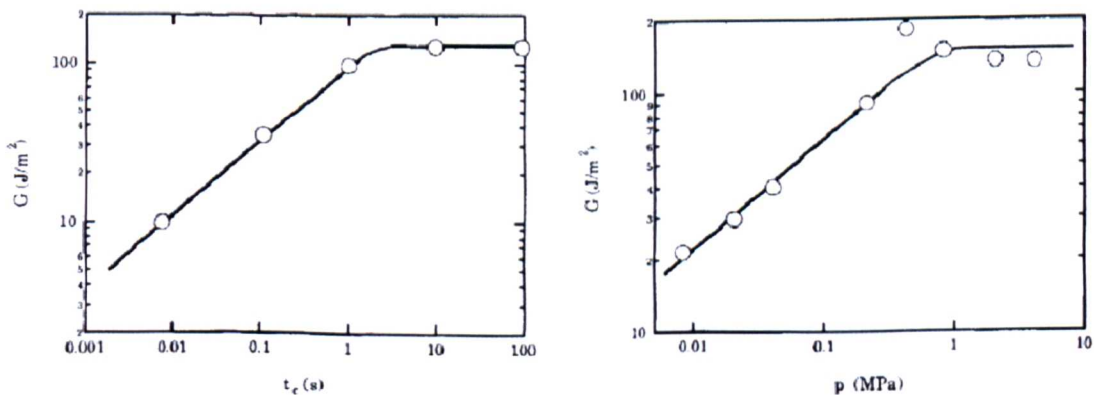


Fig 2-18 Tack energy (G) as a function of contact time (t) and pressure (p) [92]

Studies including contact area measurement have been carried out using a prism probe (Fig 2-19). Within this study, tack energy was found to be a function of wet area squared (Fig 2-20) said to be in agreement with theoretical calculations of the fracture energy between elastomers linked together by connectors. Therefore, suction and macromolecular chain disentanglement are said to be the phenomena responsible for tack properties [87]. The study concluded that results cannot be compared unless experimental conditions, such as temperature, tearing rate and actual wet contact area, are equal [87].

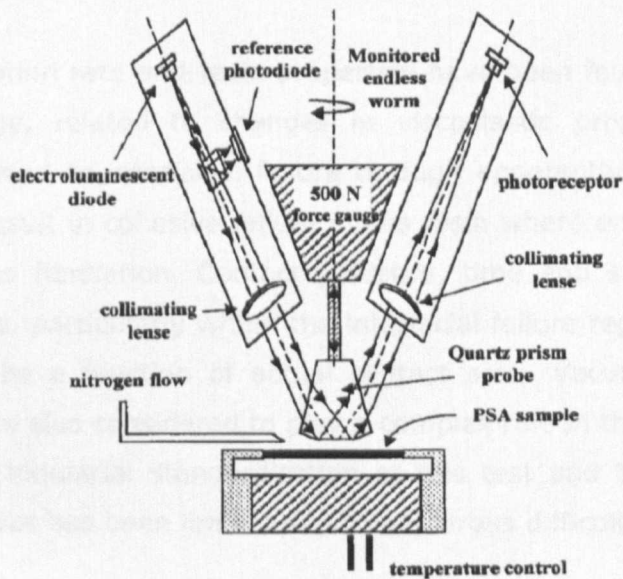


Fig 2-19 An optical probe used for measuring actual contact area [87]

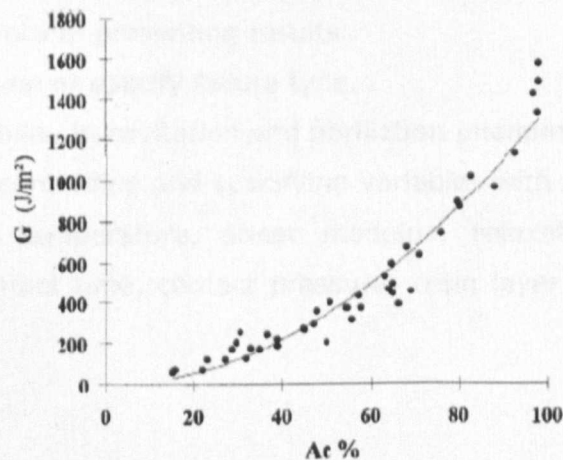


Fig 2-20 Tack energy as a function of actual contact area [87]

Summary

The probe test is the most popular method used in studying the tack mechanism. Two significant values are obtained during the test. Peak stress (σ_{\max}) is typically calculated using probe surface area. Accuracy is increased when actual contact area is considered.

However, this requires considerably more complex and expensive equipment and analysis techniques. The work of adhesion (W) or tack energy (G) is the integral of the tensile stress strain curve to failure. Two major failure types are observed. Interfacial failure occurs at the probe surface through crack propagation leaving no visual resin trace. Cohesive failure occurs within the resin typically resulting in cavitation and fibrillation with resin deposition on surfaces. The failure type may also be distinguished by the shape of the stress strain curve. A high peak stress with failure at low strain is typical of interfacial failure. A low peak with a secondary shoulder at high strain is typical of cohesive failure.

Temperature, separation rate and resin properties have been found to effect peak tack and adhesive energy, related to changes in viscoelastic properties. Highly elastic properties typically lead to interfacial failure through apparently poor surface contact. Viscous properties result in cohesive failure of the resin where energy is dissipated in a flow process such as fibrillation. Contact pressure, time and surface roughness also affect tack properties, particularly within the interfacial failure regime, where interfacial tack is believed to be a function of actual contact area. Vacuum effects along with surface roughness are also considered to play a complex role in the formation of cavities and fibrillation. The industrial standardisation of this test and the ability to compare results between studies has been limited due to numerous difficulties, including:-

- Surface alignment.
- Inability to observe surfaces under test.
- A lack of consistency in presenting results.
- Failure to determine or specify failure type.
- A lack of repeatability in cavitation and fibrillation phenomenon.
- Inconsistency in controlling and specifying variables with a known effect include; separation rate, temperature, shear modulus, relaxation properties, actual contact area, contact time, contact pressure, resin layer thickness, and surface finish

2.5.2 Peel testing

Peel tests quantify the force required to peel a PSA product such as tape or a label from a rigid substrate surface, known as peel resistance. Four types of peel tests have emerged with a variety of surfaces and peel angles (Fig 2-21) [75]. Peel methods can be classified into two groups depending on the test surface. The most popular type is peel from a rigid substrate surface which may be a plate (a) or drum (b). Peel from a

rigid substrate is then further defined by the angle which is generally constant throughout the test. Near 90° peel (a) is utilised by the floating roller method (Fig 2-7) and is typically considered the standard unless otherwise specified. For peel angles approaching 180° the method is occasionally defined as a strip back tack test (c). Peel between two flexible backing substrates (d) is referred to as cleavage or T-peel.

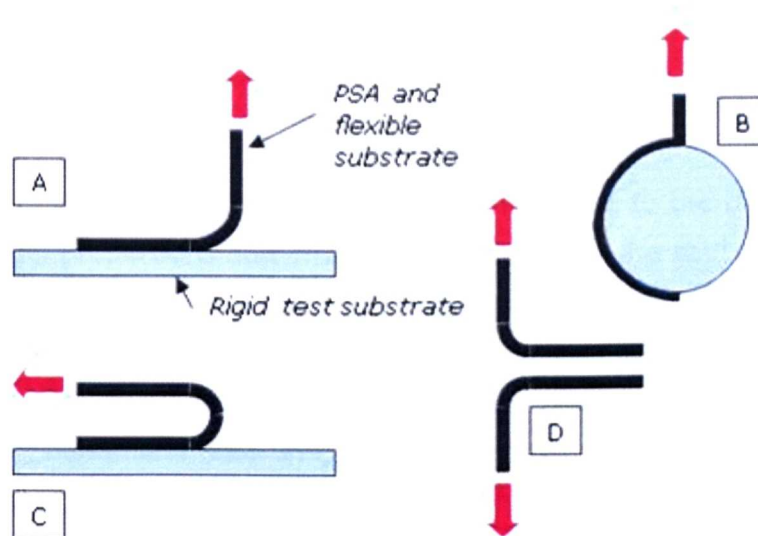


Fig 2-21 Common peel test methods, (A) 90° Standard (B) Drum (C) 180° Strip back (D) Cleavage or T-peel

The majority of testing is conducted at 90° or 180° with a 25mm wide specimen. The specimen is applied to a clean stainless steel plate without air bubbles by a constant weight roller [75] or by following the manufacturer's application guidelines [96]. After a specified bond time the sample is then clamped into the jaw with the plate constrained in a way which allows peel to proceed (Fig 2-22).

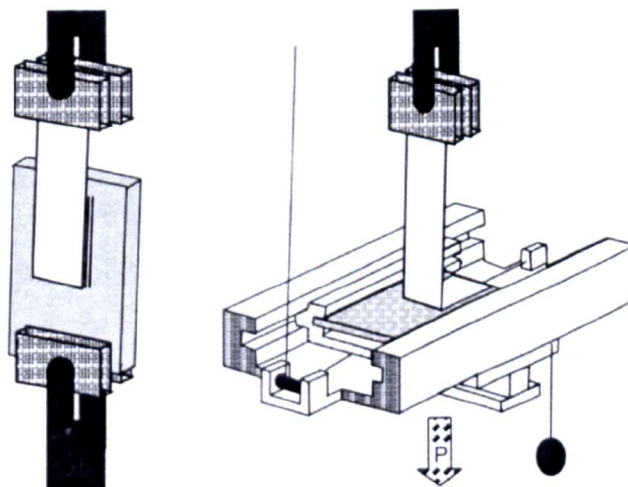


Fig 2-22 Typical 180° strip back (left) and 90° (right) Peel test apparatus [75]

A reasonably constant force is usually recorded over the length of peel. At least 115mm of peeling is recommended with the first 20-25mm disregarded [96]. An average force over the peel distance is taken as the value for peel force. Peel resistance is expressed as an average load per unit bond width, typically N/25mm (Eq 2-1) [75].

Eq 2-1 Peel resistance

$$P = \frac{F}{b}$$

P = Peel Resistance

F = Average peel force (N)

b = Tape width (mm)

Further definition of peel resistance is said to be difficult due to the many mechanisms operating in unequal proportions and direction. Contributions are said to include surface energy due to the creation of new surfaces, potential energy due to the movement of the applied force and elastic deformation [97]. 90° peel resistance is said to be a simple composition of bending and adhesive forces [98]. The adhesive forces appear to be a summation of the phenomena seen in probe testing such as cavitation and fibrillation occurring at differing positions along the peel front (Fig 2-23). Stress distributions show similarities to that of a probe test (Fig 2-10). Despite the complex relationship between bending and adhesion several predictions of peel strength have been made for particular substrate adhesive combinations with varying degrees of success [74, 98, 99].

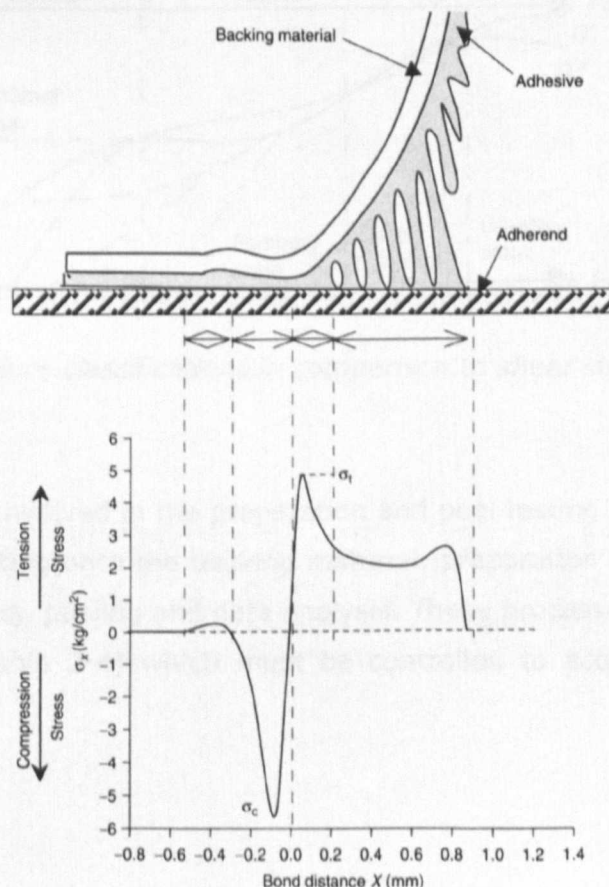


Fig 2-23 The peel front and recorded stress distribution [100]

Four types of failure have been observed in peel testing which include cohesive, interfacial, stick slip and glassy fracture and are believed to relate to rheological resin behaviour [101](Fig 2-24). Cohesive failure occurs within the resin when flow is possible. As the stiffness of the resin increases interfacial failure occurs. These failure conditions can be related to those seen in probe testing. The stick slip and glassy fracture conditions are unique to peel testing. The stick slip condition exists around the transition of failures where the constant peel rate is said to be insufficient to maintain peeling with fast interfacial mechanisms, reverting to a slow flow failure mechanism [75]. The inability of the resin to deform at high stiffness is said to result in glassy fracture separation of adhesive from the backing substrate.

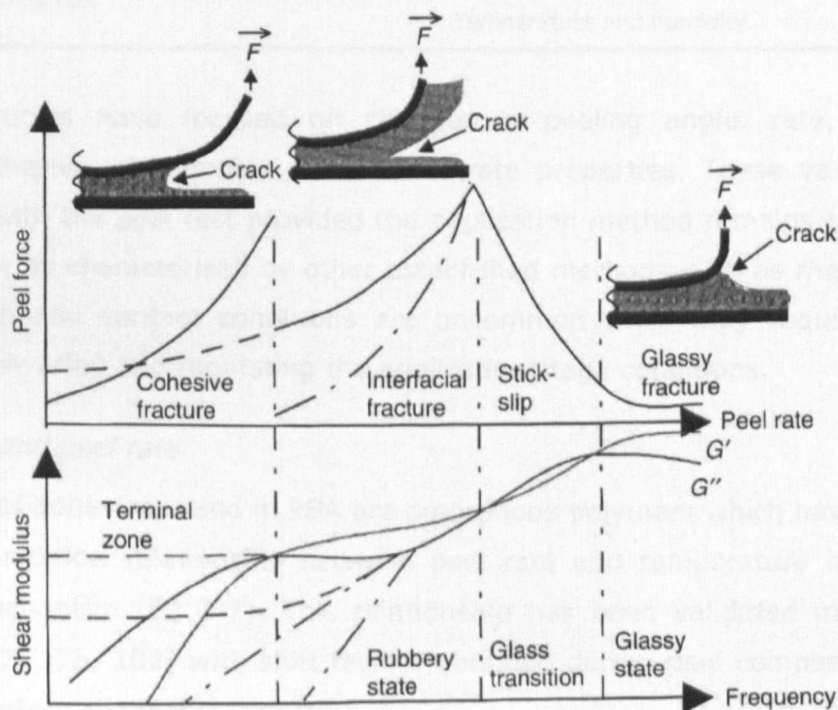


Fig 2-24 Peel Test failure classifications in comparison to shear storage modulus [75]

Effect of Variables

A number of steps are involved in the preparation and peel testing of PSA tapes such as preparing the PSA, coating onto the backing material, preparation of the strip, cleaning of the substrate, bonding, peeling and data analysis. These processes can be effected by several parameters (Table 2-4) which must be controlled to acquire meaningful and comparative data [75].

Table 2-4 Variables thought to affect peel resistance [75]

Process step	Parameters affecting peel resistance
Preparation of adhesive	Chemical composition, molecular cross-linking nature and density, miscibility of blend Viscoelastic properties
Coating onto carrier backing	Stiffness and thickness of carrier material
Preparation of sample	Adhesive layer thickness Surface properties of carrier Sample width, uniformity
Cleaning substrate	Surface energy & roughness Surface treatment & contamination
Bonding step	Application pressure & time
Peeling test	Peeling angle, geometry & rate Temperature and humidity

Generally, studies have focused on changes in peeling angle, rate, temperature, thickness, adhesive and flexible carrier substrate properties. These variables can be investigated with the peel test provided the application method remains constant. Resin properties can be characterised by other established methods such as rheology. Studies of preparation and contact conditions are uncommon since they require a separate method of measuring and regulating the application stage conditions.

Temperature and peel rate

The majority of adhesives used in PSA are amorphous polymers which have been shown to obey an empirical relationship between peel rate and temperature based on their relaxation mechanism (Eq 2-2). This relationship has been validated many times for peel testing [74, 75, 102] with shift factors obtained during peel comparable to those found in oscillatory shear rheology [98].

Eq 2-2 The Williams-Landel-Ferry(WLF) time-temperature superposition equation [103]

$$\log a_t = \frac{C_1(T - T_r)}{C_2 + T - T_r}$$

a_t = Time shift factor
 $T - T_r$ = Temp. change
 C_1 & C_2 = Empirical constants

This superposition principle can be used to construct a master peeling curve. Low $\log(a_t)$ values indicate relatively slow feed rates and high temperatures where adhesives show mostly viscous characteristics resulting in cohesive failure. Conversely, higher values of $\log(a_t)$ result in interfacial failure (Fig 2-25).

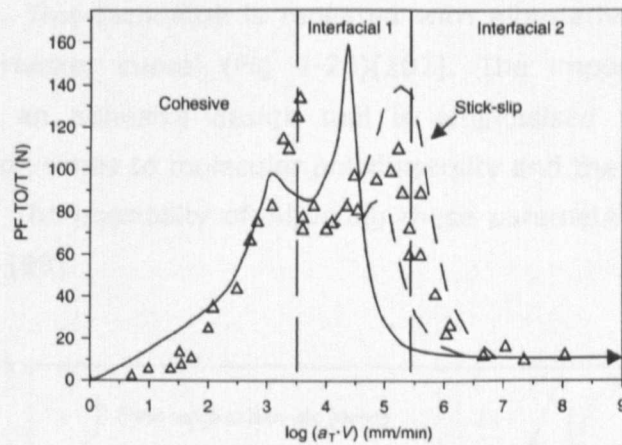


Fig 2-25 A peel master curve, constructed using the WLF equation, and observed failure modes [104]

Peel angle

Experimental results have shown that peel resistance is affected by peel angle (Fig 2-26). Results appear to confirm a theoretical inverse relationship of $1-\cos\theta$, if the summation of moments and tensional forces are unaffected and cleavage is the controlling failure mechanism [105]. The sudden drop in peel adhesion at $\theta < 40^\circ$ is attributed to a switch in the de-cohesion mechanism [75].

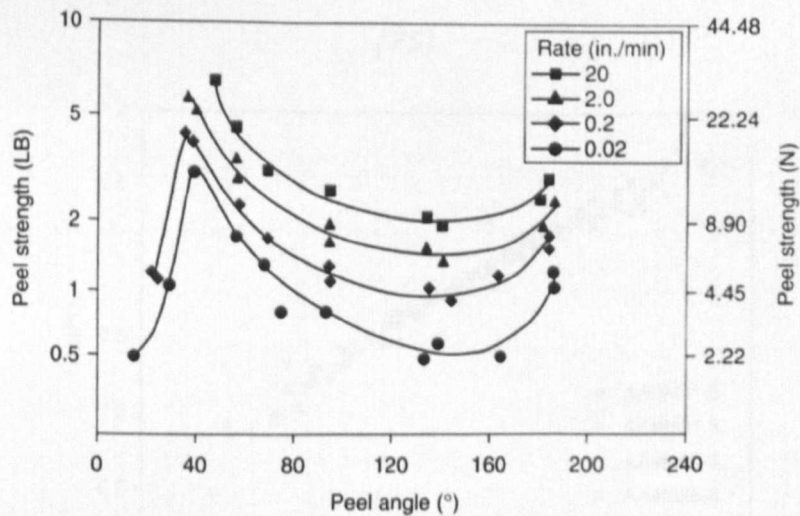


Fig 2-26 The effect of peel angle on peel resistance at various peel rates [75]

Adhesive Properties

Changes in resin properties appear to affect peel resistance through changes in viscoelastic properties. Increasing molecular weight has the effect of stiffening the resin where a shift has been observed towards interfacial failure at lower peel rates [106](Fig 2-27). The shift in properties is said to be related to the viscoelastic terminal region of relaxation. Therefore, it has been demonstrated that peel rate, temperature and adhesive formulations can be reduced to a single master curve on the basis of terminal

relaxation time [98]. This technique is repeated with alternative polymer blends and termed the 'super master curve' (Fig 2-28)[107]. The importance of the master relaxation curve as an adhesive design tool is emphasised when considering the sensitivity of relaxation times to molecular polydispersity and the sensitivity of viscosity to molecular weight. The possibility of adjusting these parameters is key to improving adhesive formulation [98].

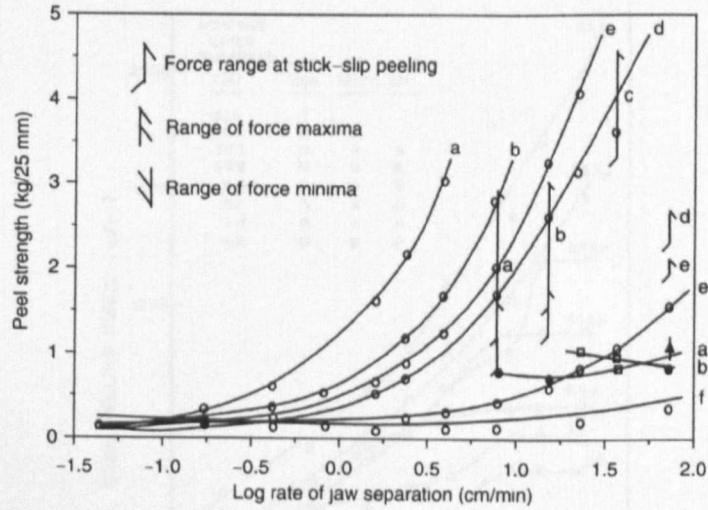


Fig 2-27 Effect of adhesive molecular weight ($a < b < c < d < e < f$) on peel resistance [75]

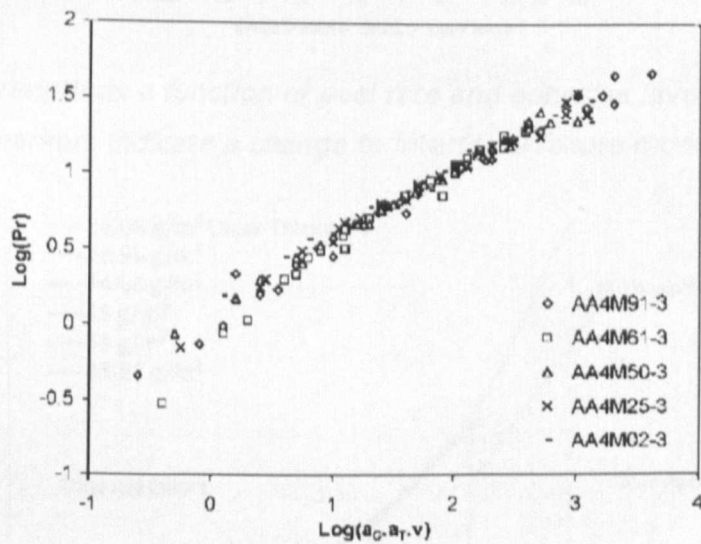


Fig 2-28 A peel resistance 'super master' relaxation curve for a range of adhesive blend molecular weights [107]

Adhesive layer thickness

The adhesive layer thickness has been shown to affect peel resistance where, at thinner coating weights, the peel resistance increases with layer thickness [74, 108]. Peel resistance as a function of coating weight has revealed an inflexion point associated with a change in failure mechanism from interfacial at thin coating to cohesive with thicker layers (Fig 2-29). However, for some adhesives increases in peel resistance is minimal, although, a shift in failure mode is still observed (Fig 2-30).

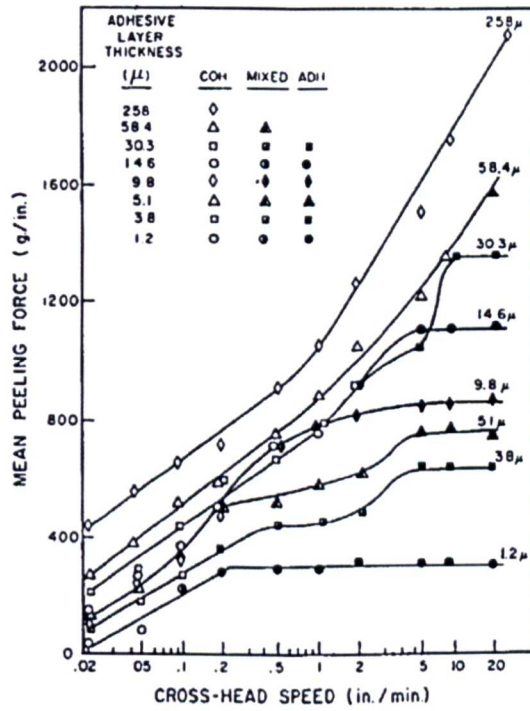


Fig 2-29 Peel strength as a function of peel rate and adhesive layer thickness where solid markers indicate a change to interfacial failure mode [109]

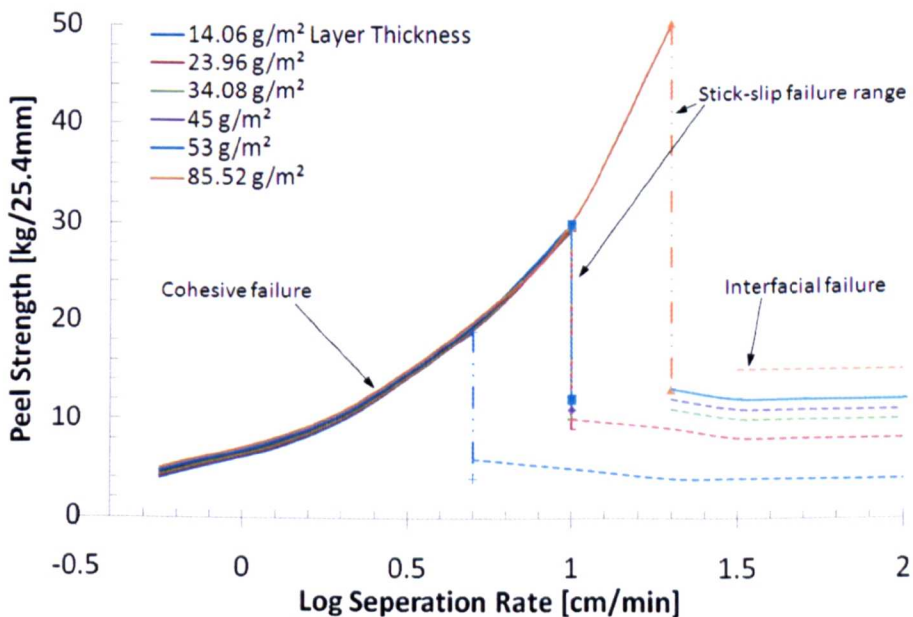


Fig 2-30 Failure mode as a function of adhesive layer thickness [106]

Contact Conditions

A refined application process with regulated application force and speed has been used with the peel test. Results are in agreement with those found during probe testing with an increase in peel resistance relating to an increase in contact force believed to increase actual contact area until full contact is achieved (Fig 2-31).

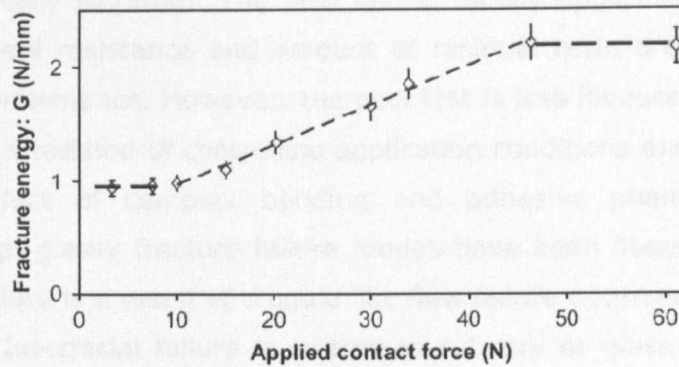


Fig 2-31 Peel fracture energy as a function of increasing application force [110]

The effect of the rigid substrate material type has also been investigated using a range of surfaces from Teflon to glass with alternate surface energies (Table 2-5). Substrates with a high surface tension mostly exhibited higher peel strength with anomalies believed to be the result of a change in failure mode (Fig 2-32) [111].

Table 2-5 Substrate surface tension determined by contact angle measurement [111]

Substrate	St/Steel	Polyethylene	Polypropylene	PVC	Bakelite	Teflon	Glass
Surface tension (γ_c)(mN/m)	Na	31	33	37	31	18	73
Symbol	□	○	△	▽	◇	◁	▷

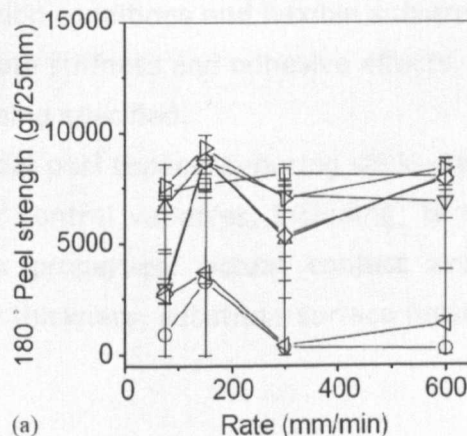


Fig 2-32 The effect of surface type on peel strength of a polymer blend [111]

Summary

The peel test is relatively simple to conduct and analyse; adhesive tapes are applied following manufacturer's instructions to a rigid substrate and then peeled at a constant rate and angle. The peeling force is measured over a typical 115mm distance and the average force is calculated. Peel resistance is expressed as the average force over bond or tape width, typically N/25mm. The peel test is mostly applicable to PSA tapes and labels where the peel resistance and amount of residual resin are key characteristics defining product performance. However, the peel test is less favoured as a research tool as it does not offer a method of controlling application conditions and the force recorded is a combined effect of complex bending and adhesive phenomenon. Cohesive, interfacial, stick-slip, glassy fracture failure modes have been observed. As with probe testing cohesive failure is a result of a liquid like flow failure occurring at low speeds and high temperature. Interfacial failure is related to rubbery or glass like fracture at the surface, associated with high feed rates and low temperature. Glassy fracture is unique to the peel test and is a result of brittle resin separating from the backing film. Stick-slip failure is also unique to the peel test and occurs during the transition between failure modes where a lack of uniformity in the peel rate results in an oscillation between two failure mechanisms. Peel resistance has been found to obey the WLF time temperature super position principle in the cohesive failure regime allowing the construction of peel master curves. The peel master curve allows prediction of peel force beyond temperature and feed rate equipment limitations. Further dimensional reductions and predictions can be made based on relaxation times of adhesives.

Only long contact times appear achievable with peel testing due to the separate application method. Additionally, distinguishing the overall effects of processing variables from multiple studies appears difficult due to:-

- Inconsistent application conditions and flexible substrates.
- An inability to separate stiffness and adhesive effects.
- Failure modes not being specified.
- Variability in interfacial peel especially during stick-slip failure.
- Failure to specify or control variables, including; temperature, peel rate, shear modulus, relaxation properties, actual contact area, contact time, contact pressure, resin layer thickness, substrate surface finish and substrate material.

2.5.3 Shear testing

PSAs in shear demonstrate creep behaviour that can lead to failure of the adhesive joint [75]. The PSA shear test is generally a measure of the adhesives rheological properties. However, the test is adapted to suit failures of PSA tape which occur over greater deflection and time scales. Typically, a weight is hung from an adhesive tape with the deflection recorded over time. The behaviour of PSAs under shear has been characterised using Maxwell and Kelvin-Voigt fluid models, using springs and dashpots to account for the elastic and viscous behaviour of the fluid. However, other viscoelastic models are available and are generally chosen to suit the experimental results [75, 98]. The loading conditions seen in shear testing can be compared to those found in plate rheology. Therefore, PSA shear testing is limited to industrial applications with shear research typically carried out using rheometers which offer greater flexibility and accuracy in results and analysis.

2.6 Rheology

PSAs and polymer resins are viscoelastic materials possessing both flow and elastic properties which play a key role in bond forming and debonding [74]. Comparisons made with rheology, peel and probe results reveal that the adhesives solid or molten state dictates tack failure type and magnitude [75, 101]. Rheology is now a well established laboratory method for determining viscoelastic properties. Many tack studies and properties are related to the rheology of the adhesive component. Although stress relaxation and creep experiments are used extensively, the small amplitude oscillatory shear experiment is the most commonly used method for determining the linear viscoelastic properties of polymer melts [112].

Method

Typically a constant thickness disc of viscoelastic material is placed between a fixed surface and a surface with a sinusoidal applied stress (Fig 2-33). A load cell and optical encoder are used to measure force and displacement response. In steady state shear the rate and stress are simply defined as a function of layer height, force and velocity (Fig 2-34). Typically, parallel plate geometry is used where the strain rate is a function of the radial position (Fig 2-35). However, small angle cone and plate geometry may be used to achieve a constant shear rate throughout the specimen. This uniform flow is advantageous when working with non-linear materials which are strain rate sensitive [113]. For viscoelastic characterisation the standardised small amplitude oscillatory shear (SAOS) experiment is commonly used. A small oscillatory shear strain is applied

to the substance and its response is recorded. The elastic and viscous components of the response can then be calculated.

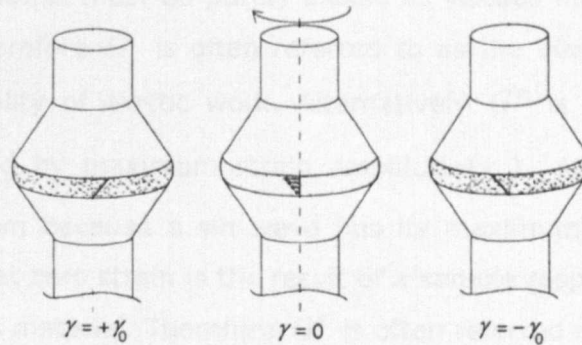


Fig 2-33 Sinusoidal strain of an adhesive in oscillatory Rheometry [114]

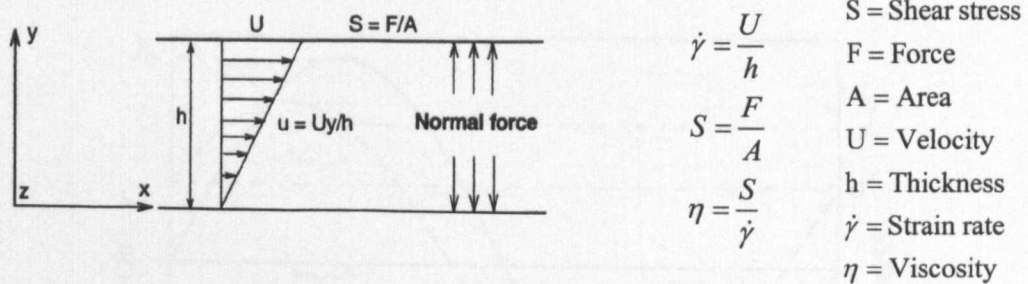


Fig 2-34 Constant velocity 'steady state' shear [115]

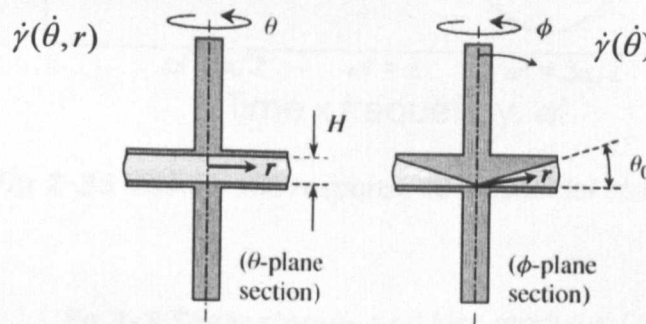


Fig 2-35 Parallel plate geometry with radius dependant strain rate (left) and cone geometry (right) [113]

Results

The motion of the driven plate and the force on the load cell are recorded. The two sinusoidal signals are then compared for phase angle, stress and strain amplitude. Stress amplitude is then calculated from force and specimen dimensions. Strain is measured as displacement. A typical viscoelastic response is defined graphically with $\gamma = \gamma_0 \sin \omega t$ defined as an input and $\sigma = \sigma_0 \sin(\omega t + \delta)$ as a response (Fig 2-36). The ratio of stress to strain is defined as a modulus each with a different physical meaning

(Eq 2-3). G' is stress (σ') measured at maximum strain ($\omega t = \pi/2$) divided by the maximum strain amplitude (γ_0). At this point the strain rate is approaching zero, consequently any response must be purely elastic as viscous materials respond only to changes in strain. Therefore G' is often referred to as the elastic or storage modulus due to the recoverability of elastic work. Alternatively G'' is the stress (σ'') at zero strain ($\omega t = 0$) divided by maximum strain amplitude (γ_0). At this point the rate of strain is at a maximum because a sin wave has its maximum rate of change at this point, thus the stress at zero strain is the result of a sample responding to strain rate as would a purely viscous material. Therefore G'' is often referred to as the viscous or loss modulus due to the fact that flow is non recoverable work dissipated through friction and heat loss [114, 116].

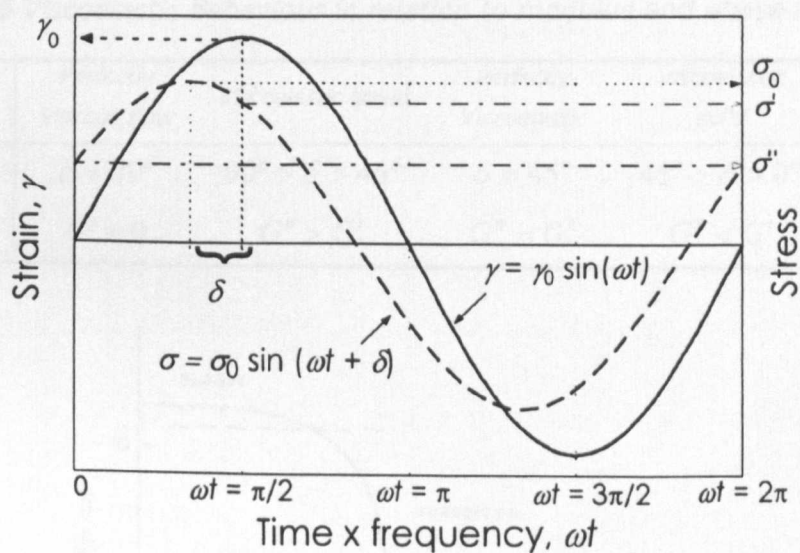


Fig 2-36 Viscoelastic response to sinusoidal strain [114]

Eq 2-3 Shear storage and loss modulus [114]

$$G' = (\sigma^0 / \gamma^0) \cos \delta$$

$$G'' = (\sigma^0 / \gamma^0) \sin \delta$$

The values of phase angle, elastic and viscous modulus can be used to define a materials state. A perfectly elastic material will have a zero viscous modulus and zero phase angle. Alternatively, a perfectly viscous material or Newtonian fluid will have no elastic modulus and a phase angle of 90° (Table 2-6). A polymer solution is found to have a range of viscoelastic properties dependant on its temperature. Typically, at very cold temperatures the polymer exhibits a brittle glassy state where low energy failure

will occur through the creation of new surfaces ($G'' \approx 0$). Increasing the temperature typically causes transition to a rubbery state often called the rubbery plateau, where properties of a viscoelastic solid are displayed. Further heating typically results in a molten polymer state displaying the characteristics of a viscoelastic fluid (Fig 2-37). Two distinct temperatures are usually defined to separate the regions (Fig 2-38). The glass transition temperature (T_g) is the midpoint of the temperature range in which glass transition takes place. The melting temperature (T_m) is the midpoint temperature between transition from the rubber-elastic to molten state [117]. The transition temperatures and dynamic modulus can be tailored to some degree by adjusting molecular weight, branching, polydispersity and cross linking, explored in greater detail in the field of polymer physics and engineering [118].

Table 2-6 Viscoelastic behaviour in relation to modulus and phase angle [117]

Behaviour	<i>Perfectly viscous flow</i>	<i>Viscoelastic liquid</i>	<i>Perfectly Viscoelastic</i>	<i>Viscoelastic solid</i>	<i>Perfectly elastic solid</i>
Phase angle	$\delta = 90^\circ$	$90^\circ > \delta > 45^\circ$	$\delta = 45^\circ$	$45^\circ > \delta > 0^\circ$	$\delta = 0^\circ$
Shear modulus	$G' = 0$	$G'' > G'$	$G'' = G'$	$G'' < G'$	$G'' = 0$

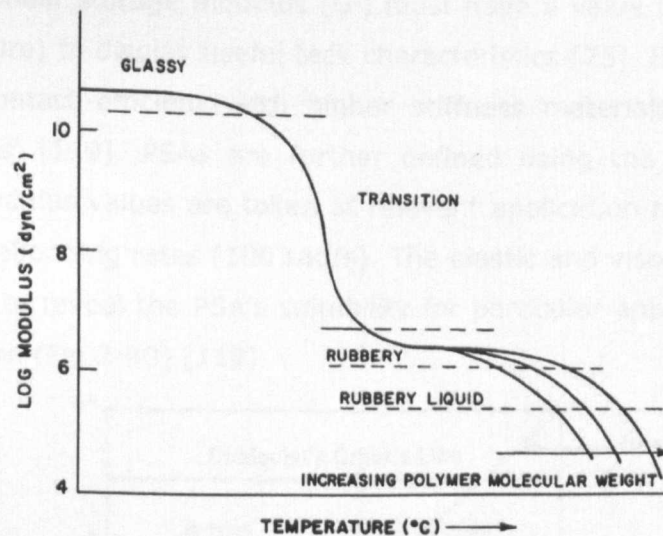


Fig 2-37 The temperature dependence of viscoelastic states in polymers [116]

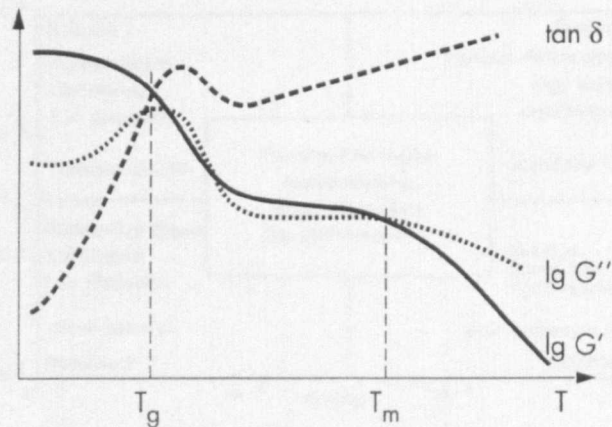


Fig 2-38 Transition temperatures defined by shear modulus [117]

Relation to PSA tack

The viscoelastic properties have been observed to affect the shape of the probe tack stress strain curve and govern the onset of failure phenomenon such as cavitation and fibrillation (Chapter 2.5). Additionally, the peel resistance and failure type appear to be governed by viscoelastic properties. Therefore, a number of attempts have been made to determine the suitability of an adhesive as a PSA based on its viscoelastic properties. The earliest rheological definition of an adhesive, known as the Dahlquist criterion, requires that the shear storage modulus (G') must have a value below 10^5 Pa (at 1Hz, ambient temperature) to display useful tack characteristics [75]. Suitable PSA materials are considered 'contact efficient' with higher stiffness materials defined as 'contact deficient non PSAs' [119]. PSAs are further defined using the viscoelastic windows concept. Shear modulus values are taken at relevant application rates (0.01 rad/s) and peel or tack test debonding rates (100 rad/s). The elastic and viscous modulus are then plotted (Fig 2-39) to reveal the PSA's suitability for particular application depending on its quadrant position (Fig 2-40) [119].

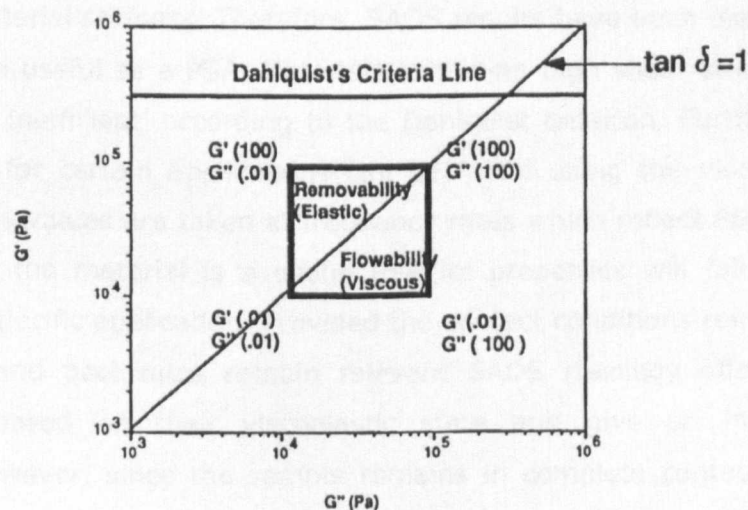


Fig 2-39 Coordinate plot for shear modulus of PSAs [119]

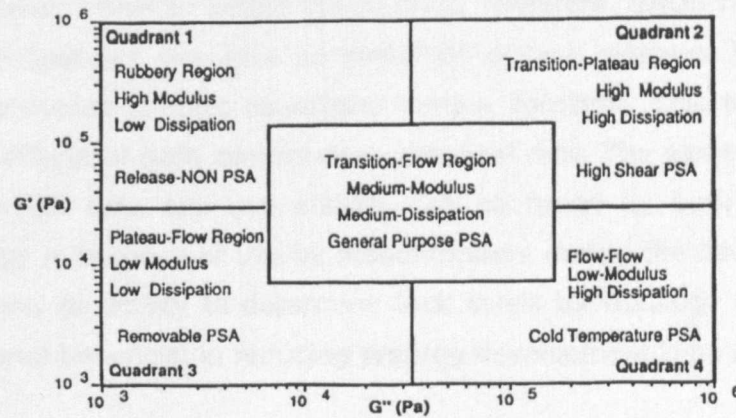


Fig 2-40 PSA type based on the viscoelastic windows principle [119]

The most convincing and quantifiable link between viscoelastic properties and tack comes from a relationship between strain rate and temperature observed in the rheology results of amorphous polymer melts [103]. An empirical equation has been developed which links the effects of the two variables with an inverse logarithmic relationship which requires two experimentally obtained constants (Eq 2-2). Essentially the relationship infers that amorphous polymers will have similar viscoelastic behaviour at high temperatures and low strain rates and vice versa. The effects on peel tack have been directly linked with equal constants found by both rheology and peel tack testing (Chapter 2.5.2) [98]. The relationship is also demonstrated less convincingly in probe tack testing [120].

Summary

Small amplitude oscillatory shear (SAOS) rheology is a well established powerful tool for determining shear modulus and phase angle. From these values it is possible to determine materials viscoelastic state and transition temperatures. Such properties give indications of material stiffness. Therefore, SAOS results have been used to determine if a material will be useful as a PSA. Materials exhibiting high shear storage modulus are deemed 'contact inefficient' according to the Dahlquist criterion. Further definition of a PSA's suitability for certain applications can be found using the viscoelastic windows principle. Modulus values are taken at frequency rates which reflect PSA application and peeling rates. If the material is a useful PSA its properties will fall into a quadrant determining its specific application. Provided the contact conditions remain constant and the application and peel rates remain relevant SAOS rheology offers the ability to classify resins based on their viscoelastic state and give an indication of tack performance. However, since the sample remains in complete contact throughout the test it does not allow the study of contact conditions. Changes in application and peel rates add the additional task of relating actual rates to test frequencies. Additionally,

the adhesive is never taken to actual failure limit. Therefore, SAOS rheology cannot be considered a tack test but may give an indication of tack response to variables which affect viscosity provided contact conditions remain constant. This is confirmed when determining the effects of both temperature and peel rate. The same constants for the WLF equation, which links the two effects, can be found by both peel testing and rheology. Rheology is in constant use by manufacturers during the development of resin systems. Therefore, an ability to determine tack levels by rheology with minimal tack testing is considered beneficial in reducing prepreg development time and costs.

2.7 Adhesives theory

Typically any adhesive bond is said to be the result of a combined effect of multiple mechanisms [121]. However, certain mechanisms may appear dominant under certain conditions. Therefore, many theories have been postulated to describe mechanisms of adhesion, with each one supported by experimental evidence under certain conditions (Table 2-7).

Table 2-7 Multiple theories of adhesion [121]

<i>Traditional</i>	<i>Recent</i>	<i>Scale of action</i>
Mechanical interlocking	Mechanical interlocking	Microscopic
Electrostatic	Electrostatic	Macroscopic
Diffusion	Diffusion	Molecular
Adsorption/surface tension	Wettability	Molecular
	Chemical bonding	Atomic
	Weak Boundary Layer (WBL)	Molecular

Mechanical interlocking adhesion is mostly applicable to adhesives which cure. It occurs by penetrating pores, cavities and other surface irregularities of the rigid substrate [121]. This theory has been formed intuitively by observations of increased adhesion of cured adhesives with increased surface roughness. However, significantly higher molecular adhesion has been achieved with two perfectly smooth surfaces [73]. Mechanical interlocking is unlikely to play a major role in prepreg tack since the resin remains uncured.

Electrostatic adhesion takes place due to electrostatic effects between the adhesive and the substrate. Electron transfer is believed to take place as a result of unlike electronic band structure. Electrostatic forces in the form of an electrical double layer are thus formed at the interface. These forces account for the resistance to separation. The electrostatic mechanism is said to be a plausible explanation for polymer-metal adhesion bonds. However, the contribution in non-metallic systems to adhesion has

been calculated and found to be small when compared to that of chemical bonding [121].

In diffusion theory, adhesion is achieved through the interdiffusion of molecules between the adhesive and the substrate. The diffusion theory is most prevalent when both surfaces are relatively long chain dynamic molecules [121]. Interdiffusion of molecular chain elements across a polymer-polymer interface (polymer healing) is considered to be the controlling factor for tack and green strength of uncured linear elastomers. Variables which control molecular diffusion may also control adhesion. Increasing temperature increases the average interdiffusion length but also decreases the stress required to pull the segment out [71].

Wetting theory proposes that adhesion results from molecular contact between two materials and the surface forces that develop. The process of establishing continuous contact between two substances is called wetting. For an adhesive to wet a solid surface, the adhesive should have a lower surface tension than the critical surface tension of the solid [121].

Chemical bonding is a general term used to describe the molecular chemical interactions which may occur at the interface. Four interactions are thought to take place during chemical bonding; covalent bonds, hydrogen bonds, Lifshitz-Van der Waals forces and acid-base interactions. The exact nature of the interactions that hold the adhesive bond depends on the chemical composition of the interface [121]. Acid-base adhesion is based on a chemical concept of polar attraction between Lewis acids and bases due to electron imbalances [121].

Weak Boundary Layer (WBL) theory dictates that any adhesive failure which is not cohesive is the result of a weak surface layer. This layer can be caused by environmental contaminants, impurities in or at the surface of the adhesive or substrate. When failure takes place, it is the weak boundary layer that fails, although failure may appear to take place at the interface [121]. Air, moisture, oxidation may all contribute to a WBL, therefore, exceptional adhesion occurring on spacecraft components such as door hinges have been attributed to the absence of a WBL normally present in earth's atmosphere [73].

2.8 Polymer melts

Polymer melt studies generally consist of characterising the mechanical response and relating behaviour, such as non-Newtonian flow and relaxation, to individual molecular structure and interaction with neighbouring molecules. Therefore, since tack is believed to be a product of such behaviour, a review of molecular principles and polymer melt theory is required.

2.8.1 Basic molecular principles

Temperature

Microscopically observable movement of particles, known as Brownian motion, is believed to be responsible for macroscopic temperature and heat flow in molecular-kinetic theory [122], the study of which has become known as thermodynamics. In kinetic molecular theory, heat energy is a measure of molecular kinetic energy and therefore velocity of molecular motion [123]. An ideal gas is the simplest form of molecular modelling. It assumes that molecular interaction takes place between the molecules and container walls, where pressure and temperature can be measured, but neglects interactions between molecules. This approximation proves reasonably accurate for simple gases at low pressures due to the relative volume of the gas molecules believed to be small in comparison to the free volume. Therefore, the effect of molecule to molecule collisions are considered negligible [124]. With negligible collisions the diffusion between two perfect gases would be instantaneous differing significantly from what is observed. Therefore, more complex modelling includes collisions with molecules modelled as hard spheres or abrupt repulsive forces increasing exponentially with approaching distance [125]. Van der Waals also considered the effect of long range attractive forces despite the average effect of these forces within the bulk, acting in all directions, being considered negligible [124]. The inclusion of attractive forces increased the accuracy of the state equation to model regions of condensation and fluid states. The state of matter is now considered to be a result of molecular packing and motion which calculation of all free linear and rotational motions is required for accurate modelling [124]. Despite the increased complexity associated with the increased molecular length of polymers generalised equations of state continue to be formed based on such molecular principles [126].

Solid flow

Elastic deformation rationalised on an atomic scale is believed to be the stretching of atomic bonds which displays a linear response since only a small portion of the near equilibrium bond is tested (Fig 2-41). Despite the apparently rigid crystalline molecular structure of most solids, flow can be observed under long periods of high loading. This

flow, known as creep, is observed experimentally to be thermally activated. The rate at which creep occurs depends on both stress and temperature and follows the empirical Arrhenius rate equation. The Arrhenius equation is found by plotting a log of rate against $1/T$ ($^{\circ}\text{K}$) which typically results in a straight line. The equation then has a comparative form to the high energy Maxwell-Boltzmann distribution for molecular energies in gases. This analogy now includes an activation energy term [127].

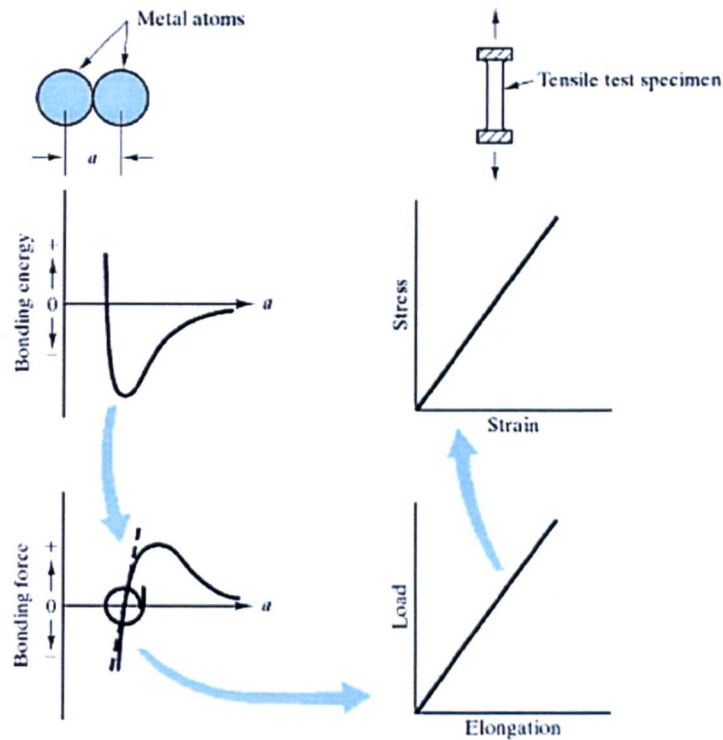


Fig 2-41 Relationship between atomic bond stretching and tensile mechanical properties of a solid [127]

Eyring's solid flow model encompasses the idea that an atom or molecule must pass over a thermally activated energy barrier in moving from one position to another in the solid [128]. The jump rate is related exponentially to temperature and occurs randomly in any direction. However, the addition of a load stress will increase the probability that a jump will occur in the direction of loading, therefore, offering some rationalisation of creep flow. Such theories have been used to predict strain rate and temperature effects on the yield behaviour of polymers [129]. These molecular activation principles have recently been applied as alternatives to free volume models in the theoretical derivation of the WLF equation [130].

2.8.2 Molecular description

A typical polymer melt consists of long chains where a number of chain lengths may exist within the melt. The distribution of lengths within the melt is known as polydispersity. Polymer chains such as epoxy are modelled traditionally using chemistry diagrams and more recently with 3D diagrams (Fig 2-42). Polymer chains have now been observed directly by atomic force microscopy (Fig 2-43). The polymers are generally thought of as a long chain of atoms held together by covalent chemical bonds [72]. Covalent chemical bonds are of short range order (0.1-0.2 nm) with high dislocation energies [131]. Covalent bonds are formed by the sharing of electrons. Atoms may also be joined by ionic bonding also of short range which involves the swapping of electrons [132].

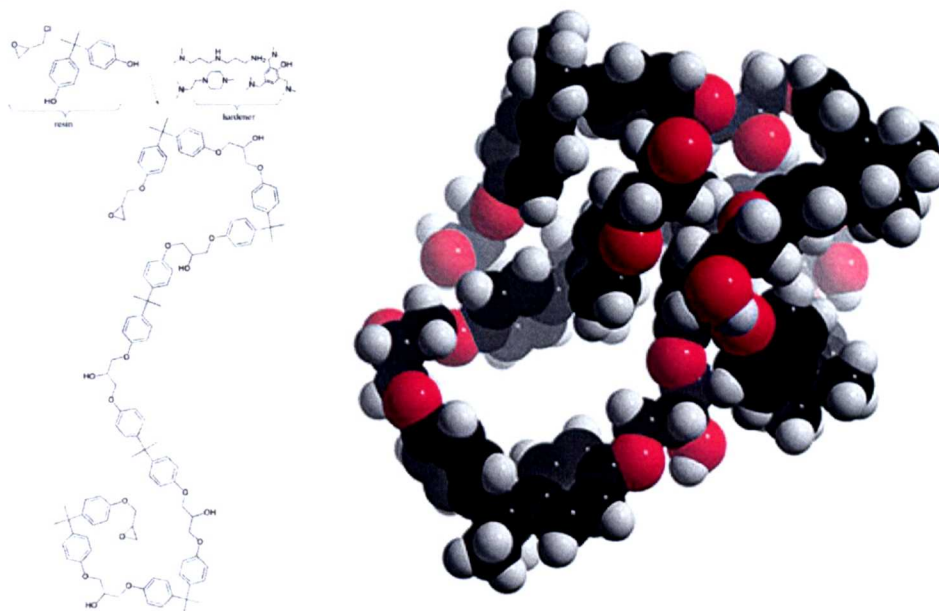


Fig 2-42 Chemical diagram (left) and 3D representational model of a typical BPA epoxy resin molecule [133]

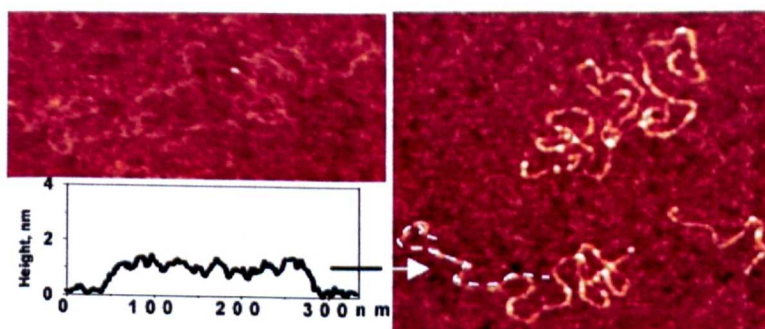


Fig 2-43 Poly 2-vinylpyridine chain observed by atomic force microscopy [134]

Covalent and ionic bonds are tightly held together and require a significant amount of energy to break. Since the energy involved in peeling is relatively low, it is assumed that the polymer chain bonds remain unbroken. These bonds are however, flexible and subject to deformation mainly through a variation in torsion angles [72]. Provided the activation energy is not reached they will return to their original bond length once the force is removed. Non-covalent attractive bonds such as van der Waals are also believed to be in effect between molecules. The van der Waals repulsive forces along with thermal vibration motions are represented as an effective co-volume in the 'vaguely defined concept' of free volume [135]. The attractive force receive little consideration since, as with a fluid, the average effect of a completely surrounded molecule vanishes [124].

2.8.3 Melt behaviour

Polymers typically have a complex mechanical behaviour resulting in strain rate, strain history and temperature sensitivity [135]. Typical polymers are also subject to relaxation processes with some polymers capable of returning to their original shape at visible rates and deflections. These properties and many others are known to relate to its molecular polymer chain structure and how the chains interact within the melt or solid state (Table 2-8).

Table 2-8 Typical polymer properties related to molecular structure [136]

	Tensile Strength	Elongation	Yield strength	Toughness	Brittleness	Hardness	Abrasion resistance	Softening temp	Melt viscosity	Adhesion	Chemical resistance	Solubility
+ Increase, - decrease, 0; little change, M; passes through a maximum, *for amorphous polymers, B; result depends on melting point, C; temperature dependant												
Increase molecular weight*	+	+	+	+	+	+	+	+	+	-	+	-
Reduce polydispersity	+	-	-	+	-	-	+	+	+	-	+	0
Increase branching / cross linking	M	-	+	-	M	+	+	+	+	-	-	M
Add polar chain units	+	+	+	+	+	+	+	B	+	+	-	+
Add polar side chains	+	+	+	+	+	+	+	+	+	+	-	+
Stiffen main chain	+	-	+	-	+	+	-	+	+	-	+	-
Increase crystallinity	-	-	+	-	-	+	+	+	+	-	+	-
Add crystallisable branches	+	+	+	+	+	+	+	0	C	0	-	+

Polymer melt theory is concerned with relating viscoelastic properties to molecular structure and dynamics. Viscoelastic polymers display both elastic and viscous deformations under applied stress. Perfectly elastic deformation is proportional to the applied stress. Once stress is removed the structure will return to its original position. Perfectly elastic behaviour is associated with high energy chemical bonds or constrained

crystalline atomic structures where bonds are stretched but remain unbroken preventing flow [127]. Perfect Newtonian fluids give a good example of purely viscous flow. Their deformation rate increases proportionately to the applied force. For a Newtonian fluid the viscosity remains constant affected only by temperature [115]. For a Newtonian fluid, viscosity can be defined by flow activation energy using the Arrhenius model (Eq 2-4). A Newtonian fluid may also exhibit non-linear flow effects, such as an object hitting water at high speed. However, these are due to inertia rather than complications of the molecular structure. If inertia effects dominate over viscous forces the flow is said to be turbulent. The ratio of inertial forces to viscous forces is commonly known as the Reynolds number [137].

Eq 2-4 Viscosity as a function of activation energy

$$\eta = Ae^{E/RT}$$

E = Activation energy
 R = Universal gas constant
 T = temperature in Kelvin

The majority of adhesives and prepreg resins consist of long chain polymer molecules, e.g. a macromolecule of molar mass $M=100,000\text{g/mol}$ has a length of approximately $1\mu\text{m}$ (1000nm) and a diameter of 0.5nm . An illustrative example is an equivalent length of spaghetti which is 1mm thick would be 2m long [117]. At rest, each macromolecule can be found in the lowest level of energy consumption. Without external load it shows the shape of a three dimensional coil. Each coil has an approximately spherical shape and each one may be entangled many times with neighbouring macromolecules. During steady state shearing the viscosity may exhibit a complex shear thinning response as the molecules become aligned. Alternatively, shear thickening flow behaviour may occur due to entanglements between molecule chains [117]. Newtonian, shear thinning and thickening responses (Fig 2-44) may all be exhibited by a polymer melt depending on its molecular configuration and loading condition.

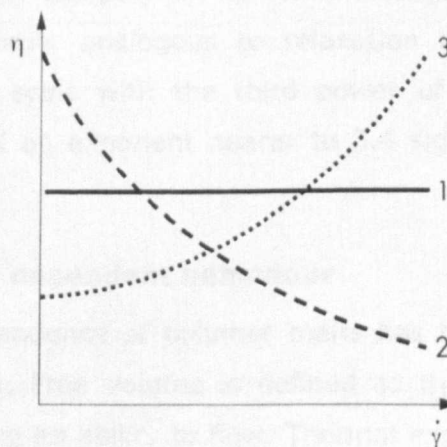


Fig 2-44 Newtonian (1), Shear thinning (2) and shear thickening behaviour(3) [117]

2.8.4 Diffusion

Diffusion is the term used to describe molecular movement within the melt. Many theoretical molecular diffusion models exist which attempt to link experimental results with molecular dynamics. The reptation or tube model is one such theory used to account for the sensitivity of viscoelastic properties to molecular length, branching and polydispersity [138]. The polymers are modelled as flexible 'snake like' objects moving through tubes constrained to travelling along their own length. This 'reptation' motion has now been observed directly within the melt using fluorescently labelled DNA [139] and at the interface [140].

Certain adhesion theories exist, where adhesion is believed to be developed through the interdiffusion of molecules between the adhesive and the adherent. The nature of materials and bonding conditions will influence whether and to what extent diffusion takes place. The diffuse interfacial layer typically has a thickness in the range of 1-100 nm. Solvent cementing or heat welding of thermoplastics is believed to be due to the diffusion of molecules [121]. Interdiffusion of chain segments across a polymer - polymer interface are also considered the controlling factor for tack and green strength of uncured linear elastomers [71]. The fracture mechanisms at polymer melt interfaces have also been found to depend strongly on the Deborah number, defined as the ratio of strain rate to polymer molecular relaxation time which is dependent on diffusion [141].

Entanglement

An increase in strain hardening is attributed to knots or 'entanglements' within the molecular chains which do not have time to break resulting in elastic behaviour. At large times the knots open by Brownian motion: the chains can slide past each other resulting in behaviour similar to a liquid [142]. This motion dictates the diffusion of the polymer melt with the time taken for the polymer to move through the tube of its own length known as the reptation time, analogous to relaxation time. The reptation time is theoretically calculated to scale with the third power of molecular length, however experimental results reveal an exponent nearer to 3.4 signifying that the theory may not be complete [72, 138].

2.8.5 Time-temperature dependant behaviour

The time-temperature dependence of polymer melts has been related to an empirical free volume concept [103]. Free volume is defined as the space a molecule has for internal movement, dictating its ability to flow. Thermal expansion is therefore believed to be responsible for the transition to a melt state (Fig 2-45) allowing greater molecular

mobility [143]. The state of a material and its ability to flow is therefore believed to be a function of molecular freedom. Polymers with great molecular freedom may crystallize under favourable conditions when the cooling rate is slow. Crystallisation is a lower energy form of matter with much tighter packing which requires an orderly structure. Polymers which do not have time to reach this ordered structure, through Brownian motion, due to rapid cooling are thought of as frozen in the molten state. Polymers which do not crystallise even when cooled extremely slowly are known as amorphous.

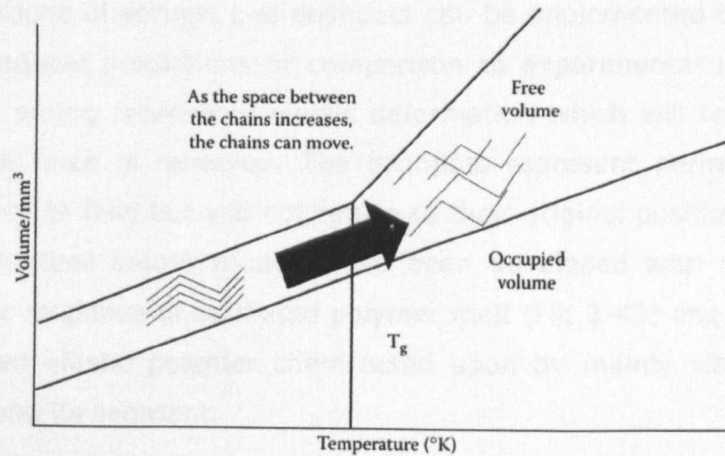


Fig 2-45 Increase in free volume occurring around T_g [143]

The main effect of cooling the melt is to decrease the thermal agitation of the molecular segments. In the melt, segments are believed to change place by thermally activated jumps. The number of jumps per second is very large (10^6s^{-1}). If cooling is continued, a temperature is reached at which the rate of segmental movement is extremely sluggish, and then further cooling finally stops the movement. The polymeric specimen then consists of long molecules tangled in a liquid like manner, with the absence of rapid molecular motion which is typical of a liquid. This glassy state is distinguished by the immobility of the molecular backbones, which are frozen in crumpled formations. A simple manifestation of this cessation of molecular motion is seen in the response of the specific volume change to temperature (Fig 2-45) where, in the glassy state the molecules simply move further apart through thermal expansion without changes in molecular conformation. The thermal expansion increases through molecular jumps throughout the transition range to reach that of a liquid on further heating [128].

Time-temperature-superposition

An empirical Williams-Landel-Ferry (WLF) relationship has been observed in the study of shear rheology measurements of amorphous polymers [103] (Chapter 2.6). Explanatory theories of the WLF relationship consider the polymer on a molecular level where

Brownian motion and free volume concepts are used to link time and temperature of amorphous polymer melt relaxation and glass transition. Essentially, increased temperature is said to result in increased molecular freedom through thermal expansion [135].

2.8.6 Mathematical models

A model consisting of springs and dashpots is conventionally used to represent a viscoelastic material and analyse its response [144]. Increasingly complex models using various configurations of springs and dashpots can be implemented to give increasingly accurate mathematical predictions in comparison to experimental response [128]. In such models the spring represents elastic deformation which will return to its original position once the force is removed. The dashpots represent permanent deformation having a resistance to flow but will not return to their original position once the force is removed. Mathematical ladder models have been developed with relative success to model viscoelastic response of undiluted polymer melt (Fig 2-46) and bear a remarkable resemblance to an elastic polymer chain acted upon by mainly viscoelastic forces at various points along its segment.

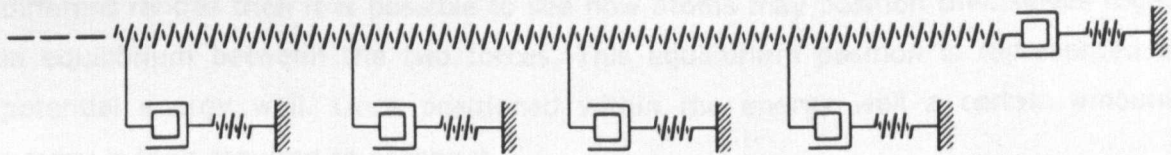


Fig 2-46 Marvin's modified ladder network for the prediction of viscoelastic properties accounting for limiting modulus at high frequencies [135]

2.8.7 Molecular adhesion

Three general laws of molecular adhesion have been suggested [73]:-

1. All atoms and molecules adhere with considerable force, if two solid bodies approach nanometer separations, they will jump into contact as a result of molecular adhesion; this behaviour differs from ordinary engineering experience.
2. The effect of contaminant molecules is to reduce adhesion.
3. Molecular adhesive forces are of such short range that various mechanisms can have large effects. Examples of such mechanisms are surface roughness, Brownian motion, cracking, viscous deformation etc. These mechanisms lead to a rich variety of adhesion phenomena which may cause macroscopic adhesion to vary, even though the molecular adhesion remains constant.

Further consideration of Brownian motion gives rise to a model of adhesion which is not static on a molecular scale. The crack tip in an adhesive system is said to be wandering kinetically as the molecules spontaneously break and rebond. Cracking is thus viewed as a chemical reaction between molecules at the crack tip. The force applied to open or close the crack is not the cause of the reaction, i.e. peeling or healing, at the crack tip. The reaction happens spontaneously and equally in both directions, causing the crack to open and close spontaneously at the molecular scale. Applying the crack driving force merely shifts the chemical equilibrium in one particular direction, either opening or closing the crack [73].

Lennard-Jones (LJ) potential

The two parameter LJ atomic model includes attractive and repulsive forces which operate over different distances (Fig 2-47). The repulsive force is short range, attributed to electron to electron repulsion, related to the Pauli Exclusion Principle in the electron shell [145]. The repulsive force is generally thought of as the atomic radius when the atom is modelled as a semi-solid sphere [73]. The adhesion term represents the attraction between the protons in the nucleus to electrons of neighbouring atoms, which extends beyond the electron shell. Since the repulsive and attractive forces operate over different ranges then it is possible to see how atoms may position themselves together in equilibrium between the two forces. This equilibrium position is represented as a potential energy well. Once positioned within the energy well a certain amount of energy is then required to escape it.

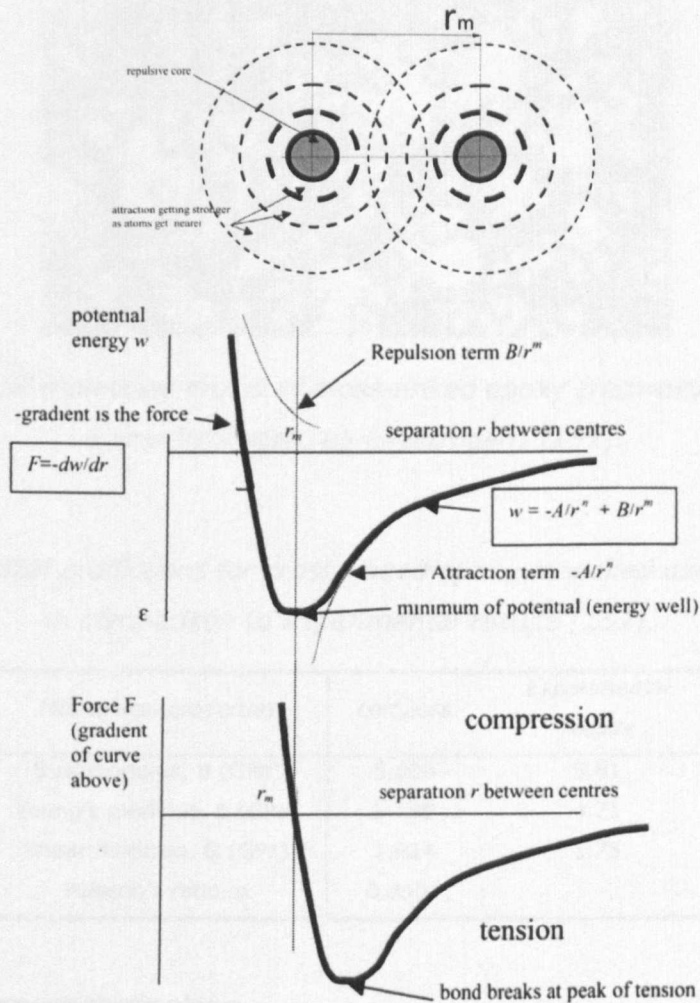


Fig 2-47 The Lennard-Jones two parameter model of atomic adhesion [73]

2.8.8 Dynamic molecular modelling

Dynamic Molecular Modelling (DMM) has been used in wetting simulations of simple liquids with reasonable results where simulation behaviour appears analogous to experimental behaviour [146, 147]. DMM generally utilises individual atomistic elements which are allowed to vibrate. The elements typically utilise a LJ type interaction in a force field model [146, 148, 149]. The LJ system is shown to allow relaxation by an increased number of molecular jumps with increasing temperature [150]. Atomistic modelling of cross-linked epoxy resin (Fig 2-48) has also shown reasonable predictions for Bulk, Young's and Shear modulus values (Table 2-9) where van der Waals forces were found to be predominant [151].

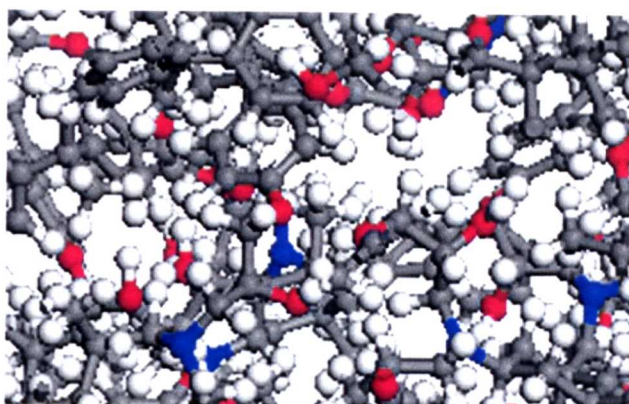


Fig 2-48 A stick-ball molecular model of cross-linked epoxy (red=oxygen, gray=carbon, white=hydrogen, blue=nitrogen) [151].

Table 2-9 Mechanical predictions for cross-linked epoxy modelled using Compass [148] in comparison to experimental results [151].

Mechanical properties	compass	Experimental results
Bulk modulus, B (GPa)	5.804	5.01
Young's modulus, E (GPa)	5.198	4.71
Shear modulus, G (GPa)	1.924	1.75
Poisson's ratio, ν	0.3507	-

2.8.9 Molecular characterisation

GPC

Gel Permeation Chromatography (GPC) is a variant of size exclusion chromatography used as an analytical procedure for separating small molecules by their difference in size. Gel particles are used to form a porous stationary phase, the molecular material which is dissolved in a solvent or elution flows through the gel bed. Smaller molecules are retained longer due to their ability to penetrate the gel pores [152]. Molecular weight averages (M_w , M_n) and information on the molecular weight distribution, termed polydispersity (P), is obtained. The raw data GPC curve is a molecular size distribution curve. When a concentration sensitive differential refractometer is used as a detector, the GPC curve is really a size distribution curve in weight concentration. With calibration, the raw data can be converted to a molecular weight distribution curve and the molecular weight averages can be calculated [153].

Rheology

Dynamic melt viscosity results found by small amplitude oscillatory shear (SAOS) rheology have also been used to characterise the molecular weight of mono and

polydisperse polystyrenes in agreement with results found by GPC [154]. The weight increase appears to shift the shear storage modulus (G') in the strain rate domain. Therefore, an increase in molecular weight stiffens the melt at any given rate (Fig 2-49) or temperature (Fig 2-37) provided transition to a glass state does not occur (Chapter 2.6).

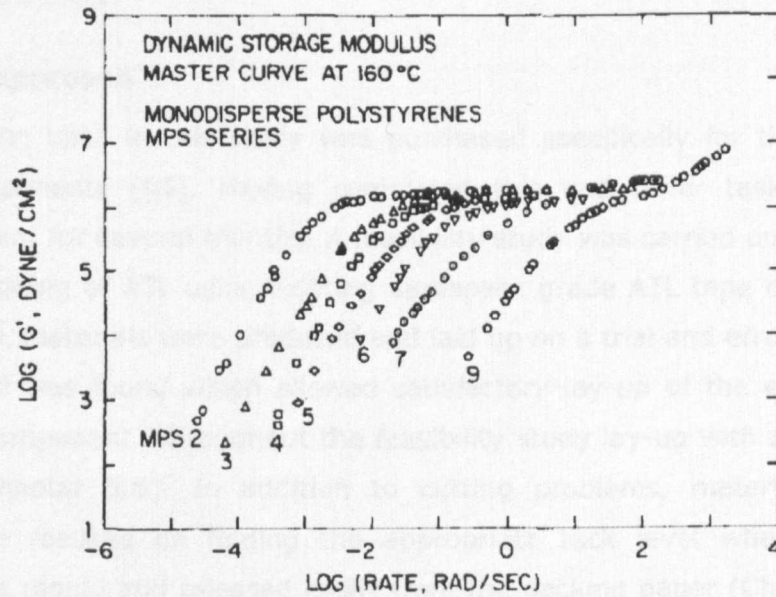


Fig 2-49 Dynamic storage modulus for monodisperse polystyrenes ranging in molecular weight from 2-Mw=547 to 9-Mw=43.1 [154]

3 Experimental methodology

The experimental work was carried out as part of a wider AIRPOWER project which incorporated the development of ATL for wind energy. The aims of the project were to construct a 7m demonstrator component, representing a section of wind turbine blade, with skins made by ATL.

3.1 General approach

The ATL machine used in this study was purchased specifically for the production of aerospace components [65]. Having completed this and other tasks the ATL had remained dormant for several months. A feasibility study was carried out which included the recommissioning of ATL using existing aerospace grade ATL tape and tooling. New wind energy ATL materials were produced and laid up on a trial and error basis (Chapter 3.2). A material was found which allowed satisfactory lay-up of the experimental 7m demonstrator component. Throughout the feasibility study lay-up with all materials was problematic (Chapter 5.6). In addition to cutting problems, material development appeared to be focused on finding the appropriate tack level where the material remained on the mould and released easily from the backing paper (Chapter 4.1). Tack was determined subjectively by touch, based on the experience of the prepreg manufacturer and recommendations by the machine operator.

A method for quantifying prepreg tack and stiffness was developed (Chapter 3.3). The method was then used to determine the effect process and material variables (Chapter 3.5). Time temperature superposition (TTS) of prepreg tack and stiffness was suspected following the investigation of variables. Although well documented for PSAs, TTS has not been observed or applied in prepreg production and was considered a useful tool with potential for regulating and controlling tack. Therefore, a further TTS investigation was carried out which included other experimental methods for supportive evidence (Chapter 3.7). The findings from this study were initially confusing and, due to progressive deadlines, did not come quickly enough to be incorporated into the development of demonstrator materials. The modification of ATL equipment to suit the findings and recommendations was also beyond the scope of this project. However, an ATL application study was conducted to ensure that experimental tack and stiffness results and findings could be directly applied to ATL equipment (Chapter 3.8).

3.2 ATL feasibility study

Feasibility trials were conducted to recommission ATL equipment which was not in continual use (Table 3-1). Initial trials were conducted on a flat stainless steel plate coated with Chemlease 41 release agent. To increase tack and reduce cleaning operations a bagging film was vacuumed to the surface. An initial flat plate lay-up was used to establish ATL ability to cut and place the prepreg tape (Fig 3-1). Trials then progressed to lay-up over a double curvature surface using aerospace alloy mould tooling (Fig 3-2). Once the demonstrator moulds became available, initial mould testing was done using carbon aerospace material to conserve newly developed wind energy material. Once acceptable lay-up was achieved a complete demonstrator lay-up of wind energy ATL tape was conducted to produce the final component.

Table 3-1 Description of the individual trials carried out within the feasibility study

Location/MC	Exp. Ref.	Description	Material	Lay-up surface
BAE Cincinnati V4 CTL	ATLF-A01	Flat panel ATL recommissioning	A-ATL-1	Flat St/St with Chemlease 41
SABCA Cincinnati V5 CTL	ATLF-W01	Initial wind energy prepreg trials carried out at SABCA	W-ATL-1	Flat surface
	ATLF-W02		W-ATL-2	
	ATLF-W03		W-ATL-3	
BAE Cincinnati V4 CTL	ATLF-W03	Flat panel wind energy tape feasibility trials. Mostly overcoming cutting issues	W-ATL-2	Flat surface covered with bagging film
	ATLF-W04		W-ATL-3	
	ATLF-W05		W-ATL-4	
	ATLF-W06		W-ATL-5	
	ATLF-W07	Flat panel wind energy tape feasibility trials	W-ATL-5	Flat polished composite panel with Chemlease 41
	ATLF-W08		W-ATL-6	
	ATLF-W09		W-ATL-7	
	ATLF-A02	Double curvature ATL (aerospace moulds)	A-ATL-2	Curved alloy moulds with Chemlease 41
	ATLF-A03	Testing wind energy moulds	A-ATL-2	GFRP wind energy moulds
ATLF-W08	Demonstrator component lay-up	W-ATL-7	with Chemlease 41	

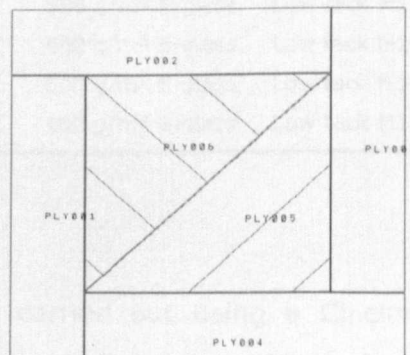


Fig 3-1 Initial test panel ply lay-up used in ATL feasibility trials



Fig 3-2 Double curvature alloy aerospace mould tool used in recommissioning ATL equipment

3.2.1 Materials

Recommissioning of the ATL and initial trials began with commercial aerospace ATL tape (Table 3-2). Experimental wind energy ATL tapes were then produced in differing tack levels to facilitate lay-up with increasing FAW. Due to a shortage of wind energy material, aerospace material A-ATL-2 was initially used to assess the feasibility of wind energy ATL tooling.

Table 3-2 Details of ATL prepreg materials used in the feasibility study

Ref.	Manufacturer Ref.	Fibre	Resin type	Content [%]		Use
				Wt.	Vol.	
A-ATL-1	8552/34%/UD268/IM7	268 g/m ² IM7 Carbon	Low tack 8552	34	41.4	Commercial Aerospace
A-ATL-2	8552/34%/UD194/AS4	194 g/m ² AS4 Carbon	Low tack 8552	34	41.4	
W-ATL-1	M19.1/32%/UD200/E	200 g/m ² E-glass	High tack M19.1	32	50.1	Experimental wind energy
W-ATL-2	M19.6/32%/UD200/E	200 g/m ² E-glass	Med tack M19.6	32	50.1	
W-ATL-3	M19.6/32%/UD400/E	400 g/m ² E-glass	Med tack M19.6	32	50.1	
W-ATL-4	M19.6LT/32%/UD300/E	300 g/m ² E-glass	Low tack M19.6LT	32	50.1	
W-ATL-5	M19.6LT/32%/UD400/E	400 g/m ² E-glass	Low tack M19.6LT	32	50.1	
W-ATL-6	M19.6LT/32%/UD600/E	600 g/m ² E-glass	Low tack M19.6LT	32	50.1	
W-ATL-7	M19.6LT/28%/UD400/E	400 g/m ² E-glass	Low tack M19.6LT	28	45.3	

3.2.2 Equipment

The majority of trials were carried out using a Cincinnati 10-axis, gantry-type V4 contour tape laying (CTL) machine. Cutting consisted of two numerically controlled knife blades capable of cutting angles from 0 to approaching 90°. Tape heating was available

via an electric hot plate positioned against the backing paper. Compaction pressure was provided by a segmented compaction shoe $\approx 30\text{mm}$ in thickness. The machine was configured to accept 150mm wide prepreg rolls. The CTL was limited to a maximum surface contour of 15° from the horizontal. Initial tests were also carried out at SABCA in Belgium using a Cincinnati V5 contour tape laying machine of a similar specification with the exception of ultrasonic knife cutters.

Process variables

A number of process variables were identified which may affect ATL performance (Table 3-3). Ambient temperature was prevalent where the heater plate was not used. Tape temperature could be increased via a hotplate against the backing paper. Feed rate was regulated within the NC program, generally slowed for cutting and intricate placement operations. Changes to contact time appeared inversely proportional to feed rate. Peel angle was believed to remain constant since the deliver head is maintained at an angle normal to the tool surface. The tool material varied from alloy to composite with release agents applied in both cases.

Table 3-3 Process variables found in ATL production which could affect performance

Variable	Range	Description
<i>Ambient Conditions;</i>		
<i>Temperature</i>	0-40°C	Ambient conditions may change according to local weather conditions
<i>Relative Humidity</i>	0-95%	
<i>Tape Temperature</i>	0-80°C	Can be adjusted using a hot plate mounted just before the compaction tool
<i>Feed Rate</i>	0-48m/min	Completely adjustable following the NC program is likely to slow for intricate cutting and placement operations
<i>Application pressure</i>	265-1300N per 150mm wide shoe	The pressure applied by the compaction shoe is adjustable, limited by the rigidity of the mould tool
<i>Tool material</i>	Aerospace - alloy Wind - composite	The mould tool can be constructed in a range of materials from steel to glass fibre composite
<i>Tool surface finish</i>	Typically smooth	Variability in tool surface finish is likely, dependant on mould tool quality and material
<i>Tool surface treatment</i>	Typically release agent	The use of release agents is likely to reduce tack significantly

Wind energy ATL moulds

The feasibility of low cost low stiffness wind energy ATL tooling in comparison to high cost high stiffness aerospace tooling was also considered within the trials. The dimensions represented the upper surface of a FFA-W3-241 typical wind turbine aerofoil [155] mirrored with a symmetrical taper for simplicity (Fig 3-3). The composite moulds

with steel lattice structure are typical of those used in the wind turbine industry with the following novel exceptions:-

- Low energy heating elements embedded within the mould laminate.
- Facility plates and blocks for post automation forming operations to overcome the 15° angle limitation of the ATL machine.

Novel low energy heating elements were used to improve temperature control and reduce thermal lag in comparison to traditional externally mounted elements. Facility plates and blocks were used in post ATL manual handling operations to form leading and trailing edge features which exceeded the 15° surface limitation. Lay-up was firstly carried out on a gently curved surface not exceeding angle limitations then blocks were inserted under the laminate to post-form the leading and trailing edge geometries (Fig 3-4).

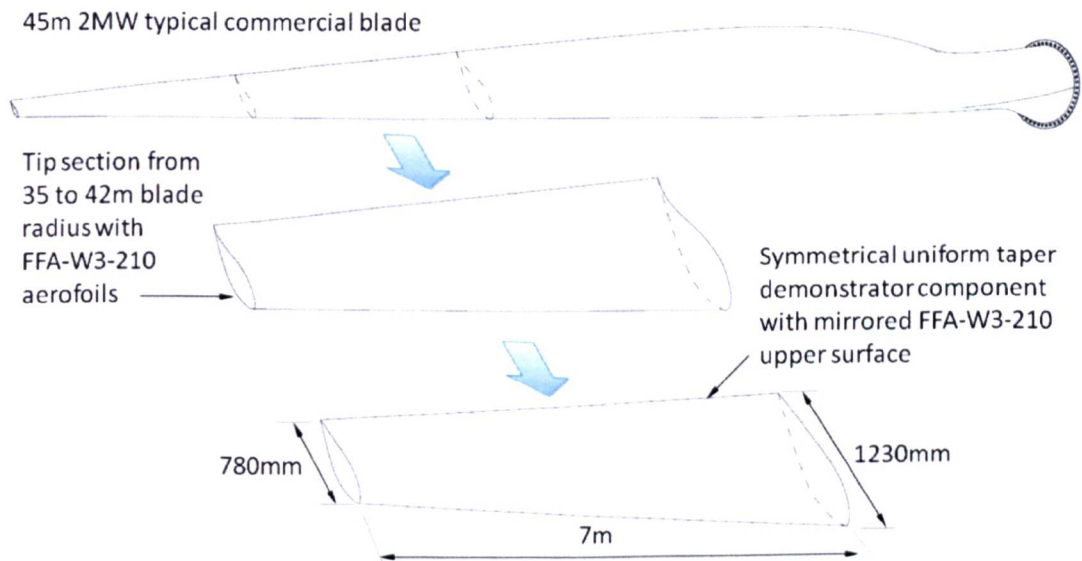


Fig 3-3 The demonstrator component which is a representative section of a typical commercial 45m turbine blade



Fig 3-4 Demonstrator moulds with plates to allow ATL lay-up on surfaces below 15° (left), blocks are then inserted to form leading and trailing edges (right)

3.3 Tack and stiffness test

3.3.1 Operation

The new peel test is a development of the floating roller method (Chapter 2.4.2). Spring loaded rollers were added to allow a regulated application method. The prepreg sample could then be instantaneously applied and peeled in a single continuous motion. Contact time is inversely proportional to feed rate which simulates the ATL process. The prepreg sample is pulled through the spring loaded rollers which provide an application force against a rigid substrate which represents the mould surface. The first rollers are used to guide the plate. The second rollers provide the peel and application force. 90° peel occurs instantaneously against the fixed top roller as the compaction force is applied by the spring loaded bottom roller.

Results were recorded for two sections in a continuous test. Stiffness was recorded for the first section of the test where the sample had a thin film covering both surfaces. The covering film was absent for the second section of the test where peel resistance was recorded (Fig 3-5). By subtracting the average stiffness from the average peel resistance a value for tack could be calculated with minor adjustment for the absence of the covering film (Appendix B).

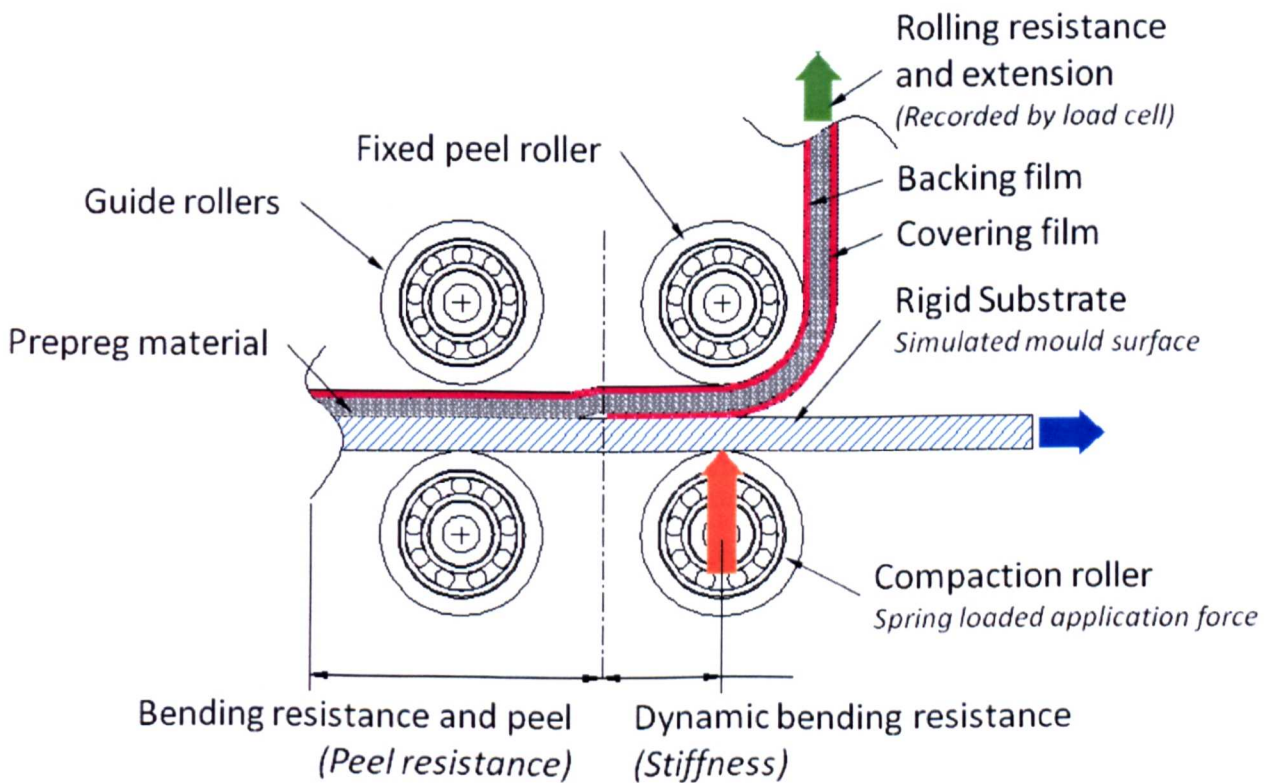


Fig 3-5 Operating principle of the new prepreg tack and stiffness test

3.3.2 Equipment

Equipment was mounted to a universal test machine. Peel resistance and stiffness was then measured continuously over a pre determined peel distance using a load cell. Extension and load values were recorded for later analysis. To allow for temperature changes the test rig was enclosed in an oven limiting the specimen size (Fig 3-6).

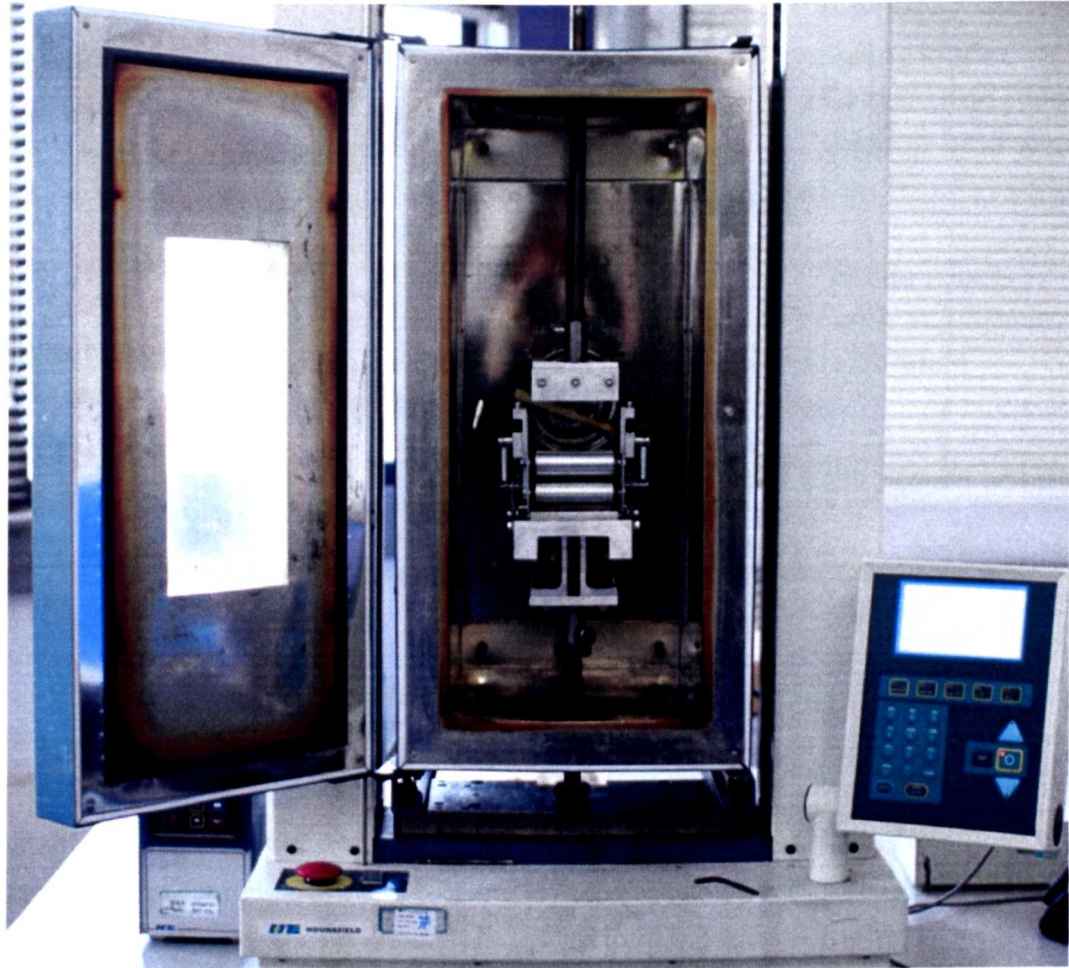


Fig 3-6 Peel test equipment mounted in a universal test machine

Design features allowed variables found in ATL production (Table 3-3) to be investigated (Fig 3-7). Commercial ATL conditions could be recreated within reasonable limitations imposed by test equipment (Table 3-4). Jacking screws were used to control the compaction force. A force of 250N was possible across the length of the roller. This force is within the lower region of the 130-650N specified by ATL manufacturers [156]. The compaction force is limited by the size of the roller bearings, springs and the cost of construction. Larger springs would require larger shaft and roller diameters resulting in a deviation from British standard specifications [96] and increased construction costs.

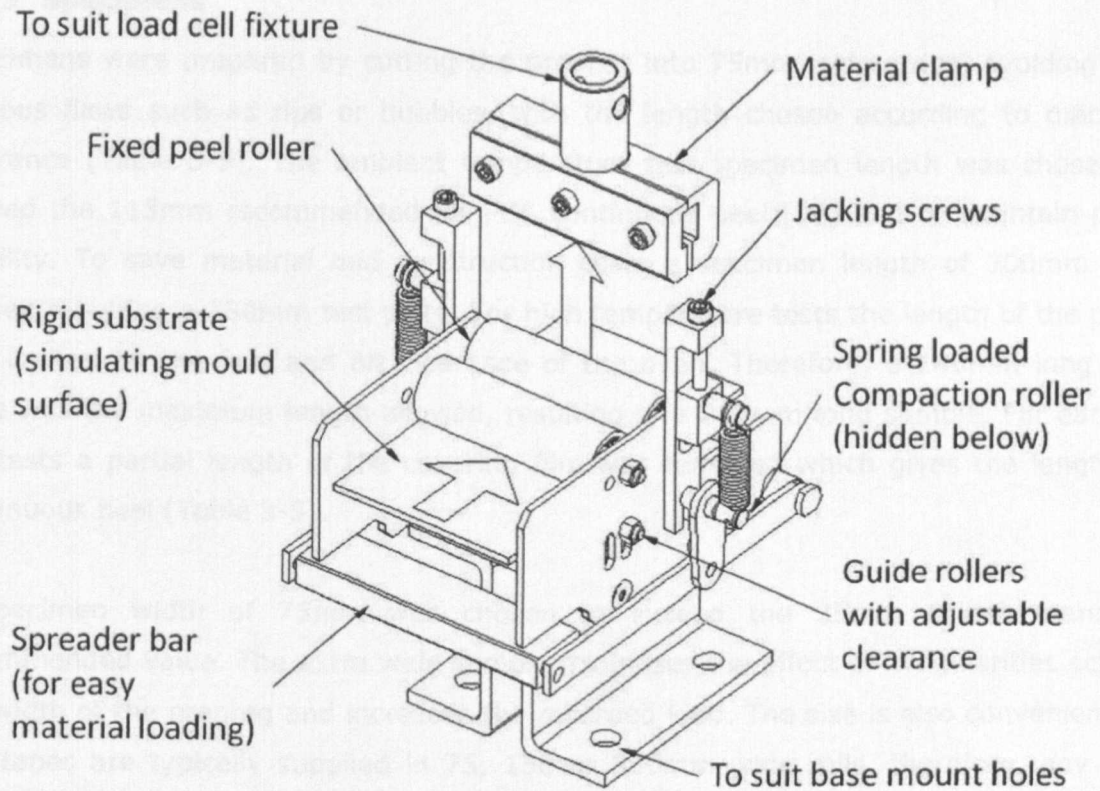


Fig 3-7 Features of the new tack and stiffness test

An environmental chamber was unavailable due to budget constraints. Therefore, relative humidity was recorded but not controlled. Feed rate was adjusted via controlling software, limited to a maximum of 1000mm/min. The solid substrate plate could be made from any rigid mould material and treated with release agents to simulate mould conditions. Adjustable clearance between the rollers allows for up to 6mm thickness of substrate and prepreg material.

Table 3-4 Production variables in comparison to test limitations

<i>Production variable</i>	<i>Production range</i>	<i>Test range</i>	<i>Limitation</i>
Temperature	Ambient-80°C	Ambient-150°C	Oven capabilities
Relative humidity	5-95%	Uncontrolled	Environmental chamber absent
Feed rate		0.01-1000mm/min	Test m/c
Application pressure	130-650N	25-250N	Springs, construction costs
Mould surface	Unlimited	Any plate and prepreg	6mm total roller clearance
ATL tape thickness	0- >1mm		

3.3.3 Specimens

Specimens were prepared by cutting the prepreg into 75mm wide strips, avoiding any obvious flaws such as rips or bubbles, with the length chosen according to machine clearance (Table 3-5). The ambient temperature test specimen length was chosen to exceed the 115mm recommended for PSA continuous peel [96] and to maintain plate stability. To save material and construction costs a specimen length of 300mm was chosen requiring a 250mm test plate. For high temperature tests the length of the plate was limited by the fore and aft clearance of the oven. Therefore, a 140mm long test plate was the maximum length allowed, resulting in a 215mm long sample. For each of the tests a partial length of the covering film was removed which gives the length of continuous peel (Table 3-5).

A specimen width of 75mm was chosen to exceed the 25mm British standard recommended value. The extra wide sample minimises the effect of irregularities across the width of the prepreg and increases the recorded load. The size is also convenient as ATL tapes are typically supplied in 75, 150 or 300mm wide rolls, therefore, any ATL tape can be tested with a minimal number of cuts.

Table 3-5 Rigid substrate and specimen dimensions used in tack and stiffness tests

Temperature chamber?	With		Without		Recommended For PSA [96]
	L	W	L	W	
Rigid substrate (test plate)	140	80	250	80	W=25
Specimen	215	75	300	75	
Results					
Length of stiffness	≈50		≈60		N/a
Length of continuous peel	80		140		115
Total test extension setting	130		200		N/a

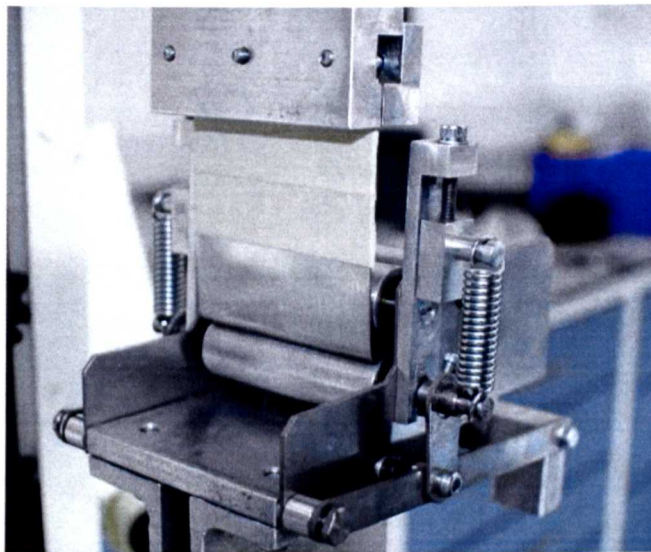
3.3.4 Accuracy

The accuracy of measurement devices exceeded that of equipment used in a production environment (Table 3-6). The peel test rig was mounted in a Hounsfield H25KS universal test machine where measurements of force and extension were taken. Ambient temperature and relative humidity was recorded in the room or oven chamber during a temperature test. Prepreg temperature was taken using an IR thermometer pointed in the centre of the peel area immediately following the test.

Table 3-6 Accuracy of measurement devices

Variable	Instrument	Range	Accuracy
Ambient relative humidity	UEI DTH10 Pen type hygrometer	5-95%	±5%
Ambient temperature		-10-80°C	±1°C
Fabric temperature	Fluke 62Mini IR Infrared thermometer	-30-500°C	±1°C
Extension	Hounsfield H.T.E H25KS Bench top universal testing machine	0-1100mm	±0.001mm or ±0.01%
Feed rate		0.001- 1000mm/min	±0.005%
Force	SM-1000N-457 1kN load cell	0-1000N	±0.5%

The compaction roller was calibrated in order to quantify the amount of application force applied to the prepreg. This was done by inserting a rigid L shaped plate connected directly to the load cell using the fabric grips (Fig 3-8). The L shape plate rests directly on the sprung roller. The spring jacking screws were then tightened to give the starting point of the calibration. Further turns were made to give a force per number of screw turns. The test was repeated to give a linear relationship. A chart was then produced to give the number of turns for the required compaction force (Fig 3-9). During testing the first sample was loaded and the screws pre-tensioned followed by the necessary number of turns using an Allen key to give the desired compaction force.

**Fig 3-8** Compaction roller force calibration using an L shaped bracket

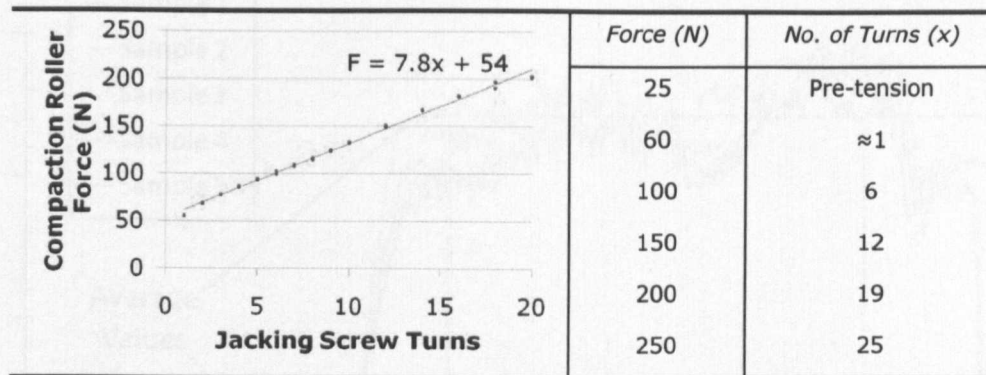


Fig 3-9 Compaction roller calibration results and jacking screw settings

Contaminates at the surface were found to affect adhesion, therefore the following cleaning procedure was observed on all rigid test plates between all tests:-

- Wipe heavy resin deposits using well soaked acetone cloth
- Wipe remaining residue using a clean cloth lightly coated in acetone
- Ensure rigid plates are streak free
- Wash with soapy water
- Wipe with clean dry cloth
- Allow plates to fully dry and return to ambient temperature before testing

3.3.5 Analysis

Typical results for a medium tack prepreg showed an increase in rolling resistance at the transition from stiffness to peel resistance sections of the test (Fig 3-10). Average values for both sections of the test were calculated over the applicable area (Table 3-7). Care was taken to exclude or avoid any unreasonable peaks resulting from surface defects in the prepreg or backing paper such as bubbles or folds. The values for stiffness and peel are expressed as force per unit width N/75mm. Standard deviation for a single sample (Eq 3-1) is shown as error bars on line or scatter plots. Where possible, for samples with high variability, batch testing was carried out using 3-5 samples. The batch standard deviation (Eq 3-2) is displayed as error bars on bar charts. The sample deviation gives an indication of the uniformity of peel in a single test. A lower value indicates steady state peel and an exceptionally high value may indicate the stick-slip condition. Batch deviation is expressed to determine the uniformity between samples, but may also appear high during unsteady peel.

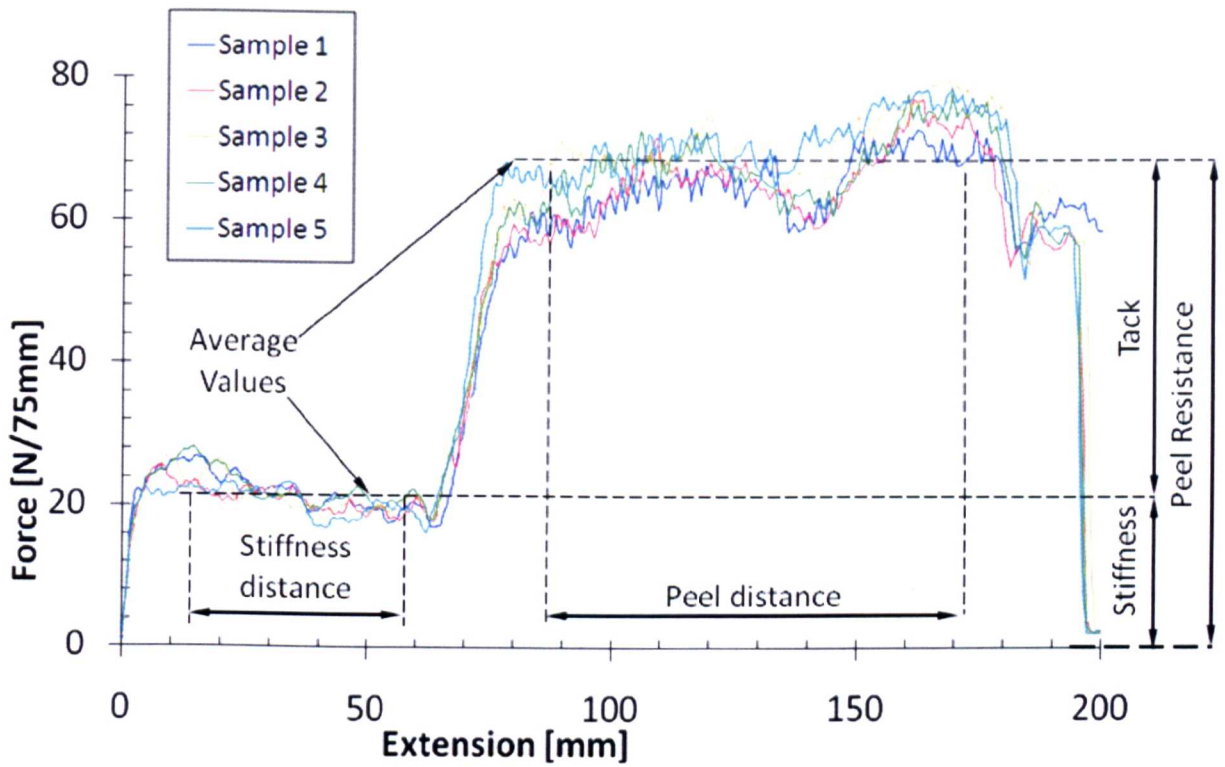


Fig 3-10 A typical five sample test result where stiffness and peel resistance are recorded allowing average tack to be calculated

Table 3-7 Typical extension range of measurement areas

Extension range	Ambient	With oven
Total	200mm	130mm
Stiffness	≈20-50mm	≈10-35mm
Peel resistance	≈80-180mm	≈55-110mm

Eq 3-1 Standard sample deviation

where :-

$$\sigma_s = \sqrt{\frac{1}{n} \sum_{i=1}^n (x_i - \mu_s)^2}$$

σ_s = Standard deviation in a sample

μ_s = Average tack or stiffness value

x = Tack or stiffness values

n = Number of values

Eq 3-2 Standard batch deviation

where :-

$$\sigma_b = \sqrt{\frac{1}{n} \sum_{i=1}^n (x_i - \mu_b)^2}$$

σ_b = Standard deviation in a batch

μ_b = Average batch tack or stiffness value

x = Average sample tack or stiffness values

n = Number of samples

3.3.6 Repeatability study

A number of experiments were repeated to ensure that the newly developed tack test gave consistent results. Initial settings were chosen based on typical ATL process parameters at the start of lay-up (Table 3-8).

Table 3-8 Settings used for initial validation tests

Test Setting	Value
Compaction Force	200N
Feed Rate	100mm/min
Temperature	20°C

Nine epoxy glass fibre prepreg samples of the same stock with a tackier control prepreg were supplied by the manufacturer and tested in batches of three samples (Fig 3-11). The nine similar materials measured an average tack level of 4.8N with a 0.8N (16%) standard deviation, which was considered acceptable considering environmental fluctuations of 20% RH and 1°C in temperature (Table 3-9). The tackier sample registered a significantly higher reading of 17N consistent with expectations.

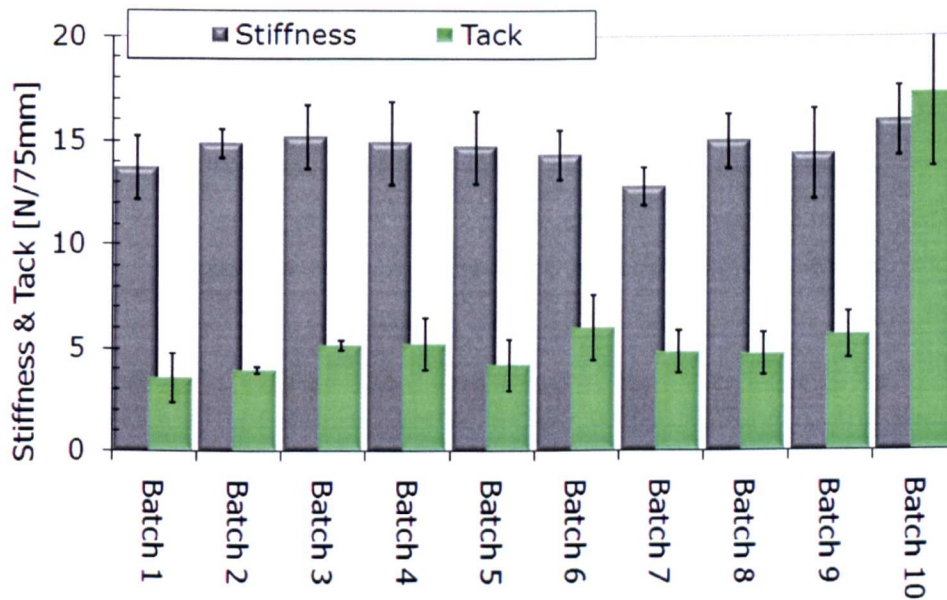


Fig 3-11 Results of a repeatability experiment (Batch 1-9) which successfully identified a tackier control sample (Batch 10)

Table 3-9 Results of the repeatability study

Sample	1	2	3	4	5	6	7	8	9	10 (Control)
Test Date	29/05/2008					30/05/2008				
Temp °C	19.2	19.4	19	19.2	19.2	19.5	19.3	18.5	18.8	19.8
%RH	44	43	43	42	42	49	46	47	57	59
Stiffness	13.69	14.86	15.19	14.9	14.69	14.3	12.8	14.97	14.36	15.91
σ_{sample}	1.53	0.67	1.53	1.98	1.73	1.17	0.92	1.3	2.16	1.65
Tack	3.58	3.94	5.14	5.2	4.16	5.96	4.81	4.71	5.62	17.2
σ_{sample}	1.2	0.16	0.25	1.26	1.24	1.58	1.01	1.02	1.12	3.5
Av. Tack	4.791									
σ_{batch}	0.786	16.4	%							
Av. stiffness	14.418									
σ_{batch}	0.756	5.2	%							

3.3.7 Controlling uncertainty

Observations during the test development revealed potential sources of error which were controlled to improve the reliability of results (Table 3-10). Cleaning and handling procedures were found to significantly affect experimental results. Therefore, a rigorous cleaning schedule was followed. Rubber gloves should be worn at all times as sweat residue deposited by finger prints on test plates before the test were seen to have a detrimental effect during the peel test (Fig 3-12). Any residue left by solvents or cleaning agents was removed from the rigid plates. Handling of the prepreg was minimised before the test to reduce body heat transfer to the sample and plate. The position of the rigid plate in relation to the prepreg appeared to cause fluctuation in results. Leaving an excessive plate overhang could cause the plate to lift and drop within the clearance of the guide rollers leading to oscillations in the recorded force. Therefore, the rigid plate was consistently positioned approximately 5-10mm from the end of the prepreg sample.



Fig 3-12 Finger print residue on the rigid substrate prior to testing was revealed in resin deposition patterns after peel

Samples where resin remained attached to the backing paper after peeling were discarded. Patches of lost resin can be seen as an area where tack is reduced in a visual inspection of rigid plate after testing (Fig 3-13). Defects in the prepreg material are seen to have a detrimental effect on results, with lumps, bumps, folds or tears showing up as artificial peaks in force as they pass through the rollers (Fig 3-13). Therefore, uniform samples with the absence of defects were chosen where possible.

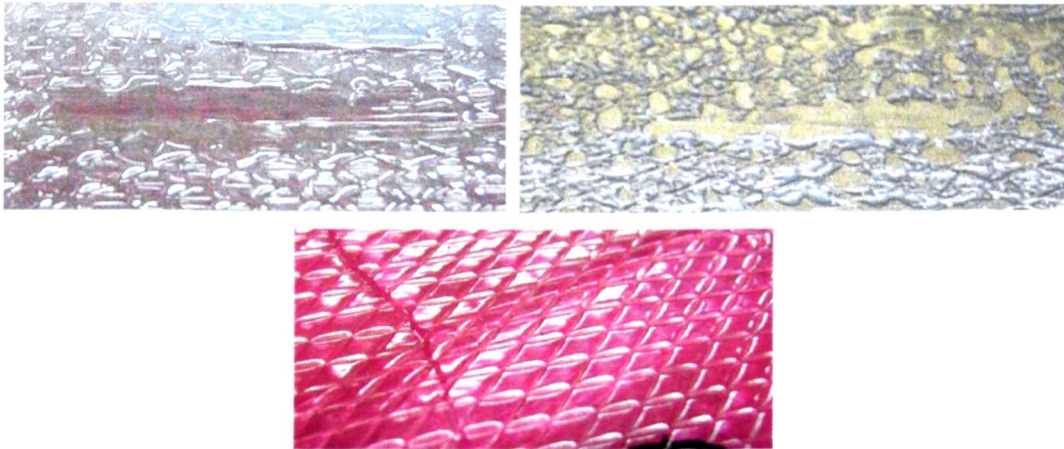


Fig 3-13 Dry resin patches on the prepreg (top left), were seen to reduce tack levels during the test, observable by lost resin patches on the test plate (top right). Bubbles and folds in the backing film (bottom) appear as artificially high levels of tack

Table 3-10 A summary of observed sources of experimental error

Cause	Effect	Control
Environmental		
Temperature fluctuations	<i>Severe</i>	Use a temperature regulated room or environmental chamber.
Relative humidity fluctuations	<i>Low</i>	
Setup and procedure		
Temperature fluctuations through excessive handling	<i>Severe</i>	Minimise handling, use rubber gloves, allow sample to cool after handling.
Sweat or grease residue on rigid plates	<i>High</i>	Avoid skin contact with rigid plates, use rubber gloves.
Excess resin on test rig	<i>Med</i>	Clean with acetone.
Plate oscillations during testing	<i>Med</i>	Ensure the rigid plate is always positioned only 10mm from the end of the prepreg.
Material		
Uncontrolled sample roll location	<i>Severe</i>	Only samples cut from the same position along the width and on the same face should be compared.
Uncontrolled sample face		
Rips, tears, folds or defects	<i>High</i>	Chose uniform samples in good condition.
Resin remains on backing film	<i>Severe</i>	Reject samples where resin remains on the backing paper after peeling.

Dwell time

Once the prepreg is loaded it is allowed to rest on the rigid substrate until the start of the test. This dwell time could potentially affect results since contact occurs. Therefore, a dwell time test was conducted over three levels; zero, two and ten minutes. The results show no noticeable effect on prepreg tack and stiffness exceeding experimental error (Table 3-11). However, a negligible rise in compliance is attributed to the formation of excess resin squeezed out in front of the compaction roller during the dwell period. A raised pull force was recorded during this initial compliance stage which is mostly outside the area of analysis but may affect the results. Therefore, although significant effects are not observed, dwell time is minimised during testing.

Table 3-11 Dwell Time Results

Dwell Time (Mins)	0	2	10		[%]
Stiffness [N/75mm]	34.06	37.2	38.32	Effect	11.1
σ	1.77	1.33	1.33	σ	4
Tack [N/75mm]	65.42	50.07	56.9	Effect	23.5
σ	24.73	21.14	23.76	σ	40.4

Radius of bending

Previously, separating material stiffness from peel resistance required a significant number of calculations and additional measurements [98]. However, in the new test, stiffness was measured during the first stage of the test where a thin film covers the tack surface. The radius of bending was seen to change between the stiffness and peel sections of the test when the peel force is high. For the stiffness section the sample typically followed the radius of the roller. During the peeling section the prepreg may be retained on the plate surface extending away from the roller, resulting in a reduced bending radius (Fig 3-14). The presence of the fibres ensures that the change in radius remains small in all but the highest tack situations, in which the bending force is considerably lower than tack. The effects of a change in radius are therefore considered negligible in the comparison of prepregs with similar stiffness.

**Fig 3-14** Deviation in bending radius from the roller radius during high tack peel

Negative tack

Negative tack values for very low tack materials were recorded. A portion of the negative tack value is attributed to the bending resistance of the covering film which is present in the stiffness section but absent from the peel resistance. Therefore, when stiffness is removed from peel resistance a negative value could be found. To account for the bending stiffness, films were calibrated (Appendix B) and the relevant value (Table 3-12) added to the average peel resistance.

Table 3-12 Backing film calibration values

Backing film	Calibration Value
Embossed polythene	4N/75mm
Red Polythene	1N/75mm
Clear PET	0.3N/75mm

A small negative value, less than 2N, for tack may still be observed in extremely low tack results after the backing film correction has been made. Negative tack values appear illogical, signifying that the surfaces are repelled, which is observed as zero tack in practice. Therefore, all negative tack values are considered negligible and regarded as zero tack. These additional small negative tack values are attributed to:-

- Unusually high average stiffness values attributed to imperfect bending or folds, most often seen in stiff samples. Efforts should be made to avoid anomalous peaks in rolling resistance when analysing results.
- A small frictional interaction between the film and the prepreg during bending which is not included in the calibration of the films.
- Changes in the bending radius between the stiffness and peel section.

3.4 Commercial prepreg tack characterisation

Several wind energy materials of various resin types, fibre weights and architecture were characterised to determine the reliability and applicability of the new tack and stiffness test to hand lay prepregs. Testing existing prepregs also allowed tack values to be compared with the 'high', 'medium' or 'low' tack levels published on accompanying datasheets.

Batches of five samples were tested for each material (Table 3-13), repeated three times, with 60 samples in total (Table 3-14). Each repeat represents testing on a different day where the rig was removed and replaced on the test machine between each occasion to include set up deviations which may occur. The position of each sample within the roll was recorded to allow for the distribution of prepreg tack across the roll width to be investigated (Fig 3-15). A further 24 experiments were carried out to

determine if tack and stiffness are dependent on the face tested. Three samples from each face (Fig 3-15) were tested for each of the four commercial prepregs, 24 samples in total. Experiments were carried out at ambient temperature (20°C), 100mm/min feed rate with 100N of compaction pressure.

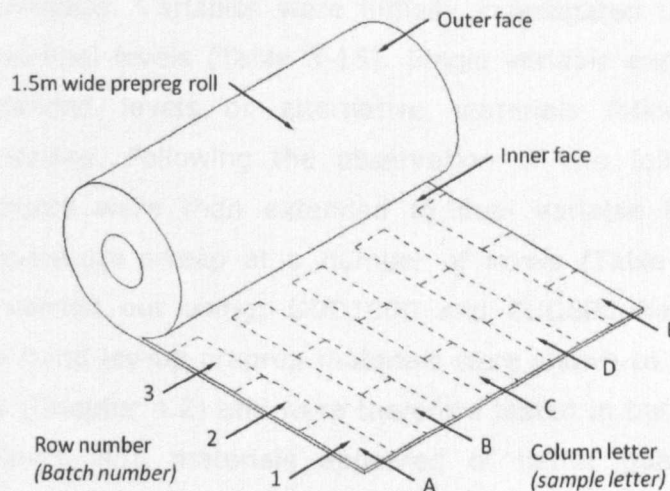


Fig 3-15 Specimen location for analysis of tack and stiffness variability as a function of roll position and face

Table 3-13 Specification of tested Hexcel commercial prepregs

Ref.	Supplier ref.	Fibre weight	Fibre direction	Resin cont.	Manf. Specified tack level
GB600	M9.6/45%/BB600/G	600 g/m ²	Biaxial $\pm 45^\circ$	45%	Medium
GT1200	M9.6/38%/LBB1200/G	1200 g/m ²	Triax 0 $\pm 45^\circ$	38%	Medium
GUD1600	M9.1F/32%/UD1600/G	1600 g/m ²	UD 0°	32%	High
CUD600	M9.6FLT/32%/UD600/CHS	600 g/m ²	UD 0°	32%	Low

Table 3-14 Experiments carried out in the characterisation of commercial prepregs

Test Type (variable)	Test ref.	Material	Details	Samples
Tack and stiffness (characterisation and roll width position)	PP-TT1	GB600	3 samples from each roll position, 1 sample between each set up for each material at 20°C, 100mm/min, 200N compaction force	15
	PP-TT2	GT1200		15
	PP-TT3	GUD1600		15
	PP-TT4	CUD600		15
Tack and stiffness (roll surface)	PP-TT5	GB600	3 samples from each face for each material, 20°C, 100mm/min, 200N compaction force	6
	PP-TT6	GT1200		6
	PP-TT7	GUD1600		6
	PP-TT8	CUD600		6

3.5 Effect of variables on tack and stiffness

3.5.1 Tack and stiffness tests

The new test method was used to investigate the effect of ATL process variables and prepreg material variables. Variables were initially investigated using single variable experiments with minimal levels (Table 3-15). Single variable experiments were then repeated with extended levels or alternative materials following results which contradicted expectations. Following the observation of two failure mode types, a number of experiments were then extended to dual variable investigations which consisted of a temperature sweep at a number of levels (Table 3-18). Single level experiments were carried out using; GUD1600 and CUD600 hand lay-up prepregs (Table 3-17). These hand lay-up prepreg materials were shown to contain a significant degree of variability (Chapter 4.2) and were therefore tested in batches of three to five samples at each level. ATL materials appeared of better quality and uniformity producing results with greater consistency. Therefore, temperature sweeps of 10-11 different temperatures at each level with a single sample for each data point was found to give reasonable results. Variables not under observation were controlled at reasonably constant values. These were chosen to represent typical ATL lay-up conditions in a UK machine shop (Table 3-16). Following feed rate experiments the feed rate constant was increased to 500mm/min in some GUD1600 experiments to maximise the measurable tack. Humidity and ambient temperatures were found to vary on a daily and seasonal basis dependant on local climate. Therefore, comparison of results between experiments was done with caution. Uncontrolled humidity and material supply constraints prevented large scale full factorial experiments.

Table 3-15 Values used in the investigation of variables

Variable	Levels	Values					Units	
Temperature	Single	16	18.3	22.3	27	30.1	°C	
	Extended	10-70 variable						
Feed rate	Single	50	250	500	750	1000	mm/min	
	Extended	1	2	5	10	20		50
Surface finish	Single	0.12	0.18	0.95	1.92		Ra	
Release agent	Single	None	3 solvent based		3 water based		-	
Surface type	Dual	Glass	Stainless steel		GFRP		-	
Compaction force	Single	100	200		300		N/80mm	
	Dual	25	80		215		wide roller	
Dwell time	Single	0	2		10		Minutes	
Resin type	Single	Low	Med		High		Tack level	
Fibre weight	Single	200	300		400		g/m ²	
Fibre type	Both	E-glass			Carbon		-	
Resin content	Both	30	40		50		%	
Fibre architecture	Both	UD			TRIAX			

Table 3-16 Constant values used in single level investigations

Variable	Fixed Value	Estimated variance
Temperature	20°C	±1.5°C
Relative Humidity	40%	±10%
Feed Rate	100mm/min	±0.005%
	500mm/min	
Compaction force	100N	±5N
Release Agent	None	N/A
Dwell time	10s	±5s

Table 3-17 Hexcel prepreg materials used in the investigation of process variables

Material	Reference	Industrial application
1600 g/m ² Unidirectional E-glass fibres with M9.1F 32% resin content epoxy resin	GUD1600	Hand lay wind energy prepreg
600 g/m ² Unidirectional carbon fibres with M9.1FLT 32% resin content epoxy resin	CUD600	Hand lay wind energy prepreg
400g/m ² Unidirectional E-glass fibres with M19.6LT 28% resin content epoxy resin	WE-ATL	Newly developed wind energy ATL tape
194g/m ² Unidirectional AS4 Carbon fibres with 8552 34% resin content toughened epoxy resin	A-ATL	Existing aerospace ATL tape

Table 3-18 Summary of experiments undertaken in the investigation variables

Variable	Test Ref	Material	Description	Levels	Samples per level	Total
Temperature	T01	GUD1600	Temp sweep	5	5	25
	T02	CUD600		4	3	12
	T03	WE-ATL	Extended temp sweep	11	1	11
	T04	A-ATL	Temp sweep	8	1	8
Feed rate	FR01	GUD1600	Feed rate sweep	5	5	25
	FR02	WE-ATL		8	1	8
Surface roughness	SR01	GUD1600	100mm/min	3	5	15
	SR02		Extended levels 500mm/min	4	5	20
	SR03	WE-ATL	Dual level temperature sweep	4x10	1	40
Release agent	RA01	GUD1600	Single level	6	5	30
	RA02	WE-ATL	Dual level temperature sweep	2X10	1	20
Compaction Force	CF01	GUD1600	100mm/min	3	5	15
	CF02		Extended levels 500mm/min	5	5	25
	CF03	A-ATL	100mm/min	3	3	9
	CF04	WE-ATL	Dual level temperature sweep	3X11	1	33
Surface type	ST01	WE-ATL	Dual level temperature sweep	3X11	1	33
Contact temperature	CT01	WE-ATL	Dual level temperature sweep	2x10	1	20
Resin Type	RT01	Custom	M19.1 (high tack), M19.6 (med), M19.6LT 32% content resins in 200g/m ² FAW prepreg	3	5	15
Fibre areal weight (FAW)	FAW01	Custom	200/300/400 g/m ² FAW in 32% M19.6 med tack resin	3	5	15
Fibre type	FT01	Custom	200g/m ² FAW carbon AS4/E-glass M19.6 30/32% resin content.	2	5	10
	FT02		Dual level temperature sweep	2x11	1	22
Resin content	RC01	Custom	200g/m ² E-glass with 30/40/50% resin content	3	5	15
	RC02		Dual level temperature sweep	3X11	1	33
Fibre Architecture	FA01	Custom	200/1200g/m ² UD/Triax 32% content M19.6 resin	2x8	1	16

3.5.2 Control of variables

Temperature

The test rig was enclosed within a temperature controlled chamber to increase accuracy. Samples and rigid substrates were allowed to dwell at the required temperature for three minutes before testing. Temperature measurements were taken at the prepreg tack surface using an IR laser thermometer immediately after testing.

Feed rate

The feed rate of the new test determines both the peel rate and contact time, where contact time is inversely proportional to peel rate. Therefore, the effect on tack will be the combined effect of an increase in peel rate with a subsequent reduction in contact time which simulates the ATL process. Feed rate is varied by adjusting test parameters within the controlling software.

Surface finish

Surface finished was adjusted by subjecting test plates to varying degrees of polishing or abrasion. Ra=0.12 finish was achieved using polish and a mechanical buffing wheel. Ra=0.18 is the brushed finish of the stainless steel plate as supplied by the manufacturer. Ra=0.95 was produced using rough sand paper. Ra=1.92 was achieved using a bastard file. Surface roughness values were measured using a Mitutoyo Surftest SV-600. Results were found to be in good agreement with observed roughness (Fig 3-16).

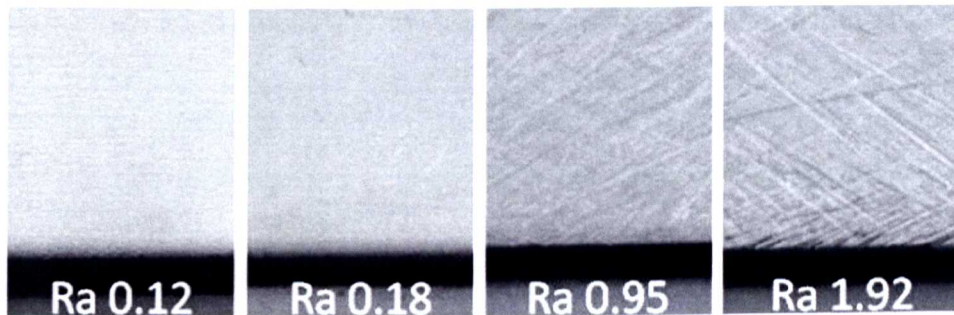


Fig 3-16 Rigid plate simulated mould surfaces with alternate surface finishes

Release agent

Test plates were coated with a range of commercial release agents (Table 3-19). Release agents were applied following manufacturers guidelines. Typically three to five coats were applied, allowing drying for 10 minutes between coats and 30 minutes after the final coat. An untreated stainless surface was also tested as a benchmark. Dual level tests were carried out using a composite test plate coated with Chemlease 41 release agent in comparison to an untreated surface.

Table 3-19 Details of the release agents used in the single level experiment (Ref.RA01)

<i>Name</i>	<i>Manufacturer</i>	<i>Carrier Base</i>
Chemlease PMR-90	Chemtrend	Solvent
Watershield	Zyvax	Water
Multishield	Zyvax	Solvent
Enviroshield	Zyvax	Water
Composite Shield	Zyvax	Solvent

Compaction force

Compaction force was varied by adjusting the tension of the springs connected to the compaction roller using jacking screws. The total force acting over the 75mm wide Ø25mm roller was calibrated using the load cell (Chapter 3.3.4). To improve repeatability the jacking screws were set using the first sample and remained in a fixed position for the duration of the experiment. The test rig allowed the springs to be spread for sample loading without tension adjustment.

Contact temperature

Contact temperature was adjusted by pre-applying prepreg samples to the test plates using the test rig without peeling. This was achieved by placing a thin film into the jaws of the test rig and through the rollers. The test plate and sample were then loaded into the rig without clamping onto the prepreg. The plate and sample and test rig were contained within the oven heated to 40°C. A dwell time of 10 minutes was allowed for the sample to reach the required temperature. The film was then pulled at 500mm/min using the universal testing machine. The result was 40°C, 500mm/min applied samples under 100N compaction force without peeling. Samples were then allowed to cool to ambient temperature before testing proceeded as normal. Samples were compared to standard testing where application is instantaneous under the compaction roller at the time of and temperature of peeling.

Surface type

Additional test plates were manufactured from tempered glass and glass fibre reinforced epoxy composite. Composite plates were constructed and finished to match the mould surface typically found with wind energy mould tools. Test plates were compared with stainless steel plates used throughout other experiments.

Resin Type

Prepreg samples were prepared by the manufacturer using unidirectional E-glass 200 g/m² impregnated with 32% BPA epoxy resin content with varying degrees of B stage reaction. Three resin types, distinguished by their tack properties, were impregnated using similar methods and equipment; M19.6LT (Low tack), M19.6 (Medium tack) and M19.1 (High tack).

Fibre areal weight (FAW)

Three prepreg materials with M19.6 resin at 32% content were supplied. FAWs were adjusted to 200, 300 and 400 g/m². Five samples were tested for each fibre weight variant. Error bars represent batch deviation within the five samples.

Fibre Type

200g/m² FAW AS4 carbon fibre M19.6 30% resin content prepreg and 200g/m² FAW E-glass M19.6 32%E were supplied by the manufacturer for comparison between glass and carbon fibres.

Resin Content

200 g/m² E-glass unidirectional fibre prepreg was supplied with M19.6 medium tack resin with 30, 40 and 50% content by weight.

Fibre architecture

A sample of triax LBB 1200 g/m² (400@±45°, 400@0°, 400@±45°) E-glass M19.6 32% resin content was prepared for comparison with 200g/m² unidirectional E-glass M19.6 30% resin content. The limitations of the prepreg production method used by the manufacturer meant that equivalent FAWs could not be produced.

3.6 Rheology

Small Amplitude Oscillatory Shear (SAOS) rheology was carried out on prepreg resin samples (Table 3-20) using Ø25mm parallel plates at 3Hz with 500µm resin layer thickness over a 10-40°C temperature range. Resin samples are generic to the resin type, not specific to the prepreg batch, tested at the point of manufacture without aging effects.

Table 3-20 SAOS rheology experiments conducted on prepreg resins

<i>Ref</i>	<i>Resin matl.</i>	<i>Prepreg reference</i>	<i>Details</i>
VI-RH1	M9.1F (High tack)	GUD1600	
VI-RH2	M9.6 (Med tack)	GB600, GT1200	
VI-RH3	M9.6LT (Low tack)	CUD600	SAOS Ø25mm parallel plate, 500µm gap, frequency 3Hz, 10-40°C.
VI-RH4	8552 (low tack)	A-ATL	
VI-RH5	M19.1 (High tack)	WE-ATL & Custom	Generic resin samples supplied independently from prepreg.
VI-RH6	M19.6 (Med tack)	materials for variable	
VI-RH7	M19.6LT (low tack)	investigation	

3.7 Time temperature superposition Investigation

Materials

Two ATL prepreg samples of the same specification (Table 3-21) from different batches and with alternate storage histories (Table 3-22) were used. Each was supplied with a separate resin sample taken immediately prior to impregnation which then experienced an equal storage history as its prepreg counterpart. Prepreg samples were tested using GPC, tack and stiffness testing. Resin samples were tested using GPC, DSC and SAOS rheology.

Table 3-21 Details of ATL prepreg used in the TTS investigation

<i>Prepreg component</i>	<i>Description</i>	<i>Designation</i>
Resin type	Low tack bisphenol-A epoxy	M19.6LT
Fibre Type	E-glass	E
Fibre weight	400g/m ²	400
Resin Content	28% by weight	28%

Table 3-22 Storage history and reference of the prepreg and counterpart resin

<i>Batch</i>	<i>Days at -18°C</i>	<i>Days at 20°C</i>	<i>Prepreg sample Ref.</i>	<i>Resin Sample Ref.</i>
One	120+	4-10	PP1	R1
Two	<30	3	PP2	R2

Tack and stiffness tests

Tack and stiffness of PP1 and PP2 prepreg samples were measured using the new tack test equipment and procedures (Chapter 3.3) in isothermal feed rate sweeps (Table 3-23, Table 3-24). The accuracy of temperature was limited by the oven chamber, which showed difficulty regulating near ambient temperatures due to its design operating temperature being significantly above ambient. Therefore, equal interval isothermal temperatures proved difficult. However, accuracy was maintained by measuring prepreg temperatures at the prepreg peel surface immediately following completion of the test. The average temperature of all samples tested at each oven set point was then used to indicate the temperature at each level.

Table 3-23 PP1 prepreg isothermal tack and stiffness test grid

Temperature (°C)	Feed rate (mm/min)									
22.1	1	2	5	10	20	50	100	250	500	1000
27.1	5	10	20	50	100	250	500	1000		
28.6	5	10	20	50	100	250	500	1000		
32.6	5	10	20	50	100	250	500	1000		
35.2	20	50	100	250	500	1000				
41.5	50	100	250	500	1000					

Table 3-24 PP2 prepreg isothermal tack and stiffness test grid

Temperature (°C)	Feed rate (mm/min)									
19.9	1	2	5	10	20	50	100	250	500	1000
25.4	5	10	20	50	100	250	500	1000		
28.2	5	10	20	50	100	250	500	1000		
30.9	20	50	100	250	500	1000				
34.4	20	50	100	250	500	1000				
38.6	100	250	500	1000						
40.9	100	250	500	1000						

Rheology

SAOS rheology experiments were carried out on a Bohlin C-VOR Rheometer with temperature control using an ETC oven with liquid nitrogen cooling. R1 and R2 resin samples were placed between Ø25mm 2.5° cone and plate geometry with a 70µm gap from the plate to truncated cone. Isothermal frequency sweeps of 0.1 to 30Hz, with 16 logarithmic intervals, were carried out at temperatures from 10-40°C at 3°C intervals.

Gel permeation chromatography

All samples were analysed for molecular weight by Gel Permeation Chromatography (GPC) using Polargel-M gel columns. R1 and R2 Resin samples were dissolved in TetraHydroFuran (THF) with a concentration of 7.5-10 mg/ml. Resin was extracted from PP1 and PP2 prepreg by dissolving a patch in THF. The patch size was calculated based on the manufacturer's quoted resin content to give the required resin concentration. The difference in mass between prepreg and un-dissolved fibres was used to ensure the correct solution was obtained. Three tests were run for each resin sample.

Differential Scanning Calorimetry (DSC)

R1 and R2 resin samples were analysed using a TA instruments Q10 DSC. Samples were placed in open aluminium hermetic pans using 50ml/min Nitrogen detector sweeping

gas. Samples of $\approx 8\text{mg}$ were subjected to a 300°C temperature ramp at 5°C per minute to determine cure enthalpy.

Summary

Four test methods were used for ten tests in total (Table 3-25).

Table 3-25 Experiments carried out in the investigation of time temperature superposition in prepreg tack and stiffness

Test Type (variable investigated)	Ref	Matl	Details	Samples
Tack and stiffness	TTS-TT1	PP1	Isothermal feed rate sweeps (Table 3-23, Table 3-24)	45
	TTS-TT2	PP2		46
Rheology (Shear modulus)	TTS-RH1	R1	SAOS $\varnothing 25\text{mm}$ cone and plate, $70\mu\text{m}$ gap, isothermal frequency sweeps of 0.1 to 30Hz, with 16 logarithmic intervals, 10 to 40°C at 3°C intervals.	<10g
	TTS-RH2	R2		
GPC (Molecular weight)	TTS-GPC1	R1	3 samples from each material, resin extracted from prepreg using THF	7.5g/ml, 800ml approx.
	TTS-GPC2	R2		
	TTS-GPC3	PP1		
	TTS-GPC4	PP2		
DSC (Cure enthalpy)	TTS-DSC1	R1	300°C temperature ramp at $5^\circ\text{C}/\text{min}$	$\approx 8\text{mg}$ each
	TTS-DSC2	R2		

3.8 ATL applicability study

WE-ATL material was characterised for tack and stiffness under simulated commercial ATL lay-up conditions using the new test method. Test results were then used to determine the feed rate which gave good tack performance at ambient temperature. ATL lay-up then proceeded using a feed rate which was increased with or without adding temperature according to the WLF time temperature relationship. The aim of this test was to determine if tack and stiffness results and the WLF time temperature relationship are directly applicable to the ATL process.

Materials

Newly developed wind energy ATL prepreg tape (WE-ATL) was used throughout the applicability study. The material was 400 g/m^2 unidirectional E-glass fibres with batch two M19.6LT resin at 28% by wt. content. Therefore, results and WLF equation constants from the time temperature superposition investigation could be used.

Tack tests under ATL production conditions

The following production mould surface conditions were simulated and investigated using the new tack and stiffness test (Table 3-27):-

- Untreated composite test plates replicated the mould material and surface roughness. Rigid plates were cut from the actual ATL lay-up surface and used as a baseline comparison. This surface is not currently viable in production since a release agent is needed for the removal of cured components (Ref. ATL-TT1).
- Chemlease 41 release agent was applied using the recommended application method recreating production conditions without tackifier (Ref. ATL-TT2).
- Chemlease was applied as above. Plates were then brushed with dichloromethane and allowed to dry. This test is used to assess the possible degradation effects on release agent caused by dichloromethane (Ref. ATL-TT3).
- Chemlease was applied as above. Plates were then brushed with tackifier and allowed to dry. Tackifier consisted of 0.16 g/ml of M19.6LT resin dissolved in dichloromethane (Ref. ATL-TT4).

The exact compaction pressure of the ATL head was unknown. Therefore, a roller force of 100N was used to allow for comparison between existing results. A feed rate of 500 mm/min was used as an estimate of ATL speed and to give a comparison between existing results. A temperature sweep of $\approx 20-45^{\circ}\text{C}$ was carried out with a single sample at each temperature, 10-12 samples in total per temperature sweep. Temperatures were recorded at the peel surface using an IR thermometer immediately following the test.

ATL trials

The lay-up of WE-ATL tape at ambient temperature proved problematic and required mould surface tackifier. Tack testing at 500mm/min revealed that a peak tack is obtainable without tackifier at a higher temperature ($\approx 34^{\circ}\text{C}$) exceeding the tack available with tackifier at ambient (20°C) temperature (Chapter 4.6.1). To validate the tack and stiffness results ATL lay-up was attempted at this higher peak tack level without tackifier. To validate the use of time-temperature superposition the WLF equation with constants taken from rheology (Chapter 3.7) were used to determine this peak tack feed rate at ambient temperature. Lay-up began at this feed rate increasing until lay-up failure occurred by lack of mould tack. The experiment was then repeated with temperature increased according to the WLF relationship, where tack was expected to remain constant (Table 3-27).

A Cincinnati V4 contour tape layer was utilised. The ATL's heated shoe was not used, considered wrongly positioned against the backing paper, since heating was required at the mould surface side. Therefore, heating was provided by a digitally controlled heat gun and monitored using an IR thermometer (Fig 3-17). Temperature measurements revealed significant difficulties in maintaining a uniform temperature across the tape using this method.

Peak tack was transposed to ambient temperature using the WLF equation (Eq 4-1) with constants ($C_1=13.76$ & $C_2=59.471$) from rheology (Chapter 3.7). Peak tack without tackifier was calculated to occur at $\approx 4\text{mm/min}$ (Table 3-26). Therefore, ATL processing began at 4mm/min at ambient temperature. Feed rate was then increased without heating. In a separate experiment feed rate was also increased with heating according to the WLF relationship (Table 3-27).

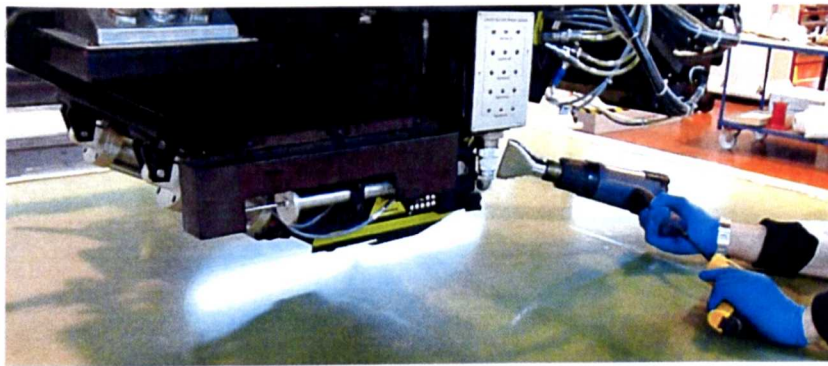


Fig 3-17 ATL heating method using a heat gun and IR thermometer

Table 3-26 Peak tack feed rate at given ATL tape temperatures according to the WLF relationship with constants found by rheology (Chapter 3.7)

Temp °C	20	22	24	25	26	27	28	29	30	31	32	33	34
Feed Rate	4.3	8.5	17	24	33	47	65	91	128	180	253	356	500

Table 3-27 ATL applicability trial experiments

Test Type	Ref	Details	Samples
Tack and stiffness test	ATL-TT1	Temperature sweep on a composite plate	11
	ATL-TT2	Temperature sweep with Chemlease 41 release agent	11
	ATL-TT1	Temperature sweep with Chemlease 41 and dichloromethane	11
	ATL-TT1	Temperature sweep with Chemlease 41 and tackifier	11
ATL lay-up	ATL-1	Lay-up at 4, 20, 50, 100, 200 & 400 mm/min on a composite surface with Chemlease 41 release agent at 20°C fixed	12m
	ATL-2	Lay-up at 400 mm/min temperature increased according to WLF relationship (34°C)	12m

4 Results and observations

Details of each test methodology can be found in Chapter 3 along with experiment reference numbers and material details.

4.1 ATL feasibility trials

Flat panel BAE ATL recommissioning

Recommissioning the Cincinnati V4 ATL (Ref. ATLF-A01) began with existing aerospace ATL tape at ambient temperature. Difficulties in lay-up were observed with an inability to stick plies to the mould surface where prepreg was retained on the backing paper. This became increasingly problematic in laying the small triangular pieces of the test panel. Problems were associated with a low tack level to the mould surface. Covering the mould with a vacuum bag surface allowed successful lay-up and recommissioning (Fig 4-1).

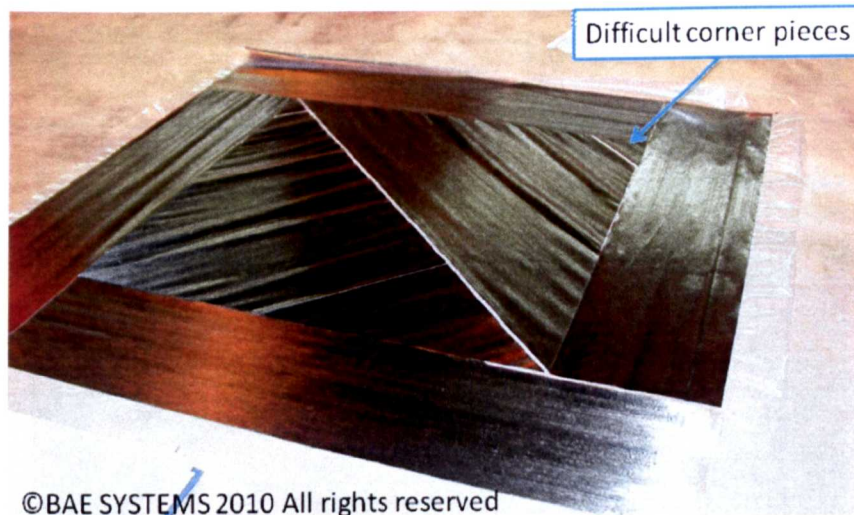


Fig 4-1 Flat panel ATL lay-up of aerospace prepreg over bagging film

Wind energy ATL prepreg trials

The use of M19.1 high tack resin prepreg (Ref. ATLF-W01) was immediately ruled out by the machine operator, considered unsuitable due to too high tack level. Concern was raised over resin build up on ATL machine components, difficulty in unwinding the prepreg roll and inability to remove and reposition misplaced plies.

Lay-up using M19.6 resin, 300 and 400 g/m² E-glass prepreg was also attempted (Ref. ATLF-W02 and 3). The FAW increase was initially minimised to 400 g/m² due to anticipated cutting problems. Positive lay-up performance was achieved, although the tack levels were believed by the operator to be too high, with significant noise and unwanted tack when unwinding the delivery roll. Difficulty in repositioning misplaced

plies was also considered detrimental. No difficulty in cutting was experienced using the Cincinnati V5 standard equipped with ultrasonic cutter knives.

Wind energy prepreg trials

ATL lay-up using the Cincinnati V4 was attempted using 300 to 400g/m² E-glass with M19.6 (medium tack) and M19.6LT (Low tack) 32% resin content (Ref. ATLF-W03 to W06). Lay-up of both materials was hampered by cutting problems (Table 4-1). The problematic cutting was mostly associated with resin build up on the cutter blade (Fig 4-2).

Table 4-1 Cincinnati V4 ATL lay-up failures associated with cutting

Failure	Cause	Description
Incomplete cut	Cutter depth wrong setting	Depth of cut not adequate
	Resin build up	Clean cutting is prevented by blade tip fouling
	Fibres pulled from tape edges	Small bundles of fibres are dragged from the edges of the tape
Backing paper failure	Cutter depth wrong setting	Backing paper breaks due to being scored or cut



Fig 4-2 Resin build up on Cincinnati V4 blades believed to cause cutting difficulties

Cutting was not considered an issue warranting significant research since no problems were found during the SABCA trials when using ultrasonic knives. However, the cutting issue did need to be addressed in order to allow V4 trials to continue. Several changes were implemented during subsequent trials to alleviate cutting difficulties:-

- Changes to the geometry of the cutter blade
- Reducing resin content to 28%
- Utilising M19.6LT low tack resin

Wind energy prepreg trials

Changes to the cutter blade geometry were found to improve cutter performance significantly allowing trials to continue (Ref. ATLF-W07 to 09). A build up of resin on the cutter blade main body remained, however the actual cutting tip appeared to stay clean. Concerns were raised over the excess resin dropping from the cutter blade into the laminate. Therefore, the ATL machine was paused at regular intervals to clean the cutter blades. A low tack resin system (M19.6LT) and reduced resin content (28%) were then preferred on the basis of a reduction in resin build up on the cutter. Other observations were made on material performance. The 600 g/m² prepreg was attempted but proved too difficult to cut. Therefore, FAW was limited to 400g/m² based on cutter performance. The M19.6 resin system displayed marginal difficulty in separating from the backing paper indicating that tack to the backing paper was too high. M19.6LT resin appeared to separate much easier from the backing paper. M19.6 showed moderately improved mould tack in comparison to M19.6LT. A number of methods were then employed to improve mould tack:-

- The temperature of the hot shoe was increased. This appeared to increase tack to the backing paper preventing release with little effect on mould tack.
- A homemade tackifier consisting of prepreg resin dissolved in tetrahydrofuran was applied to the mould surface. Lay-up performance was then considered acceptable.

Despite poor mould tack performance M19.6LT 400g/m² 28% resin content (W-ATL-7) material was selected for lay-up of the demonstrator component since the issue of poor mould adhesion could be overcome using tackifier (Table 4-2).

Table 4-2 Summary of ATL material performance in feasibility trials

Material	Performance				Effect of		Highest score
	Cutting	Backing paper release	Mould tack	Reposition -ability	Mould tackifier	Increased temperature	
A-ATL-1	10	8	2	9	Increased mould tack to 7	Increased mould tack to 5	34
A-ATL-2							
W-ATL-1	1P	1P	10P	1P	Unknown		1
W-ATL-2	5 (Resin build up)	4	5	3	Increased mould tack to 7	Reduced backing paper release to 2	19
W-ATL-3		6	5	3			21
W-ATL-4		7	2	6			25
W-ATL-5		8	2	6			26
W-ATL-6		1 (FAW too high)	NA				1
W-ATL-7	6 (reduced resin build up)	9	2	6	28		

Scale 1=Unable to process, to 10=excellent no problems (P= Predicted result)

Aerospace double curvature contour recommissioning

Successful lay-up of aerospace ATL tape was achieved on a double curvature high stiffness alloy aerospace tool (Ref. ATLF-A02) (Fig 4-3). However, poor mould adhesion was observed with the use of Chemlease 41 release agent. Improvements in mould adhesion were achieved by utilising the hot shoe to increase prepreg temperature and applying tackifier to the tool surface.



Fig 4-3 Aerospace ATL prepreg lay-up on a double curvature mould surface

Wind energy moulds

Wind energy moulds coated with Chemlease 41 release agent were tested using aerospace prepreg materials (ATLF-A03). Tackifier was applied to the mould surface to overcome issues of low tack (Fig 4-4). Full ATL lay-up could not be achieved for any ply direction with a percentage of each ply finished by hand lay-up (Table 4-3). Full lay-up was prevented by Z axis tracking machine errors. These errors are associated with mould dimensions which do not match pre-programmed tool paths based on a 3D CAD model of the mould. The mismatch is associated with:-

- Mould construction tolerances which exceed that of ATL limits
- Mould deflection caused by the compaction force of the ATL head



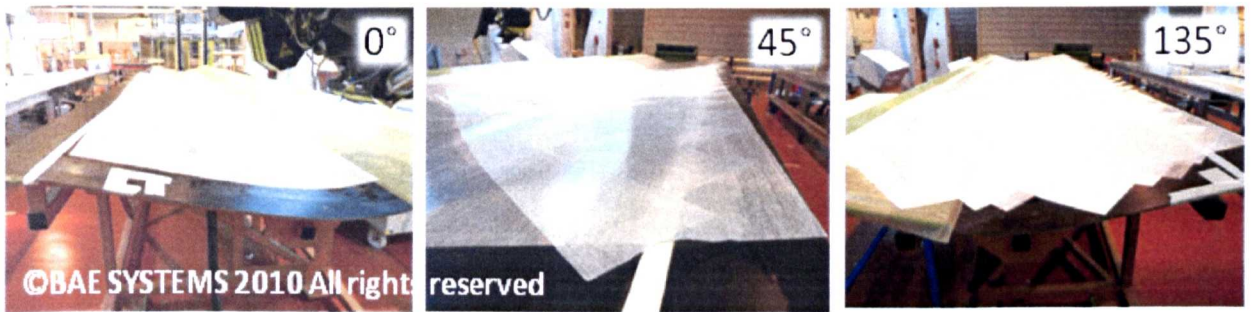
Fig 4-4 ATL aerospace prepreg lay-up on wind energy moulds

Table 4-3 ATL lay-up achieved for each ply direction

Ply direction	Successful ATL Lay-up (approx)
0°	75%
45°	60%
135°	60%

Demonstrator component lay-up

A significant portion (Table 4-3) of each ply direction was laid successfully using ATL (Fig 4-5) (Ref. ATLF-W08). Complete lay-up of each ply was prevented by machine errors as experienced during the previous lay-up (Ref. ATLF-W07). Tackifier was applied to the mould surface to relieve issues of low tack. Incomplete plies were finished by hand to complete the lay-up of the 7m wind turbine representative blade skin (Fig 4-6).

**Fig 4-5** Extent of ATL lay-up of wind energy prepreg plies**Fig 4-6** Hand finishing of plies (left) to complete 7m blade skin lay-up (right)

4.2 Commercial prepreg characterisation

4.2.1 Roll position effects

The majority of commercial prepregs showed differences in stiffness across the roll (Fig 4-7) (Ref. PP-TT1 to 4). The glass triax material showed the greatest increase with up to 10N stiffness towards the centre of the roll. Tack variability was also displayed across most rolls, with the exception of CUD600 carbon sample which displayed insignificant tack levels throughout (Fig 4-8). The GT1200 sample showed a significant increase in tack towards the centre of the roll.

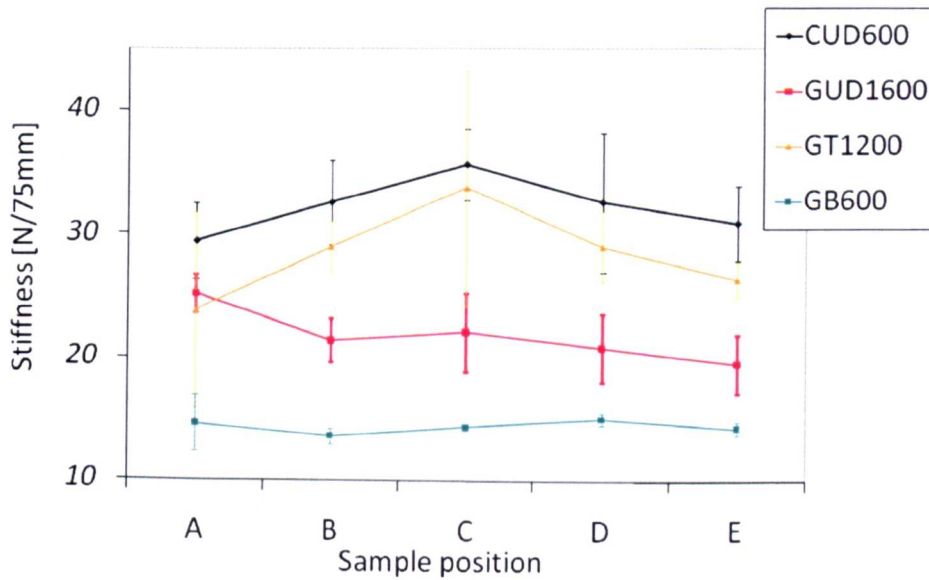


Fig 4-7 Stiffness distribution across the commercial prepreg roll width

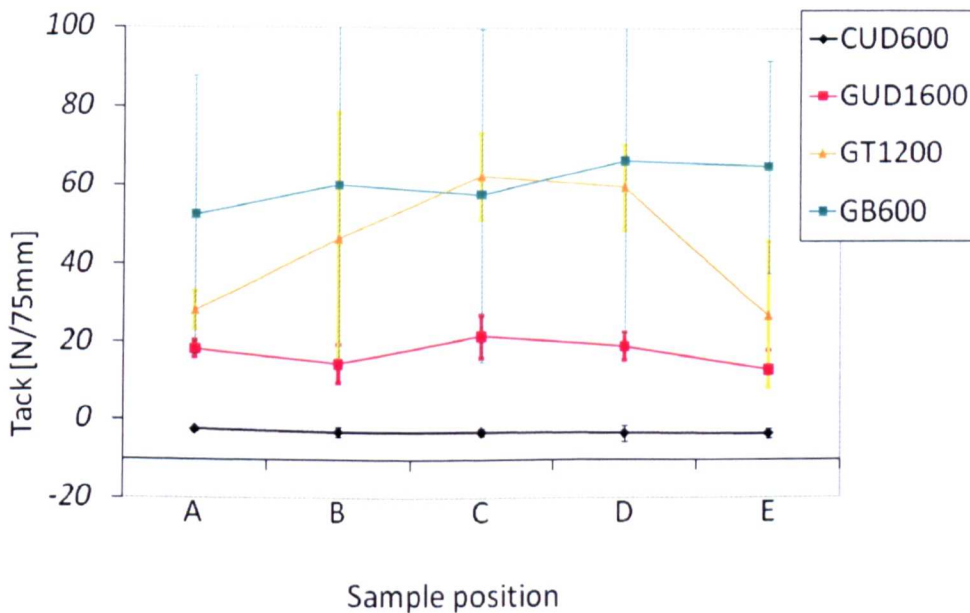


Fig 4-8 Tack distribution found across the commercial prepreg roll width

4.2.2 Face position effects

When testing for differences in tack and stiffness between faces (Ref. PP-TT5 to TT8) stiffness values remained reasonably consistent for all materials (Fig 4-9). However, tack values were found to vary significantly between faces in most prepregs. GT1200 triax sample showed the greatest variation between faces. CUD600 displayed little variation due to its overall low tack properties.

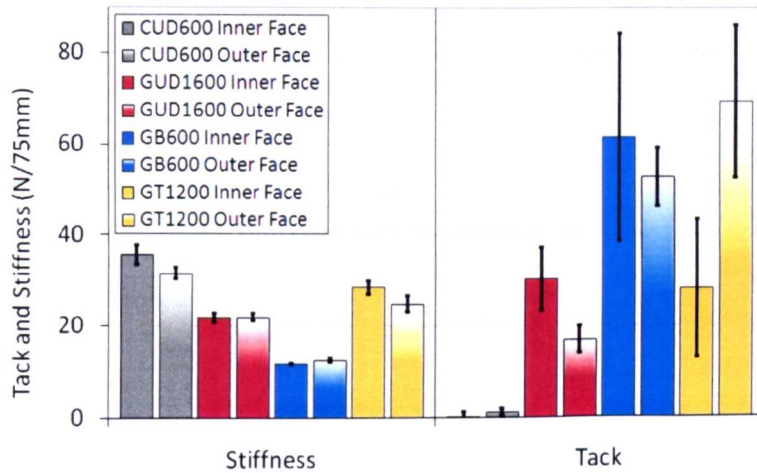


Fig 4-9 Tack and stiffness values between alternate faces of the prepreg roll

4.2.3 Overall characterisation

When comparing prepregs in the characterisation of roll width position (Ref. PP-TT1 to 4) stable and repeatable values were recorded for all stiffness values with minimal standard deviation. Tack values appeared stable and repeatable for unidirectional prepregs with reasonably low standard deviation. However, multidirectional prepregs with increased resin content showed inconsistent tack results with significant deviation between samples and batches (Fig 4-10). These prepregs also differed significantly from manufacturers specified tack levels (Table 4-4).

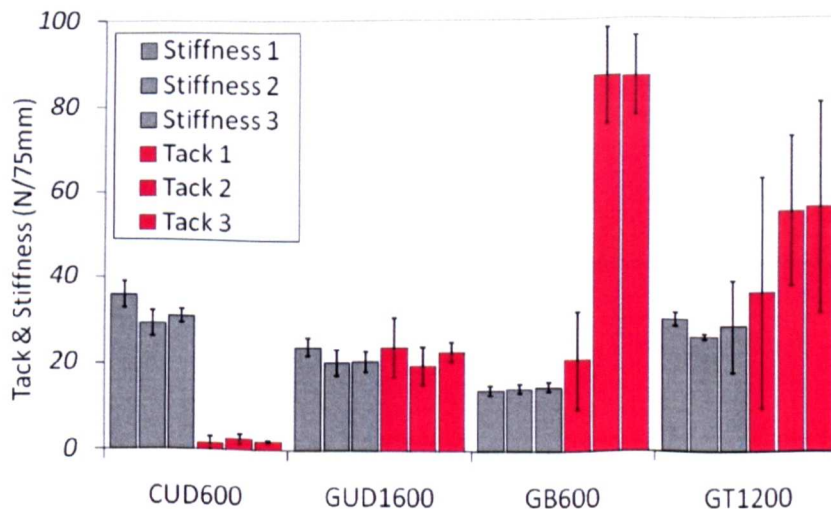


Fig 4-10 Three batch repeatability experiment results (Ref. PP-TT1 to 4)

Table 4-4 Tack and stiffness characterisation results (Ref. PP-TT1 to 4) for existing wind energy prepreg in comparison to specified tack levels

Ref.	Stiffness		Tack		Specified tack level
	[N/75mm]	σ [%]	[N/75mm]	σ [%]	
GB600	14.4	7.4	60	56.2	Medium
GT1200	28.4	20.9	44.4	48.8	Medium
GUD1600	21.8	12.9	17.22	28.44	High
CUD600	32.2	11.9	0	37.9	Low

When comparing the two characterisation studies (Ref. PP-TT1 to 4 and PP-TT5 to 8), the values for prepreg stiffness appeared logical and were consistent between roll position and face studies (Table 4-5). The highest stiffness was measured for CUD600 due to the increased stiffness of carbon fibres in comparison to E-glass. It may be logical for the stiffness of glass fibre prepreg to be directly proportional to material weight. However, GT1200 showed increased stiffness in comparison to GUD1600. Therefore, fibre architecture and increased resin fraction also have an effect. The values for tack are repeatable experimentally but are not always consistent with manufacturer's specified values (Table 4-5). Manufacturers specify tack values based on results of constituent resin tests without the presence of fibres. Multidirectional fabrics display the highest deviation. Therefore, it is likely that fibre direction and resin content also contribute to tack, possibly changing the surface resin layer characteristics, consistent with the findings of prepreg probe test results [83].

Table 4-5 Commercial stiffness and tack results compared to manufacturers values

Matl. Ref.	Fibre type	Resin Content [%]	Fibre weight [g/m ²]	Stiffness [N/75mm]		Tack [N/75mm]		Manufacturers Specified tack level
				position study	Face study	position study	Face study	
GB600	Glass	45	600	14.4	12	60	52.2	Medium
GT1200	Glass	38	1200	28.4	26.7	44.4	43.9	Medium
GUD1600	Glass	32	1600	21.8	21.9	17.22	18.6	High
CUD600	Carbon	32	600	32.2	33.7	0	0	Low

4.3 Effect of tack variables

Results were analysed for consistency maintaining the definition for batch and sample deviation (Chapter 3.3.5). Overall effects were calculated by comparing maximum and minimum values obtained (Appendix C). Dual interaction effects of temperature were found by comparing the integral of each temperature curve (Appendix D). The experimental reference grid can be found in Chapter 3.5 along with details of method and materials used.

4.3.1 Temperature

Results for single level experiments (Ref. T01) with GUD1600 prepreg show a reduction in stiffness and tack with increased temperature (Fig 4-11). Values for standard deviation reveal good levels of certainty (Table 4-6).

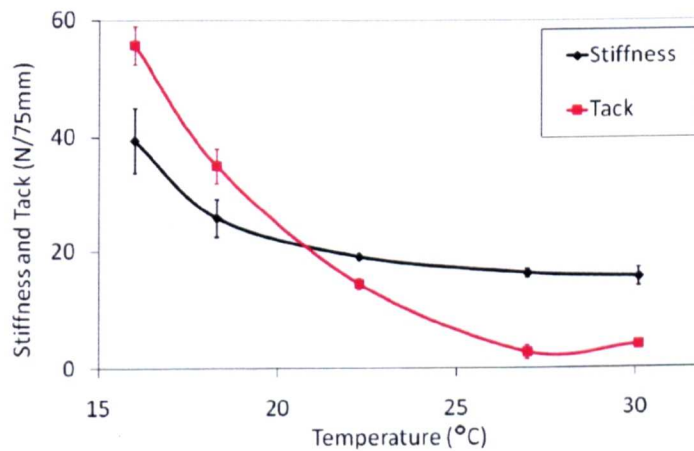


Fig 4-11 Tack and stiffness response to temperature in GUD1600 prepreg (Ref. T01)

Table 4-6 Standard batch deviation in the effect of temperature results

Temperature [°C]	16	18.3	22.3	27	30.1		[%]
Stiffness [N/75mm]	39.37	25.97	19.18	16.36	15.64	Effect	60.27
σ	5.59	3.26	0.48	0.75	1.53	σ	9.96
Tack [N/75mm]	55.73	35	14.49	2.68	3.93	Effect	95.2
σ	3.26	2.98	1	1.12	0.16	σ	7.62

CUD600 prepreg (Ref. T02) showed a similar stiffness decrease response to temperature. However, a contradictory tack response was found showing a significant increase in tack with a 97% effect compared to 23% error (Fig 4-12).

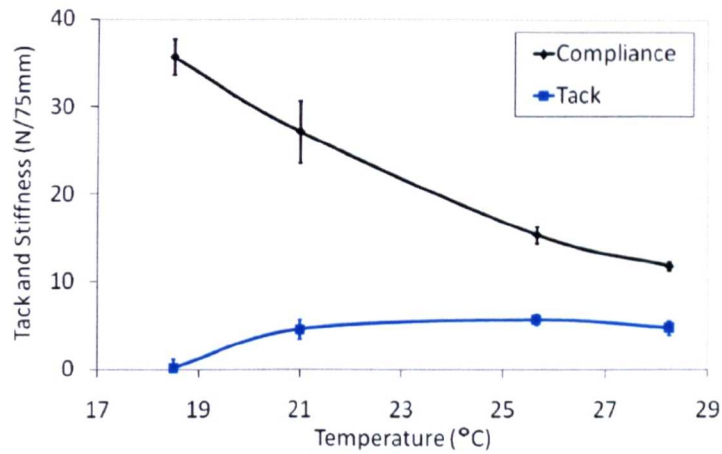


Fig 4-12 Tack and stiffness response to temperature in CUD600 prepreg (T02)

The contradiction in temperature response between GUD1600 and CUD600 prepreps was attributed to an observed change in failure mode (Fig 4-13). At room temperature the CUD600 appeared to exhibit mostly dry failure at the surface whereas GUD1600 was mostly wet viscous failure within the resin.

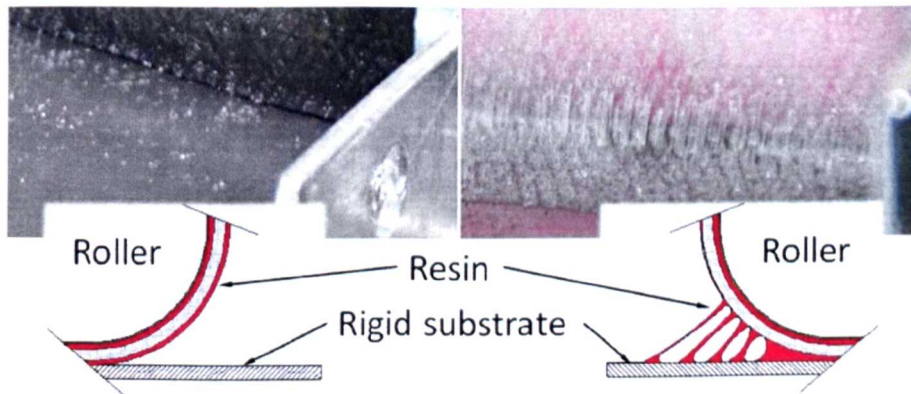


Fig 4-13 CUD600 (left) and GUD1600 (right) peel failure modes at ambient temperature (20°C)

Newly developed wind energy ATL tape (Ref. T03) exhibited both failure modes and a peak in recorded tack over a temperature range (Fig 4-14). The transition in failure mode was evident by examination of the peeling process and rigid substrate following the test. At low temperature surface failure revealed a mostly clean plate with little resin deposition, but as the temperature was increased resin failure was observed with significant resin deposition (Fig 4-15). The transition in failure mode appeared at a temperature consistent with the peak in recorded tack.

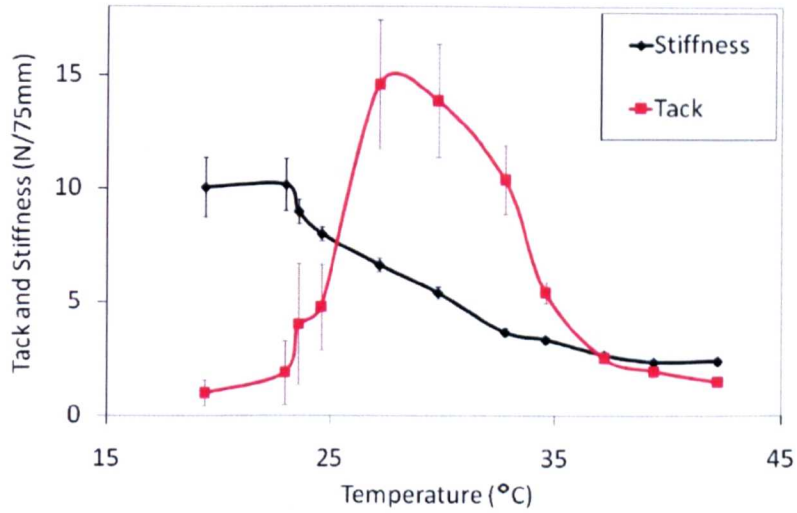


Fig 4-14 Tack and stiffness of WE-ATL prepreg (Ref. T03) temperature response

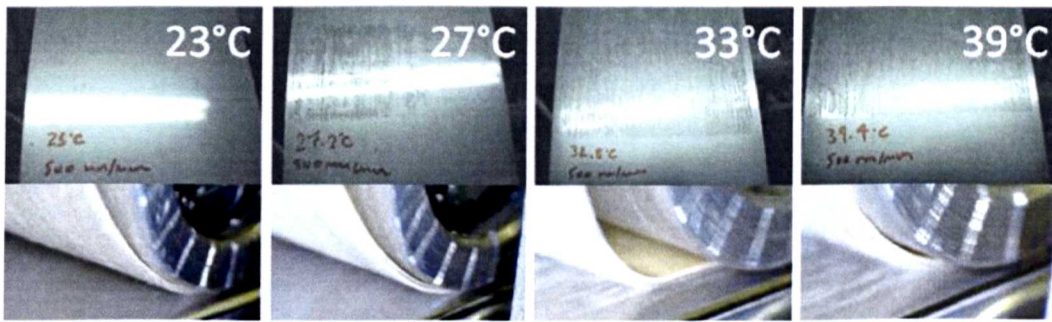


Fig 4-15 Resin deposition of WE-ATL prepreg (Ref. T03) with increasing temperature

Existing aerospace A-ATL tape (Ref. T04) revealed only a modest peak in recorded tack with a transition in failure mode observed at a higher temperature. The transition in failure mode observed by resin deposition on test plate again appears to correspond with the peak in tack (Fig 4-16).

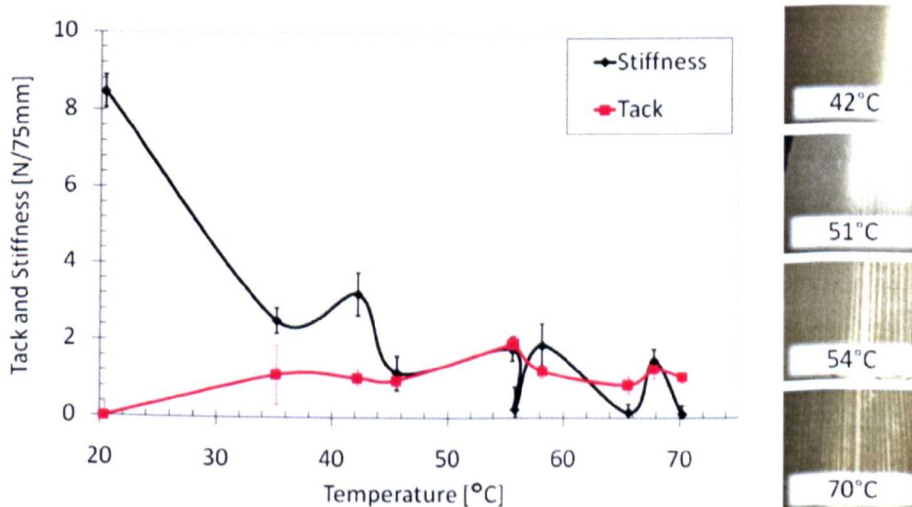


Fig 4-16 A-ATL (Ref.T04) Tack and stiffness temperature response (left) and resin deposition (right)

4.3.2 Feed rate

Feed rate was shown to have a significant effect on tack (96.8%) and stiffness (52.4%) of GUD1600 prepreg (Ref. FR01) (Fig 4-17) with a reasonably low degree of standard deviation which appears to increase with feed rate (Table 4-7).

Table 4-7 Effect of feed rate on GUD1600 prepreg

Feed Rate [mm/min]	50	250	500	750	1000		[%]
Stiffness [N/75mm]	21.39	29.74	36.15	38.78	44.9	Effect	52.4
σ	0.85	1.56	1.19	1.34	2.83	σ	4.5
Tack [N/75mm]	2.51	32.46	65.94	79.08	78.65	Effect	96.8
σ	0.81	2.29	9.57	9.02	23.49	σ	17.5

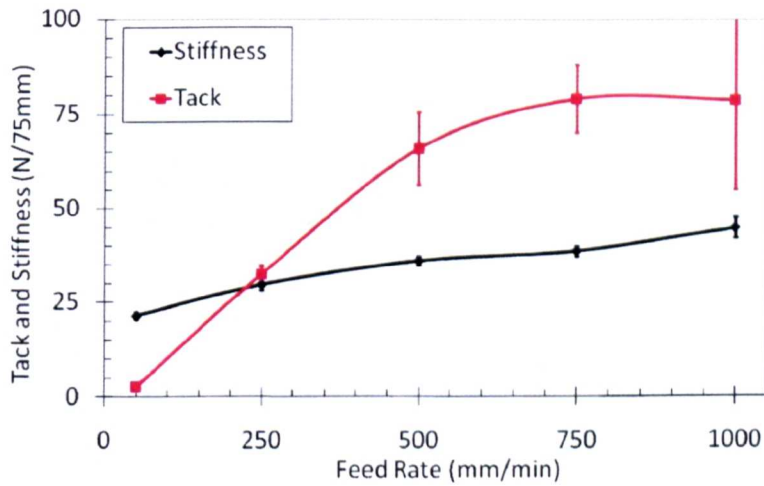


Fig 4-17 Tack and stiffness of GUD1600 prepreg in response to increasing feed rate

An increase in tack and stiffness with increasing feed rate was also recorded for WE-ATL prepreg (Ref.FR02) (Fig 4-18). However, a peak in tack was reached which appeared to correspond with a change in failure mode observed at the rollers and by resin deposition on the rigid test plate (Fig 4-19). An increase in experimental error was also observed during failure mode transition and interfacial failure at increased feed rates.

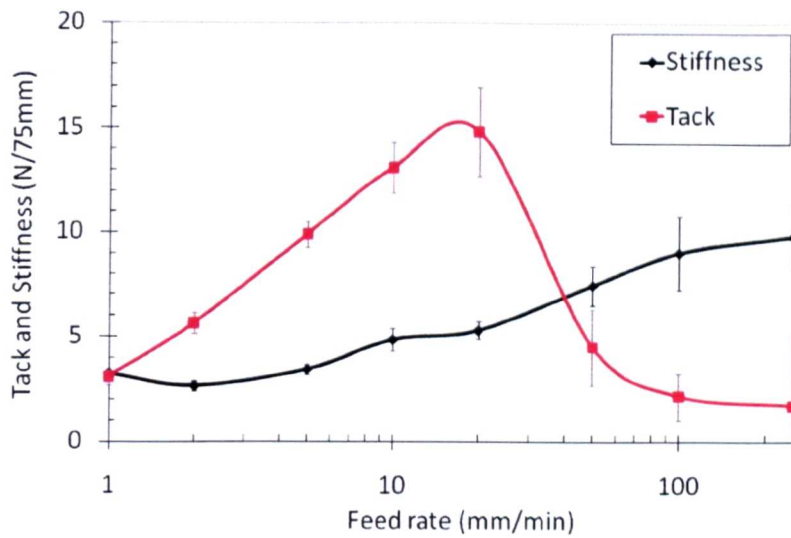


Fig 4-18 WE-ATL prepreg tack and stiffness response to feed rate (Ref. FR02)

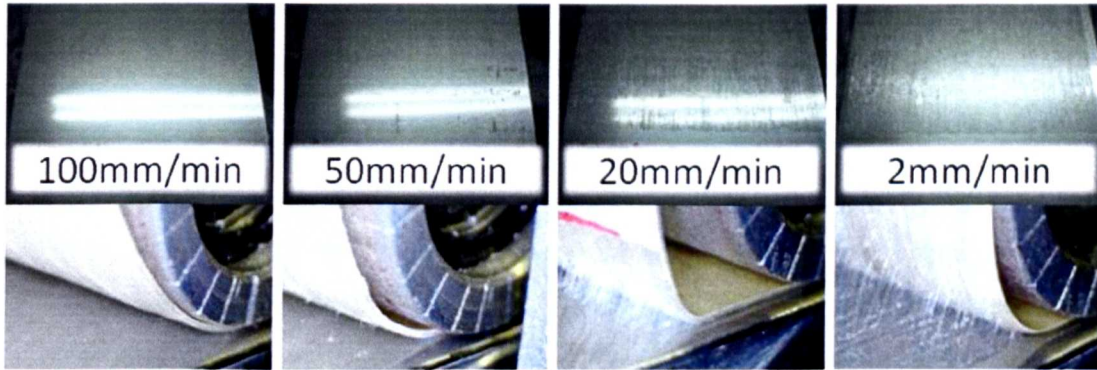


Fig 4-19 WE-ATL prepreg failure mode and deposition feed rate response (Ref. FR02)

4.3.3 Surface roughness

The results of the initial surface roughness investigation (Ref. SR01) showed no significant effect. However, the Ra=1.92µm plate appeared to show a 20% rise in tack with a 10% experimental error (Table 4-8).

Table 4-8 GUD1600 prepreg surface roughness response (100mm/min) (Ref. FR01)

Av. Surface Roughness (Ra) [µm]	0.12	0.18	1.92		[%]
Stiffness [N/75mm]	20.9	18.56	22.24	Effect	16.5
σ	0.28	2.08	1.54	σ	6.4
Tack [N/75mm]	10.72	10.03	12.79	Effect	21.6
σ	0.39	1.89	1.39	σ	10.9

The experiment was repeated with an additional Ra=0.95 plate to investigate any possible trend in increasing tack towards the increasingly rough surface (Ref. SR02). The repeated experiment showed no obvious trend in tack levels. A 27% rise in tack was again recorded for the Ra 1.92 μm plate (Table 4-9) with 29% uncertainty. Both tests showed large standard deviation in comparison to any effects. A minor trend was observed, with an increase in tack levels for the 1.92μm plate. However, effects did not significantly exceed standard deviation. Resin failure was mostly observed at 100mm/min. At 500mm/min signs of a change in failure mode were beginning to occur, but complete surface failure was never observed.

Table 4-9 Effects of surface roughness on GUD1600 prepreg at 500mm/min feed rate (Ref. FR02)

Av. Surface Roughness (Ra) [μm]	0.12	0.18	0.95	1.92		[%]
Stiffness [N/75mm]	34.46	34.2	34.31	34.29	Effect	0.8
σ	3.46	1.94	3.02	1.61	σ	7.3
Tack [N/75mm]	46.3	45.56	45.39	62.59	Effect	27.5
σ	14	7.25	19.43	17.64	σ	29.2

WE-ATL temperature sweeps (Ref. SR03) showed no significant stiffness (Fig 4-20) or tack response to surface finish (Fig 4-21). A familiar peak in tack appeared to occur alongside a change in failure mode at a consistent temperature for all surfaces (Fig 4-22). Increased error was observed with the polished plate around the transition in failure mode, believed to be due to the onset of an unsteady 'stick-slip' peel condition.

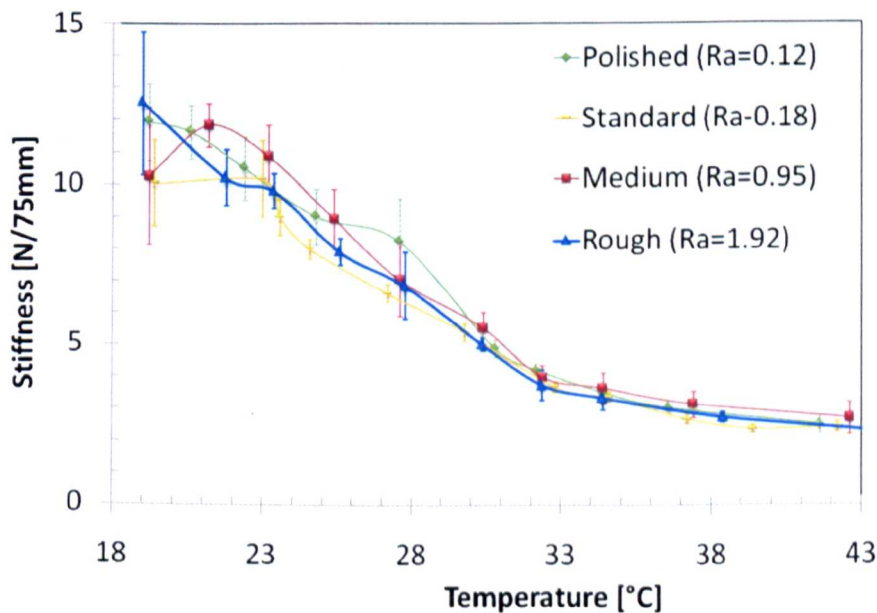


Fig 4-20 Effect of surface finish on stiffness of WE-ATL prepreg (Ref. SR03)

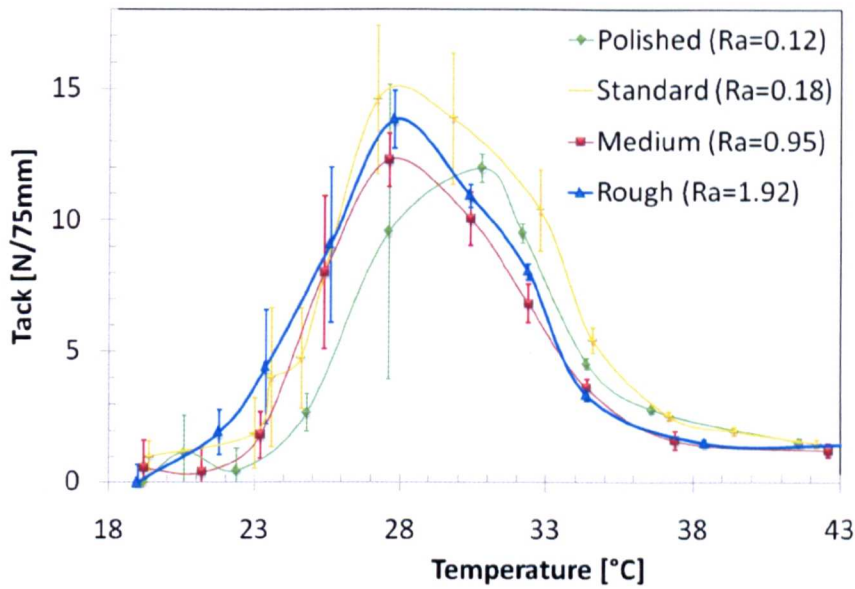


Fig 4-21 WE-ATL tack response to surface finish over a temperature range (Ref.SR03)

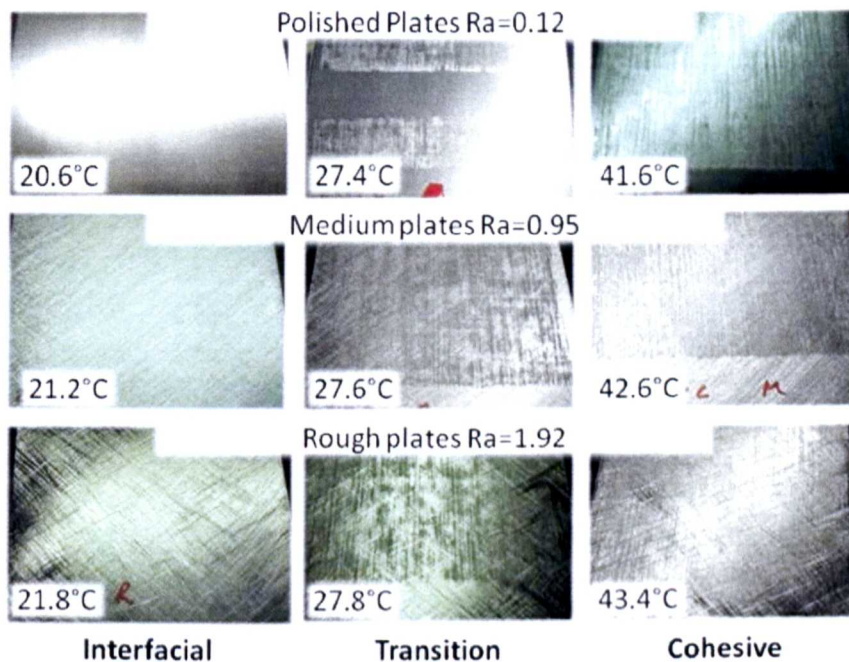


Fig 4-22 WE-ATL test plate resin deposition indicating a consistent change in failure mode over a temperature range (Ref. SR03)

Further analysis (Appendix D) of the effects of surface finish on WE-ATL prepreg allows a comparison of average tack and stiffness effect with standard deviation (Table 4-10). The results show that surface finish has no significant effect over a temperature range which includes both types of failure modes.

Table 4-10 WE-ATL prepreg tack and stiffness response over a temperature range including average standard deviation (Ref. SR03)

Av. Surface Roughness (Ra) [μm]	0.12	0.18	0.95	1.92		[%]
Tack [N/75mm]	4.77	6.32	4.71	5.22	Effect	25.5
σ	1.19	1.30	0.88	0.79	σ	19.8
Stiffness [N/75mm]	6.28	5.48	6.16	5.71	Effect	12.7
σ	0.59	0.39	0.70	0.55	σ	9.5

4.3.4 Release agents

The stiffness of GUD1600 prepreg at 20°C (Ref. RA01) appears unaffected by release agents, with minor effect attributed to experimental error (Table 4-11). A significant reduction in tack, with 99.5% effect, can be seen with all release agents indicating a significant effect in comparison to 31.4% standard deviation (Fig 4-23). Additionally, solvent based composite, Multishield and PMR-90 release agents showed a higher residual tack than water based types. A change in failure mode was also observed. Heavy resin deposition seen on untreated test plates is not present on those treated with release agent.

Table 4-11 GUD1600 prepreg response to release agents (Ref. RA01)

Release agent	None	Water Shield	Multi Shield	Enviro Shield	Composite Shield	PMR-90		[%]
Stiffness	31.47	30.31	29.17	31.05	30.8	30.55	Effect	7.3
[N/mm] σ	2.53	1.84	0.61	1.77	0.82	4.94	σ	6.8
Tack	58.29	1.38	8.62	0.27	8.78	3.95	Effect	99.5
[N/mm] σ	8.64	1.96	5.35	0.49	6.35	2.71	σ	31.4

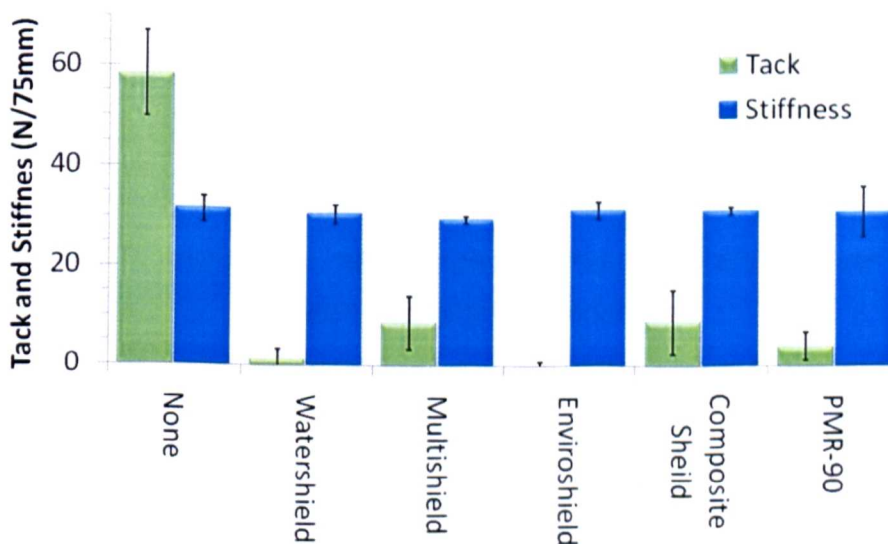


Fig 4-23 GUD1600 prepreg tack and stiffness response to release agents (Ref. RA01)

Temperature sweep experiments using WE-ATL prepreg (Ref. RA02) also show that release agents have a significant effect on tack. The peak in tack appears to be significantly reduced. The peak remains at a consistent temperature as the apparent shift in failure mode observed by resin deposition for each temperature sweep. However, the failure mode transition appears to occur at a higher temperature when a release agent is used (Fig 4-24).

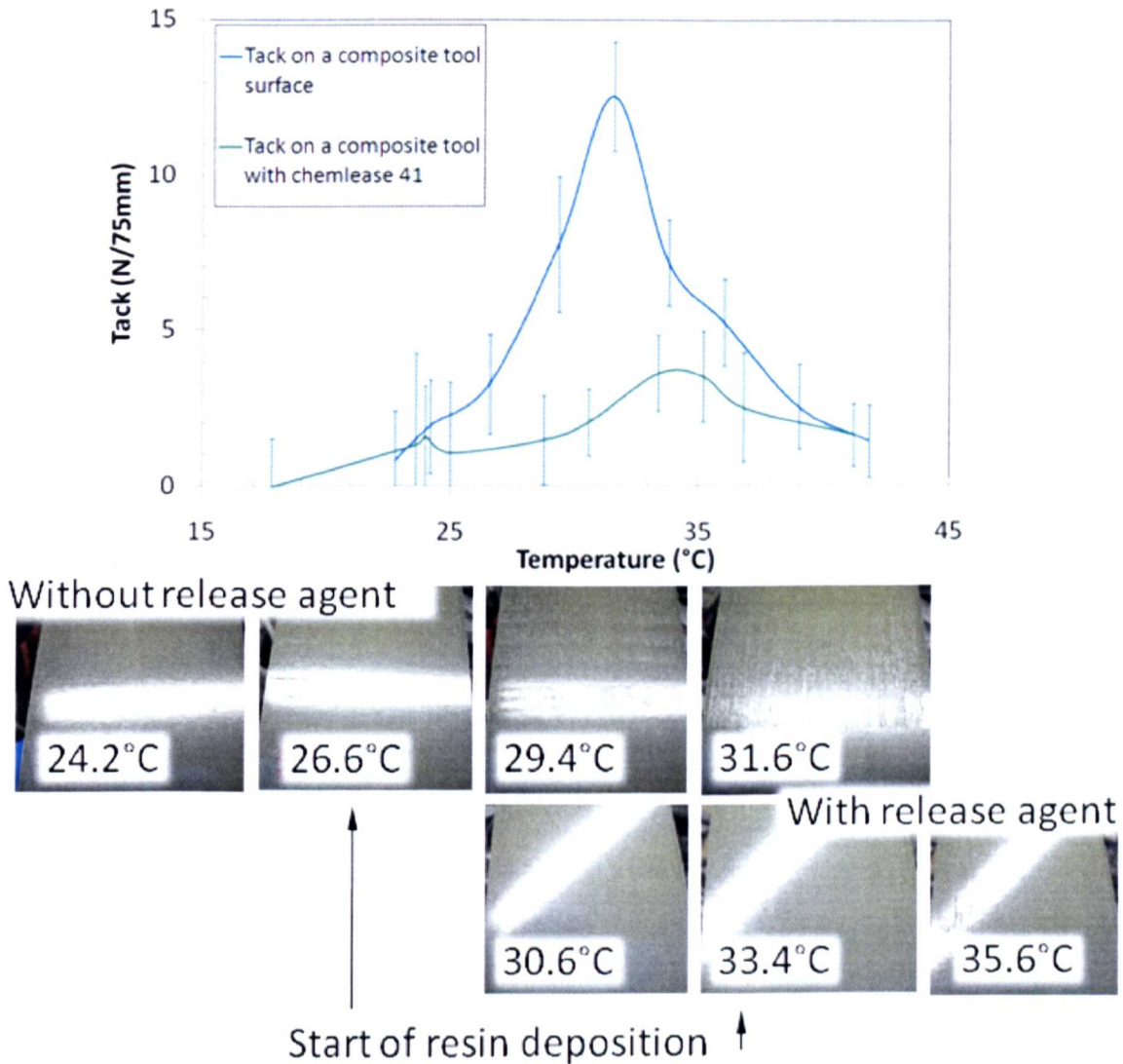


Fig 4-24 WE-ATL response to release agent over a temperature range with test plate resin deposition observations

4.3.5 Compaction force

Testing GUD1600 at 100mm/min, 20°C (Ref. CF01) revealed a trend of increasing stiffness with compaction force. A decreasing trend of tack was observed with a 40.5% effect in comparison to 14% standard deviation (Table 4-12).

Table 4-12 GUD1600 tack and stiffness response to compaction force at 20°C and 100mm/min feed rate (Ref. CF01)

Compaction Force [N]	100	200	300		[%]
Stiffness [N/75mm]	21.53	25.35	32.78	Effect	34.2
σ	1.3	3.48	2.75	σ	9.5
Tack [N/75mm]	39.84	30.93	23.7	Effect	40.5
σ	3.38	3.26	6.3	σ	13.7

Testing GUD1600 prepreg at 500mm/min, 20°C (Ref. CF02) showed a repeated trend of increasing stiffness with increased compaction force. The trend of decreasing tack was also repeated with 37% effect in comparison to 14% error (Table 4-13).

Table 4-13 GUD1600 tack and stiffness response to compaction force at 20°C and 500mm/min feed rate (Ref. CF02)

Compaction Force [N]	75	100	150	200	250	300		[%]
Stiffness [N/75mm]	19.59	20.17	24.9	27.65	29.16	30.78	Effect	36.4
σ	1.24	1.62	1.21	1.53	2.81	4.25	σ	8.3
Tack [N/75mm]	42.16	43.63	35.99	27.59	31.77	30.63	Effect	36.8
σ	6.41	6.89	4.7	5.74	1.37	5.1	σ	14.3

Testing aerospace A-ATL prepreg at 100mm/min, 20°C (Ref. CF03) showed a confident repeated trend of increasing stiffness with increased compaction force. The trend of decreasing tack was also repeated with 44% effect, however, standard deviation increased to 45%.

Table 4-14 Aerospace A-ATL tack and stiffness response to compaction force at 20°C and 100mm/min feed rate (Ref. CF03)

Compaction Force [N]	100	200	300		[%]
Stiffness [N/75mm]	9.56	12.19	14.89	Effect	35.8
σ	0.24	0.19	0.55	σ	2.7
Tack [N/75mm]	2.48	1.63	1.38	Effect	44.4
σ	0.54	0.9	1.02	σ	44.8

Temperature sweeps using WE-ATL (Ref. CF04) show the familiar peak in tack at a consistent temperature regardless of compaction force (Fig 4-25). An increase in peak tack was observed with increasing compaction force. However, the increase appears to occur mainly within the failure mode transition region ($\approx 25-35^\circ\text{C}$). The temperature sweep confirms the lack of compaction pressure effect at ambient (20°C) temperatures. A consistent increase in stiffness was observed with increasing compaction force

independent of temperature (Fig 4-24), suggesting that this effect is likely to be due to increased friction within the rig.

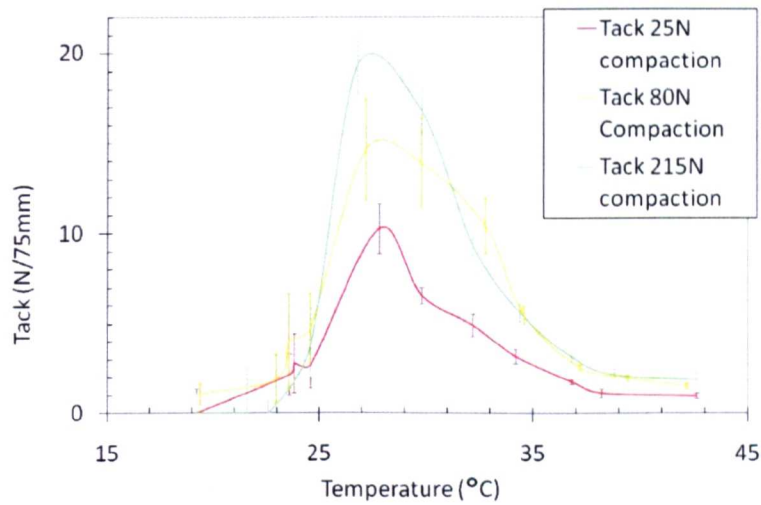


Fig 4-25 WE-ATL tack response to compaction force over a temperature range (Ref. CF04)

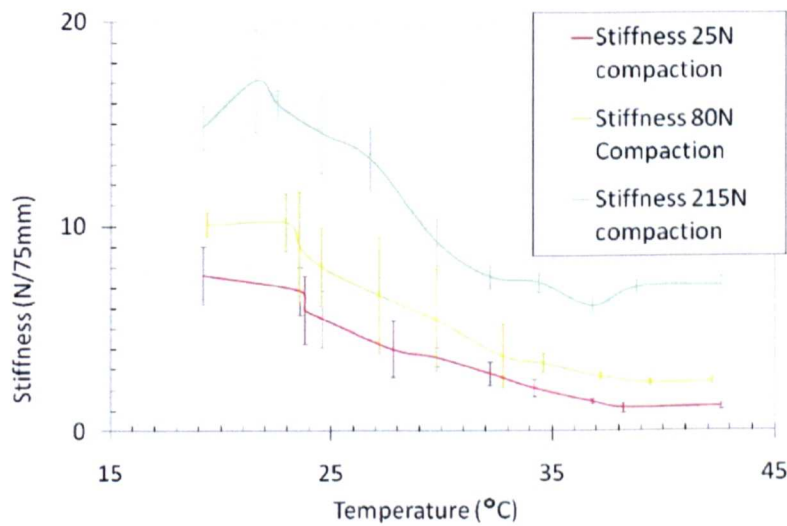


Fig 4-26 WE-ATL stiffness response to compaction force over a temperature range (Ref. CF04)

4.3.6 Surface material

Results of temperature sweeps using WE-ATL on alternate surface types (Ref. ST01) revealed a peak in tack for all surfaces (Fig 4-27). However, peaks were shown to change in magnitude and transition temperature. The peak in tack for each surface appeared consistent with the change in failure mode observed by resin deposition (Fig 4-28). Effects over the temperature range (Appendix D) showed a 69% effect on tack with 23% error and 25% effect on stiffness with 11.3% error (Table 4-15). Increased stiffness for the composite plate remained consistent throughout the temperature range

(Fig 4-29). Therefore, the effect on stiffness was mostly attributed to the rough lower surface of the composite plate, believed to result in increased rolling friction.

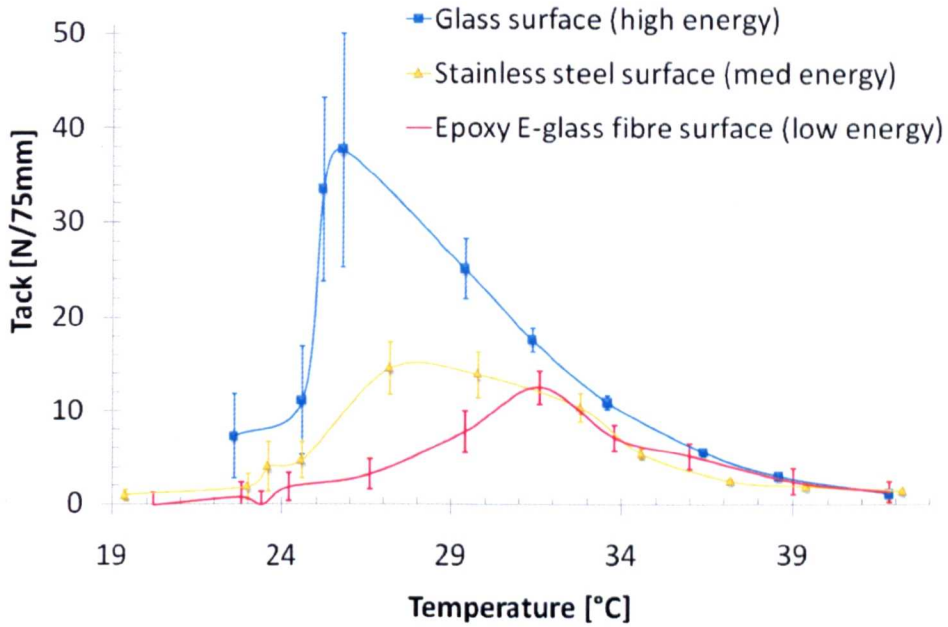


Fig 4-27 WE-ATL tack response to surface type over a temperature range (Ref. ST01)

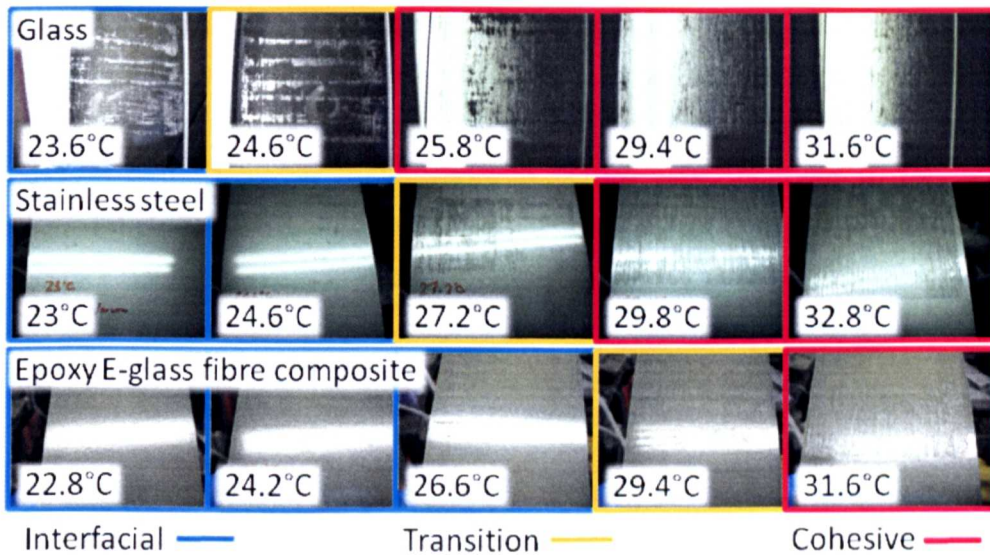


Fig 4-28 WE-ATL resin deposition response to surface type (Ref. ST01)

Table 4-15 Effect of surface type on WE-ATL prepreg tape (Ref. ST01)

Surface Type	St/St	Glass	Epoxy E-GF		[%]
Stiffness [N/75mm]	5.48	5.39	7.22	Effect	25.3
σ	0.39	0.38	1.27	σ	11.3
Tack [N/75mm]	6.32	14.57	4.56	Effect	68.7
σ	1.30	3.10	1.55	σ	23.4

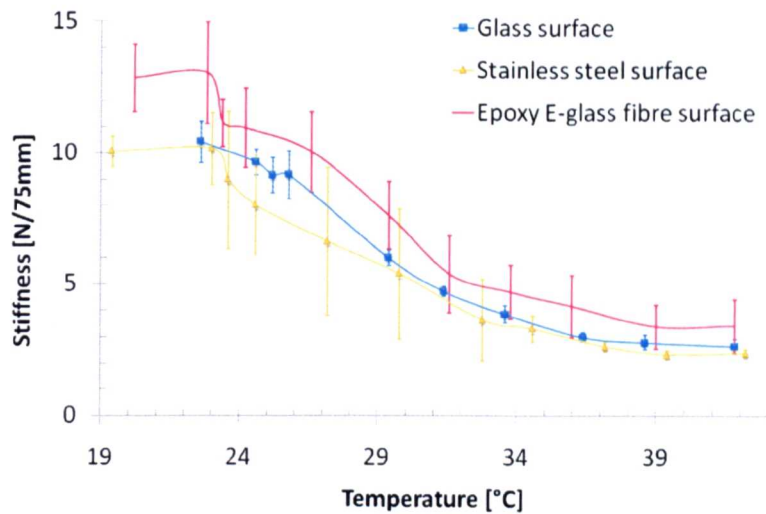


Fig 4-29 WE-ATL stiffness response to surface type over a temperature range (Ref. ST01)

4.3.7 Contact temperature

The contact temperature experiment (Ref. CT01) revealed a significant effect of 69% overall average increase in tack with a 40°C, 100N, 500mm/min pre-application stage (Table 4-16). A low standard deviation of 5.3% indicates a good degree of confidence in the observed effect. Observations over the peel temperature range show that tack is significantly increased mostly at a lower temperature. Both failure modes are observed in the standard test. However, only cohesive failure was observed in the pre-applied high contact temperature sample displayed which did not exhibit a peak in tack (Fig 4-30). No effect was observed on prepreg stiffness.

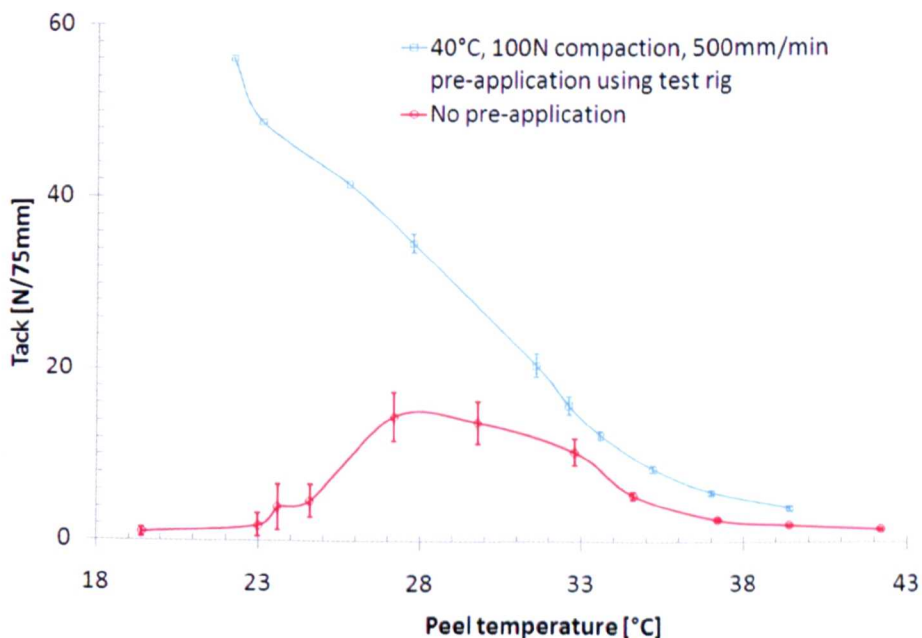


Fig 4-30 Effect of a 40°C pre-application on tack over a subsequent peel temperature range (Ref. CT01)

Table 4-16 Effects of increased temperature application on WE-ATL (Ref. CT01)

	No Pre-application [N]	With Pre-application [N]	Effect (N)	Effect [%]	σ [%]
Tack	7.6	24.6	17.0	69.0	6.5
σ	1.5	0.6			
Stiffness	5.7	5.3	0.4	7.9	7.8
σ	0.4	0.5			

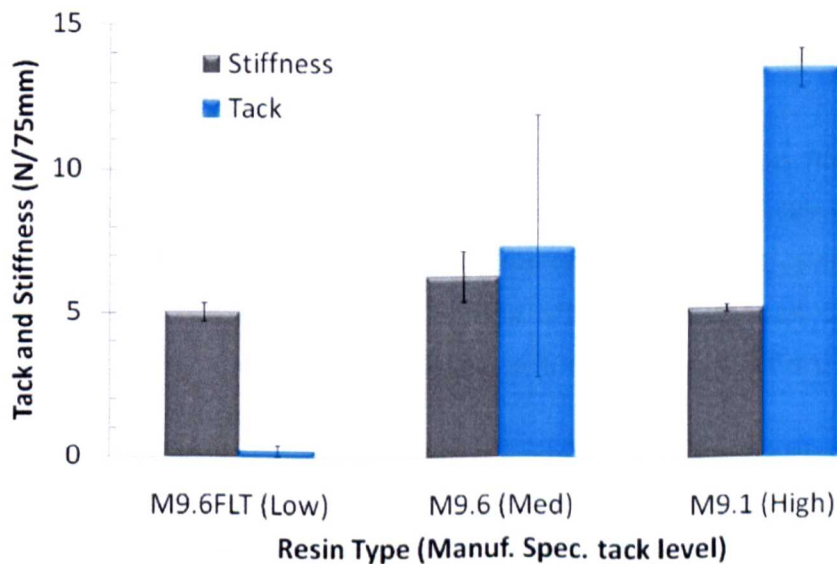
4.3.8 Resin type

The testing of three custom made preregs with matching fibre specification and alternate resin types, formulated based on tack levels (Ref. RT01), revealed a moderate effect (19.4%) on stiffness with 8% uncertainty (Table 4-17).

Table 4-17 Effects of resin type on prepreg tack (Ref. RT01)

Tack level	Low	Med	High		
Resin Type	M9.6LT	M9.6	M9.1F		[%]
Stiffness [N/75mm]	5.07	6.29	5.17	Effect	19.4
σ	0.3	0.89	0.13	σ	8
Tack [N/75mm]	0.24	7.3	13.44	Effect	98.2
σ	0.19	4.51	0.68	σ	25.6

The tack response was shown to be in agreement with tack levels specified by the manufacturer (Fig 4-31). A 98.2% effect with 25.6% uncertainty reveals a dominant effect on tack at ambient temperature.

**Fig 4-31** Tack and stiffness response to resin type at ambient temperature (Ref. RT01)

4.3.9 Fibre areal weight

The testing of three matching prepregs with increasing Fibre Areal Weight (FAW) (Ref. FT01) revealed an almost proportional 57.3% increase in stiffness with 12.8% uncertainty (Fig 4-32). A 46.8% effect on tack is overshadowed by 54.7% uncertainty without a noticeable trend (Table 4-18).

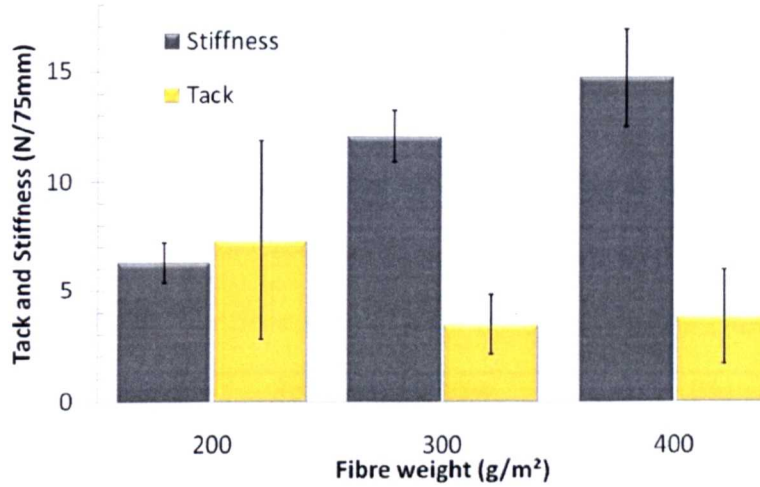


Fig 4-32 Tack and stiffness response to FAW at ambient temperature (Ref. FAW01)

Table 4-18 Effect of FAW on tack and stiffness (Ref. FAW01)

Fibre weight [g/m ²]	200	300	400		[%]
Stiffness [N/75mm]	6.29	12.05	14.73	Effect	57.3
σ	0.89	1.15	2.2	σ	12.8
Tack [N/75mm]	7.3	3.49	3.88	Effect	46.8
σ	4.51	1.36	2.16	σ	54.7

4.3.10 Fibre type

A comparison of matching prepregs with alternate carbon and E-glass fibres (Ref. FT01) was made at ambient (20°C) conditions. The stiffness of carbon fibre prepregs was shown to increase by 38% with 12% uncertainty in comparison to E-glass (Fig 4-33). A significant 87.1% with 64.4% standard deviation effect on tack was observed with a change in fibre type, with significantly increased tack in the E-glass fibre samples (Table 4-19) at ambient temperature.

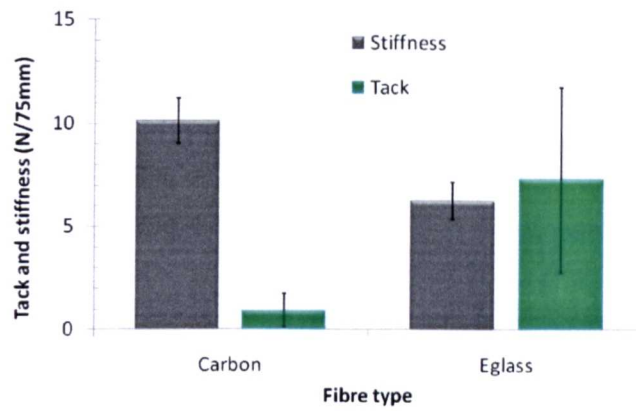


Fig 4-33 tack and stiffness response to fibre type at ambient temperature (Ref. FT01)

Table 4-19 Effect of fibre type at ambient temperature (Ref. FT01)

Fibre type	Carbon	E-glass		[%]
Stiffness [N/75mm]	10.14	6.29	Effect	38
σ	1.08	0.89	σ	12
Tack [N/75mm]	0.94	7.3	Effect	87.1
σ	0.8	4.51	σ	64.4

Temperature sweeps (Ref. FT02) appeared to demonstrate a consistently higher stiffness in carbon prepreg irrespective of the temperature effects on resin viscosity (Fig 4-34). A familiar peak in tack was observed with the E-glass sample. However, the peak for the carbon sample appeared truncated (Fig 4-35). The temperature at which a transition in failure mode occurs appears to be independent of fibre type (Fig 4-36)

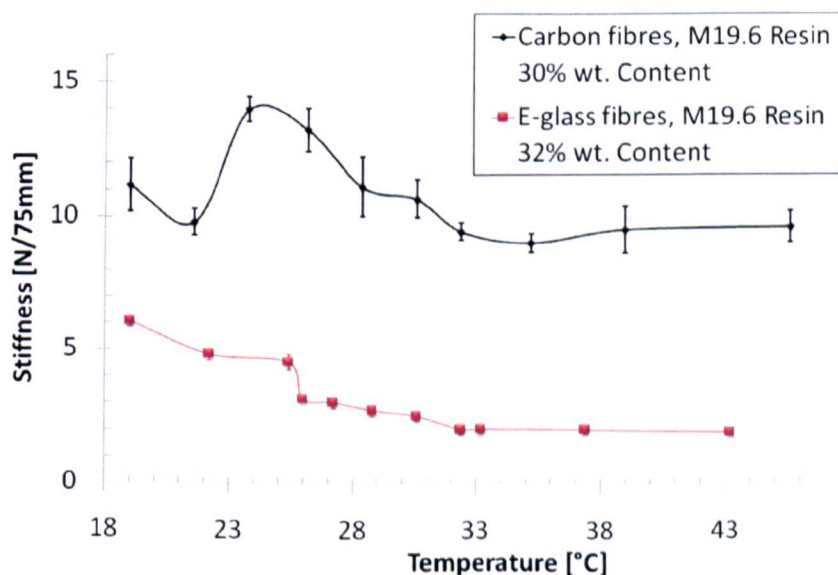


Fig 4-34 Stiffness response to fibre type over a temperature range (Ref. FT02)

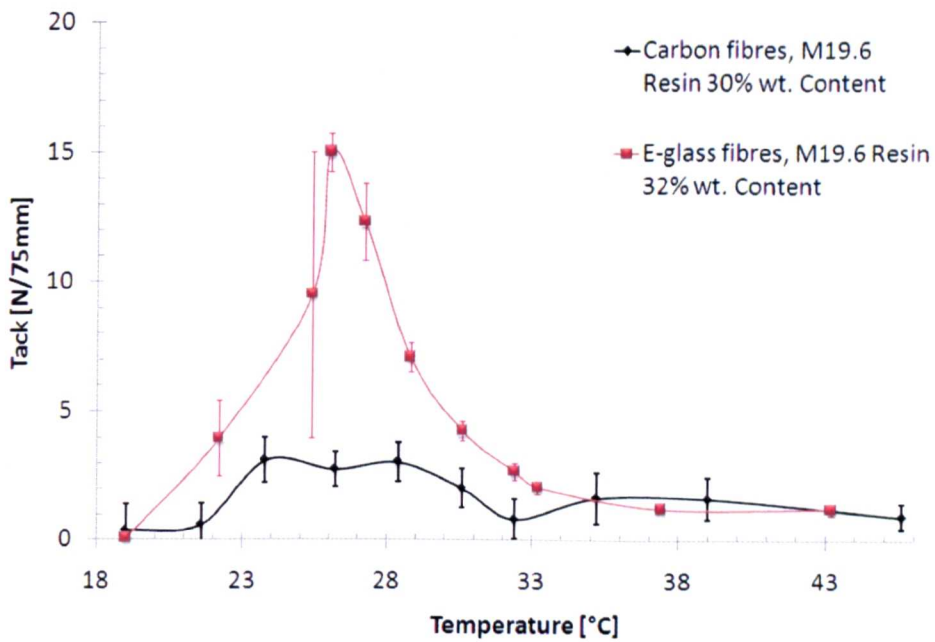


Fig 4-35 Tack response to fibre type over a temperature range (Ref. FT02)

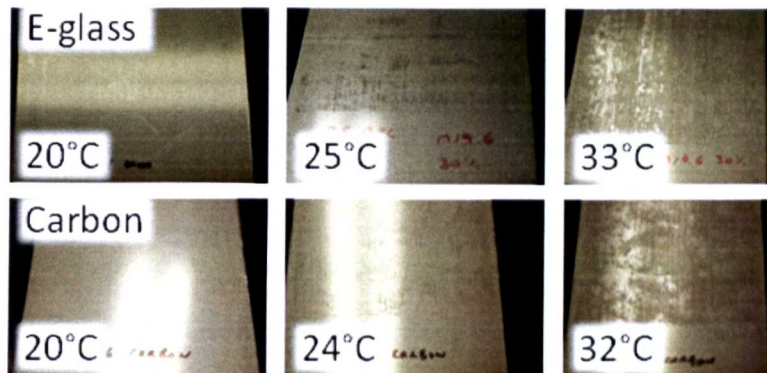


Fig 4-36 Resin deposition response to fibre type over a temperature range (Ref. FT02)

4.3.11 Resin content

Testing alternate resin contents at 20°C 500mm/min (Ref. RC01) reveals a 25.8% effect on stiffness with 6.1% deviation with no apparent trend (Table 4-20). A general trend of increasing tack was observed with 64.6% effect. However overall tack levels are low, resulting in relatively high experimental noise ($\sigma=89.4\%$).

Table 4-20 Effect of resin content at 20°C 500mm/min (Ref. RC01)

Resin Content	30%	40%	50%		[%]
Stiffness [N/75mm]	6.52	5.62	7.57	Effect	25.8
σ	0.28	0.33	0.6	σ	6.1
Tack [N/75mm]	0.34	0.86	0.96	Effect	64.6
σ	1.2	0.44	0.29	σ	89.4

Once again a familiar peak tack was observed in temperature sweeps (Ref. RC02) consistent with a change in failure mode observed by resin deposition. The effect of increased resin content on tack was shown to greatly increase within the peak tack temperature range of 24-34°C (Fig 4-37). Analysis over the temperature range revealed a significant 65.5% effect on tack with 24.2% standard deviation (Table 4-21). A 37.3% increased effect on stiffness with 9.1% uncertainty was calculated (Table 4-21).

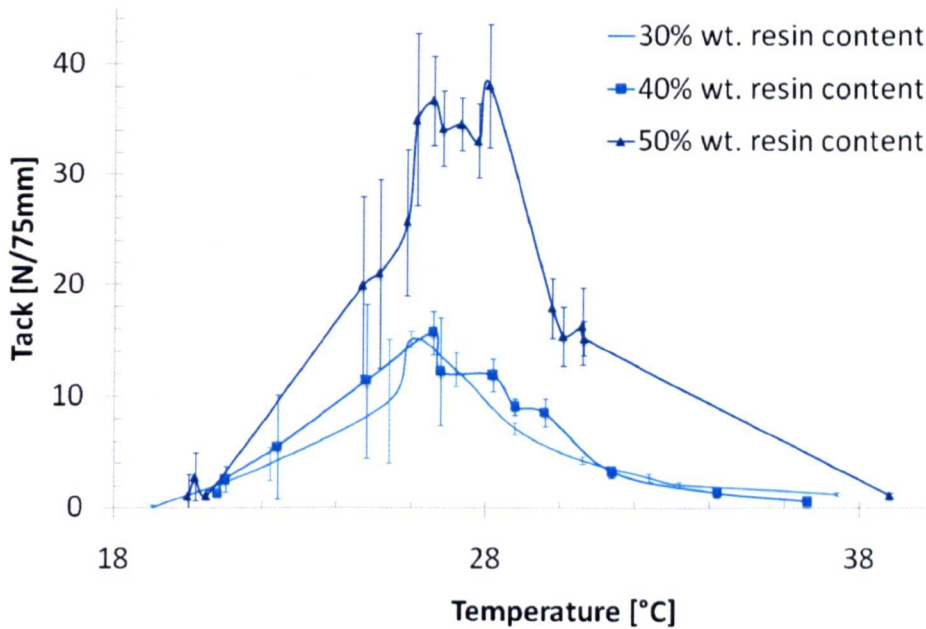


Fig 4-37 Tack response to resin content over a temperature range (Ref. RC02)

Table 4-21 Effect of resin content over a temperature range (Ref. RC02)

Resin Content	30%	40%	50%		[%]
Stiffness [N/75mm]	3.39	5.41	5.15	Effect	37.3
σ	0.19	0.41	0.67	σ	9.1
Tack [N/75mm]	5.05	6.52	14.63	Effect	65.5
σ	1.16	2.28	2.88	σ	24.2

4.3.12 Fibre architecture

A temperature sweep of 1200g/m² tri-axial (triax) fibre and 200g/m² Uni-Directional (UD) fibre (Ref. FA01) showed a familiar peak in both tack levels. However, the triax sample showed a significantly increased peak occurring at a lower temperature (Fig 4-38). Stiffness appeared to be consistently six times higher than unidirectional fabrics (Fig 4-39) attributed to the six fold increase in overall prepreg areal weight. An average overall tack increase effect of 81% with 25% uncertainty was observed (Table 4-22).

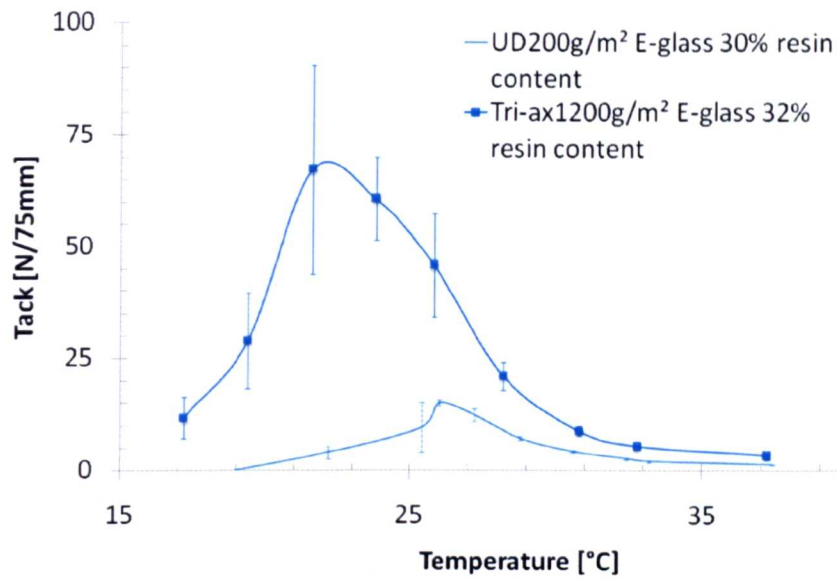


Fig 4-38 Tack response to fibre architecture and FAW over temperature (Ref. FA01)

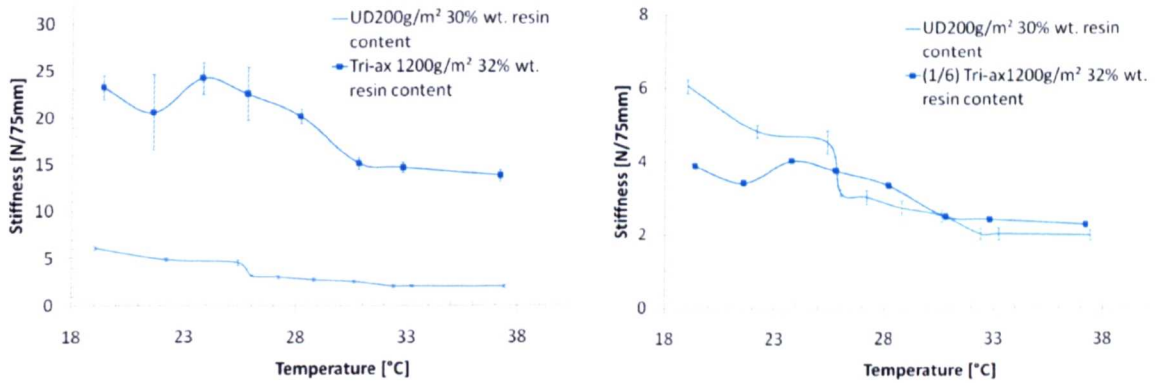


Fig 4-39 Stiffness response to fibre architecture and FAW (Ref. FA01) (left) normalised for a 6 times increase in FAW (right)

Table 4-22 Effects of fibre architecture and FAW on tack and stiffness over a temperature range (Ref. FA01)

Fibre architecture	UD	Triax		[%]
Av. Stiffness [N/75mm]	3.39	19.83	Effect	82.9
σ	0.19	1.45	σ	7.1
Av. Tack [N/75mm]	5.05	26.63	Effect	81.0
σ	1.16	6.90	σ	25.4

4.3.13 Stiffness summary

A comparison of effects on prepreg stiffness in single level experiments at ambient temperature show that temperature, feed rate and fibre weight have the greatest effect (Table 4-23). The results are mostly confirmed when considering temperature interactions (Table 4-24). However, certain variables could not be retested for temperature interaction effects due to material availability constraints.

Table 4-23 Summary of the effects of variables on prepreg stiffness at ambient 20°C

Variable	Exp. Ref.	Range	Stiffness [%]		Comments
			Effect	σ	
Temperature	T01	16-30.1°C	60.3	10	Noticeable trend of decreasing stiffness
Fibre Weight	FAW01	200-400 g/m ²	57.3	12.8	Increases with increased weight
Feed Rate	FR01	50-1000	52.4	4.5	stiffening trend
Fibre type	FT01	Eglass/carbon	38	12	Carbon prepreg significantly stiffer
Compaction force	CP01	75-300N	36.4	8.3	Increases may be due to increased roller friction
	CP02	100-300N	34.2	9.5	
Resin Content	RC01	30-50%	25.8	6.1	Increases with increasing content
Resin type	RT01	Low-High tack	19.4	8	Minimal effect
Surface finish	SR01	0.12-1.92Ra	16.5	6.4	Frictional effects only
Release Agents	RA01	With-without	7.3	6.8	No effect
Surface Finish	SR02	0.12-1.92Ra	0.8	7.3	No effect

Table 4-24 Summary of the effects of variables on stiffness over a temperature range

Variable	Exp. Ref.	Range	Stiffness [%]		Comments
			Effect	σ	
Fibre weight & architecture	FA01	UD200/ Triax1200	82.9	7.1	Increase due to combined effect of 6x FAW increase
Temperature	T03	19.4-42.2°C	76.9	7.3	Apparent trend of decreasing stiffness with increased temperature
Feed rate	FR02	1-250mm/min	73.1	12.9	Apparent trend of increasing stiffness with increased feed rate
Fibre type	FT02	Eglass/Carbon	70.9	6.1	Carbon significantly stiffer
Compaction pressure	CP04	25-300N	65	8.2	Increases may be due to increased roller friction
Resin content	RC02	30-50%	37.3	9.1	Increases with increased resin content
Surfaces	ST01	Glass-composite	25.3	11.3	Effect may be due to increased surface roughness underside of composite plate
Surface finish	SR03	0.12-1.92Ra	12.7	9.5	Frictional effects only
Release Agent	RA02	Without-Chemlease 41	5.1	16.2	No effect

4.3.14 Tack summary

The effects of variables at ambient conditions show that resins, release agents, feed rate and temperature have an overwhelming effect on tack with a significant degree of confidence in comparison to standard deviation (Table 4-25). When temperature interaction effects are considered (Table 4-26) the dominant effects appear to be temperature, feed rate and surface energy. Release agents appear much less effective. Compaction force and surface finish appear to have the least significant effect.

Table 4-25 Summary of the single level effect of variables on tack at 20°C

Variable	Ref.	Range	Tack [%]		Comments
			Effect	σ	
Release Agents	RA01	Without - water & solvent based	99.5	31.4	Decreases with the addition of release agent. Failure mode changes to interfacial
Resin type	RT01	Low-High tack	98.2	25.6	Increases with increased specified tack level
Feed rate	FR01	50-1000	96.8	17.5	Increases with increasing feed rate until a plateau is reached
Temperature	T01	16-30.1°C	95.2	7.6	Decreases with increasing temperature
Fibre type	FT01	Eglass/carbon	87.1	64.4	Significant loss of tack in carbon
Resin content	RC01	30-50%	64.6	89.4	Inconclusive, slight increase
Fibre weight	FAW01	200-400 g/m ²	46.8	54.7	No trend, negligible effect
Compaction force	CP01	100-300N	40.5	13.7	Decreases
	CP02	75-300N	36.8	14.3	
Surface Finish	SR01	0.12-1.92Ra	27.5	29.2	No trend, negligible effect
	SR02	0.12-1.92Ra	21.6	10.9	

Table 4-26 Summary of the effect of variables on tack including temperature interaction effects

Variable	Ref.	Range	Tack [%]		Comments
			Effect	σ	
Temperature	T03	19.4-42.2°C	93.1	23.2	Increases with increasing temperature during interfacial failure then reaches a peak at transition, falling during cohesive failure
Feed rate	FR02	1-250mm/min	88.6	20.2	Increases with increasing feed rate during cohesive failure, decreases during interfacial failure
Fibre weight & architecture	FA01	UD200/ Triax1200	81	25.4	Increases with triax, most likely due to combined effects of a 6x FAW increase
Surfaces	ST01	Glass-St/St-composite	68.7	23.4	Increases with increased surface energy, the onset of cohesive failure is delayed with low surface energy surfaces
Resin content	RC02	30-50%	65.5	24.2	Generally increasing with significant increase between 40-50%
Release agent	RA02	None-Chemlease 41	61.3	51.9	Decreases with the addition of release agent, delays the onset of cohesive failure
Fibre type	FT02	E-glass/Carbon	58.8	29.5	Significant loss of tack in carbon prepreg
Compaction force	CF04	25-300N	48.2	18.4	Increases with increased pressure around the peak only
Surface finish	SR03	0.12-1.92Ra	25.5	19.8	No trend, negligible effect

4.4 Rheology

The rheology results for shear storage modulus (VI-RH1 to 7) of all the resin systems used show that generally shear storage modulus is found to decrease consistently at all temperatures above glass transition for each of the BPA epoxy resins (Fig 4-40). The 8552 resin system is shown to differ significantly in temperature response most probably due to the inclusion of thermoplastic toughening additives.

BPA epoxy resin systems also show a decrease in shear storage modulus with increasing specified tack level at temperatures above T_g . The reduction in modulus is consistent with increased perceived tack levels for all M9/M19 BPA epoxy resin systems at ambient ($\approx 20^\circ\text{C}$) temperature.

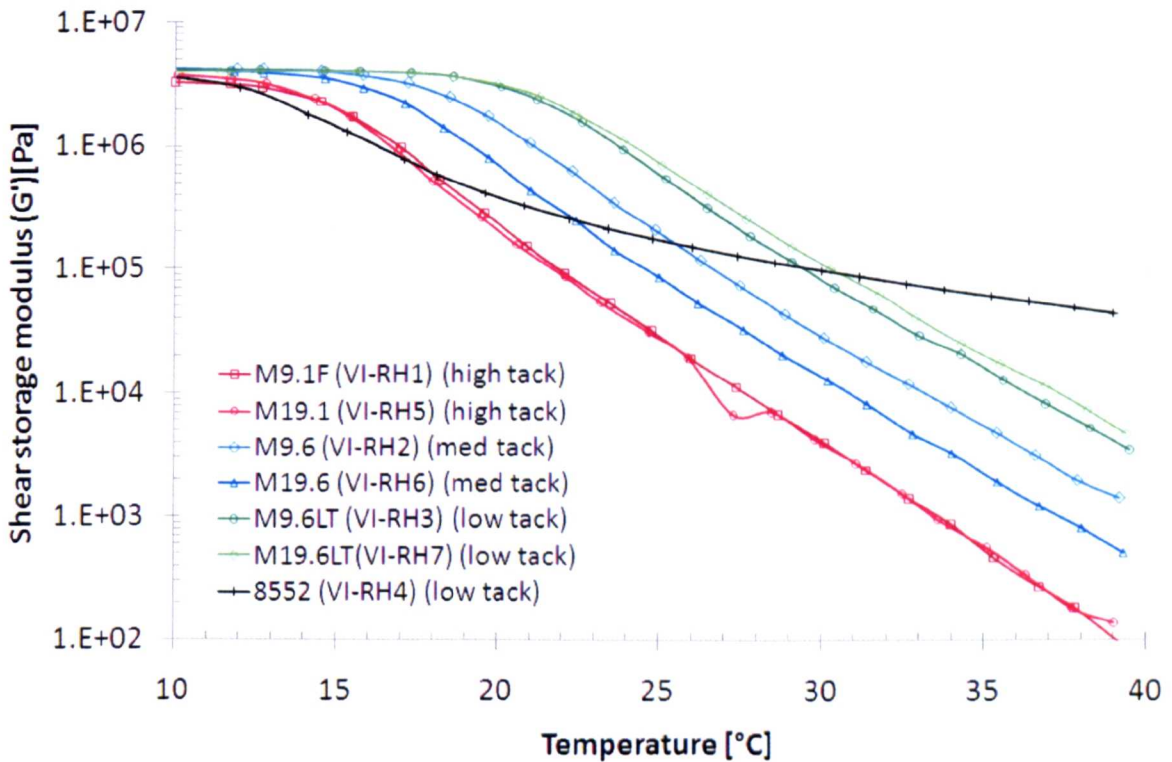


Fig 4-40 Viscoelastic shear storage modulus response, of prepreg resin systems used in tack testing, to temperature (Ref. VI-RH1 to 7)

4.5 Time temperature superposition

4.5.1 Gel permeation chromatography

Three peaks were identified by GPC analysis software (Fig 4-41). The large low molecular weight peak was attributed to the THF solvent which is not applicable to the analysis. The three peaks considered are likely to relate to the differing chemical components and polymerisation of epoxy Bisphenol-A resin. The exact components are considered commercially sensitive by the manufacturer and not disclosed. These peaks were consistent in all tests and were used to compare samples based on molecular weight.

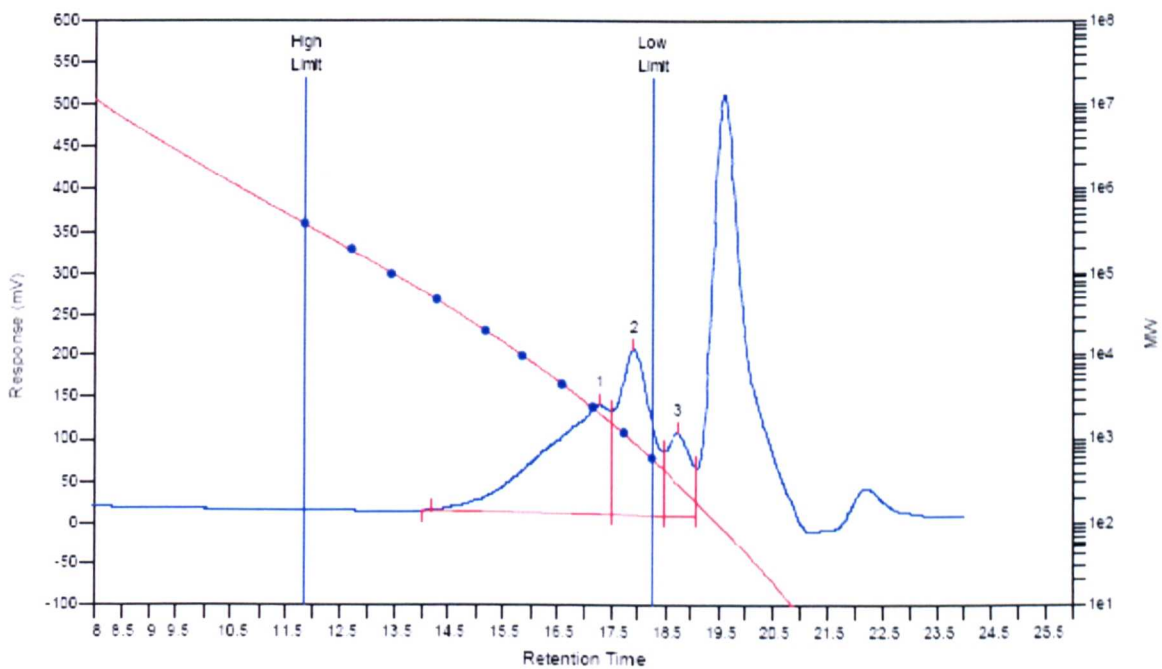


Fig 4-41 Typical GPC results showing three peaks with significant molecular weight

Results are presented in number average molecular weight (M_n), weight average molecular weight (M_w) and polydispersity (P). Number average is the mass of the specimen divided by the total number of moles present. Weight average is defined as the molecular mass multiplied by the mass divided by the total mass of the mixture. Polydispersity gives a measure of the range of molecular sizes and can be expressed as M_w/M_n [128]. Results are presented as average values for M_n , M_w of peaks, with standard deviation between the three tests. M_n , M_w and P results indicate no significant differences between prepreg and resin samples (Table 4-27 to Table 4-29). However, significant molecular changes are observed in peaks 1 and 2 between batches.

Table 4-27 Molecular weight (M_n) [g/mol] of resin and prepreg samples found by GPC

Sample	Peak 1	σ	Peak 2	σ	Peak 3	σ
Batch 1 resin (TTS-GPC1)	3792	± 108	863	± 21	286	± 9
Batch 1 prepreg (TTS-GPC3)	3816	± 53	865	± 12	286	± 5
Batch 2 resin (TTS-GPC2)	3431	± 46	834	± 11	284	± 4
Batch 2 prepreg (TTS-GPC4)	3439	± 11	842	± 1	285	± 0
Avg. batch diff.	369		26		1.5	
Avg. resin-prepreg diff.	16		5		0.5	

Table 4-28 Molecular weight (M_w) [g/mol] of resin and prepreg samples

Sample	Peak 1	σ	Peak 2	σ	Peak 3	σ
Batch 1 resin (TTS-GPC1)	6613	± 225	962	± 23	304	± 8
Batch 1 prepreg (TTS-GPC3)	6532	± 125	967	± 12	305	± 5
Batch 2 resin (TTS-GPC2)	5582	± 95	926	± 11	302	± 4
Batch 2 prepreg (TTS-GPC4)	5502	± 64	934	± 1	304	± 0
Avg. batch diff.	1030.5		34.5		1.5	
Avg. resin-prepreg diff.	80.5		6.5		1.5	

Table 4-29 Polydispersity (P) of resin and prepreg samples found by GPC

Sample	Peak 1	σ	Peak 2	σ	Peak 3	σ
Batch 1 resin (TTS-GPC1)	1.74	± 0.014	1.115	± 0.0025	1.064	± 0.0036
Batch 1 prepreg (TTS-GPC3)	1.711	± 0.0085	1.119	± 0.003	1.065	± 0.0015
Batch 2 resin (TTS-GPC2)	1.627	± 0.0069	1.11	± 0.0021	1.062	± 0.0026
Batch 2 prepreg (TTS-GPC4)	1.6	± 0.013	1.11	± 0.004	1.067	± 0
Avg. batch diff.	0.112		0.007		0.002	
Avg. resin-prepreg diff.	0.028		0.002		0.003	

4.5.2 Differential scanning calorimetry

Both resin samples displayed a similar cure profile when subjected to a 5°C per minute up to 300°C temperature ramp. Batch one (TTS-DSC1) displayed a lower cure enthalpy of 182.1 J/g compared to 192.7 J/g in batch two (TTS-DSC2) (Fig 4-42).

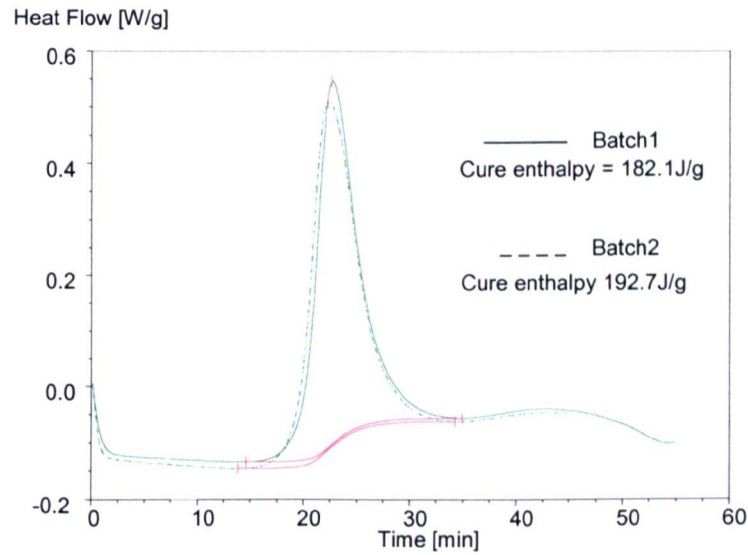


Fig 4-42 DSC results showing cure enthalpy for batch one and two resin (Ref. TTS-DSC)

4.5.3 Rheology

Batch one

The results for batch one (Ref. TTS-RH1) shear storage modulus (G') show increasing apparent stiffness with increasing frequency (ω) in the molten state (Fig 4-43). As temperature is reduced further the stiffening effect is reduced as the material appears to enter a glassy state.

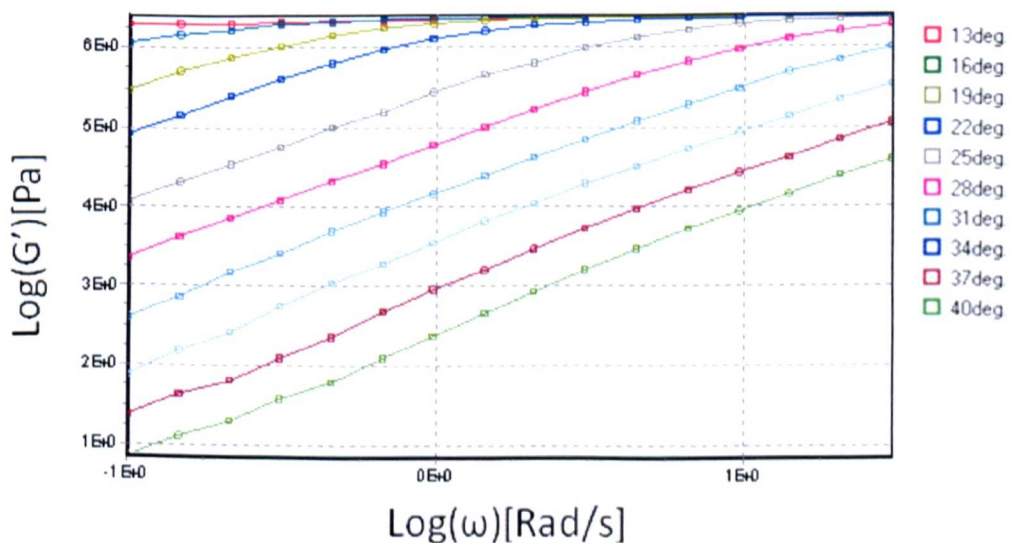


Fig 4-43 Shear storage modulus results for batch one resin (Ref TTS-RH1)

The results indicate characteristics of time temperature superposition. Recently developed Reptate [157] software was used to establish WLF parameters (Table 4-30) for the WLF equation as presented by Reptate authors (Eq 4-1). Once shifted using these parameters, a master curve could be compiled which indicates a molten to glass transition within the strain rate and temperature range of the experiment (Fig 4-44).

Table 4-30 Batch one resin (R1) WLF parameters

Parameter	Value
C ₁	12.8
C ₂	46.8
T ₀	20°C

Eq 4-1 The WLF equation as implemented by Reptate software [157]

$$\log(a_T) = \frac{-C_1(T - T_0)}{T + C_2}$$

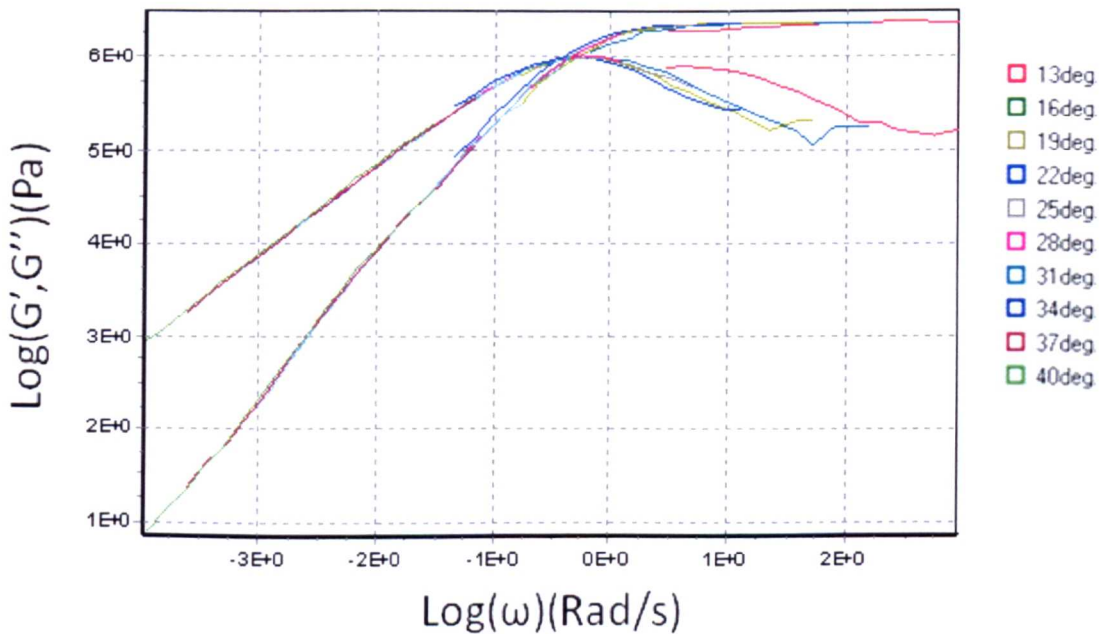


Fig 4-44 Viscoelastic master curve for batch one resin (R1) obtained by WLF time temperature superposition

Batch two

The procedure was repeated for batch two (Ref. TTS-RH2) and showed similar results (Fig 4-45). However, marginal differences in WLF constants are observed (Table 4-31). Construction of a reasonable master curve using the WLF equation was again possible (Fig 4-46).

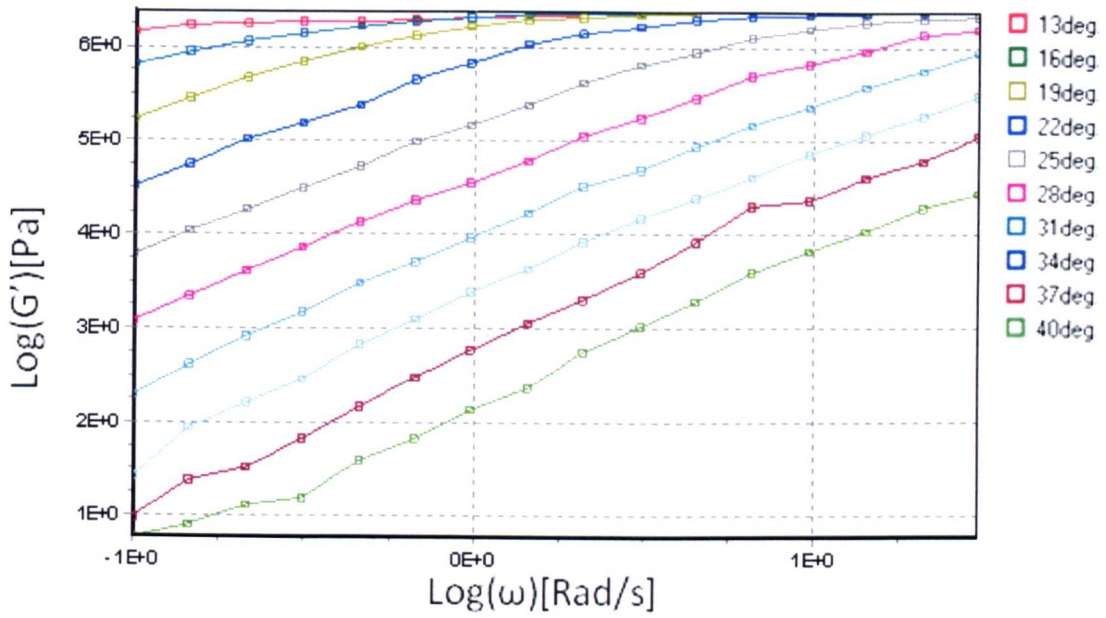


Fig 4-45 Viscoelastic modulus (G') results for batch two resin (Ref. TTS-RH2)

Table 4-31 Batch two WLF parameters

Parameter	Value
C_1	13.7
C_2	59.4
T_0	20°C

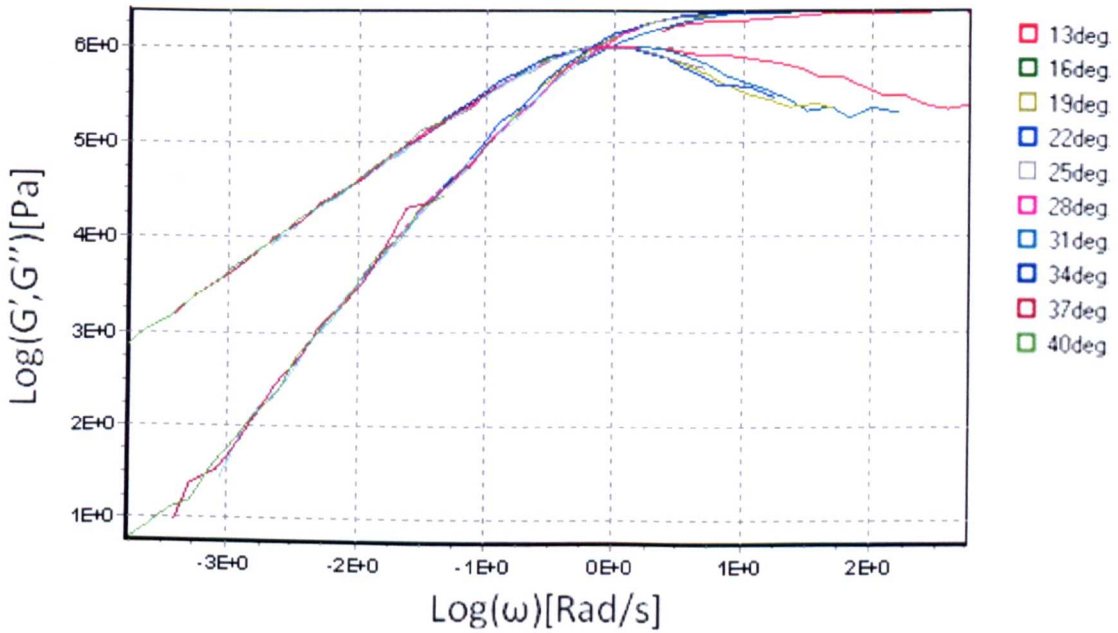


Fig 4-46 Viscoelastic master curve for batch two resin (R2) obtained by WLF time temperature superposition

Comparison

A comparison of master curves reveals that batch one appears to have increased stiffness at all points below glass transition (Fig 4-47).

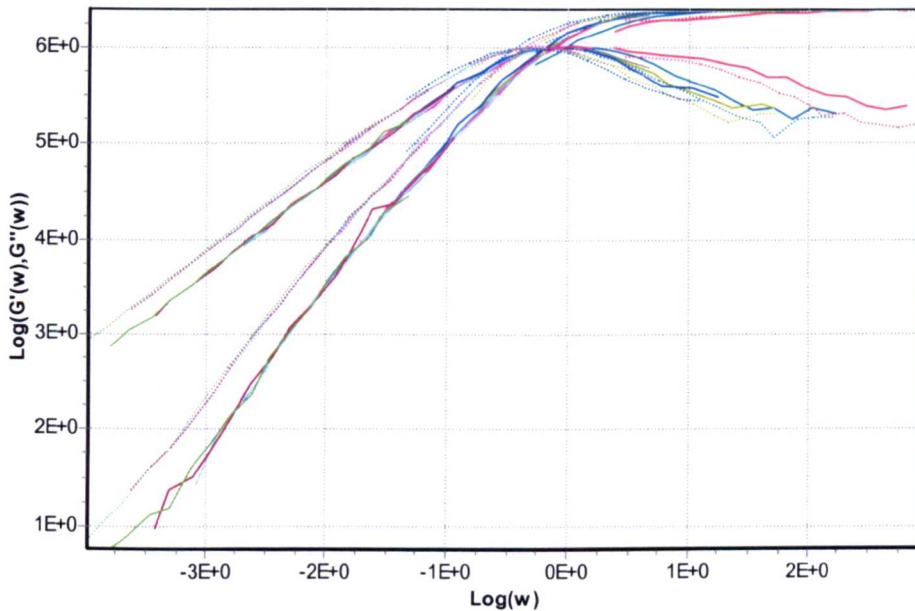


Fig 4-47 Comparison of rheology master curves between batch one (TTS-RH1, dashed line) and batch two (TTS-RH2, solid line) resins

4.5.4 Peel testing

The TTS shifting of peel results was conducted using the WLF equation and constants obtained from rheology of the constituent resin (Chapter 4.5.3). To reduce error each individual data point was shifted based on the prepreg peel surface temperature immediately after the test.

Batch one results

Isothermal peel results (Ref. TTS-TT1) confirm the findings of the temperature and feed rate investigation where a peak in tack is observed in near ambient temperature tests (Fig 4-48). As temperature was increased a higher feed rate was required to initiate peak tack and the transition from cohesive to interfacial failure. WLF TTS of results using constants obtained from rheology (Ref. TTS-RH1) showed that prepreg tack appears to follow the time temperature superposition principle with reasonable accuracy (Fig 4-49). Tack results appear well aligned in both cohesive and interfacial failure modes. The peak tack where failure mode transition occurs is also consistent. Time-temperature equivalency was also observed in resin deposition patterns at equivalent temperatures and feed rates (Fig 4-50).

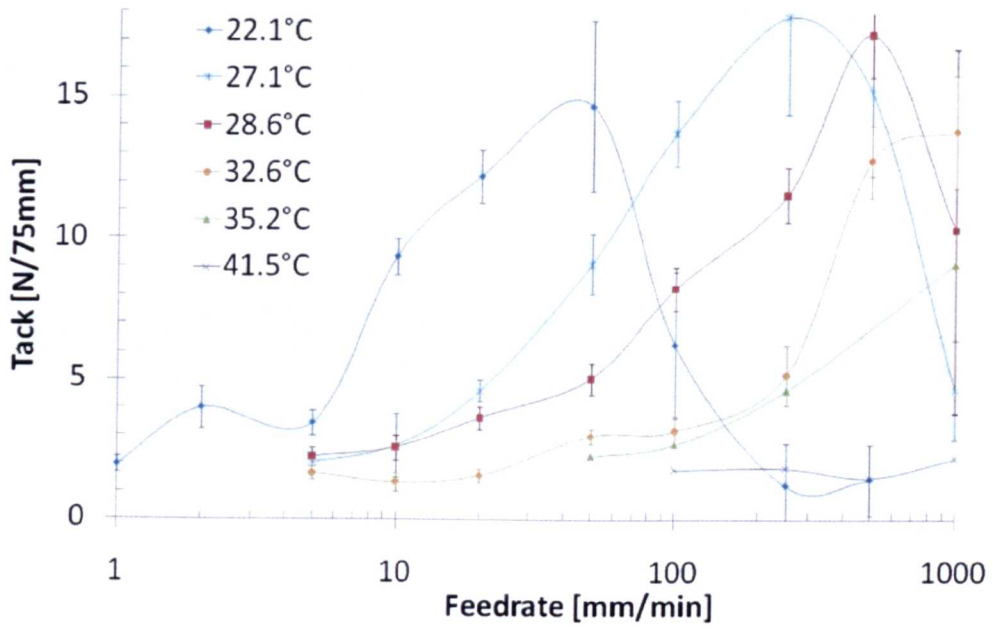


Fig 4-48 Isothermal tack results for batch one prepreg (Ref. TTS-TT1)

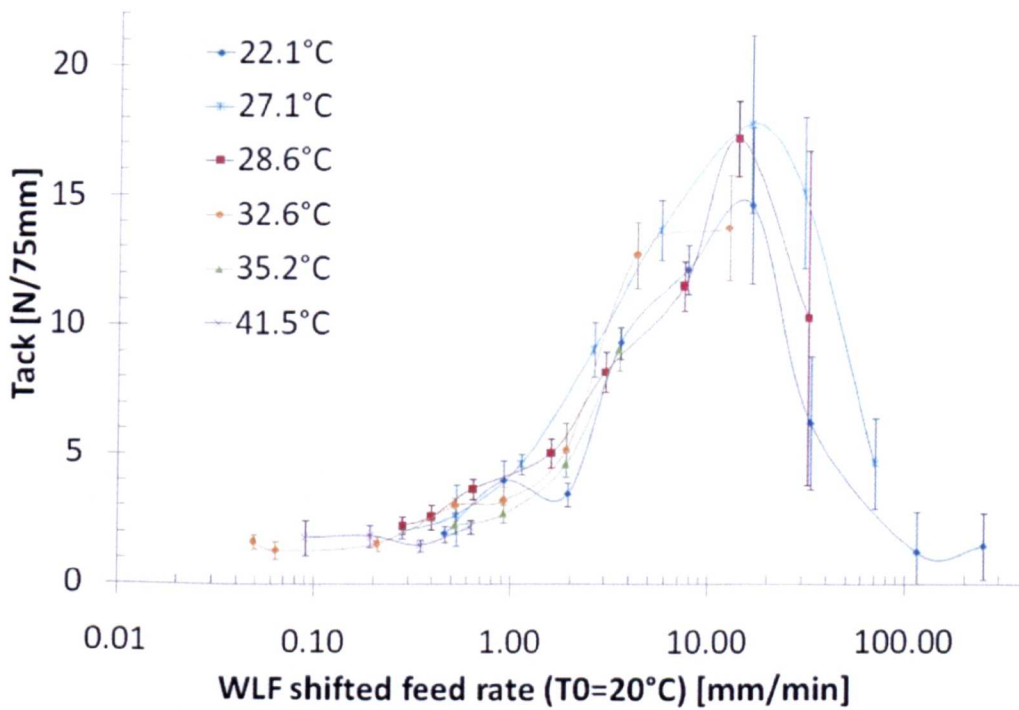


Fig 4-49 Isothermal tack results for batch one prepreg (Ref. TTS-TT1) shifted by WLF transposition using equation constants found by rheology (Ref. TTS-RH1)

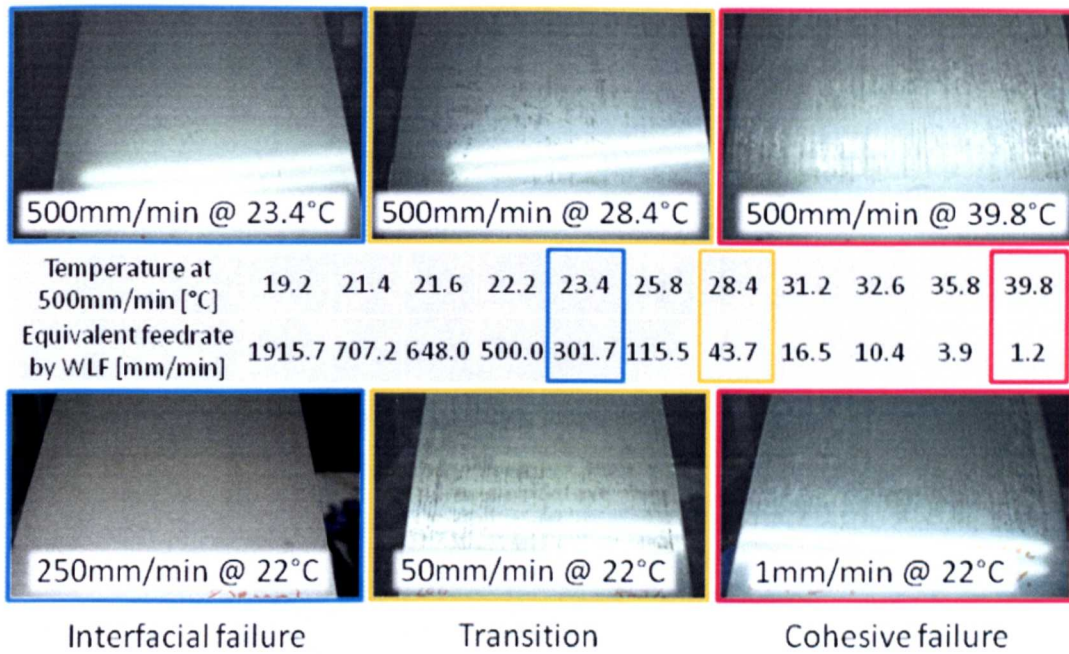


Fig 4-50 WLF time-temperature equivalence observed by resin deposition on test plates following peel (Ref. TTS-TT1)

The stiffness of batch one prepreg (Fig 4-51) (P1) was also transposed using the WLF equation and constants from resin rheology (Fig 4-52). The increasing stiffness appears to be in good agreement with the time temperature superposition principle.

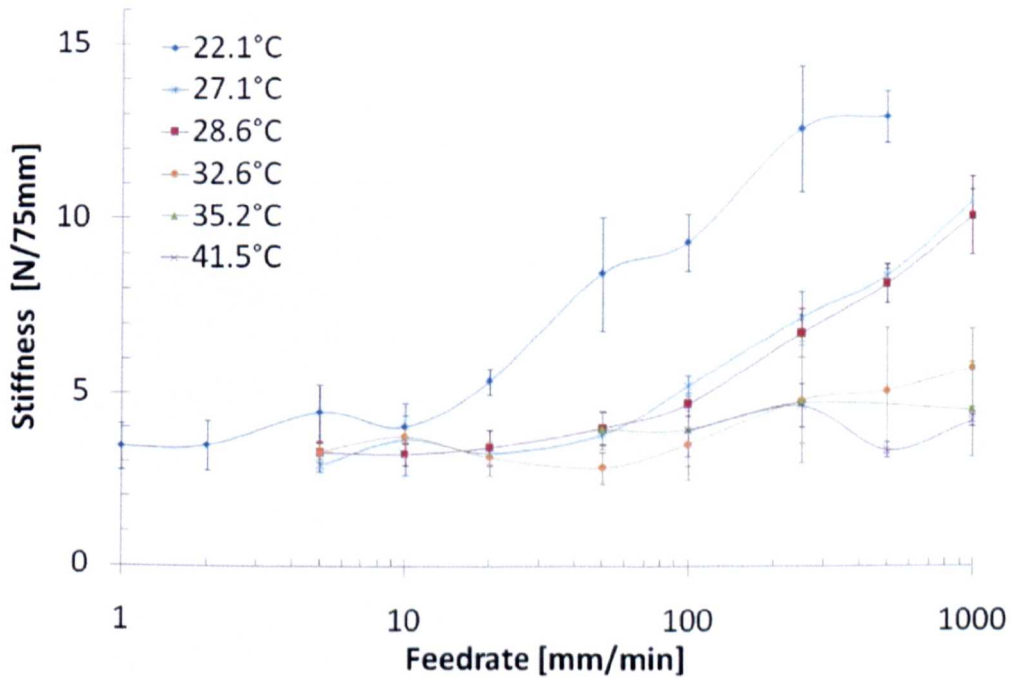


Fig 4-51 Isothermal stiffness results for batch one prepreg (Ref. TTS-TT1)

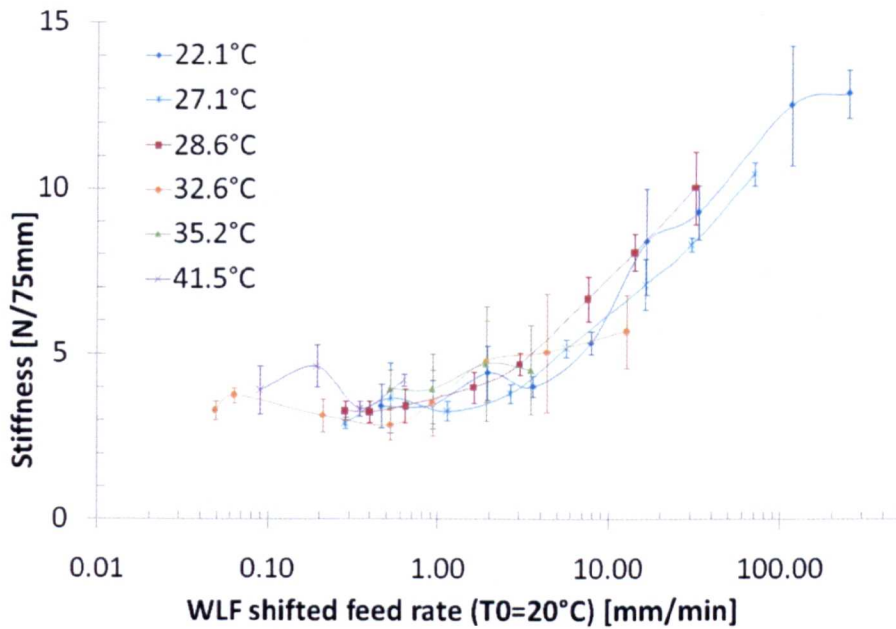


Fig 4-52 Isothermal stiffness results for batch one prepreg (Ref. TTS-TT1) shifted by WLF transposition using equation constants found by rheology (Ref. TTS-RH1)

Batch two results

The procedure was repeated for batch two prepreg (Ref. TTS-TT2) (Fig 4-53). Batch two prepreg was also shown to obey the time temperature superposition principle with reasonable accuracy (Fig 4-54).

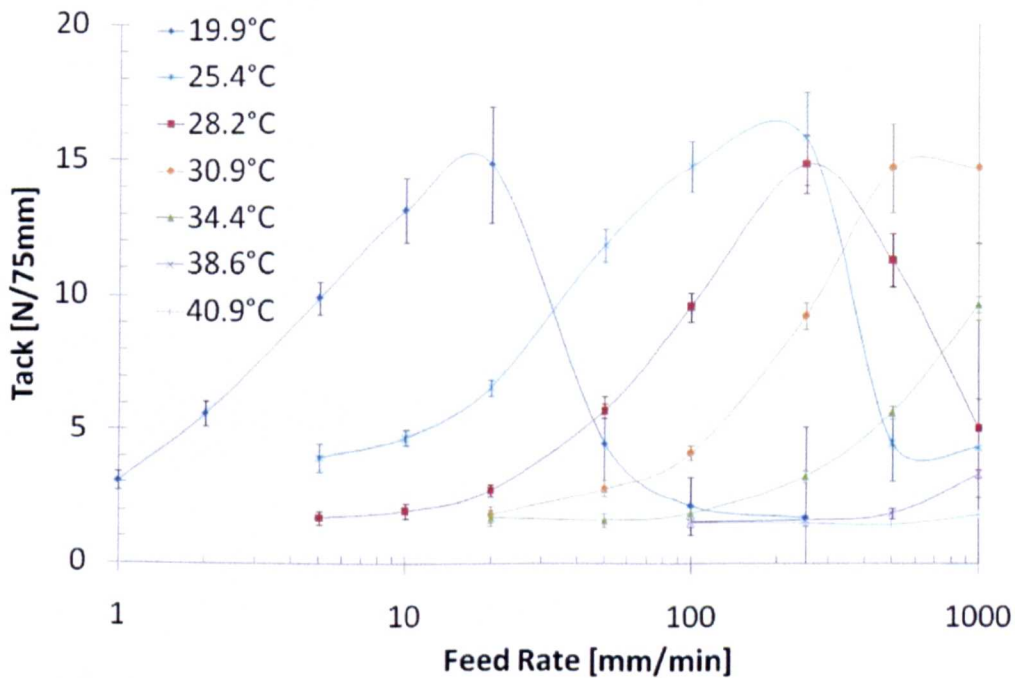


Fig 4-53 Isothermal tack results for batch two prepreg (Ref. TTS-TT2)

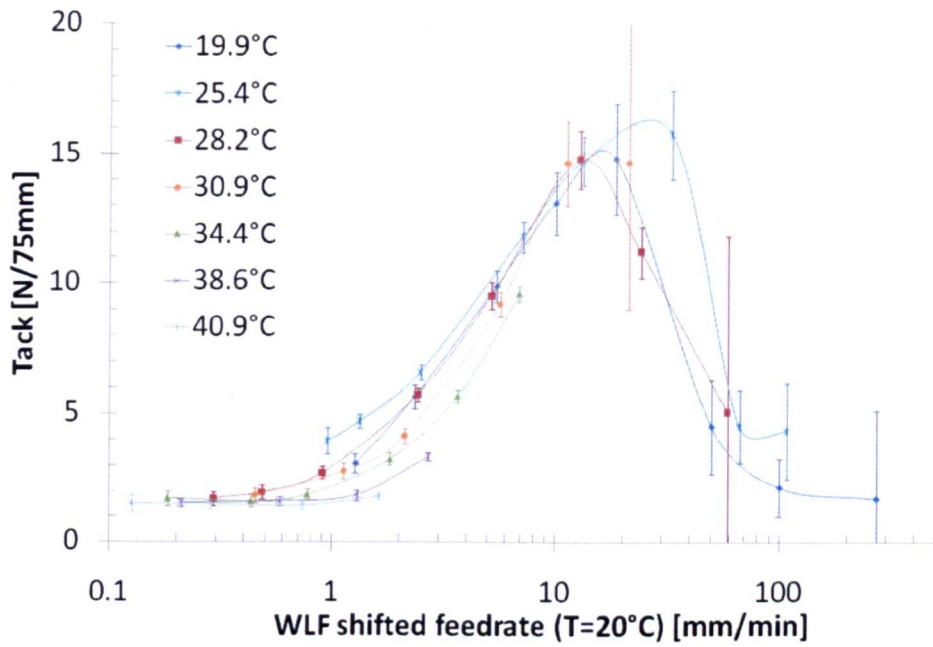


Fig 4-54 Isothermal tack results for batch two prepreg (Ref. TTS-TT2) shifted by WLF transposition using equation constants found by rheology (Ref. TTS-RH2)

The stiffness of batch two prepreg again showed similar results (Fig 4-55) demonstrating conformity to the time temperature superposition principle (Fig 4-56).

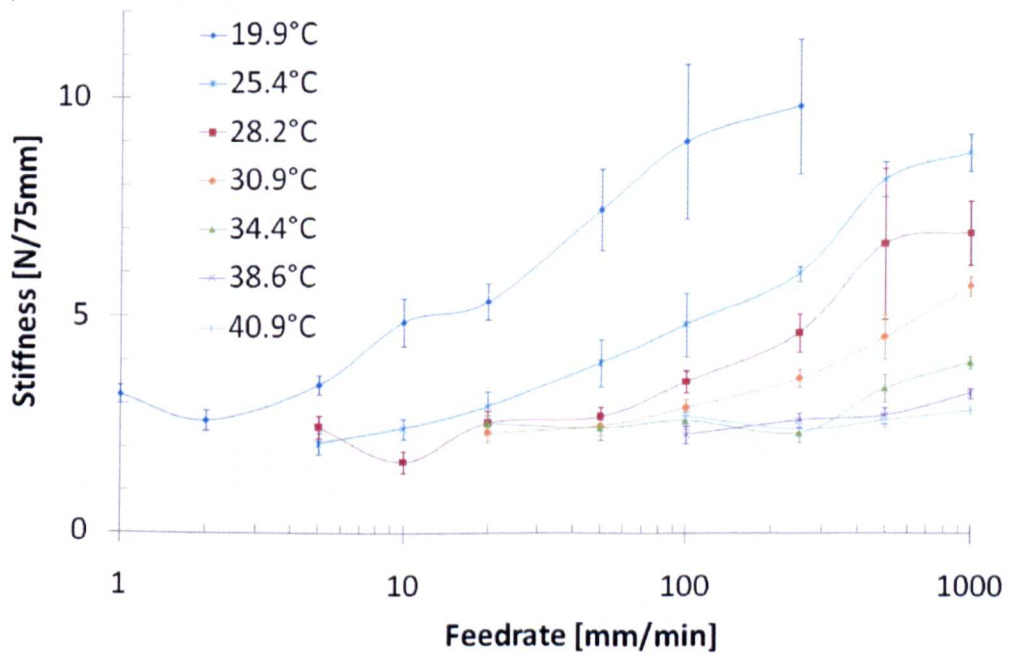


Fig 4-55 Isothermal stiffness results for batch two prepreg (Ref. TTS-TT2)

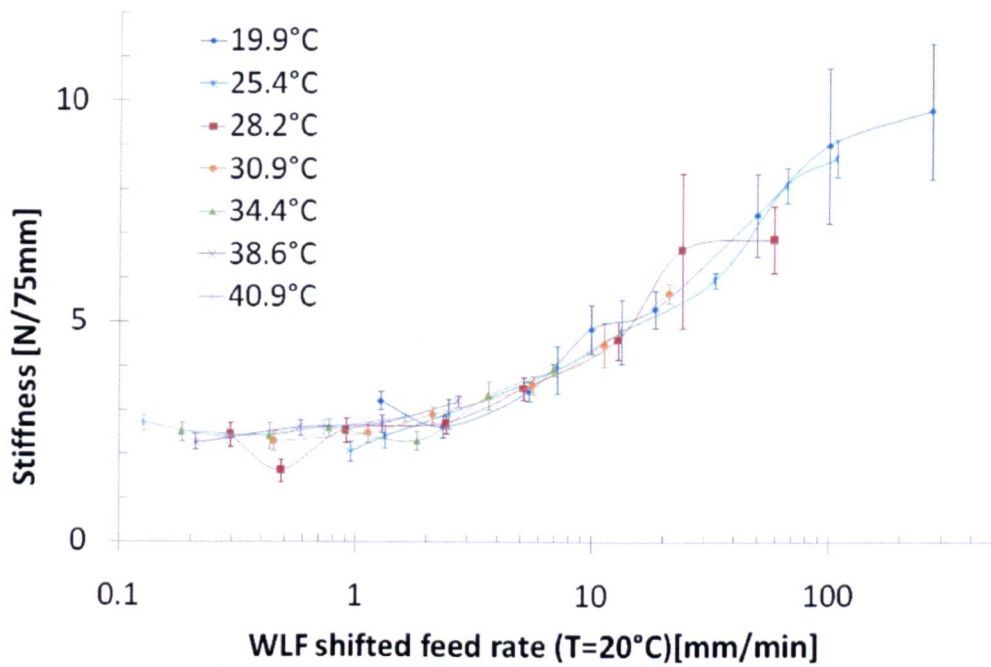


Fig 4-56 Isothermal stiffness results for batch two prepreg (Ref. TTS-TT2) shifted by WLF transposition using equation constants found by rheology (Ref. TTS-RH2)

Comparison

When transposed to ambient 20°C and compared the two batches display similar stiffness and tack properties. However, batch one (Ref. PP1) appears marginally stiffer than batch two (Ref. PP2) prepreg (Fig 4-57). Comparison of the master tack curves also reveals that both batches have similar tack levels (Fig 4-58).

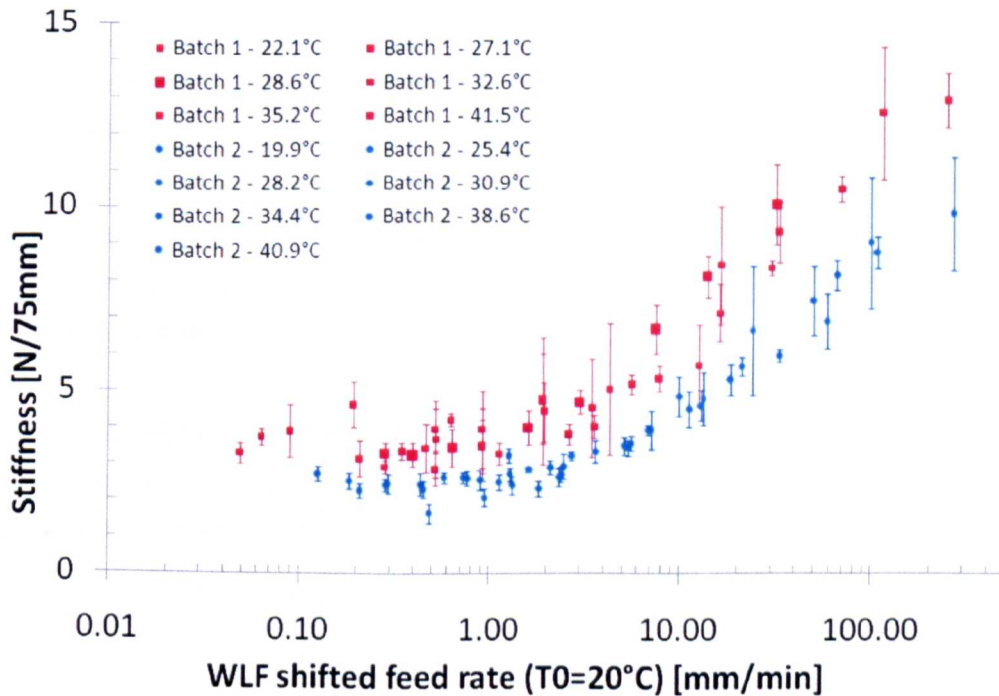


Fig 4-57 Comparison of stiffness for batch one and two (Ref. TTS-TT1 and TT2) prepregs

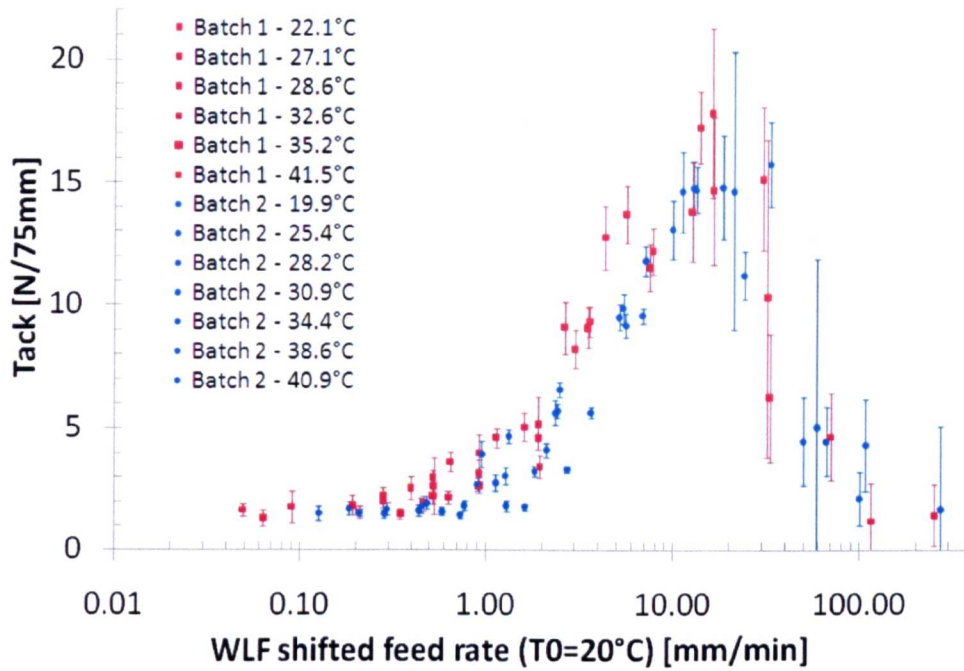


Fig 4-58 Comparison of tack batch one and two (TTS-TT1 and TT2) prepregs

4.6 ATL applicability study

4.6.1 Prepreg tack in commercial conditions

Tack testing of simulated ATL lay-up conditions (Ref. ATL-TT1 to TT4) suggests that the addition of Chemlease 41 significantly reduces available tack (Fig 4-59). The results for tests involving release agent are subsequently low in comparison to experimental error. Therefore, a statistical analysis (Appendix E) is performed to better access confidence levels between these results (Table 4-32). The overall effect of release agent is a 61% reduction in tack within a 99.5% confidence interval. The effect of dichloromethane is 16% in comparison to Chemlease alone with less than 80% confidence, indicating that this effect is mostly due to experimental noise. The effect of tackifier is a 45% increase in tack with 90% confidence.

The results also show that peak tack without tackifier occurs at 34°C and is greater than tack with tackifier at ambient (20°C) temperatures. Therefore, provided tack results can be directly related to ATL, 34°C, 500mm/min would be an optimum mould surface tack operating point on a composite surface coated with Chemlease 41 release agent (Fig 4-59).

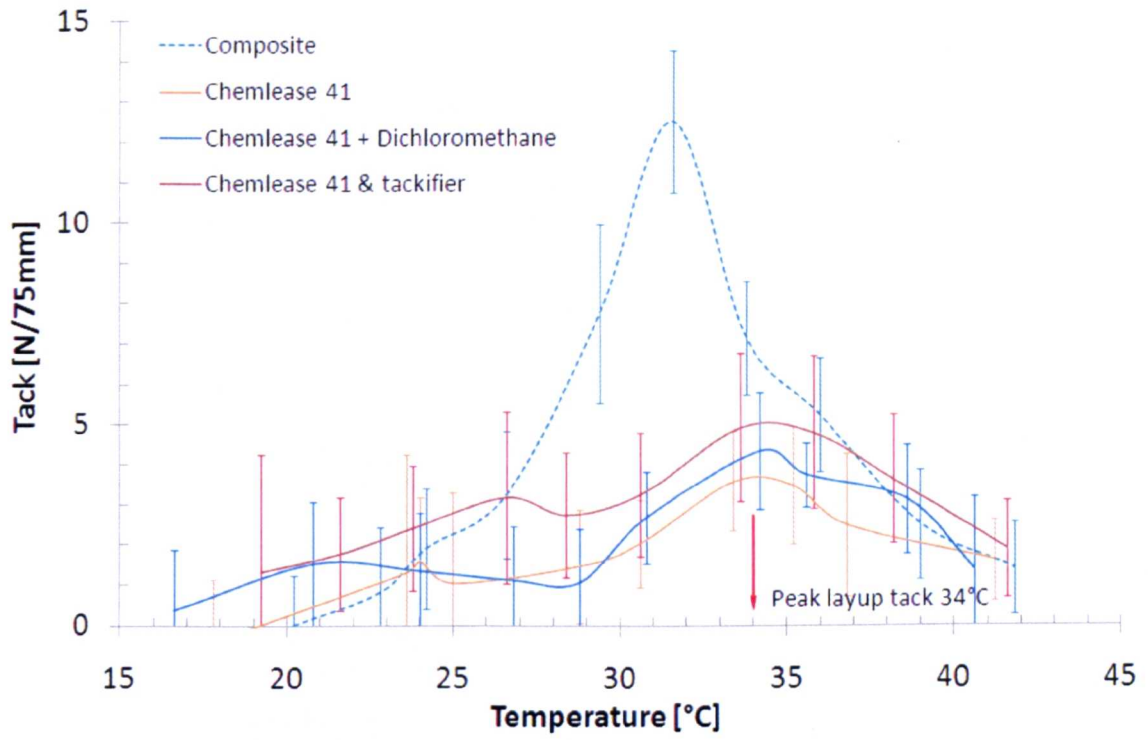


Fig 4-59 Comparison of the tack of WE-ATL prepreg tape under simulated ATL production conditions (Ref. ATL-TT)

Table 4-32 Comparison of simulated production conditions (Ref. ATL-TT) and statistical analysis of the effects of release agent, dichloromethane and tackifier

Surface	Composite	Chemlease	Chemlease & Dichloromethane	Chemlease & tackifier
Av. Stiffness	7.25	7.63	8.23	7.41
Av. $\sigma \pm$	1.30	1.11	1.36	1.36
Av. Tack	4.50	1.74	2.09	3.16
Av. $\sigma \pm$	1.55	1.69	1.37	1.72

Effect of release agent in comparison to composite plate

Effect	2.76	61%
σ_e (estimated total standard deviation)	1.62	36%
t-statistic	3.989	
Confidence Interval	99.5%	(n=11 DOF)

Effect of dichloromethane in comparison to Chemlease alone

Effect	0.35	16%
σ_e (estimated total standard deviation)	1.54	74%
t-statistic	0.537	
Confidence Interval	<80%	(n=11 DOF)

Effect of tackifier in comparison to Chemlease alone

Effect	1.42	45%
σ_e (estimated total standard deviation)	1.7	54%
t-statistic	1.95	
Confidence Interval	90%	(n=11 DOF)

4.6.2 ATL trials

The results of ATL trials showed good correlation with tack test results and use of the time temperature superposition (TTS) principle (Table 4-33). Running at the TTS transposed optimum tack operating point of 20°C, 4mm/min revealed significant tack to the mould surface without the use of tackifier (Fig 4-60). However, edges of the prepreg tape were seen to separate from the main body of the tape.

Table 4-33 Results of ATL applicability trials

Experiment ref.	Feed rate [mm/min]	Temperature [°C]	Lay-up mould tack performance
ATL-1	4	20	Excellent mould tack level, tape splitting at edges
	20	20	Good tack level
	50	20	Acceptable, some tack available
	100	20	poor
	200	20	Lay-up failure, zero tack
	400	20	Lay-up failure, zero tack
ATL-2	400	≈34	Good tack levels in patches, through thickness tape splitting



Fig 4-60 ATL lay-up at ambient temperature ($\approx 20^\circ\text{C}$) and 4 mm/min feed rate

Increasing feed rate without increasing heat shows a progressive loss of tack with negligible tack observed at 100mm/min resulting in lay-up failure (Fig 4-61). Laying up at 400mm/min and attempting to reach a peak tack temperature of 33°C, according to the WLF relationship, revealed an increase in tack. However, uniform heating using a hand operated heat gun was unachievable. Patches with lower temperatures displayed lack of adhesion compared to patches of correctly heated material. Overheated patches were observed to fail cohesively leaving resin patches on the mould surface accompanied by through thickness splitting of ATL tape in these areas (Fig 4-62).



Fig 4-61 ATL lay-up at 20°C and 100 mm/min feed rate (Ref. ATL-1)

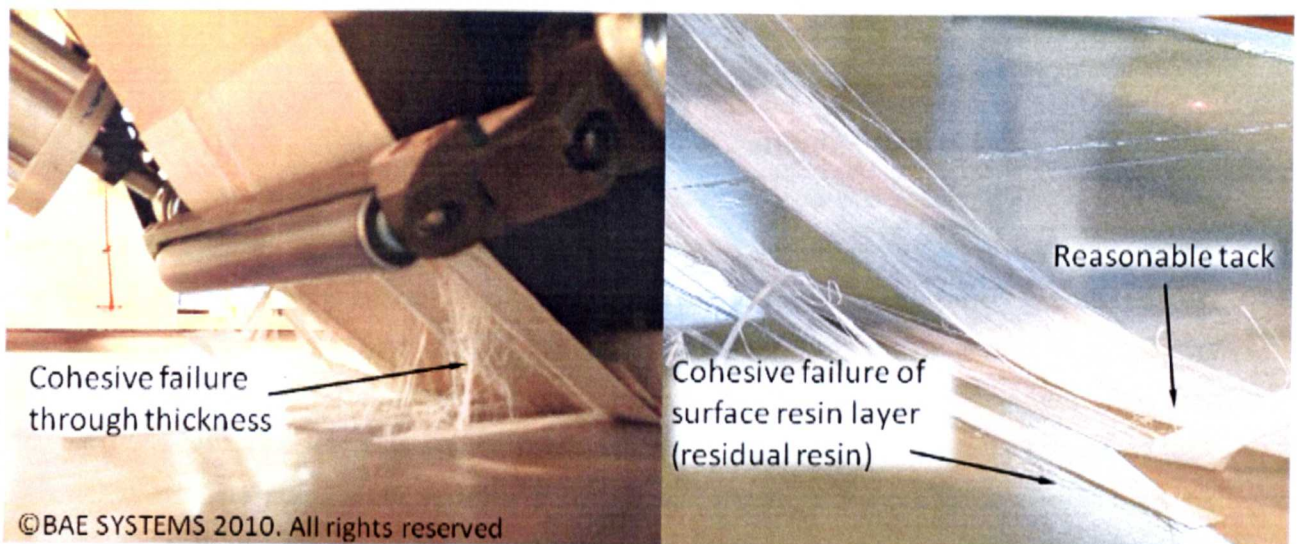


Fig 4-62 ATL lay-up at a non-uniform optimised temperature of 25-45°C and 400 mm/min feed rate (Ref. ATL-2)

5 Discussion

5.1 Tack and stiffness methodology

A standardised method for tack and stiffness testing of uncured prepreg is not apparent. At present, commercial prepreg tack appears to be analysed by simple subjective methods. Subjective specifications of low, medium and high tack are seen on product datasheets. Experimental methods of quantifying tack exist within research, where prepreg is quantified using methods taken from the pressure sensitive adhesives (PSA) field. PSA methods are often complicated and affected by many variables. Therefore, the lack of quantification of tack is possibly due to the lack of an easily understood method of characterisation and standardisation of test variables. Further development is therefore needed considering the importance of prepreg tack in lamination [36], production [46] and shelf life [53].

PSA probe methods (Chapter 2.5.1) give force and extension values for a typically flat circular probe surface and disc of resin. Normally, stress values are calculated using the surface area of the probe without the actual resin contact area being known. Optical methods for determining actual contact area are available at significantly increased cost and complication. The probe test is typically favoured over other methods since the application or compression stage can be carefully controlled during the test. The test also has the advantageous ability to record force throughout the various stages of tack increasing its analytical ability. Values for peak stress and work of adhesion can be calculated from results. The work of adhesion appears to be analogous to peel strength (Fig 5-1). However, during the peeling process the angle of each stage in relation to the direction of peel is likely to change resulting in inconstant values between the two methods.

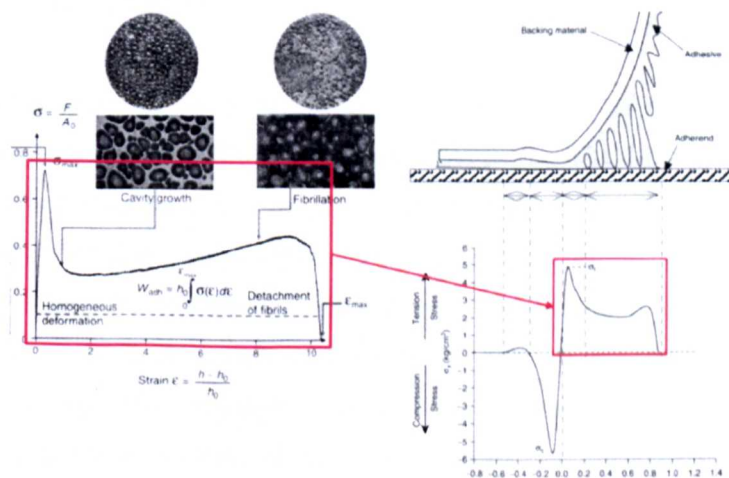


Fig 5-1 Comparison of probe results (left [75]) with measurements taken along the peel front (right [100])

Probe results may be complicated due to phenomenon such as cavitation and fibrillation, thought to be effected by vacuum pressure and surface irregularities. The effects of these complications are likely to be increased by surface patterns of fibres in prepreg [83]. The probe method also appears to be significantly affected by alignment issues [158].

The peel test was favoured in this study mostly for its similarity to the ATL process. However, the peel test is considered inferior to probe testing as an analytical tool due to an inability to:-

- control application conditions
- analyse individual stages of separation
- separate the effects of peel from bending stiffness

The newly designed peel method allows control of application conditions and has the ability to isolate peel and bending stiffness effects. A single value for peel resistance, considered analogous to work of adhesion in probe testing (Fig 5-1), was considered acceptable since this study sought to compare the tack of materials rather than study the tack mechanism.

The new peel method also allowed the investigation of a number of variables which are found within the ATL process (Table 3-3). In addition to these variables humidity is believed to effect tack and the aging of prepreg materials [159]. An environmental chamber was unavailable to control humidity and quantify its effect. The humidity was found to change 15-80% R.H. depending on weather conditions. Therefore, tests for establishing the effects of variables were carried out within the shortest time period possible limiting full factorial experiments. Comparisons between variable investigations are therefore made with caution.

The level of repeatability was found to be good. Low rig friction was recorded $>0.7\text{N}$ and variability in rolling tests of thin films was less than 0.3N . The higher variability found in tack testing was attributed to the material itself and the nature of the peeling process. Variability could be reduced somewhat by stringent handling and cleaning methods (Chapter 3.3.4). However, variability was found to increase when approaching the interfacial failure domain and is believed to be an inherent property of the interfacial peeling process through the storage and sudden release of elastic energy. Overall, results were comparable to perceived tack levels and the repeatability was considered acceptable for materials characterisation.

5.2 Effect of variables on tack and stiffness

5.2.1 Temperature

Initial findings using GUD1600 material showed a decrease in tack. This result was in contradiction to manufacturer's expectations since low tack materials are often heated to improve tack. Therefore, the range of materials was extended to include low tack materials. Temperature was subsequently found to increase the tack of low tack materials. Further observations revealed a visual change in failure mode between the two materials. An extended temperature sweep using WE-ATL material found that both failure modes could be observed. At low temperatures a dry surface failure was apparent and at high temperatures a wet fibrillation failure was observed. A peak in tack force was also observed to be consistent with transition between failure modes for all experiments.

The two failure modes appear analogous to interfacial and cohesive failure found in PSA peel [75]. The additional interfacial failure modes found at the backing substrate in PSAs [75, 104] are prevented in prepreg due to the fibres being gripped. Therefore, peeling appears to occur between the fibres and surface interfaces. Rationalisation of the failure mode and tack response in PSAs is found by comparing rheological data [75]. At lower temperatures the resin appears too stiff to deform to the surface irregularities. Therefore the resin is unable to achieve the intimate contact required for adhesion, resulting in interfacial failure. The resin would be considered contact inefficient at this temperature according to the Dahlquist criterion (DC), as the shear storage modulus lies above 3×10^5 pa [119]. The rheology of prepreg resin appears to show good agreement with the DC concept in some cases (Fig 5-2). The high tack resin meets the criteria at ambient temperature where low tack resins require increased temperature. The peak tack found in WE-ATL (M19.6LT) appears to be at a consistent temperature with the point at which the DC is met. However, aerospace (8552) is not consistent with the DC and changes in prepreg architecture are shown later to effect the point of peak tack. Therefore, this indicates that the actual value for a Dalquist style prepreg criterion is likely to be a function of both shear modulus and surface conditions.

In summary, tack appears to be a function of interface and cohesive resin strength. Whichever is the weaker will dictate the failure mode and tack force recorded. The effect of temperature on each phenomenon is contradictory. Temperature increases interfacial but decreases cohesive strength, therefore the maximum tack value in a temperature sweep will occur at the point where interfacial and cohesive strength are equal. A

reduction in prepreg stiffness is observed in agreement with the reduction in shear storage modulus of the resin component with increased temperature.

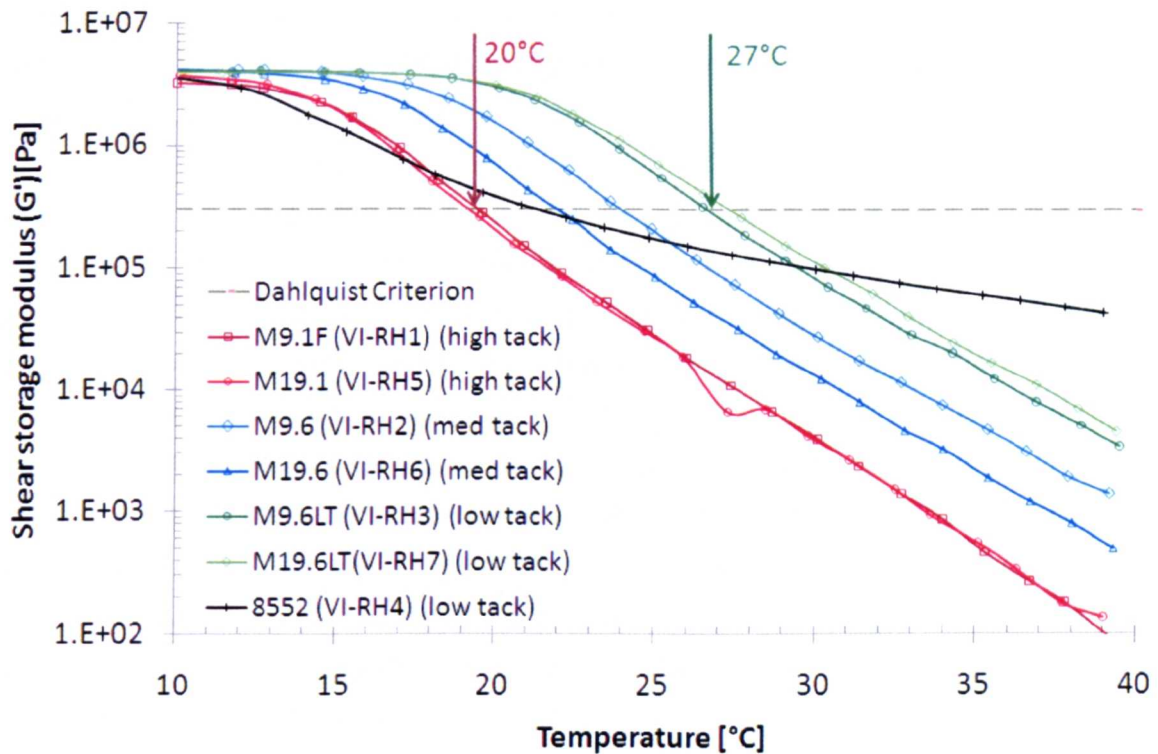


Fig 5-2 A comparison of prepreg resin shear storage modulus to the Dahlquist criterion

5.2.2 Feed rate

Prepreg materials appear to be equally responsive to changes in feed rate as changes in temperature. Both the interfacial and cohesive failure modes are observed in a single sample over a feed rate range of 1-1000mm/min and peak tack is evident at a consistent point with the transition between failure modes. The prepreg resin is later shown to obey the time temperature superposition principle found in rheology of amorphous polymers [103] and PSA peel testing [98] (Chapter 4.5). The result is an apparent stiffening of the resin at increased strain rates, or in this case feed rate.

The measured bending stiffness is consistent with an increase in apparent resin stiffness. The increasing apparent stiffness increases tack in the cohesive failure condition with increased feed rate. However, interface strength appears reduced through reduced contact time and poor wetting. The peak is again observed at a point where cohesive and interface strength is equal.

5.2.3 Surface roughness

Interactions with the surface are not expected during the bending portion of the test since both surfaces of the prepreg are covered. Therefore, the lack of effect of surface finish on bending stiffness is unsurprising with minimal effect attributed to a change in rolling friction between the surfaces.

Surface roughness was found to have a minimal effect on tack. This result were considered surprising in comparison to the significant effect found in probe testing [95]. The lack of effect could be attributed to the change in surface roughness of the test plate being low in comparison to the prepreg surface roughness (Fig 5-3). Surface profiles of prepreg samples were also obtained. The tack of the prepreg samples required that the samples be frozen or air cured to avoid damaging the test probe. A comparison of prepreg and the roughest test plate reveal that the prepreg has a significantly rougher surface. In practice, mould surfaces are typically much smoother than $R_a=1.92$. Therefore, the variation in mould surface finish is now considered to be insufficient to affect prepreg tack. However, effects due to changes in the surface finish of the prepreg remain possible.

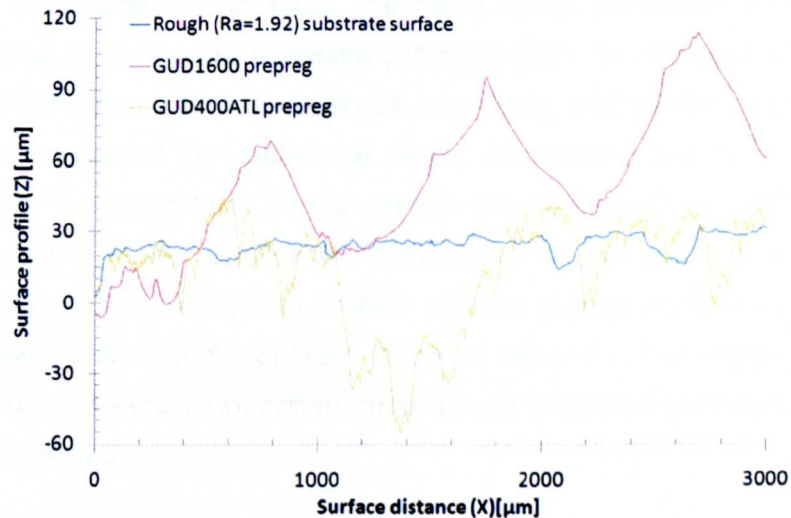


Fig 5-3 A comparison of rigid substrate ($R_a=1.92$), WE-ATL and GUD1600 prepreg surface profiles over 3mm

5.2.4 Release agent

No effect on prepreg stiffness was observed. This was considered a logical result since the only available mechanism for release agent effect appears to be through reduced friction on test plate, the effects of which are found to be minimal.

A significant reduction in tack is demonstrated with the use of release agent at ambient temperatures. When considering temperature interaction effects, release agents also appear capable of increasing the transition temperature to cohesive failure. For cohesive failure to occur adequate surface adhesion is required. The presence of a release agent appears to effectively act as a weak boundary or contaminate layer preventing interfacial adhesion of the polymer resin to the rigid surface [73]. However, some adhesion and cohesive failure may still be observed, albeit significantly reduced, at a higher temperature (Fig 4-24) signifying that a minimal amount of penetration of the layer may still be possible.

5.2.5 Compaction force

The apparent increase in stiffness is likely to be the result of increased friction in the roller bearings and material due to the increased reaction forces. This is most apparent when considering a temperature sweep where the increase in stiffness remains constant throughout the temperature range. Therefore, stiffness values can only be compared with those tested at equal compaction force.

Results at ambient temperature (Ref CF01-3) show a decrease in tack levels which is repeatable but not entirely understood. The result is also inconsistent with the generally perceived increase in tack with increased pressure [61]. In the case of CF01 and CF02 fully developed cohesive failure is observed, signifying that surface wetting is complete and cannot be improved by additional force, consistent with the suggestion that application force is unimportant during certain lay-up conditions [64]. A reduction in tack observed with a higher application force could be the result of a greater area of resin being displaced to give fibre to surface contact reducing the resin layer thickness. During experiment CF03 interfacial resin failure is observed, here improved tack should be observed with increased compaction force due to improved surface contact, however no increase is observed.

Testing over a temperature range (Ref. CF04) which included both failure modes gives a clearer indication of the effects of compaction force on tack, showing that increased compaction force is most effective within the failure mode transition region (25-45°C). This appears logical for fully cohesive failure since full wetting has already occurred and failure is reliant on resin strength which is not improved by increased pressure. During interfacial failure it is possible that the increase in compaction force is supported mostly by the fibres and therefore does not improve resin contact.

5.2.6 Surface type

The significant increase in peak tack and overall tack levels (Fig 4-27) appear to be consistent with the increase in adhesion energy found when comparing Epoxy-A to stainless steel and glass surfaces (Fig 5-4). The maximum effect appears to be on the interfacial failure mode where transition to cohesive failure is seen to occur at a lower temperature with increased surface energy. This is consistent with the findings of PSA peel experiments [111]. Once cohesive failure is initiated in all three surfaces the tack values are relatively similar for the remainder of the temperature increase (Fig 4-27). Since the resin rheology remains constant and only the surface is changed, it appears to again indicate that overall tack is a measure of two components; an interfacial surface component, which is a product of interfacial contact, and a cohesive viscoelastic component, a product of resin cohesive strength. The peak tack appears to occur where the two components are equal. The new test may offer an alternative simplified means of comparing solid surface energy, considering the difficulty of existing methods [160].

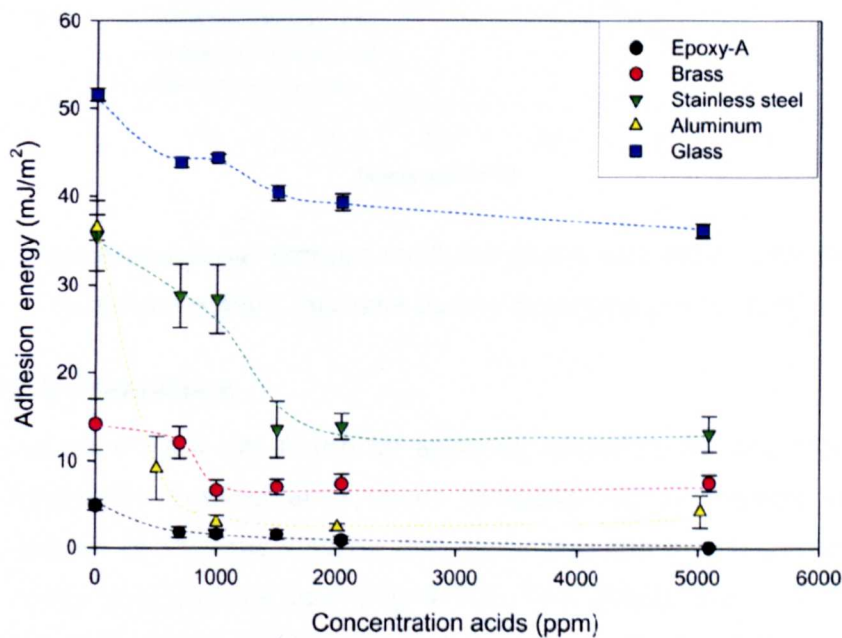


Fig 5-4 Adhesion energy between buffer solution and solid surfaces in petroleum ether with different concentrations of naphthenic acids [160]

5.2.7 Resin type

A significant effect on tack was recorded at ambient temperatures. A change in failure mode was also observed from cohesive failure in high tack resins to interfacial failure. When shear storage modulus of the resin systems are compared the high tack resin is shown to satisfy the Dahlquist criterion for contact efficiency. Tack appears to be reduced in medium and low tack resin through a change in failure mode from cohesive to interfacial failure as shear storage modulus is increased (Fig 5-5). The increased

shear storage modulus of the resin is consistent with an increase in molecular weight [116, 154] (Fig 5-5). The increase in molecular weight is consistent with the B-stage reaction used during the prepregging process of simple BPA Dicyandiamide cured resin systems [161] (Chapter 2.1.1) where the degree of reaction or polymerisation dictates molecular weight, resin stiffness and therefore tack.

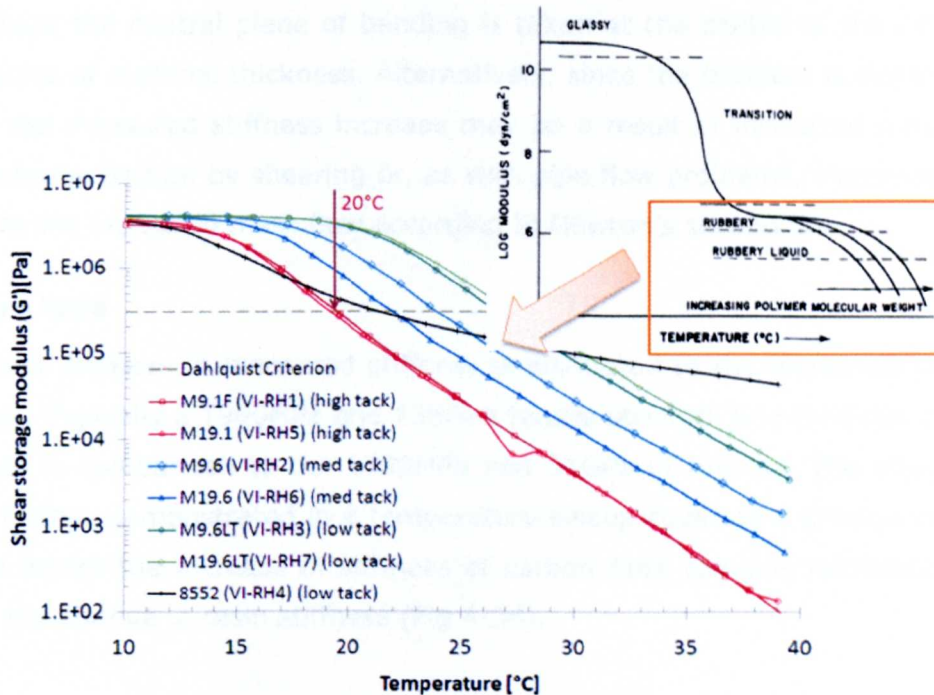


Fig 5-5 The increased shear storage modulus of low tack resins consistent with a molecular weight increase during b-staging resin [116]

5.2.8 Contact temperature

Significant increases in tack are found by applying materials at increased temperature and then subsequently peeling at a lower temperature. Increasing the application temperature appears to improve wetting and eliminates the interfacial failure mode for subsequently lower temperature peel (Fig 4-30). The effects are seen to reduce with increasing temperatures particularly after both samples enter the cohesive failure mode. The difference between the two samples could be the loss of tack due to incomplete surface contact.

5.2.9 FAW

No significant effect on tack was found in comparison to experimental deviation for an increase in fibre areal weight. Resin weight is increased proportionately with fibre weight signifying that the resin layer on the surface would theoretically remain unaffected. However, it is expected that tack would be affected by a change in impregnation or resin distribution caused by a change in FAW, although it has not been observed here.

There appears to be a linear relationship between increasing FAW and increasing stiffness. This relationship is not consistent with basic beam bending principles where a cubed increase in stiffness would be expected with increased thickness. However, the behaviour would be consistent with a membrane under tension and the parallel axis theorem where the central plane of bending is taken at the centre of the roller rather than the centre of material thickness. Alternatively, since the problem is dynamic rather than static the measured stiffness increase may be a result of increased roller friction, increased internal friction by shearing or, as with pipe flow problems, increased reaction forces due to the increased mass flow according to Newton's second law.

5.2.10 Fibre type

The significant increase in measured stiffness is attributed to the increased stiffness of carbon fibres. Typically a 1900MPa and 135GPa tensile strength and modulus is found in carbon fibres in comparison to the 1300MPa and 51GPa of E-glass. The effect of fibre stiffness is further demonstrated in a temperature sweep covering a change in viscosity of the resin where the increase in stiffness of carbon fibre remains relatively constant throughout the change in resin stiffness (Fig 4-34).

There is a significant reduction in tack for carbon fibre prepreg which is apparent throughout the temperature sweep. Both failure modes are observed in resin deposition of both specimens with the exception that the carbon sample does not have a corresponding distinct peak in tack (Fig 4-35). There are three possible hypotheses to account for the effect:-

- Differing impregnation and resin volume affecting the surface resin layer
- Electrostatic effect
- Failure at the fibre interface

Impregnation effects

Differences in resin deposition patterns on rigid test plates are observed between glass and carbon prepreps. Carbon samples exhibit a more defined stripe pattern (Fig 5-6). Microscopic inspection of carbon and glass samples shows that carbon samples consist of variably impregnated resin-dry bundles with the majority of resin occupying trenches between bundles (Fig 5-7) unlike glass samples which show less defined bundles and greater resin layer uniformity (Fig 5-8). Therefore, it is likely that difference in tack is due to a reduced actual contact area of the resin as the carbon fibre bundles support the majority of the applied compaction load. The change in impregnation is most likely due to a change in resin volume. Although resin content by weight increases by only 2%, the volumetric ratio of resin increases from 41.4% in the carbon to 50.1% in the E-

glass due to the lower density of carbon fibres (1.78 g/cm^3) in comparison to glass (2.56 g/cm^3). The resultant loss of resin volume appears to show a reduction in the thickness of the surface resin layer indicating that a larger deformation is required in carbon tapes for resin contact. This distance is not achievable until the resin becomes viscous at higher temperatures at which point the cohesive strength of the resin is too low to maintain the tack load.

Electrostatic effect

Despite the difference in impregnation between the two materials an additional electrostatic effect is not completely ruled out since an electrostatic field is shown to affect wetting and contact angle of fluids [162]. There are also suggestions that electrostatic forces could be used as an independent means for controlling tack during the ATL processing of glass-epoxy materials [64]. The glass prepreg is non conductive and could allow a static potential voltage to form, favourable for electrostatic adhesion, between the fabric and test plate. The electrical conductive properties of the carbon fibres could allow this voltage potential to dissipate for the entire sample on initial contact.

Interfacial failure at the fibre interface

Interfacial failure at the glass fibre interface is dismissed due to the high surface energy of glass (Chapter 5.2.6) and evenly impregnated resin distribution. However, the lower energy of carbon and poor impregnation may allow for failure at the resin-fibre interface. In this case plate depositions would appear to show cohesive failure since the resin layer remains on the ridged substrate. Therefore, this effect cannot be dismissed completely as it is difficult to observe requiring microscopic images of the peeling process.



Fig 5-6 A comparison of E-glass and carbon fibre prepreg resin deposition pattern on rigid substrates

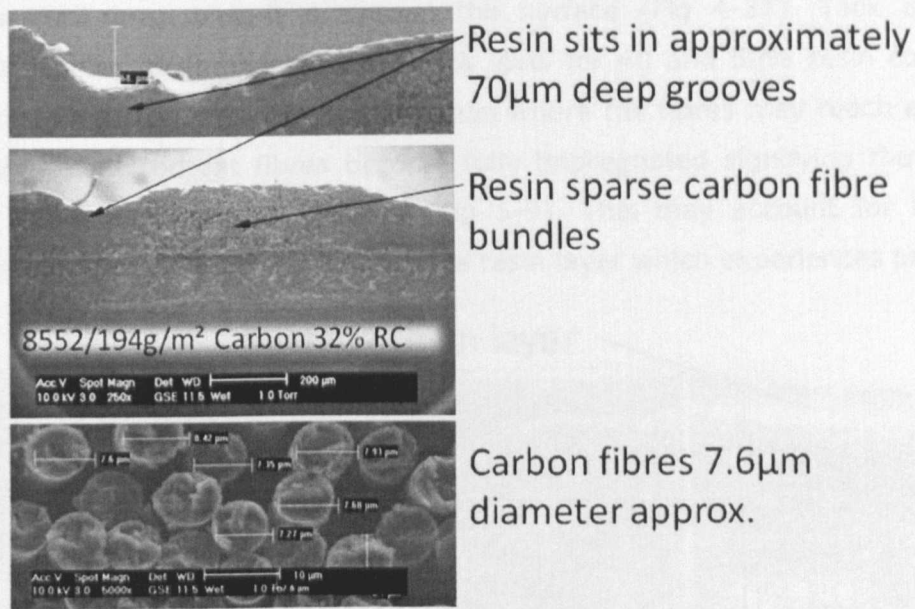


Fig 5-7 Resin impregnation of carbon fibre ATL prepreg tape

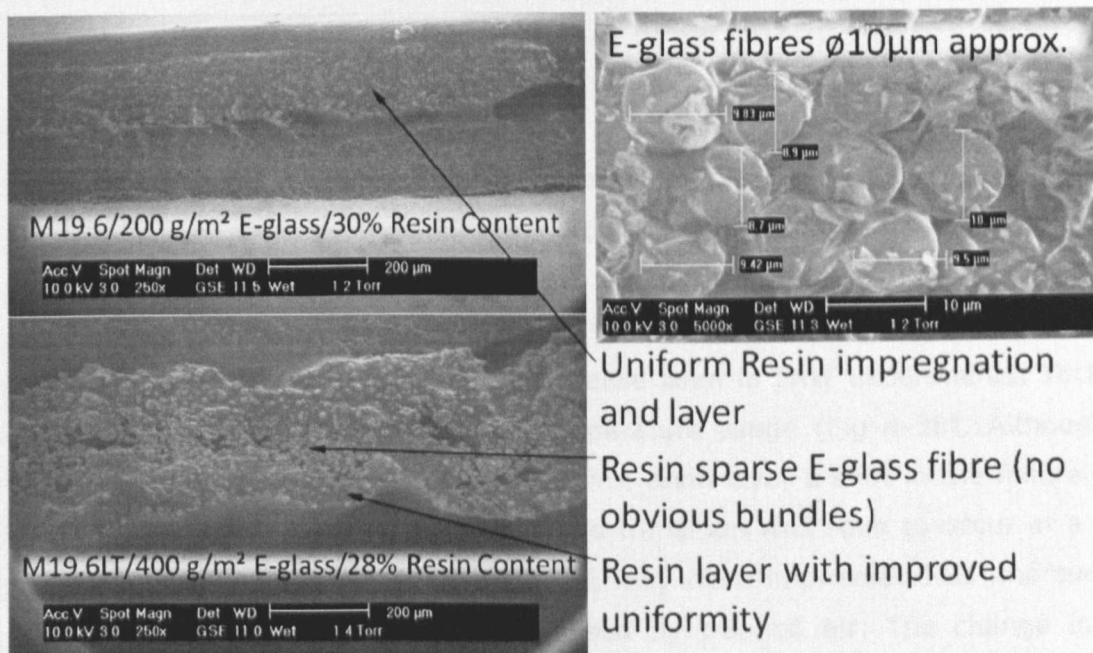


Fig 5-8 Resin impregnation of glass fibre prepreg

5.2.11 Resin content

A 64.6% increase in tack is observed between the 30 and 50% resin content prepreg. However, 89.4% uncertainty dictates that no significant conclusion can be gained from such results at ambient conditions (20°C) (Table 4-20). A significant 65.5% effect with 24.2% uncertainty is observed on temperature sweeps where both cohesive and interfacial failure modes are observed (Table 4-21). The discrepancy is likely to be due to interfacial failure, mostly seen at ambient conditions (20°C), being less affected by

resin layer thickness since it occurs at the surface (Fig 4-37). Tack is however, significantly increased around the peak tack level for 40 and 50% resin content. This sudden increase could be due to impregnation where the fibres may reach a saturation point. At this resin content fibres become fully impregnated signifying that additional resin may then reside on the surface (Fig 5-9). This may account for the sudden increase in tack since it is mostly the surface resin layer which experiences peel.

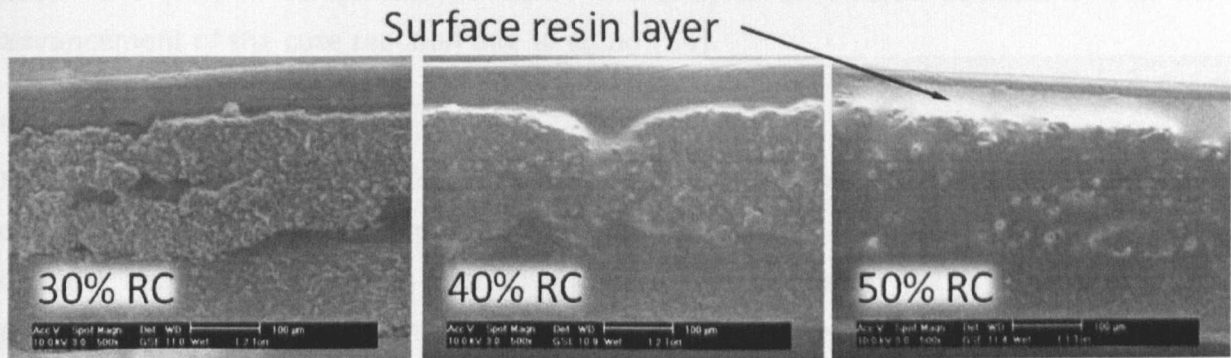


Fig 5-9 Impregnation of M19.6 200g/m² 30, 40 & 50% resin content prepreg

5.2.12 Fibre architecture

The effects of fibre architecture cannot be isolated completely using this experiment due to a rise in fibre areal weight from 200 to 1200g/m². This was the minimum weight that could be produced for multidirectional fabrics on the prepreg pilot line that was used. The stiffness was found to be consistently six times higher throughout the temperature sweep (Fig 4-39) showing a proportional increase seen in FAW experiments. Tack was also significantly higher throughout the temperature range (Fig 4-38). Although the increase is consistent with an increase in surface resin layer a shift in the failure mode transition temperature was also observed. The transition was seen to occur at a lower temperature indicating that interfacial contact may have improved. This improvement could be attributed to a vacuum effect caused by trapped air. The change in fibre pattern, where fibres now run transverse to the rollers, allow air to be trapped rather than escaping along the groves created by unidirectional fibres normal to the rollers. The trapped air could be subject to a vacuum force at the early stages of peeling [94]. Such an effect is also experienced in probe testing of prepregs [83] and may account for the significantly higher than expected tack of multidirectional commercial prepregs (Chapter 4.2.3).

5.3 Time temperature superposition investigation

5.3.1 DSC

The initial cure enthalpy of both resins at the point of manufacture is assumed equal since both resins are formulated with matching ingredients, procedure, operator and equipment. Excluding the effects of batch variation the 5.5% lower cure enthalpy of batch one (R1) in comparison to batch two (R2) is considered consistent with the advancement of the cure reaction due to aging [54].

5.3.2 GPC

Molecular weight and polydispersity (M_w , M_n , and P) results indicate insignificant differences in molecular weight between prepreg resins (PP1-2) and resins taken directly before impregnation (R1-2) (Table 4-27 to Table 4-29). Therefore, the prepregging process is shown not to significantly alter the resins molecular state. M_n results do however indicate significant differences in molecular weight exceeding experimental error between batch one (R1 and PP1) and batch two (R2 and PP2) (Table 4-27). Batch one is shown to have increased molecular weight indicating that the polymers have advanced through cross linking, consistent with the effects of aging or curing. This result is in line with expectation considering the extended storage history of batch one samples (Table 3-22). Results are confirmed by increases in M_w , which is typically more sensitive to larger molecules (Table 4-28).

5.3.3 Rheology

Rheology results are in good agreement with the time temperature superposition (TTS) principle (Fig 4-44 and Fig 4-46). The uncross-linked epoxy resin is therefore believed to be an amorphous polymer melt. Therefore, it does not possess a crystalline structure and may readily transition between a glassy and melt state without structural changes, dependent upon temperature. This is provided that the effects of cross linking remain negligible. Shifting of the isothermal curves in the strain rate domain allows constants for the WLF equation to be calculated and a master curve to be constructed [103]. Comparison of batch one (R1) and batch two (R2) master curves show that batch one is shifted marginally to the left consistent with the effects of a molecular weight increase (Fig 5-10).

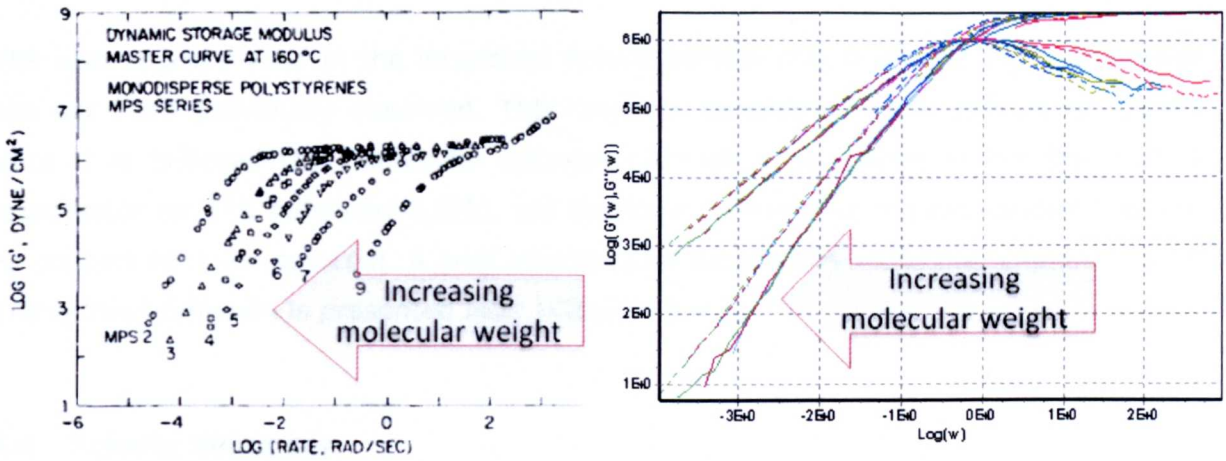


Fig 5-10 Effect of increasing molecular weight on shear storage modulus in monodisperse polystyrenes (Left) [154] and epoxy BP-A (right) (Chapter 5.3.3)

5.3.4 Tack and stiffness results

Both prepreg tack and stiffness are found to obey the time temperature superposition principle. The WLF equation, with constants found by rheology, is shown to give good agreement between isothermal tests in both tack (Fig 4-49 and Fig 4-54) and stiffness (Fig 4-52 and Fig 4-56). The convincing result is attributed to the new test setup, where both the application and peel process is scalable in the time domain, since a change in feed rate results in a directly proportional change in strain rate. TTS has also been previously applied in PSA peeling [98] and with reduced accuracy in probe testing [120] indicating that PSA principles are somewhat relevant to prepreg. Comparisons between the two batches also show that both stiffness (Fig 4-57) and tack (Fig 4-58) are seen to shift marginally to the left in the time domain consistent with the marginal increase in molecular weight [154].

The TTS principle has also been demonstrated in thermoplastic polypropylene tapes [163]. Additionally, the superposition of secondary variables, such as force-velocity, have been observed in thermoset tape laying [64] and the superposition of temperature-pressure-velocity in the prepregging production process [47]. The effect of time, temperature and pressure on the behaviour of polymer melts has been readily demonstrated to be interchangeable following empirical based superposition formulas with their theoretical origins based on free volume theory and molecular diffusion [135]. It is now believed that these relationships can be applied to the time scaling rate dependant processing of polymer composites. Consistent laminate properties and tack behaviour may be achieved by maintaining a constant polymer diffusion rate using these relationships throughout changes in feed rate of the process.

TTS also appears valid in the interfacial failure domain (Fig 4-49 and Fig 4-54) which has not been previously observed. This result is considered more difficult to explain since it is believed that molecular diffusion through free volume within the melt is responsible for TTS behaviour [135], yet molecular diffusion is not necessarily required for contact adhesion to occur. A brief attempt at a satisfactory molecular explanation for TTS without diffusion is presented later (Chapter 5.4.3).

5.4 Results Summary

5.4.1 Stiffness

Any variable which results in an increase in fabric, fibre or resin stiffness or thickness results in an overall stiffer prepreg. Therefore, temperature, fibre weight, feed rate and fibre type have a significant effect (Table 4-23). Typically, factors which affect only the surface such as release agents and surface finish show no effect. This is logical since the prepreg is covered with resin film preventing surface interaction during the stiffness section of the test. Anomalous results such as compaction force, surface type (Table 4-24) and finish do show an unexpected effect on stiffness. However, this effect can be attributed to an increase in rolling friction caused by increased reaction forces or increasingly rough surfaces. This may signify that stiffness values are not comparable between alternate plates and compaction pressures without correction. However, tack values remain comparative since stiffness is removed from peel resistance highlighting the self-corrective nature of the test with regards to quantifying tack. A linear increase in stiffness has been observed with increased thickness (Ref. FAW01 and FA01) indicating that stiffness is a complex problem which better resembles a membrane, shear, frictional or flow issue rather than a simple beam bending problem.

5.4.2 Tack

Throughout all of the tack tests two failure modes have become apparent and shown to be affected differently by each variable (Table 5-1). The first failure mode is characterised by poor surface contact resulting in very low values of tack and negligible resin deposition on the rigid test plate and is likened to interfacial failure found in PSA's. The second failure mode is characterised by good surface contact and the formation of resin fibrillations which eventually fail leaving significant resin deposition on the rigid test surface. The second failure mode is likened to cohesive failure found in PSA's [75]. Other failure modes found in PSA's are generally associated with failure at the flexible tape substrate interface [75, 104]. Since the fibres are gripped during prepreg peeling,

failure at the fibre interface is considered as another possible failure mode. Fibre interface failure is not suspected in all glass-epoxy samples due to the high surface energy of glass and even resin impregnation. However, this failure mode may play a role in the reduction of tack due to carbon fibres (Chapter 5.2.10).

Table 5-1 Failure mode occurrence observations made by resin deposition throughout prepreg tack testing

Variable	Failure mode type and occurrence	
	Interfacial	Cohesive
Temperature	Low	High
Feed rate	High	Low
Surface roughness	Both, no effect	
Release agent	With	without
Compaction force	Both, no effect	
Surface type	Low energy	High energy
Resin type	Low tack	High tack
Increased contact temperature	Not observed	constantly
Fibre areal weight	Both, no effect	
Fibre type	Possible carbon fibre-resin interface failure	
Resin content	Both, no effect	
Fibre architecture	UD	Triax

Each failure mode appears to have a contradictory response to variables indicating a difference in mechanism between the two. This phenomenon often results in a peak in tack when measured in a temperature or feed rate sweep. The peak is also found to correspond with the change in failure mode indicating that tack is a balance of good contact and cohesive strength. The phenomenon becomes more obvious when variables are investigated including the interaction effects of temperature, which increases the likelihood that both failure modes are observed for each variable (Fig 5-11).

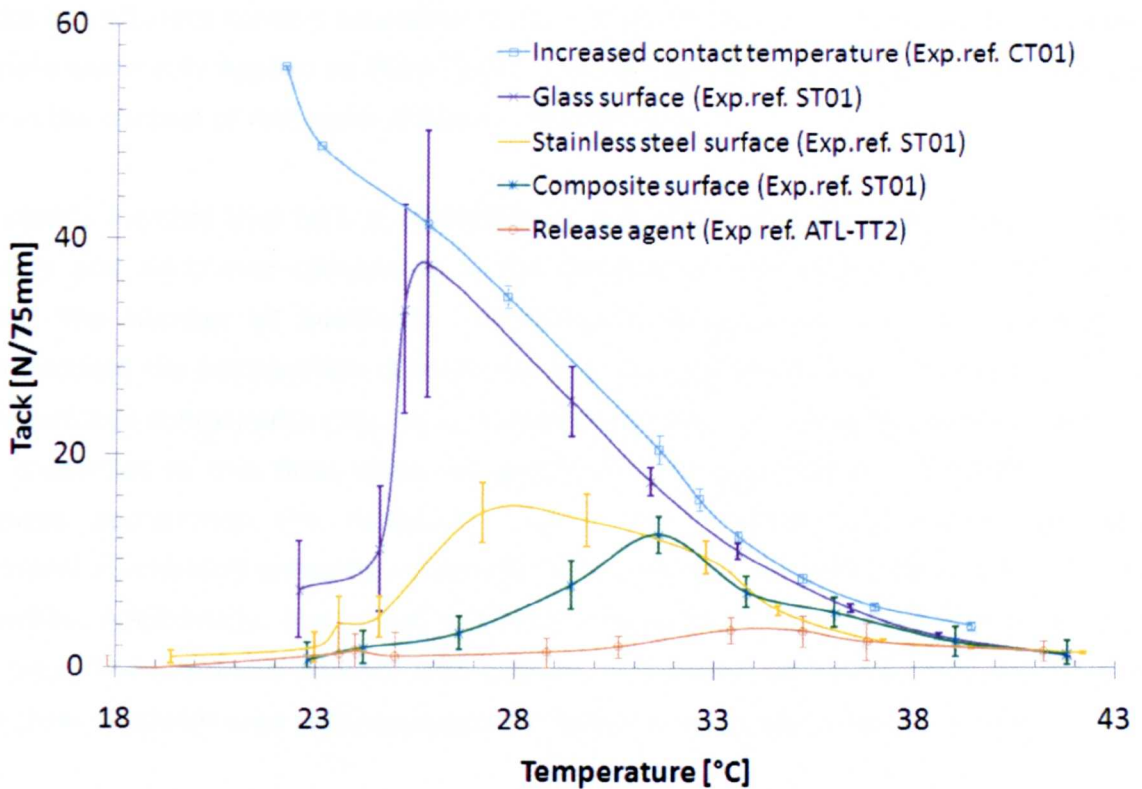


Fig 5-11 A comparison of surface variables effects on WE-ATL prepreg including temperature interaction effects

Essentially, increasing surface adhesion conditions, by increasing surface energy, causes a shift to cohesive failure at lower temperatures where the resin stiffness is higher and able to maintain a higher load. Once cohesive failure is initiated all samples appear to show a similar tack load based on the volume of resin in shear. The introduction of a weak boundary layer such as Chemlease is shown to prevent adequate contact initiating apparent interfacial failure. The effect of humidity is likely to be the increased quantity of water molecules at the surface acting in this way [73].

The time temperature superposition principle has been shown to apply indicating that logarithmically inverse effects on rheology are demonstrated in the time domain. Therefore, the effect of increasing feed rate and reducing temperature is to increase the shear loss modulus of the resin, which has a stiffening effect. The stiffening is said to be a result of reduction in free volume or allowed molecular diffusion time of the polymer melt [135]. The increase of molecular weight of resin types is also shown to have a stiffening effect (Chapter 4.3.8). This indicates that molecular weight, temperature and feed rate all have interchangeable effects on tack. The interchangeable effects have also been observed in PSAs where a 'super master curve' has been proposed as a useful tool for materials development based on tack levels [107]. The effect of stiffening the resin

results in inefficient contact according to the Dahlquist criteria and viscoelastic windows principle commonly applied to PSAs [119]. The effective build up of contact is discussed later in the context of molecular diffusion (Chapter 5.4.3).

The results indicate that tack is effectively a chain of components rather than a single property and whichever component is the weakest at any given time will determine failure. The number of interfacial and cohesive components may be increased to accommodate the introduction of weak boundary layers which may also have cohesive and interfacial components (Fig 5-12). However, caution should be taken when applying bulk properties to thin films since the properties are expected to change as the film thickness approaches the molecular length. The interface component has time dependant mechanical properties which differ from that of the time dependant bulk melt properties. Additionally, the actual cross sectional area for each component may vary with time. The interfacial contact area appears to increase with time whereas the bulk resin cross sectional area reduces during formation and elongation of fibrils (Fig 5-13).

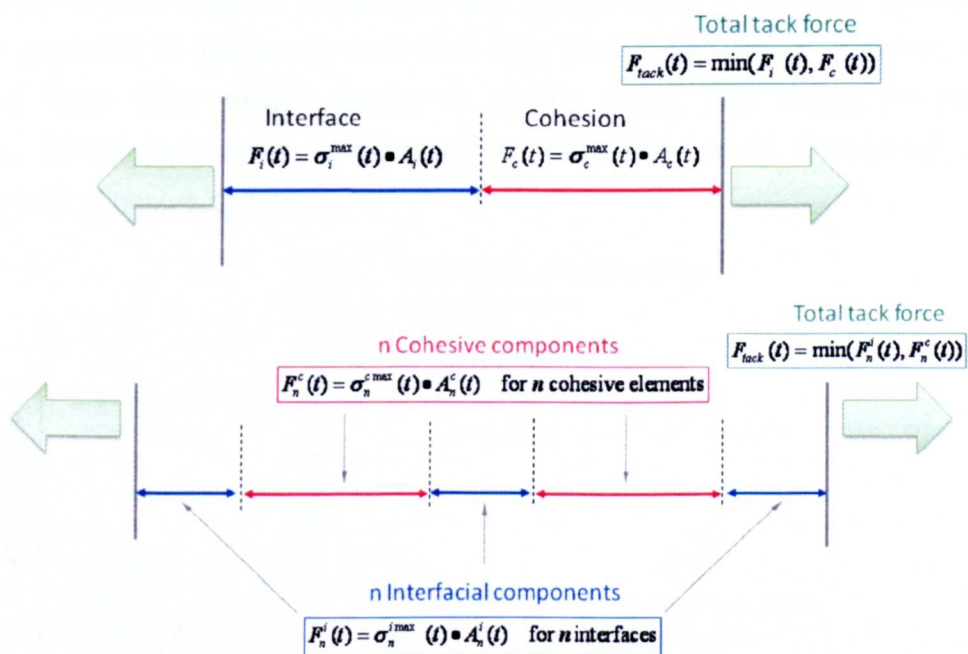


Fig 5-12 Tack force modelled as a chain with cohesive resin and rigid surface interface components (above) which may increase in number with the addition of weak boundary layers (below).

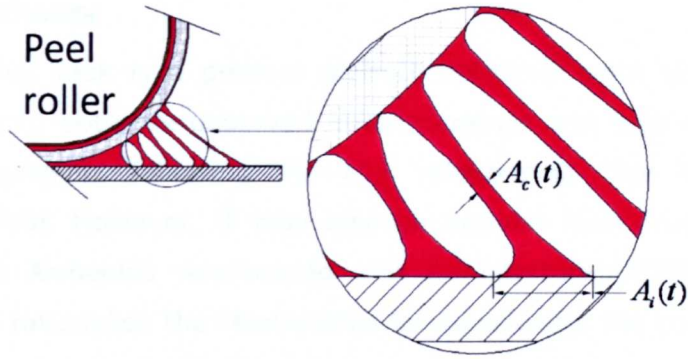


Fig 5-13 Cross sectional area of tack components during peeling

A curve may now be constructed for the new peel experiment based on experimental results and theoretical reasoning which gives some indication of the effects of variables on tack (Fig 5-14). Molecular diffusion rate in comparison to experiment time, known as Deborah number [141], is recognised as the primary variable with temperature and a reduction in molecular weight resulting in increased relative diffusion rate. The curve is valid only for a time scalable application and peel process. A perfectly uniform system would be expected to follow red and blue lines (Fig 5-14) where variation in surface finish and resin layer height results in patchy areas with mixed failure modes. Therefore, actual tack level is expected to fall below ideal theoretical combined interfacial and cohesive curves.

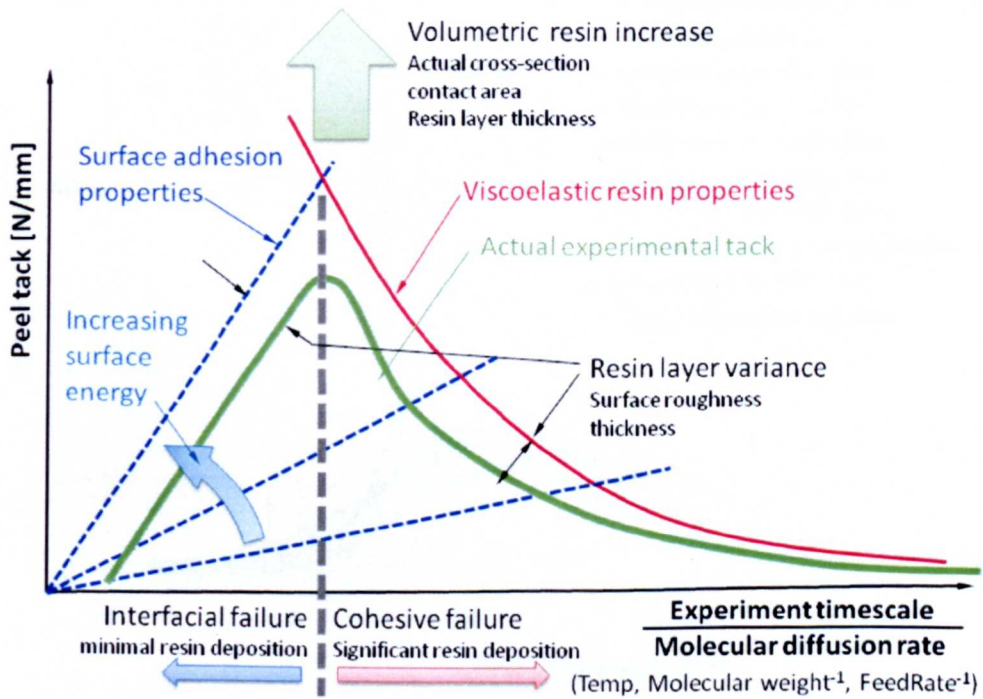


Fig 5-14 A tack curve based on empirical findings for use in predicting the effect of variables on time scalable application and peel processes

5.4.3 Molecular theory

Results indicate that tack is a product of both cohesive resin strength and surface wetting phenomenon, both are observed in temperature and feed rate experiments to be reasonably equivalent following the WLF relationship. The WLF relationship is traditionally empirical. However, it may also be derived from free volume principles which leads to an Arrhenius relationship with temperature [135]. The free volume approach seeks to rationalise the relationship by introducing the concept of free space between molecules. This space is thought to expand with thermal expansion increasing molecular mobility, indicating that flow, or molecular jumps, only occur if it has sufficient space [72, 143]. Free volume may explain the tack processes sensitivity to diffusion by preventing molecular flow and therefore contact. However, experimental results show that the effects of contact area variables on tack are low in comparison to surface energy and thermodynamic effects (Fig 5-15). Additionally, free volume theory (Chapter 2.8) wrongly implies that melts would diffuse into neighbouring gasses which have greatly increased free volume. This inability to describe interfaces stems from the omission of molecular adhesive forces which are considered negligible as they act equally in all directions within the melt [124]. However, this is insufficient to describe interfaces where intermolecular forces differ at the external face resulting in surface tension.

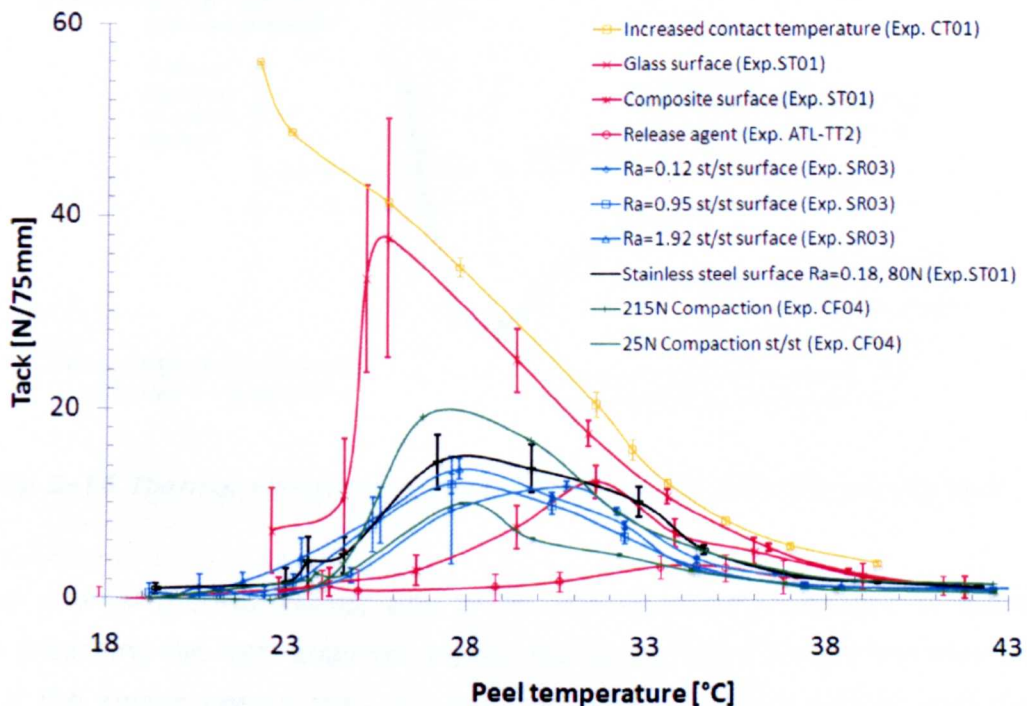


Fig 5-15 A comparison of increased diffusion rate at the point of contact (orange) surface energy (red), surface roughness (Blue) and compaction force (green) effects on prepreg tack including temperature interaction effects

The Lennard-Jones (LJ) two parameter model is typically used to represent molecular adhesion (Chapter 2.8.7). The LJ energy barrier is consistent with activation energy in reactions and solid flow phenomenon such as Eyring's solid flow model and Gibbs free energy [128]. Eyring proposes that 'molecules oscillate in a potential energy well and occasionally, by random fluctuation, draw enough energy from the thermal bath to escape' [128]. Such an oscillation is allowed within the LJ energy well by a constant cycle of internal kinetic and potential energy (Fig 5-16), or enthalpy in a simplified one dimensional system. The actual atomic positions are in constant flux oscillating around a central position where kinetic energy is equal to attractive and repulsive potential energy. Since the LJ forces are not symmetrical it can be seen that the central atomic position would shift outward with increased amplitude of internal thermal energy, observed macroscopically as thermal expansion, consistent with free volume theory.

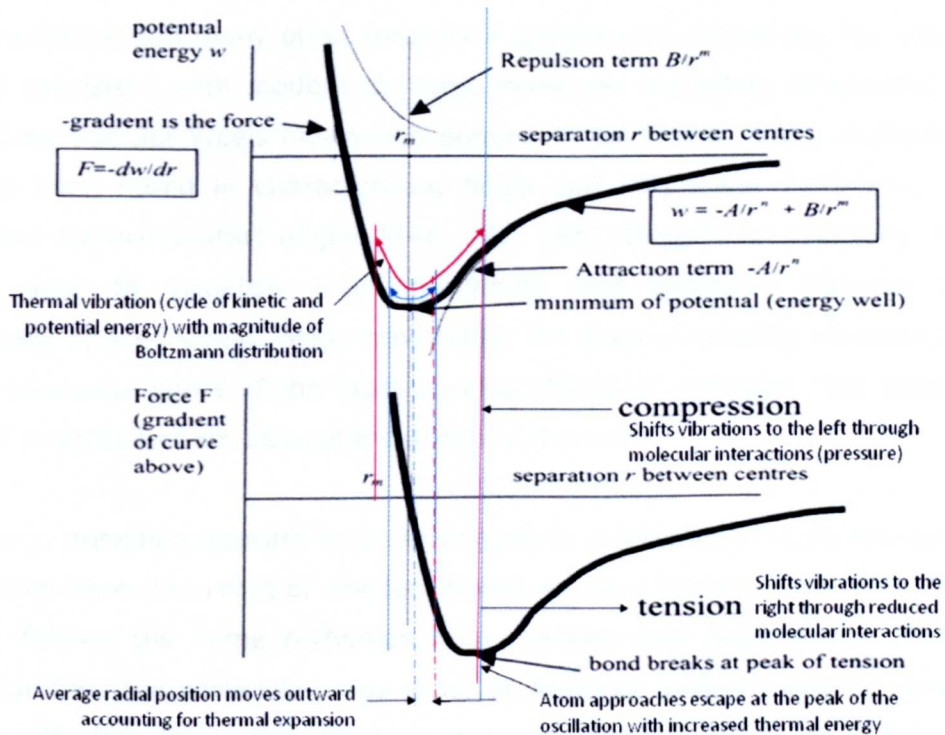


Fig 5-16 Thermal vibrations within a Lennard Jones potential energy well

Increased internal thermal energy also brings the peak radial distance of oscillations closer to exceeding the total potential energy well and allowing separation which results in flow. If the kinetic energy then exceeds that of the potential energy well then the adhesion force is exceeded and a jump may occur. The magnitude of individual internal thermal oscillations is likely to follow a statistical distribution. A high energy Maxwell-

Boltzmann (MB) type distribution may be applicable and is also comparable to the Arrhenius equation from which the WLF equation may be derived.

The applicability of the MB distribution and Arrhenius equation to solid state kinetics is questionable since the molecules are thought to be immobilized [164, 165]. However, the dynamic LJ model allows thermal vibrations within the energy wells and effectively interactions without molecular jumps. The high molecular population will result in an exceptionally large number of interaction events, where rare interaction events will allow atoms to occasionally exceed the required activation energy to allow a molecular jump. Following this probabilistic approach it is possible to see that longer experiment times will result in an increased number of jump events accounting for the time dependant component.

This analogy is greatly simplified since it ignores rotational momentum, polar alignment, thermal radiation and many other force field components. However, the visualisation is generally consistent with modern dynamic molecular modelling of epoxies, where the non covalent van der Waals interaction dominates behaviour [151]. Reasonable results have also been found in characterising fluids and interaction behaviour, particularly wetting and surface contact angles [146, 147, 166]. Despite its simplicity, the analogy may be used to visualise strain hardening and thermally induced flow under mechanically applied stress. Most importantly the theory includes adhesion and can be used to rationalise some of the more curious effects of variables. The exact details of molecular interactions are beyond the scope of this work.

In summary, adhesion appears to be analogous to a reaction with an activation or bond energy much lower than that of covalent bonds required to form molecules. Therefore, it generally follows the same Arrhenius type reaction rate dependency. The low bond energy signifies that molecules may react or jump at ambient energy levels allowing flow and diffusion. Neglecting physical distance, adhesion may be a function of the frequency of molecular jumps which is in turn a function of internal energy and activation energy of the LJ relationship. The quantity of jumps is probabilistic, increasing with time and thermal energy. A lack of molecular mobility results in interfacial failure through a lack of reaction with the surface. In this case molecules may rest against the surface but remain in their LJ energy well until an interaction event occurs which allows it enough energy to escape to the next nearest well which may be the surface [167]. Excessive mobility results in a bulk melt with poor mechanical properties due to a high frequency of jumps. Therefore, the whole process is determined by atomic motion of which diffusion is an accurate measure.

Increased molecular weight (without branching)

Covalent bonds may also be modelled using the LJ equation. The atoms may share one or more electrons allowing closer attraction before the repulsion term becomes effective. As a result a higher potential energy well and shorter bond distance is achieved. Since the covalent bonds now require greater energy to escape they can accommodate increased thermal energy. The polymer chain is considered to be a chain of covalently bonded atoms immersed in non-covalent bonds. It is then possible that once a single atom in a chain reaches an energy state higher than the non-covalent bonds of its neighbours it is held in position in a higher state of thermal oscillation by the covalent bond. Once all atoms of the polymer chain exceed the non-covalent energy of their neighbours the entire chain may jump. Allowing for a flexible backbone and without applied stress, segments of the polymer chain are most likely to escape non-covalent bonds by rotating and diffusing randomly around covalent bonds. Once stress is applied, the polymers are now most likely to jump non-covalent bonds in the direction of the applied stress. This would eventually lead to an aligned polymer which requires all atoms to reach the required energy for the complete chain to make a non-covalent jump.

Weak boundary layers

The dominant effect of release agents (Chapter 4.3.4) and surface contaminants (Chapter 3.3.7) can be attributed to the weak boundary layer (WBL) principle. The LJ attractive forces are most significant over a distance of a few atomic diameters. Therefore, the presence of an apparently invisible atomically thin layer can significantly affect tack. The atomic layer may work by positioning itself over the surface creating a layer with a low LJ potential energy. Alternatively, if the surface energy is sufficient, a sufficiently thick contaminant layer may fail cohesively. It may also be possible for such molecular layers to be squeezed out or penetrated during molecular jumps [73]. This offers some explanation as to why peak tack may be observed at higher temperatures, with increased energy molecular jumps, where a WBL is present. The significant effect of water molecules and oxide layers [73] may also account for some variability in tack observed by manufacturers in climates with differing humidity.

Surface energy and finish

Dynamic molecular analysis using LJ interactions have been used to model surface adhesion [73] with simplifications allowing an effective analysis [168]. It is assumed that the atomic radius at which the repulsive term becomes significant is determined by the electron shell which varies between atomic and molecular species [73]. The values for the atomic radius, also known as the equilibrium distance, are believed to have a

significant effect on the prediction of adhesion [169]. It can now be seen that surfaces consisting of molecules with a greater attractive force may attract molecules and subsequently retain them within a deeper potential energy well. Therefore, the interfacial bond is achievable with reduced thermal energy.

5.5 Commercial prepreg

Production process variability

Variation in commercial prepreg stiffness along the width of the roll has been found to in most samples (Fig 4-7). This is likely to be the result of variations in fibre tows according to manufacturer's tolerances. The way in which fibre tows are spread across the roll may also be subject to some degree of variance. However, variance appears to be contained to the roll width rather than through thickness, since the prepreg demonstrates minimal variance in stiffness between bending direction when faces are reversed (Fig 4-9).

Minimal variance in tack is shown across the roll width for most specimens with the exception of triax 1200g/m² E-glass which shows significantly reduced tack towards the edges of the roll (Fig 4-8). This could be due to poor wetting, uneven roller pressure or resin bleed-out from the edges in the production process. The greatest variance in prepreg tack comes from the testing of alternate faces shown in all samples (Fig 4-9). The greatest effect in the change of tack between faces is seen in triax 1200g/m² which has alternate fibre directions at each surface indicating that fibre pattern at the surface also affects tack.

Characterisation

When the roll position and face position studies are compared an overall repeatable value for tack and stiffness is found (Table 4-5). This indicates that the new test is a useful tool for quantifying tack and stiffness. However, these repeated values are not in complete agreement with specified values. The 'low tack' CUD600 is in good agreement. However, 'medium tack' multidirectional higher resin content prepreps exhibit a higher value than 'high tack' unidirectional glass fabrics. Prepreg tack levels are specified based on resin tack level. However, temperature, feed rate, fibre surface pattern, fibre type and resin content have all shown some effect on tack over a temperature range (Chapter 4.3). Therefore, tack would be better specified based on actual prepreg measurements. The test has also shown sensitivity to prepreg quality issues such as rips, bubbles and resin layer variations which result in lost resin on peeling of the backing film (Chapter 3.3.7). Therefore, quality, or uniformity is shown to affect tack and may be quantified in terms of experimental noise over a larger sample base to fully

characterise prepreg. In this case visible quality variations were screened out of the sample group before testing to increase the effect of variables in comparison to experimental noise.

5.6 ATL feasibility and application

5.6.1 Performance observations

The feasibility study identified four key problem areas; cutting, backing paper release, mould tack and repositionability (Chapter 4.1). The cutting performance was related in some way to material properties, with increased fibre areal weight (FAW) proving more difficult to cut due to the increased thickness. Fibre bundling, seen in early versions of experimental E-glass prepreg, was also problematic where bundles were pulled from the edge of the tape by the blade without being cut. This was relieved by improved tow spreading during prepregging. The cutting configuration of the V4 machine limited material weight ($FAW \leq 400\text{g/m}^2$) with resin content minimised (28% wt.) to prevent build up on the cutters. Overall, cutting was considered to be a mechanical design issue which could be remedied with the ultrasonic cutter knives of the latest machines. Therefore, these material limitations were expected not to apply to newer machines and further cutter investigations were not warranted.

Repositionability was considered to be a product of the materials tack level and considered important only for manual handling, which is what automation seeks to avoid. Lowering the tack level improves repositionability yet it also increases the probability that manual intervention is required, since a ply is more likely to move out of position after being laid. Therefore, aiming for good material repositionability is counter intuitive to the automation process. However, hand lay-up of the ATL material was required to finish plies as a result of mould tracking machine errors. Therefore, for this experimental program repositionability was considered favourable and preferred by operators.

Backing paper release and mould tack are considered fundamental to the lay-up process. However, the tack and removal mechanism and the interaction of stiffness are not clearly defined. Closer inspection of the material head accompanied by a force diagram (Fig 5-17) allows the following observations:-

- Peel appears to be the dominant removal mechanism.
- Application and peel appear instantaneous in a continuous process.
- Contact time is inversely proportional to feed rate.
- Application pressure is maintained by the tool head compaction shoe.

- Tape stiffness is favourable in holding the tape to the tool surface and releasing it from the backing paper.
- Additional shear forces may occur with incorrect spool tension.

Effectively the mould, or ply to ply, tack and the bending stiffness should always exceed tack to the backing paper for successful lay-up. However, some tack to the backing paper is required to hold prepreg tape in place for intricate cutting operations. These require that the prepreg is wound past the compaction tool whilst cutting and then wound back and positioned later. The ATL process is therefore a delicate balance of reduced backing paper tack, stiffness and reasonable mould tack.

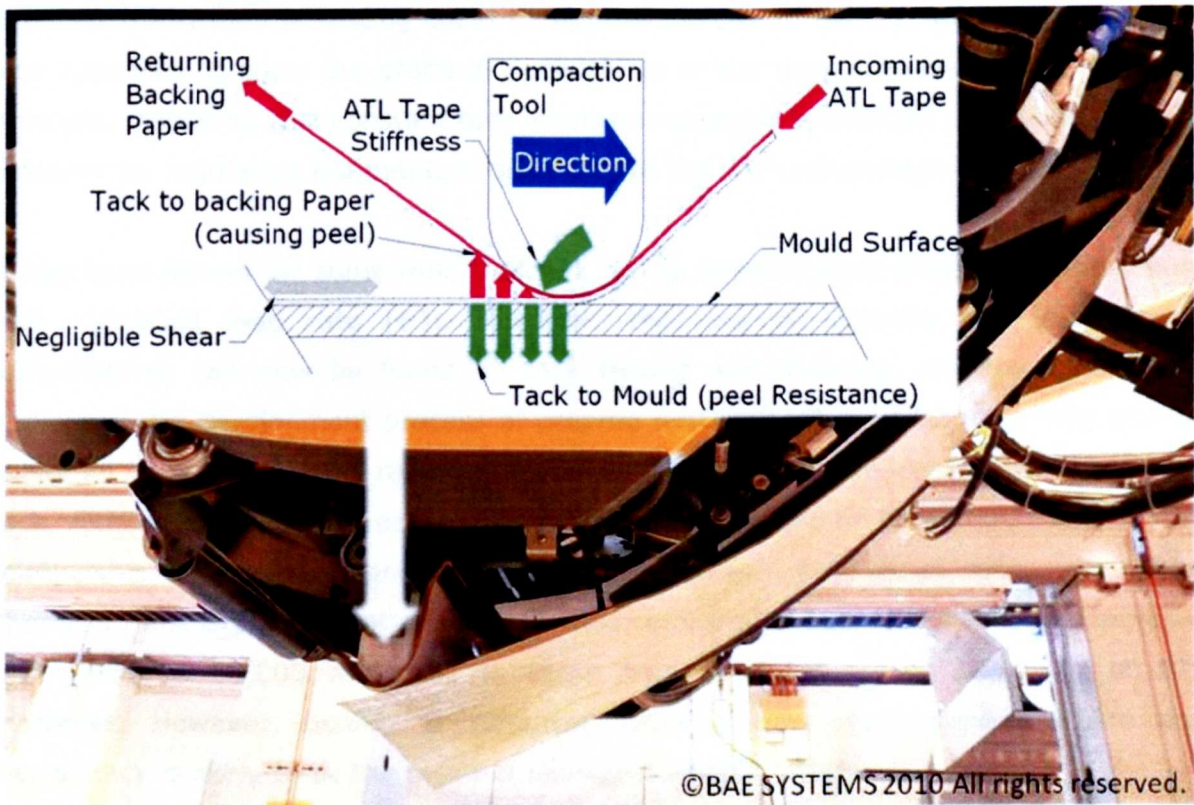


Fig 5-17 Force diagram of the ATL application process shown against the Cincinnati V4 CTL delivery head

5.6.2 Applicability results

Observations made during the feasibility trials (Chapter 5.6.1) show that the new tack and stiffness test method is a good representation of the ATL process. However, exact compaction pressures and tape tension is likely to differ. Therefore, the main aim of the applicability trials was to show that results found in testing could be related to ATL lay-up performance. Successful lay-up on a composite surface at 20°C had been previously achieved only with the use of tackifier. Tack testing showed that a higher peak in tack could be found at 34°C without the use of tackifier (Fig 4-59). Time temperature super

position was used to find the equivalent feed rate at which this peak would occur (4 mm/min). Running the ATL at this feed rate was found to give good results, increasing the feed rate showed progressive loss of tack. Increasing the feed rate with heat added according to TTS appeared to give improved tack but unpredictability in the heating method resulted in uneven tack levels and tape splitting. Splitting was believed to occur in overheated sections of the tape which failed cohesively. Without cross-stitching the resin is responsible for prepreg integrity, therefore cohesive failure of the resin would be expected to cause tape splitting.

The application study was believed to be a success since it showed that high tack operating points found by tack and stiffness testing could be exploited on the machine and that the results of testing could be applied directly to the ATL procedure. The test also appeared to show the practical applicability of the time temperature transposition principle, indicating that constant tack levels and possibly lamination conditions could be achieved by regulating temperature according to the WLF parameters of the resin.

It has been known for some time that ATL lay-up benefits from increased temperature with increased feed rate [63]. However, the rate of increase and ideal lay-up temperatures can now be found by tack testing and rheology, thereby significantly improving the development process of prepreg materials. The relationship may also be exploited to increase feed rates of processes which have previously been limited by tack. Although lay-up and testing speeds have been limited to 1000 mm/min, the WLF relationship is logarithmic and appears valid for several decades of strain rate [135]. Therefore, it is expected that results will scale comfortably over the two decade increase (from 500 to 50,000 mm/min) to reach the maximum lay-up capability of ATL machines. However, testing at increased rates is now recommended where any discrepancy is likely to be the result of increased inertial effects.

The consistency of lamination quality may also be regulated by this method since TTS regulated lay-up is effectively maintaining a constant polymer diffusion rate. TTS regulated lay-up of thermoplastics may possibly yield improvements since they have demonstrated mechanical properties in agreement with the TTS principle [163]. Transposition of time-temperature variables have also been demonstrated in the prepreg production process [47].

5.6.3 Tape performance

A comparison of experimental ATL materials at ambient lay-up conditions shows that 'high' and 'medium' tack resins (W-ATL-1 to W-ATL-3) are abandoned in favour of less problematic lower tack high stiffness tapes (W-ATL-7) which better match the properties of existing aerospace (A-ATL-1 & 2) materials (Fig 5-18). The results of tack under commercial conditions (Fig 4-59) show that limited tack is available at the mould surface due to the use of mould release agent. Therefore, low tack stiff prepreg appears to be preferred on the basis of improved release from the backing paper. The lack of tack to the mould surface can then be overcome with the use of tackifier. Therefore, a study of tack to the release paper would be beneficial. However, this would require increased sensitivity in measuring equipment.

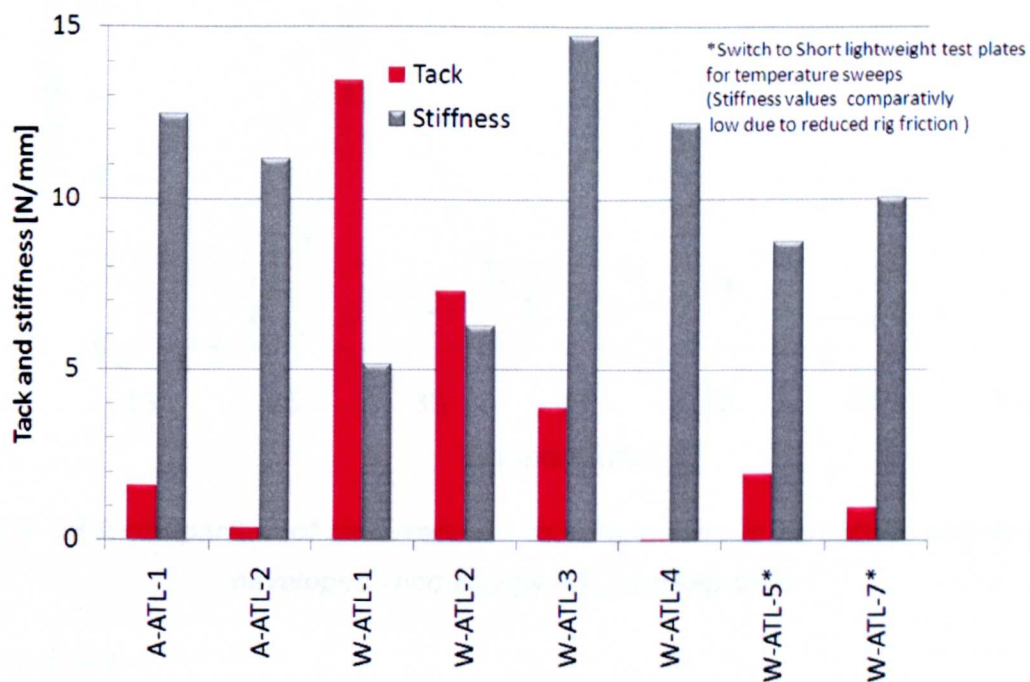


Fig 5-18 Tack and stiffness of experimental wind energy ATL prepregs (W-ATL) in comparison to existing aerospace (A-ATL) preprep at ambient conditions

Temperature effect

Increased temperature of 40-50°C was found to be beneficial in the lay-up of 8552 aerospace (A-ATL1 and 2) tapes. Tack appeared to be moderately increased without significant decrease in the material stiffness. When the same level of heat was applied to wind energy tapes the tapes became overly flexible and showed difficulty releasing from the backing paper. The effect is attributed to the resin shear storage modulus response to temperature (Chapter 5.2.1). The position of the heater plate against the

backing paper on the ATL machine was also considered to be detrimental. This could cause tack to be improved at the backing paper rather than at the mould surface.

Both interfacial and cohesive failure modes were observed with wind energy ATL tapes. Cohesive failure became apparent at higher temperatures leaving resin deposition or causing through thickness splitting of the prepreg tape. The two failure modes are consistent with the two distinctly different lay-up behaviours observed in previous studies of ATL lamination [64].

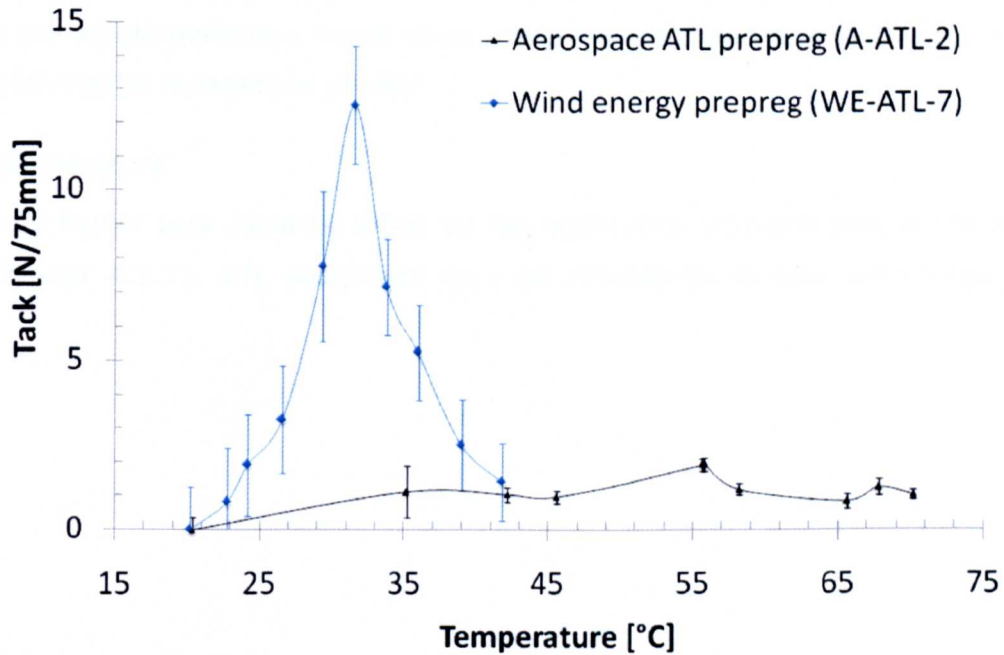


Fig 5-19 A comparison of tack response to temperature in aerospace and newly developed wind energy ATL prepreg tape

Feed rate effect

Prepreg has also been shown to be sensitive to feed rate with a logarithmic relationship to temperature effects through TTS. Therefore, the effects seen with temperature may be repeated within the feed rate of the ATL. Essentially, higher tack and a shift to the cohesive failure mode may be seen at increasingly lower feed rates. Interfacial failure and a lack of tack consistent with cold temperature behaviour may be seen when feed rate is increased. For consistent tack throughout feed rate a constant molecular diffusion rate is recommended (Chapter 5.3) which is dependent on temperature and resin molecular weight.

Release agents

Release agents appear detrimental to mould tack and the lay-up process. They subsequently require the use of tackifier which significantly increases production times

by increasing the number of mould coating and drying operations. The ATL process would benefit from a specifically designed mould release agent, which allowed residual tack, or a gel coat with a high energy surface finish.

Compaction force

Compaction force was found to be ineffective at increasing tack outside of the failure mode transition zone (25-35°C) (Chapter 4.3.5). Significant levels of tack could be found with 80N compaction. This value is much lower in comparison to the 265-1300N typically applied by the ATL [55]. Therefore, compaction pressures could be reduced to eliminate the mould deflection found when using low cost wind energy tooling provided it is not detrimental to laminate quality.

Contact temperature

Significantly higher tack could be found by hot application and cold peel of the backing paper (Chapter 4.3.7). ATL equipment may be redesigned to take advantage of this effect.

6 Conclusions

6.1 Tack and stiffness

6.1.1 Method and observations

A new tack and stiffness test has been developed which is an extension of the floating roller peel method. Peel methods have been less favoured in the past due to lack of a controlled application method and difficulty in isolating adhesion and bending forces from the results. This new method allows simultaneous application under a controlled force. Bending and tack forces are also isolated in separate stages of the test. The test was originally designed to replicate the ATL application method but has also been used to characterise hand lay-up prepregs. Consistent results were found in the characterisation of wind energy grade prepreg materials despite an overall high level of uncertainty. Repeatable results have also been produced with a standard deviation of 5.2% in stiffness and 16.4% in tack over 27 samples. A tackier control sample was correctly identified. The test method may also be applied to PSA tapes and surface adhesion with further refinement.

The new test method allowed for the investigation of the effects of twelve variables on both tack and stiffness. During this investigation interfacial and cohesive failure modes were observed. These failure modes appear analogous to those found in PSA peel testing where any additional modes, not observed in E-glass prepreg, are believed to be associated with failure at the flexible substrate prevented from occurring in prepregs since the fibres are gripped. The equivalent failure in prepreg would be at the fibre interface. However, this is believed not to occur in E-glass since the resin is assumed to be well impregnated within the fibres resulting in a poorly defined interface. However, the fibre-resin interface failure is one of the possible scenarios offered to account for the reduction in tack found in carbon prepregs. Typical interfacial failure is attributed to failure at the interface between the polymer melt and the rigid test plate resulting in a mostly clean surface. Cohesive failure appears to occur within the resin polymer melt and is attributed to the viscoelastic properties of the resin resulting in significant resin deposition on the test plate. A patchy mix of failure modes can be observed over the peel area, particularly around the point of transition between failure modes. This is attributed to the variability in resin layer thickness and contact. Increased unpredictability is also observed during interfacial failure attributed to the elastic storage and sudden release of energy, known as the stick-slip condition when observed in PSAs.

In all experiments where a peak in tack was recorded, it was found to be consistent with the transition point between failure modes. This is believed to be the point where contact adhesion and cohesive resin strength are equal. This indicated that tack is a function of two mechanisms rather than a property itself. A chain model is now considered the most appropriate method to represent prepreg tack. The number of interfacial and cohesive components will depend on the number of layers and interfaces within the boundary of the applied force. Relative molecular diffusion rate, often referred to as the Deborah number, was found to have opposing effects on the two failure phenomenon. An empirical tack curve has been produced for a two component system to assist with the prediction of the response of prepreg tack to a number of variables. Short relative diffusion times result in mostly interfacial failure which may be affected by surface conditions. Long relative diffusion times result in mostly cohesive failure which is affected mostly by resin properties. The variation found in the resin layer and surfaces is likely to account for mixed or patchy failure modes. The whole curve appears to scale upward depending on the volumetric increase in resin involved in the peeling process.

6.1.2 Variable effects

Temperature, feed rate and resin type

The effect of changes in temperature on tack appeared to be dependent on the dynamic shear storage response of the resin. The results are supportive of the PSA Dahlquist criterion concept which states that the dynamic shear storage must fall below a value $\approx 3 \times 10^5$ Pa to become contact efficient. However, the actual value for prepreg contact efficiency also appears to be a function of surface conditions, specific to each surface and prepreg. Resin type investigations show that with constant fibres, surfaces and resin impregnation, tack can be controlled by increasing molecular weight. The molecular weight increase is typically achieved through a secondary reaction which in turn stiffens the resin and reduces tack at a particular operating temperature. Similar effects were found with inverse changes in feed rate leading to the discovery of time temperature superposition applicability in prepreg tack and stiffness.

Release agents

Release agents were shown to virtually eliminate all useful tack. They appeared to lower surface energy and prevent the onset of cohesive failure. They appear to act by either reducing surface energy or producing a weak boundary layer with low cohesive strength that is easily sheared. Residual tack was observed to be higher at increased

temperature and with solvent based release agents in comparison to water based. Humidity is also thought to affect tack in a similar manner.

Surface roughness and energy

Surface roughness was found to have minimal effect. This could be attributed to the surface roughness of the prepreg which was found to be large in comparison to all the substrate surfaces tested. Changes in surface energy were found to be significantly greater, leading to the possibility that tack could be a thermodynamically molecular adhesion controlled mechanism rather than a diffusion controlled physical mechanism of surface contact spreading.

Fibre type

Carbon fibre prepregs were found to have significantly reduced tack in comparison to equivalent E-glass prepregs. The effect was attributed to a difference in impregnation, an electrostatic effect, failure at the fibre-resin interface or a combination of all three.

Fibre areal weight (FAW)

Increasing fibre areal weight showed no effect on tack. However, a proportional increase in prepreg stiffness was observed.

Resin Content

Resin content was found to have minimal effect on tack during fully interfacial failure. However, increasing tack was found with increasing resin content throughout the failure mode transition region and during cohesive failure.

Fibre architecture

The fibre architecture effects were difficult to isolate due to an unwanted increase in FAW imposed by the manufacturing process. However, early onset of cohesive failure appears to have occurred which could possibly be attributed to a vacuum effect of trapped air due to a change in resin layer surface pattern.

Contact temperature

Hot application cold peel was found to significantly improve tack by improving interfacial strength. The interfacial failure mode appeared to be eliminated from peeling at a lower temperature.

Compaction force

Compaction force was found to have minimal effect on tack outside of the failure mode transition region (25-35°C) where significant tack could be found with 80N compaction force.

General

Overall variables which were found to affect the apparent shear storage modulus and therefore stiffness of the resin were found to show the greatest magnitude of effect on tack. Changing the apparent shear storage modulus and subsequently diffusion rate of the resin is able to affect both the build up of interfacial strength and the cohesive strength of the resin. Yet changes to surface contact conditions are only able to affect the interfacial failure mode mostly by delaying the onset of cohesive failure. Therefore, surface variables can also appear dominant at certain low temperatures but appear less effective over a temperature sweep which encompasses both failure modes.

Stiffness was found to be unaffected by changes in surface conditions. Only variables which affect the thickness of the prepreg or the stiffness of fibre or resin components are shown to effect prepreg stiffness.

6.1.3 Time temperature superposition

The effects of feed rate and temperature on both tack and stiffness were found to conform to the time-temperature superposition (TTS) principle using the Williams-Landel-Ferry (WLF) equation, previously observed in rheology and PSA peel testing. Constants for the WLF equation can be found using rheology and used to superposition prepreg peel and stiffness results. This method then allows for the construction of prepreg peel and stiffness master curves and the prediction of feed rate response based on temperature response and vice versa. A tack investigation of resin formulation also shows promising signs in supporting the 'super master curve principle' allowing tack predictions to be made based on molecular weight.

6.1.4 Molecular theory

A thermodynamic Lenard-Jones (LJ) model, typical of that utilised in molecular dynamics, is proposed to descriptively rationalise results. Adhesion and flow is essentially envisaged as a reaction with a low activation energy and relatively long bond length. Therefore, a molecular jump is required for initiation of both adhesion and flow signifying that both processes are governed by an Arrhenius type relationship, such as WLF. Surface energy, thermal expansion and thermally induced flow under stress may also be accounted for. A semi-empirical model based on the dynamic LJ relationship may offer reasonable predictions for the future in the absence of true molecular modelling, which may be limited by a lack of computational power and molecular

information. Simplifications to the LJ relationship and increased time step intervals, useful in reducing computations, should be made with caution. They may result in an inability to capture the true nature of the molecular jump and associated thermal vibrations.

6.2 Prepreg characterisation

The new tack test method is considered equally applicable to hand-lay and ATL prepreg characterisation since it quantifies both tack and stiffness, giving an indication of its ability to stick and be formed around the mould surface.

A degree of variability was found in the tack levels of commercial prepregs dependant on roll position and which face was tested. Repeatable results for tack and stiffness could be found in large batch sizes containing an equal number of samples taken from each face and roll position. Tack levels were not always in agreement with specified levels. The most significant discrepancies are found in prepregs with multidirectional fibres. Therefore, the fibres are believed to play a complex role in determining tack. Prepreg tack is typically specified as 'high', 'medium' or 'low' based on the tack level of the constituent resin. Fibre type and resin content have also been shown to have an effect. Therefore, testing of the prepreg is preferable to resin only tests.

GPC analysis of prepreg resin and constituent resin has shown that no significant molecular changes have occurred during the prepregging process. Therefore, aging and cross linking of the resin can be presumed negligible. This allows for the rheological analysis of resin samples, taken immediately before the prepregging process, to be compared to the properties of the prepreg. Molecular differences are recorded between batches with alternate storage histories. Increased molecular weight and reduced cure enthalpy is observed with longer storage, consistent with increased cross linking through aging. A stiffening of the prepreg resin is observed with aging which appears analogous to the stiffening seen in increasingly low tack resin formulations suggesting that molecular weight is used as a control of resin tack by manufacturers. Therefore, a molecular diffusion based time-temperature-super position principle could also apply to resin formulation and aging.

6.3 ATL development

6.3.1 Feasibility

The following material developments were made to facilitate the use of ATL as a wind turbine production method:-

- An increase in fibre areal weight (FAW) from 200 to 400g/m², improving deposition rates.
- High performance aerospace toughened epoxy 8552 resin has been replaced with low exotherm low cost epoxy M19.6LT resin system, allowing the cost effective production of thick laminates using vacuum bagging.
- High cost carbon fibres have been replaced with cost effective E-glass fibres.
- High cost, high accuracy alloy aerospace mould tooling has been replaced with a cost effective mould construction typical of that found in the wind turbine industry.

ATL Materials were developed and evaluated based on cutting performance, tack to the mould surface, backing paper release and repositionability. Cutting problems were alleviated by changing the mechanical design of the cutter. Repositionability was found to be a counterproductive method for evaluation since designing materials to be easily repositioned results in an increase in the likelihood that they will move out of place after lay-up. Observation and a force diagram of the ATL process reveal that:-

- Peel appears to be the dominant failure mechanism.
- Application and peel appear instantaneous in a continuous process.
- Contact time is inversely proportional to feed rate.
- Tape stiffness is favourable in holding the tape to the tool surface.

Therefore, backing paper release and tack to the mould surface are believed to be fundamental in the lay-up process and subsequently a product of prepreg tack and stiffness. A new peel method which simulates the ATL process was developed and used to characterise tack and stiffness where values obtained were compared to ATL performance. High tack levels were found to be detrimental due to poor release from the backing paper and inability to be repositioned should an error occur. Existing aerospace materials were shown to be much lower tack than that of wind energy prepreg. A low tack stiff prepreg was eventually favoured by ATL operators with the use of an in-house tackifier to alleviate the problem of poor mould adhesion

Compatibility problems arose between low cost mould tooling typical of that used in wind turbine blade manufacture and ATL machinery. The wind turbine blade moulds were found to deform under the compaction pressure of the ATL head. The deformations and large tolerances ($\pm 15\text{mm}$) exceeded that of typical aerospace mould accuracy with stiff high cost alloy tooling. These out of tolerance deviations from the programmed surfaces caused the ATL to generate errors. The ATL was eventually reprogrammed using actual surfaces measured from the mould, resolving the error. Therefore, a reduction in compaction pressure and an ability to map actual mould surfaces in situ would be beneficial when using low cost mould tooling.

6.3.2 Application

Manufacturing conditions were recreated in tack and stiffness testing using a composite mould surface rigid substrate coated with release agent. A peak mould tack was identified and considered an optimum lay-up point for increased tack. The optimum point was recreated using ATL equipment and found to give increased tack. Increasing feed rate showed loss of tack. Increasing feed rate with temperature increases according to the time temperature superposition principle showed signs that the optimum tack conditions could be maintained. Therefore, results indicate that tack and stiffness test results can be directly related to ATL performance and the time temperature superposition principle can be applied to stabilise tack levels throughout the feed rate range.

Interfacial and cohesive failure modes observed in tack testing could also be observed during ATL lay-up and can be seen to correspond to pressure driven and surface tension driven behaviours previously identified [64]. Cohesive failure during lay-up was believed to result in tape splitting due to low resin stiffness. Therefore, the optimum lay-up condition appears to be in the interfacial failure domain at the point closely before failure mode transition, when tack to the mould surface is high. The ability to relate tack and stiffness results to ATL performance allows the effect of variables on ATL to be discussed based on tack and stiffness test findings.

Temperature, feed rate and resin type

Tack appears to be sensitive to shear storage modulus of the resin. The effect of stiffening the resin by lowering the temperature, increasing the feed rate or the molecular weight of the resin results in a shift to interfacial failure and a stiffer prepreg. The three variables appear to be linked by the relative diffusion rate of the polymer. The relative diffusion rate may be held constant during the change in one variable by

adjusting another. For example, a higher molecular weight prepreg may display similar tack properties as a low molecular weight polymer at higher temperatures. Additionally, tack properties at low feed rates can be recreated at higher feed rates with increased temperature. Essentially, the effects of resin aging, which changes molecular weight and changes in feed rate, required for various mechanical operations of ATL, could be compensated for by changes in temperature to maintain consistent laminating conditions. Resins such as that used in existing aerospace ATL tapes appear less sensitive to changes in temperature and demonstrate improved lay-up consistency. Therefore, an alternative strategy would be to formulate resins which are less sensitive to temperature and therefore feed rate changes.

Release agents

Release agents were found to significantly reduce available mould tack, which is detrimental to ATL performance. Therefore, development of an ATL friendly release agent or gel coat would be beneficial.

Compaction force

Compaction force appeared to be ineffective at increasing mould tack outside of the failure mode transition region (25-35°C). Within this region significant tack could be found with as little as 80N. Therefore, compaction pressure could be reduced to facilitate the use of reduced stiffness low cost mould tools.

Contact temperature

Hot application cold peel showed significantly improved tack and could therefore be utilised for future ATL designs.

Fibre areal weight (FAW)

Increasing fibre FAW results in a stiffer prepreg with no significant increase in tack, thought to be beneficial in improving backing paper release.

6.4 Major conclusions

This section contains a summary of the major conclusions arising from the work described in this thesis:-

- I. Development of new wind energy E-glass fibre ATL tape has been achieved with significant difficulty to produce a 7m representative section of a 45m commercial wind turbine blade using ATL and low cost mould tooling.

- ii. Tack and stiffness properties were found to be critical in achieving good ATL lay-up performance. Tack to the mould surface combined with material stiffness must exceed tack to the backing paper for successful lay-up.
- iii. A new prepreg tack and stiffness test has been developed. The test is advantageous due to a regulated application force, the ability to differentiate between tack and bending stiffness, and a contact time which is proportionate to peel rate, simulating the ATL process.
- iv. The effects of temperature, feed rate, surface finish, release agents, compaction pressure, surface energy, resin type, fibre weight, fibre type, resin content and fibre architecture have been investigated with most variables demonstrating significant effect on either tack, stiffness or both.
- v. Tack variables were found to be effected either by changing surface properties or the shear storage modulus of the melt.
- vi. Two failure modes were observed. Interfacial failure appeared to occur at the surface leaving little resin deposition on rigid test plates. Cohesive failure appeared to occur within the bulk resulting in significant resin deposition and fibril formation.
- vii. During temperature or feed rate sweeps a peak in peel tack was recorded and observed to occur at the transition between failure modes. The peak occurred against a trend of falling stiffness for the resin component and was somewhat supportive of the Dahlquist criterion concept. However, the actual value of the criterion for prepreg is believed to be dependent on contact conditions.
- viii. Both the tack and stiffness response of prepreg to feed rate and temperature were found to follow the time temperature superposition principle using the WLF equation. Consistent WLF constants could be found from rheology of the resin component before impregnation.
- ix. The impregnation process was found, by GPC and DSC, not to affect the molecular size and distribution of the resin melt. Aging was found to increase molecular weight believed to be the result of cross-linking.

- x. Results from the tack and peel test were related directly to ATL performance. Optimum high tack operating points were located by tack testing and recreated on ATL equipment. Operating points were then transposed using the WLF equation showing reasonable signs that the WLF relationship can be used to improve ATL tack consistency and increase feed rates.
- xi. It is proposed that engineering tack is not a single property but a chain of interfacial and cohesive components. Each is believed to have time dependant properties and cross sectional area. Experiment time should begin at the point of influential molecular contact. Whichever component is weakest at any given time will determine failure. To account for the effect of contaminates, the chain should be extended to include interfacial and cohesive components of any weak boundary layer.
- xii. A descriptive engineering tack curve has been devised where tack is normalised against relative diffusion rate. Increasing interfacial and reducing viscoelastic curves are believed to meet at a point of peak tack where actual experimental tack is thought to fall below the lower of the two curves.
- xiii. The apparent ability of an Arrhenius type equation to govern both viscoelastic and interfacial properties has been discussed. The traditional free volume theory was not considered satisfactory in accounting for interface behaviour. Alternatively, a thermodynamic Lennard-Jones molecular approach has been proposed to account for experimental results.

7 Recommendations and future work

7.1 Tack and stiffness

The tack and stiffness test is proposed for use in other fields such as PSAs and surface energy studies. The study of polymers in accurate dimensionally controlled resin films without fibre effects may allow for improved isolation of variable effects. Surface energy may also be correlated using standardised resin films.

Uniform resin films with perfectly smooth surfaces could be investigated to confirm the lack of surface finish effect observed here. The results may help to determine whether tack is diffusion or thermodynamically controlled.

The electrostatic effect requires further investigation since it could yield a useful tool in automated handling of prepregs. It would also be useful to quantify the effects of humidity as it is considered an important factor effecting lay-up performance.

The effect of molecular length and configuration on viscoelasticity and tack could be investigated. A number of molecular configurations and dispersions could be tested to gain an accurate picture of how features such as molecular weight, branching and polymeric dispersity effect tack. The differing melts may also be tested to confirm the validity of the WLF time temperature relationship in both tack and rheology.

The effects of surface energy also require further investigation. It is likely that the gradient at which interfacial failure meets cohesive failure in a tack temperature sweep may be directly correlated to surface energy.

Molecular changes during aging and its effect on tack would also benefit from investigation. The results may lead to the possibility of extending prepreg out life which is generally determined by useful tack.

Thermodynamic Lenard Jones modelling is recommended as the method most likely to yield accurate results. However, this type of modelling requires accuracy on an atomic scale including contaminant layers. Prediction of WLF constants could offer a simplified test of bulk dynamic properties of the model before moving on to contact simulations. Testing in a vacuum may also offer a simplified experimental comparison.

7.2 Prepreg

The adoption and standardisation of the tack and stiffness test method for prepregs is recommended. For maximum benefit, resin manufacturers could include a tack and stiffness to temperature plot using a standardised feed rate, application pressure, humidity level, and surface. Inclusion of the resin's WLF constants, found by rheology, would allow the superposition of tack and stiffness levels to suit the production environment by adjusting lay-up feed rates or temperature. The standardisation of measurement, calculation and specification of data is recommended and could lead to the development of a British standard with the help of manufacturers and consumers.

The effects of aging would also require that tack properties be given some adjustment depending on their storage history. Alternatively, since tack appears to be the variable limiting shelf life, manufacturers may wish to consider producing all prepreg at the highest possible tack level and allowing it to age during transport and storage to give the required tack level at the time of lamination. A time temperature indicator could be included in the packaging to show when the prepreg is ready. Alternatively, customers could perform their own b-staging within a short cycle in a low temperature oven essentially accelerating the aging procedure. This method would take advantage of the curing process, increasing the molecular weight to give the required tack level, and could remove the need for freezer delivery and storage, further reducing the cost of prepreg.

7.3 ATL

Modification of ATL equipment is proposed in an attempt to improve performance. Essentially, a favourable tack gradient through the prepreg thickness could be attempted, where the tack to the mould surface exceeds that of the backing paper. The tack gradient may be created by tailoring viscoelastic properties. This may be done by resin formulation, where resin at the mould surface has a lower shear storage modulus than that of the backing paper side. Alternatively, the favourable tack gradient could be induced by a temperature gradient with heat applied at the mould surface side which would require repositioning of the heater element.

Significantly improved ATL feed rates could be attempted by exploring the limits and application of the WLF relationship (Chapter 4.5). Control of the heater element via the CNC program is recommended. Changing temperature with feed rate according to the WLF relationship, and relevant constants for a particular material, should enable any successful operating point to be maintained at a significantly higher feed rate,

approaching that of the machines feed rate limit. For Example if M19.6LT 400g/m² 28% resin content ATL prepreg was B-staged to give an optimum tack operating point of 100 mm/min at 20°C then a temperature increase of 19.5°C is required to maintain this operating point at a maximum output of 50,000 mm/min. At this speed, approximately 1.4 kW of heat is needed to achieve the required temperature. Therefore, a 3kW heater element positioned against the mould side of the prepreg would be recommended based on a heating efficiency of around 50%. The difficulty of delivering such a rapid temperature increase may be overcome with the use of laser, microwave or electron beam heating.

In addition to maintaining tack performance the constant diffusion rate may also produce a laminate with more consistent mechanical properties and is recommended for further investigation. An alternative strategy may also be employed in formulating ATL prepreg resins with reduced response to temperature and strain rate changes. Essentially a reduced gradient of shear storage modulus response to temperature is required for more reduced sensitivity to feed rate changes. More flexibility in tracking of the mould surface and a reduced compaction pressure are also recommended to facilitate the use of low cost mould tooling.

Appendix

A. Publications arising from this thesis

*Crossley, R.J., Schubel, P. J., Warrior, N. A. *The Experimental Determination and Control of Prepreg Tack for Automated Manufacture*. In 14th European Conference on Composite Materials (ECCM), June 2010, Budapest, Paper ID.403-ECCM14.

*The paper has been accepted for publication in the journal of Plastics, Rubber and Composites ECCM14 special edition, Due 2011.

Crossley, R.J., Schubel P.J., Warrior N.A., *Automated tape lay-up (ATL) of wind energy grade materials*, in the 2010 European Wind energy conference (EWEA 2010), May 2010, Warsaw, Poland.

Crossley, R.J., Schubel, P.J., Warrior, N.A., *The experimental characterisation of prepreg tack*, in The 17th International Conference on Composite Materials (ICCM-17), 2009, IOM Communications Ltd, Edinburgh.

Crossley, R.J., Kemp, G., Hudson, N., Schubel, P., *AIRPOWER** - Materials Development and Strain Sensor Integration*, July 2009, Technology Strategy Board (TSB): Swindon.

Crossley, R.J., Schubel P.J., Mead F., *AIRPOWER** - Response to Breakpoint Conditions milestone report WP1*, 2007, Technology Strategy Board (TSB): Swindon.



**The AIRPOWER project was selected as a finalist in the wind energy category of the JEC Composites 2011 Innovation awards

B. Calibration of rolling friction and backing film

Calibration of films and rolling friction was done with a 100N compaction force. A thin clear film strip with negligible bending stiffness was passed through the rollers to give an average rolling friction of approximately 0.7N over 190mm extension at 500 mm/min (Fig B-1). The rig friction was then subtracted from the average rolling resistance of backing films to yield the correction factors required to be added to the average tack values to give the true tack value (Table B-1).

Changes in rig friction and bending resistance of films are acknowledged with changes in compaction force, feed rate and temperature. However, such changes are considered negligible in comparison to the typical stiffness and tack forces recorded.

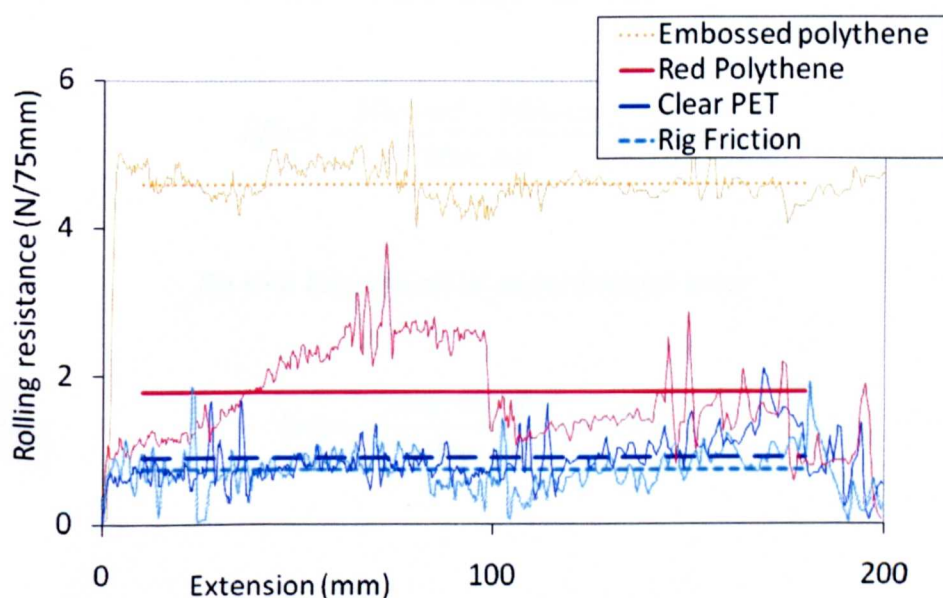


Fig B-1 Calibration of rig friction and backing films

Table B-1 Rig friction and film calibration values

Film	Value
Embossed Polythene	4 N/75mm
Red Polythene	1 N/75mm
Clear PET	0.3 N/75mm
narrow paper strip (Rig friction)	0.7 N

C. Analysis of single level results

In order to quantify the effect of multiple level experiments further analysis was required. The effect of the variable under consideration was defined by the maximum change in tack as a percentage of the maximum recorded value for tack (Eq C-1). This method proved effective for results where large changes of tack were recorded. However, the value of the effect appeared exaggerated where very low values of tack were recorded overall. Therefore, for comparison the experimental error must also be considered. The average experimental batch standard deviation is taken for all levels and then divided by the average value (Eq C-2). If the error value approaches or exceeds the effect then result is considered less conclusive.

Eq C-1 Expression of effect

$$\text{Effect} = \frac{\text{Max. val} - \text{Min. val}}{\text{Max. val}} \times 100\%$$

Eq C-2 Expression of experimental error

$$\text{Error} = \frac{\text{Avg. std. dev.}}{\text{Avg. val}} \times 100\%$$

D. Analysis of temperature sweep results

In order to quantify the effect of multiple level experiments over a temperature sweep range further analysis was required. The average tack level over a temperature sweep range encompassing both failure modes is considered (Fig D-1). The average tack is expressed as the average integral of tack (Eq D-1). The overall experimental error is expressed in the same manner taking error values at y_n and y_{n+1} ensuring that high values of error which occur over a short temperature range are not over emphasised.

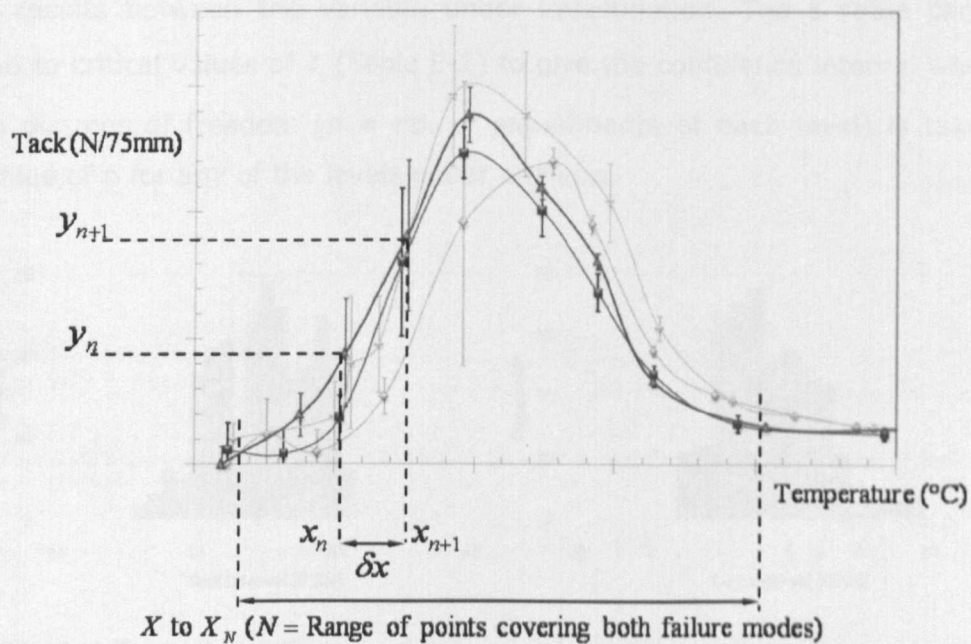


Fig D-1 Numerical analysis of results for temperature sweeps at a number of variable levels

Eq D-1 The average tack of a temperature sweep experiment

$$Av.Tack = \frac{1}{X_N - X} \cdot \int_{x_n}^{x_N} y \cdot dx$$

E. Statistical confidence

The continuous tack data appears to follow a bell shaped normal distribution (Fig E-1). The total variance is unknown, therefore, confidence intervals are calculated using the t-distribution [170]. A comparison is made between two results to give an indication of whether the observed effect is mostly due to chance through random fluctuation or actual effect. Firstly the estimated true standard deviation σ_e is calculated (Eq. E-1). Then the t statistic can be calculated (Eq. E-2) where $\bar{x}_1 - \bar{x}_2$ is the difference in the average results between the variable under investigation. The t value can then be compared to critical values of t_c (Table E-1) to give the confidence interval where in this case the degrees of freedom ($n = \text{no. of experiments at each level}$) is taken as the lowest value of n for any of the levels under analysis.

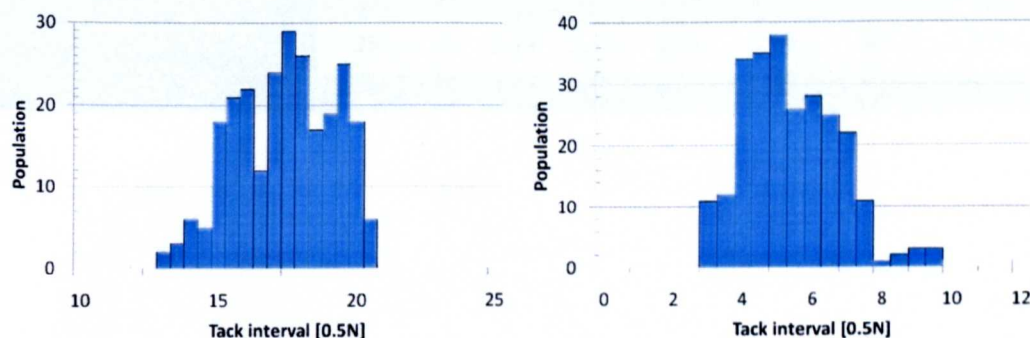


Fig E-1 Typical distribution of values recorded during a tack experiment

Eq. E-1 Estimated standard deviation for two datasets [171]

$$\sigma_e = \frac{(n_1 - 1)\sigma_1^2 + (n_2 - 1)\sigma_2^2}{n_1 + n_2 - 2}$$

Eq. E-2 t-statistic for the comparison of two variables [171]

$$t = \frac{\bar{x}_1 - \bar{x}_2}{\sigma_e} \sqrt{\frac{n_1 n_2}{n_1 + n_2}}$$

Table E-1 Critical confidence intervals for *t*

Confidence Interval (%)	80	90	95	99	99.5	99.99	99.995	99.999
Degrees of freedom (n)								
2	1.89	2.92	4.3	9.92	14.09	31.6	44.7	100.14
3	1.64	2.35	3.18	5.84	7.45	12.92	16.33	28.01
4	1.53	2.13	2.78	4.6	5.6	8.61	10.31	15.53
5	1.48	2.02	2.57	4.03	4.77	6.87	7.98	11.18
6	1.44	1.94	2.45	3.71	4.32	5.96	6.79	9.08
7	1.41	1.89	2.36	3.5	4.03	5.41	6.08	7.89
8	1.4	1.86	2.31	3.36	3.83	5.04	5.62	7.12
9	1.38	1.83	2.26	3.25	3.69	4.78	5.29	6.59
10	1.37	1.81	2.23	3.17	3.58	4.59	5.05	6.21
11	1.36	1.8	2.2	3.11	3.5	4.44	4.86	5.92
12	1.36	1.78	2.18	3.05	3.43	4.32	4.72	5.7
13	1.35	1.77	2.16	3.01	3.37	4.22	4.6	5.51
14	1.35	1.76	2.14	2.98	3.33	4.14	4.5	5.36
15	1.34	1.75	2.13	2.95	3.29	4.07	4.42	5.24

References

- [1] Houghton, J., *Global warming*. Reports on Progress in Physics, 2005. 68(6): p. 1343-403.
- [2] Q&A: *The Kyoto Protocol*. BBC News 2005 Available from: <http://news.bbc.co.uk/1/hi/sci/tech/4269921.stm>.
- [3] Rose, C. *2008 Annual Report*. 2008 EWEA, Report No., Available from: www.ewea.org.
- [4] Anon. *Global Wind 2008 Report*. 2009 GWEC, Report No. N/a, Available from: www.gwec.net.
- [5] Schubel, P.J., *Technical cost modelling for a generic 45-m wind turbine blade produced by vacuum infusion (VI)*. Renewable Energy, 2010. 35(1): p. 183-9.
- [6] Red, C. *Wind turbine blades: Big and getting bigger*. Composites Technology 2008 6/1/2008 Available from: www.compositesworld.com.
- [7] EWEA. *Wind Energy, The Facts*. 2008 Available from: www.wind-energy-the-facts.org.
- [8] Anon. *Automating wind turbine manufacture*. Reinforced plastics.com 2009 Available from: www.reinforcedplastics.com.
- [9] Hau, E., *Wind Turbines, Fundamentals, Technologies, Application, Economics*. 2nd ed. 2006, Berlin: Springer.
- [10] Gasch, R., Tvele J., *Wind Power Plants*. 2002, Berlin: Solarpraxis.
- [11] Brondsted, P., Lilholt H., Lystrup A., *Composite materials for wind power turbine blades*. Annual Review of Materials Research, 2005. 35: p. 505-38.
- [12] Anon. *Clipper Windpower announces groundbreaking offshore wind blade factory in England*. Windpower Monthly 2010 Available from: <http://www.windpowermonthly.com/news/985112>.
- [13] Gorban', A.N., Gorlov A.M., Silantyev V.M., *Limits of the turbine efficiency for free fluid flow*. Journal of Energy Resources Technology-Transactions of the Asme, 2001. 123(4): p. 311-7.
- [14] Hansen, M.O.L., *Aerodynamics of wind turbines*. 2008, London: Earthscan.
- [15] Fuglsang, P., Bak C., *Development of the Riso wind turbine airfoils*. Wind Energy, 2004. 7(2): p. 145-62.
- [16] Burton, T., Sharp D., Jenkins N., Bossanyi E., *Wind Energy Handbook*. 2006 ed. 2001, Chichester: John Wiley & Sons Ltd.
- [17] Kong, C., Bang J., Sugiyama Y., *Structural investigation of composite wind turbine blade considering various load cases and fatigue life*. Energy, 2005. 30(11-12): p. 2101-14.
- [18] Habali, S.M., Saleh I.A., *Local design, testing and manufacturing of small mixed airfoil wind turbine blades of glass fiber reinforced plastics Part I: Design of the blade and root*. Energy Conversion and Management, 2000. 41(3): p. 249-80.
- [19] Anon. *Euros blades production catalogue*. 2010 Available from: http://www.euros.de/en/products_blades_production.html.
- [20] Quinn, J.A., *Composites Design Manual*. 1999, Lancaster, USA: Technomic Publishing.
- [21] Schubel, P.J., Parsons A.J., Lester E.H., Warrior N.A., *Characterisation of thermoset laminates for cosmetic automotive applications: Part II - Cure and residual volatile assessment*. Composites, 2005. Part A(37): p. 1747-56.
- [22] Hull, D., Clyne T.W., *An Introduction to Composite Materials*. 2002, Cambridge, UK: Cambridge University Press.
- [23] Ponten, A., Carstensen O., Rasmussen K., Grubberger B., et al., *Epoxy-based production of wind turbine rotor blades: occupational dermatoses*. Contact Dermatitis, 2004. 50(6): p. 329-38.
- [24] Khoun, L., Hubert P., *Cure Shrinkage Characterization of an Epoxy Resin System by Two in Situ Measurement Methods*. Polymer Composites, 2010. 31(9): p. 1603-10.

- [25] Adams, R.D., Yu H., Karachalios V.F., *Cure shrinkage in epoxy adhesives*, in *EURADH 2000 5th European adhesion conference*. 2000, SFV, Paris: Lyon, France.
- [26] Veers, P.S., Ashwill T.D., Sutherland H.J., Laird D.L., et al., *Trends in the design, manufacture and evaluation of wind turbine blades*. *Wind Energy*, 2003. 6(3): p. 245-59.
- [27] Astrom, B.T., *Manufacturing of Polymer Composites*. 1997, London: Chapman & Hall.
- [28] Griffin, D.A., *Cost & performance tradeoffs for carbon fibers in wind turbine blades*. *Sampe Journal*, 2004. 40(4): p. 20-8.
- [29] Harris, B., *Engineering Composite Materials*. 1999, London: IOM Communications Ltd.
- [30] Rudd, C.D., Long A.C., Kendall K.N., *Liquid moulding technologies*. 1997, Cambridge, England: Woodhead Publishing Ltd.
- [31] Chambers, A.R., Earl J.S., Squires C.A., Suhot M.A., *The effect of voids on the flexural fatigue performance of unidirectional carbon fibre composites developed for wind turbine applications*. *International Journal of Fatigue*, 2006. 28(10): p. 1389-98.
- [32] Cairns, D.S., Skramstad J.D., *Evaluation of hand lay-up and resin transfer moulding in composite wind turbine blade structures*, in *45th International SAMPE symposium*. 2000: Long Beach, CA, USA.
- [33] Chatting, I. *Resin Infusion Project*. 2002 Department of Trade & Industry, Report No. ETSU W/45/00542/00/REP.
- [34] Summerscales, J., Searle T.J., *Low-pressure (vacuum infusion) techniques for moulding large composite structures*. *Proceedings of the Institution of Mechanical Engineers Part L-Journal of Materials-Design and Applications*, 2005. 219(L1): p. 45-58.
- [35] Long, A.C., *Design and manufacture of textile composites*. 2005, CRC Press: Cambridge.
- [36] Newell, G.C., Buckingham R.O., Khodabandehloo K., *The automated manufacture of prepreg broadgoods components - A review of literature*. *Composites Part A - Applied Science and Manufacturing*, 1996. 27(3): p. 211-7.
- [37] Goode, K., *Automated Ply Lamination*, in *ASM Handbook volume 21, Composites*. 1987, ASM International.
- [38] Grimshaw, M.N., Grant C.G., Diaz J.M.L., *Advanced technology tape laying for affordable manufacturing of large composite structures*. *Polymer Composites*, 2007. 13(3): p. 197-206.
- [39] Lubin, G., *Handbook of composites*. 1982, London: Chapman & Hall.
- [40] Evans, D.O., *Fiber Placement*. ASM International, 2001. 1: p. 477-9.
- [41] Black, S. *Getting to know "Black Aluminium"*. *Modern Machine Shop* 2008 Available from: <http://www.mmsonline.com/articles/getting-to-know-black-aluminum>.
- [42] Skinner, M.L., *Trends, advances and innovations in filament winding*. *Reinforced Plastics*, 2006. Feb(Feb): p. 28-33.
- [43] srl, C.T.S. *Lamellar line for the continuous production of GRP/GRE Pipe ND 100 - 600mm*. 2007 Available from: www.cimtec-holding.it/lamellar.htm.
- [44] Technobell, L. *Continuous Filament Winding machine CFW4000*. 2007 Available from: <http://www.technobell.info/>.
- [45] Crossley, R.J., Schubel P.J., Mead F. *AIRPOWER - response to Breakpoint conditions milestone report WP1*. 2007 01/11/2007 Technology Strategy Board, Report No.
- [46] Molyneux, M., *Prepreg, Tape and Fabric Technology for Advanced Composites*. *Composites*, 1983. 14(2): p. 87-91.
- [47] Ahn, K.J., Seferis J.C., *Prepreg Process Analysis*. *Polymer Composites*, 1993. 14(4): p. 349-60.
- [48] Saunders, K.J., *Organic polymer chemistry*. 1994: Chapman & Hall.
- [49] Allcock, H.R., *Introduction to materials chemistry*. 2008: John Wiley & Sons.

- [50] Rosu, D., Cascaval C.N., Mustata F., Ciobanu C., *Cure kinetics of epoxy resins studied by non-isothermal DSC data*. *Thermochimica Acta*, 2002. 383(1-2): p. 119-27.
- [51] Banks, R., Mouritz A.P., John S., Coman F., et al., *Development of a new structural prepreg: characterisation of handling, drape and tack properties*. *Composite Structures*, 2004. 66(1-4): p. 169-74.
- [52] Anon. *Prepreg Technology*. 2011 Available from: www.hexcel.com.
- [53] Akay, M., *Effects of Prepreg Aging and Post-Cure Hygrothermal Conditioning on the Mechanical-Behavior of Carbon-Fiber Epoxy Laminates*. *Composites Science and Technology*, 1990. 38(4): p. 359-70.
- [54] Ahn, K.J., Peterson L., Seferis J.C., Nowacki D., et al., *Prepreg Aging in Relation to Tack*. *Journal of Applied Polymer Science*, 1992. 45(3): p. 399-406.
- [55] Grimshaw, M.N., *Automated Tape Laying*, in *ASM Handbook volume 21, Composites*. 2001, ASM International. p. 480-5.
- [56] Grimshaw, M., Grant C., Diaz J., *Advanced technology tape laying for affordable manufacturing of large composite structures*, in *46th International SAMPE Symposium*. 2001: Long Beach, CA.
- [57] Sloan, J., *ATL and AFP: Defining megatrends in composite aerostructures*. *High-Performance Composites*, 2008. July 2008.
- [58] Repecka, L., *Prepreg Characteristics and Their Effects on Automated Tape Laying Machines*, in *SAMPE 88*. 1988, New Generation Materials and Processes: Milan. p. 55-64.
- [59] Shirinzadeh, B., Alici G., Foong C.W., Cassidy G., *Fabrication process of open surfaces by robotic fibre placement*. *Robotics and Computer-Integrated Manufacturing*, 2004. 20(1): p. 17-28.
- [60] Lukaszewicz, D.H.-J.A., Potter K.D., *The internal structure and confirmation of prepreg with respect to reliable automated processing*. *Composites Part a-Applied Science and Manufacturing*, 2010. Online (Awaiting publication).
- [61] Olsen, H.B., Craig J.J., *Automated Composite Tape Lay-up Using Robotic Devices*. *Proceedings : Ieee International Conference on Robotics and Automation*, Vols 1-3, 1993: p. C291-7.
- [62] Ruth, D.E., Mulgaonkar P. *Robotic lay-up of prepreg composite plies*. in *Robotics and automation, IEEE international conference on*. 1990. Cincinnati: IEEE Xplore.
- [63] Schulz, M.D., Grimshaw M.N., Beard J. *Tape Temperature Control System For Automated Tape-Laying of Low Tack Prepregs*. in *33rd International SAMPE Symposium*. 1988. California: SAMPE.
- [64] Gutowski, T.G., Bonhomme L., *The Mechanics of Prepreg Conformance*. *Journal of Composite Materials*, 1988. 22(3): p. 204-23.
- [65] Owen, P.S. *Eurofighter Typhoon production*. 2005 Available from: www.typhoon.starstreak.net/Eurofighter/production.html.
- [66] Benson, V.M., Arnold J. *Automated fiber placement of advanced materials*. 2006 Wright-Patterson airforce base, Report No. AFRL-ML-WP-TP-2006-424.
- [67] Lin, H., Wang J., Long A.C., Clifford M.J., et al., *Predictive modelling for optimization of textile composite forming*. *Composites Science and Technology*, 2007. 67(15-16): p. 3242-52.
- [68] Ondarcuhu, T., *Tack of a polymer melt: Adhesion measurements and fracture profile observations*. *Journal De Physique II*, 1997. 7(12): p. 1893-916.
- [69] Cottingham, W.N., Greenwood D.A., *An introduction to the standard model of particle physics*. 2nd ed. 2007, Cambridge: Cambridge University Press.
- [70] Anon. *Brian Cox: Large Hadron Collider is all about understanding the forces of nature*. 2009 Available from: <http://www.belfasttelegraph.co.uk>.
- [71] Lee, L.-H., *Fundamentals of adhesion*. 1991, New York: Plenum Press.
- [72] Rubinstein, M., Colby R.H., *Polymer physics*. 2006, Oxford: Oxford university press.
- [73] Kendall, K., *Molecular Adhesion and its Applications, The Sticky Universe*. 2001, London: Plenum Publishers.

- [74] Benedek, I., *Pressure sensitive adhesives and applications*. 2nd ed. 2004, Wuppertal, Germany: Marcel Dekker Inc.
- [75] Benedek, I., Feldstein M.M., *Fundamentals of pressure sensitivity*. 2009, London: CRC Press.
- [76] Putnam, J.W., Seferis J.C., Pelton T., Wilhelm M., *Perceptions of Prepreg Tack for Manufacturability in Relation to Experimental Measures*. *Science and Engineering of Composite Materials*, 1995. 4(3): p. 143-54.
- [77] Ahn, K.J., Seferis J.C., Pelton T., Wilhelm M., *Analysis and characterization of prepreg tack*. 1992. 13(3): p. 197-206.
- [78] McMurtrie, R. *Accutac Inc.* 2009 Available from: <http://www.antronics.com/accutac/>.
- [79] Inc., T.M. *Lab Master Loop Tack Tester*. 2009 Available from: <http://www.testingmachines.com/80-94-lab-master-loop-tack-tester.html>.
- [80] Seferis, J.C., Meissonnier J., *Development of a Tack and Drape Test for Prepregs Based on Viscoelastic Principles*. *Sampe Quarterly-Society for the Advancement of Material and Process Engineering*, 1989. 20(3): p. 55-64.
- [81] Ahn, K.J., Seferis J.C., Pelton T., Wilhelm M., *Deformation Parameters Influencing Prepreg Tack*. *Sampe Quarterly-Society for the Advancement of Material and Process Engineering*, 1992. 23(2): p. 54-64.
- [82] Putnam, J.W., Hayes B.S., Seferis J.C., *Prepreg process-structure-property analysis and scale-up for manufacturing and performance*. *Journal of Advanced Materials*, 1996. 27(4): p. 47-57.
- [83] Dubois, O., Cam J.B.L., Beakou A., *Experimental Analysis of Prepreg Tack*. *Experimental Mechanics*, 2009. Online.
- [84] Anon. *World pressure sensitive tapes to 2012*. 2009 Freedonia, Report No., Available from: www.freedoniagroup.com.
- [85] Gierenz, G., Karmann W., *Adhesives and Adhesive Tapes*. 2001, New York: Wiley-VCH.
- [86] Lin, Y.Y., Hui C.Y., Conway H.D., *A detailed elastic analysis of the flat punch (Tack) test for pressure-sensitive adhesives*. *Journal of Polymer Science Part B-Polymer Physics*, 2000. 38(21): p. 2769-84.
- [87] Tordjeman, P., Papon E., Villenave J.J., *Tack properties of pressure-sensitive adhesives*. *Journal of Polymer Science Part B-Polymer Physics*, 2000. 38(9): p. 1201-8.
- [88] Good, R.J., *Theory of Cohesive Vs Adhesive Separation in an Adhering System*. *Journal of Adhesion*, 1972. 4(2): p. 133-8.
- [89] Creton, C., Hooker J., Shull K.R., *Bulk and interfacial contributions to the debonding mechanisms of soft adhesives: Extension to large strains*. *Langmuir*, 2001. 17(16): p. 4948-54.
- [90] O'Connor, A.E., Willenbacher N., *The effect of molecular weight and temperature on tack properties of model polyisobutylenes*. *International Journal of Adhesion and Adhesives*, 2004. 24(4): p. 335-46.
- [91] Zosel, A., *Adhesion and Tack of Polymers - Influence of Mechanical-Properties and Surface Tensions*. *Colloid and Polymer Science*, 1985. 263(7): p. 541-53.
- [92] Creton, C., Leibler L., *How does tack depend on time of contact and contact pressure?* *Journal of Polymer Science Part B-Polymer Physics*, 1996. 34(3): p. 545-54.
- [93] Gay, C., *Stickiness - Some fundamentals of adhesion*. *Integrative and Comparative Biology*, 2002. 42(6): p. 1123-6.
- [94] Gay, C., Leibler L., *Theory of tackiness*. *Physical Review Letters*, 1999. 82(5): p. 936-9.
- [95] Chiche, A., Pareige P., Creton C., *Role of surface roughness in controlling the adhesion of a soft adhesive on a hard surface*. *Comptes Rendus De L Academie Des Sciences Serie Iv Physique Astrophysique*, 2000. 1(9): p. 1197-204.
- [96] Anon, *Adhesives - Determination of peel resistance, floating roller method*. British standards institute, 1995. BS EN 1464:1995.

- [97] Kendall, K., *Thin-Film Peeling - Elastic Term*. Journal of Physics D-Applied Physics, 1975. 8(13): p. 1449-52.
- [98] Derail, C., Allal A., Marin G., Tordjeman P., *Relationship between viscoelastic and peeling properties of model adhesives. Part 1. Cohesive fracture*. Journal of Adhesion, 1997. 61(1-4): p. 123-57.
- [99] Christensen, S.F., McKinley G.H., *Rheological modelling of the peeling of pressure-sensitive adhesives and other elastomers*. International Journal of Adhesion and Adhesives, 1998. 18(5): p. 333-43.
- [100] Kaelble, D.H., *Peel adhesion: Micro-fracture mechanics of interfacial unbonding of polyers*. Transactions of the society of rheology, 1965. 9(2): p. 135-63.
- [101] Gibert, F.X., Allal A., Marin G., Derail C., *Effect of the rheological properties of industrial hot-melt and pressure-sensitive adhesives on the peel behavior*. Journal of Adhesion Science and Technology, 1999. 13(9): p. 1029-44.
- [102] Gent, A.N., Petrich R.P. *Adhesion of viscoelastic materials to rigid substrates*. in Royal Society of London 1969.
- [103] Williams, M.L., Landel R.F., Ferry J.D., *The Temperature Dependence of Relaxation Mechanisms in Amorphous Polymers and Other Glass-Forming Liquids*. Physical Review, 1955. 98(5): p. 3701-7.
- [104] Aubrey, D.W., Sherriff M., *Peel Adhesion and Viscoelasticity of Rubber-Resin Blends*. Journal of Polymer Science Part a-Polymer Chemistry, 1980. 18(8): p. 2597-608.
- [105] Kaelble, D.H., *Theory and Analysis of Peel Adhesion - Bond Stresses and Distributions*. Transactions of the Society of Rheology, 1960. 4: p. 45-73.
- [106] Aubrey, D.W., Welding G.N., Wong T., *Failure Mechanisms in Peeling of Pressure-Sensitive Adhesive Tape*. Journal of Applied Polymer Science, 1969. 13(10): p. 2193-8.
- [107] Gower, M.D., Shanks R.A., *The effect of chain transfer agent level on adhesive performance and peel master-curves for acrylic pressure sensitive adhesives*. Macromolecular Chemistry and Physics, 2004. 205(16): p. 2139-50.
- [108] Poh, B.T., Yong A.T., *Dependence of Peel Adhesion on Molecular Weight of Epoxidized Natural Rubber*. Journal of Adhesion, 2009. 85(7): p. 435-46.
- [109] Gardon, J.L., *Peel Adhesion. I. Some phenomenological Aspects of the Test*. Journal of Applied Polymer Science, 1963. 7(1): p. 625-41.
- [110] Horgnies, M., Darque-Ceretti E., Felder E., *Relationship between the fracture energy and the mechanical behaviour of pressure-sensitive adhesives*. International Journal of Adhesion and Adhesives, 2007. 27(8): p. 661-8.
- [111] Kim, D.J., Kim H.J., Yoon G.H., *Effect of substrate and tackifier on peel strength of SIS (styrene-isoprene-styrene)-based HMPSAs*. International Journal of Adhesion and Adhesives, 2005. 25(4): p. 288-95.
- [112] Mark, J.E., Eisenberg A., Graessley W.W., Mandelkern L., et al., *Physical Properties of Polymers*. 2nd ed. 1993, Washington DC: American Chemical society.
- [113] Morrison, F.A., *Understanding Rheology*. 1st ed. 2001, Oxford: Oxford University Press Inc.
- [114] Shaw, M.T., MacKnight W.J., *Introduction to polymer viscoelasticity*. 3rd ed. 2005, Hoboken. New Jersey: John Wiley & Sons.
- [115] Phan-thien, N., *Understanding Viscoelasticity*. 2002, Berlin: Springer.
- [116] Rudin, A., *The Elements of Polymer Science and Engineering*. 2nd ed. 1999, London: Academic Press.
- [117] Mezger, T.G., *The Rheology Handbook*. 2nd ed. 2006, Hannover, Germany: Vincentz Network GMBH.
- [118] Gedde, U.W., *Polymer Physics*. 1995, London: Chapman & Hall.
- [119] Chang, E.P., *Viscoelastic Windows of Pressure-Sensitive Adhesives*. Journal of Adhesion, 1991. 34(1-4): p. 189-200.
- [120] Lakrout, H., Sergot P., Creton C., *Direct observation of cavitation and fibrillation in a probe tack experiment on model acrylic Pressure-Sensitive-Adhesives*. Journal of Adhesion, 1999. 69(3-4): p. 307-59.

- [121] Ebnesajjad, S., *Adhesives Technology Handbook*. 2nd ed. 2008, New York: William Andrew Inc.
- [122] Einstein, A., *Investigations on the Theory of Brownian Movement*, ed. Furth R. 1926, London: Methuen & Co. Ltd.
- [123] Malone, L.J., Dolter T.O., *Basic Concepts of Chemistry*. 8th ed. 2010, Hoboken, New Jersey, USA: John Wiley & Sons.
- [124] Helrich, C.S., *Modern Thermodynamics with Statistical Mechanics*. 2009, Berlin: Springer-Verlag.
- [125] Blundell, S.J., Blundell K.M., *Concepts in Thermal Physics*. 2nd ed. 2010, Oxford: Oxford University Press.
- [126] Sabbagh, H., Eu B.C., *Generic van der Waals equation of state for polymers, modified free volume theory, and the self-diffusion coefficient of polymeric liquids*. *Physica a-Statistical Mechanics and Its Applications*, 2010. 389(12): p. 2325-38.
- [127] Shackelford, J.F., *Introduction to materials science for engineers*. 7th ed. 2009, Upper Saddle River N.J.: Pearson Prentice Hall.
- [128] McCrum, N.G., Buckley C.P., Bucknall C.B., *Principles of Polymer Engineering*. 2nd ed. 1997, Oxford: Oxford University Press.
- [129] Richeton, J., Ahzi S., Daridon L., Remond Y., *Modeling of strain rates and temperature effects on the yield behavior of amorphous polymers*. *Journal De Physique Iv*, 2003. 110: p. 39-44.
- [130] van der Put, T.A.C.M., *Theoretical derivation of the WLF- and annealing equations*. *Journal of Non-Crystalline Solids*, 2010. 356(6-8): p. 394-9.
- [131] Lide, D.R., Hayes W.M., *CRC Handbook of chemistry and physics*. 2009, London: CRC press.
- [132] Puddephatt, R.J., Monaghan P.K., *The periodic table of the elements*. 1994, Oxford: Clarendon press.
- [133] Harrison, K. *Epoxy Resin @ 3Dchem.com*. 2007 Available from: <http://www.3dchem.com/molecules.asp?ID=326>.
- [134] Kiriya, A., Gorodyska G., Minko S., Tsitsilianis C., et al., *Chemical contrasting in a single polymer molecule AFM experiment*. *Journal of the American Chemical Society*, 2003. 125(37): p. 11202-3.
- [135] Ferry, J.D., *Viscoelastic properties of polymers*. Third ed. 1980, New York: John Wiley & Sons.
- [136] Collins, E.A., Bares J., Billmeyer F.W., *Experiments in polymer science*. 1973, New York: John Wiley & Sons.
- [137] Severs, E.T., *Rheology of polymers*. 1962, New York: Reinhold Publishing corp.
- [138] Degennes, P.G., Leger L., *Dynamics of Entangled Polymer-Chains*. *Annual Review of Physical Chemistry*, 1982. 33: p. 49-61.
- [139] Perkins, T.T., Smith D.E., Chu S., *Direct Observation of Tube-Like Motion of a Single Polymer-Chain*. *Science*, 1994. 264(5160): p. 819-22.
- [140] Russell, T.P., Deline V.R., Dozier W.D., Felcher G.P., et al., *Direct Observation of Reptation at Polymer Interfaces*. *Nature*, 1993. 365(6443): p. 235-7.
- [141] Schach, R., Creton C., *Adhesion at interfaces between highly entangled polymer melts*. *Journal of Rheology*, 2008. 52(3): p. 749-67.
- [142] DeGennes, P.G., *Introduction to polymer dynamics*. 1990, Cambridge: Cambridge university press.
- [143] Menard, K.P., *Dynamic Mechanical Analysis, A practical Introduction*. 2008, London: CRC Press.
- [144] Lakes, R.S., *Viscoelastic solids*. 1999: CRC press.
- [145] Israelachvili, J., *Intermolecular & surface forces*. 2nd ed. 2007, London: Academic press.
- [146] De Coninck, J., Blake T.D., *Wetting and molecular dynamics simulations of simple liquids*. *Annual Review of Materials Research*, 2008. 38: p. 1-22.
- [147] Ingebrigtsen, T., Toxvaerd S., *Contact angles of Lennard-Jones liquids and droplets on planar surfaces*. *Journal of Physical Chemistry C*, 2007. 111(24): p. 8518-23.

- [148] Sun, H., *COMPASS: An ab initio force-field optimized for condensed-phase applications - Overview with details on alkane and benzene compounds*. Journal of Physical Chemistry B, 1998. 102(38): p. 7338-64.
- [149] MacKerell, A.D., Bashford D., Bellott M., Dunbrack R.L., et al., *All-atom empirical potential for molecular modeling and dynamics studies of proteins*. Journal of Physical Chemistry B, 1998. 102(18): p. 3586-616.
- [150] Vollmayr-Lee, K., *Single particle jumps in a binary Lennard-Jones system below the glass transition*. Journal of Chemical Physics, 2004. 121(10): p. 4781-94.
- [151] Wu, C.F., Xu W.J., *Atomistic molecular modelling of crosslinked epoxy resin*. Polymer, 2006. 47(16): p. 6004-9.
- [152] L.Fischer, *An introduction to gel chromatography*, in *Labratory techniques in biochemistry and molecular biology*, Work TS, Work E, Editors. 1969, North Holland Publishing Company: Amsterdam.
- [153] Striegel, A.M., Yau W.W., Kirkland J.J., Bly D.D., *Modern Size-Exclusion Liquid Chromatography*. 2nd ed. 2009, New York: John Wiley & Sons.
- [154] Wu, S.H., *Polymer Molecular-Weight Distribution from Dynamic Melt Viscoelasticity*. Polymer Engineering and Science, 1985. 25(2): p. 122-8.
- [155] Timmer, W.A., van Rooij R.P.J.O.M., *Summary of the Delft University wind turbine dedicated airfoils*. Journal of Solar Energy Engineering-Transactions of the Asme, 2003. 125(4): p. 488-96.
- [156] Grimshaw, M.N. *Automated Tape Laying*. 2007 Available from: <http://www.cincinnatiilamb.com/downloads/AutomatedTapeLaying.pdf>.
- [157] Ramirez, J., Likhtmen A. *Reptate: Rheology of Entangled Polymers Toolkit for Analysis of Theory and Experiment*. 2009 Available from: www.reptate.com.
- [158] Gillanders, A.M., *Determination of prepreg tack*. Int. J. Adhesion and adhesives, 1981. 1(3): p. 125-34.
- [159] Sanjana, S.N., *Overage Indicators for Prepreg Products*. Sampe Journal, 1980. 16(1): p. 5-11.
- [160] Aspenes, G., Hoiland S., Barth T., Askvik K.M., *The influence of petroleum acids and solid surface energy on pipeline wettability in relation to hydrate deposition*. Journal of Colloid and Interface Science, 2009. 333(2): p. 533-9.
- [161] Murphy, J., *Additives for Plastics*. 2nd ed. 2001, Oxford: Elsevier Science Ltd.
- [162] Kang, K.H., *How electrostatic fields change contact angle in electrowetting*. Langmuir, 2002. 18(26): p. 10318-22.
- [163] Abraham, T., Banik K., Karger-Kocsis J., *All-PP composites (PURE (R)) with unidirectional and cross-ply lay-ups: dynamic mechanical thermal analysis*. Express Polymer Letters, 2007. 1(8): p. 519-26.
- [164] Galwey, A.K., Brown M.E., *A Theoretical Justification for the Application of the Arrhenius Equation to Kinetics of Solid-State Reactions (Mainly Ionic-Crystals)*. Proceedings of the Royal Society of London Series a-Mathematical and Physical Sciences, 1995. 450(1940): p. 501-12.
- [165] Galwey, A.K., Brown M.E., *Application of the Arrhenius equation to solid state kinetics: can this be justified?* Thermochemica Acta, 2002. 386(1): p. 91-8.
- [166] Johnson, J.K., Muller E.A., Gubbins K.E., *Equation of State for Lennard-Jones Chains*. Journal of Physical Chemistry, 1994. 98(25): p. 6413-9.
- [167] Larson, R.S., Lightfoot E.J., *Thermally Activated Escape from a Lennard-Jones Potential Well*. Physica A, 1988. 149(1-2): p. 296-312.
- [168] Johnson, K.L., *Mechanics of adhesion*. Tribology International, 1998. 31(8): p. 413-8.
- [169] Yu, N., Polycarpou A.A., *Adhesive contact based on the Lennard-Jones potential: a correction to the value of the equilibrium distance as used in the potential*. Journal of Colloid and Interface Science, 2004. 278(2): p. 428-35.
- [170] Box, G.E.P., Hunter J.S., Hunter W.G., *Statistics for Experimenters*. 2005, Hoboken, New Jersey: John Wiley & Sons.
- [171] Hodgkinson, J.M., *Mechanical testing of advanced fibre composites*. 2000, Cambridge, England: Woodhead publishing Ltd.